In Vivo Fluorescence Imaging of E-Selectin: Quantitative Detection of Endothelial Activation in Arthritis

A thesis submitted for the degree of PhD

by

Luke Gompels

August 2010

Kennedy Institute of Rheumatology

Faculty of Medicine

Imperial College

SUPERVISORS

Dr Ewa Paleolog

Prof. Dorian Haskard

Abstract

Rheumatoid arthritis (RA) is a chronic progressive systemic inflammatory disease, characterized by synovial inflammation and localized destruction of cartilage and bone. Heterogeneity in the clinical presentation of RA and uncertainty about which patients will respond to treatment makes diagnosis and management challenging. Fluorescent imaging in the near infrared (NIR) spectrum significantly decreases tissue autofluorescence offering unique potential to detect specific molecular targets *in vivo*. E-selectin or endothelial adhesion molecule-1 (ELAM-1), a 115kDa glycoprotein induced on endothelial cells in response to pro-inflammatory cytokines involved in RA, such as interleukin (IL)-1β and tumour necrosis factor α (TNFα). E-selectin has been well validated as a potential biomarker of disease activity.

My study aimed to investigate whether E-selectin targeted optical imaging *in vivo* could be developed as a sensitive, specific and quantifiable preclinical molecular imaging technique, and also whether this approach could be used to delineate the molecular effects of novel therapies. I utilised anti-E-selectin antibody labelled with NIR fluorophore in a mouse model of paw swelling induced by intra-plantar injection of TNFα, and in acute collagen-induced arthritis (CIA) in DBA/1 mice, a widely used model of RA. E-selectin generated signal, localised to points of maximal clinical inflammation in the inflamed mouse paw in both models with significant differences to control antibody. Binding of anti-E-selectin antibody was also demonstrated by immunohistochemistry in both models. The ability of E-selectin targeted imaging to detect sub-clinical endothelial activation was also investigated, demonstrating that E-selectin may be an excellent way of determining subclinical vascular activation in CIA. Finally the effect of novel targeted therapy – RB200 which blocks epidermal growth factor (EGF) signalling was investigated. This demonstrated that E-selectin targeted signal could be absolutely abrogated to a level seen in unimmunised healthy control animals, following combination treatment with RB200 and the TNFα inhibitor etanercept.

E-selectin targeted optical imaging is a viable *in vivo* imaging technique that can also be applied to quantify disease and investigate the effects of novel molecular therapies. It holds significant promise as a molecular imaging technique for future translation into the clinic for patients with rheumatoid arthritis and other inflammatory diseases.

Table of Contents

List of Figures

List of Tables

List of Appendices

List of Abbreviations

Ab	antibody
ABP	activity based probe
ACPA	antibodies to citrullinated protein antigens
ANOVA	analysis of variance
AR	amphiregulin
au	arbitrary units
BCA	bicinichoninic acid
bCII	bovine type II collagen
BTC	betacellulin
CCD	charge coupled detector
CF	correction factor
CFA	complete Freund's adjuvant
CIA	collagen induced arthritis
CW	constant wave
DMARD	disease modifying antirheumatic drug
DMEM	Dulbecco's modified eagles medium
DNP	dinitrophenol
DPJ	distal phalangeal joint
EC	endothelial cells
EGF	epidermal growth factor
EGFR	epidermal growth factor receptor
ELAM-1	endothelial adhesion molecule-1
ELISA	enzyme Linked Immunosorbant Assay
EPG	epigen
EPR	epiregulin
FCS	foetal calf serum
FGF	fibroblast growth factor
FMT	fluorescence molecular tomography
FRI	fluorescence reflectance imaging
GFP	green fluorescent protein
GM-CSF	granulocyte-macrophage colony-stimulating factor
H&E	haematoxylin and eosin
HAMA	human anti-mouse antibody
HER	human epidermal growth factor receptor
HRP	horseradish peroxidase
HSA	human serum albumin
ICAM-1	intracellular adhesion molecule-1
ICG	indocyanine green
Ig	immunoglobulin
IL	interleukin
IL-1ra	IL-1 receptor antagonist
LP	left paw

MAC1	macrophage antigen 1
MAdCAM1	mucosal vascular addressin cell-adhesion molecule 1
MAPK	mitogen activated protein kinase
MES-1	mouse E-selectin-1
MFI	mean fluorescence intensity
MHC	major histocompatibility complex
MoAb	monoclonal antibody
MPO	myeloperoxidase
MRI	magnetic resonance imaging
MTX	methotrexate
MW	molecular weight
NADH	nicotinamide adenine dinucleotide
NGF	nerve growth factor
NIR	near infrared
NIRF	near infrared fluorophore
NRG	neuregulin
OA	osteoarthrtitis
PBS	phosphate buffered saline
PDGF	platelet derived growth factor
PECAM1	platelet/endothelial-cell adhesion molecule 1
PEG	polyethelene glycol
PET	positron emission tomography
PFA	paraformaldehyde
PGI2	prostacyclin
PI3K	phosphoinositide 3-kinase
PPJ	proximal phalageal joint
PSGL1	P-selectin glycoprotein ligand 1
RA	rheumatoid arthritis
RP	right paw
RTK	receptor tyrosine kinase
SCID	severe combined immunodeficiency
SDS	sodium dodecyl sulphate
sFlt-1	soluble fms-like tyrosine kinase-1
sFV	single-chain variable fragment antibodies
SPECT	single photon emission computed tomography
Tc	technetium
TGF	transforming growth factor
TNF	tumour necrosis factor
Treg	regulatory T-cell
TTJ	tibiotarsal joint
VCAM	vascular cell adhesion molecule
VEGF	vascular endothelial growth factor
VLA4	very late antigen 4 (also known as $\alpha 4\beta 1$-integrin)
vWF	von Willebrand factor

Statement of Originality

The material in this report has not previously been submitted, and to the best of my knowledge contains no material previously published or written by another person except where due acknowledgement is made in the report itself.

Acknowledgements

I am indebted to my acting supervisor Dr Ewa Paleolog for her constant advice and attention throughout this project.

I would also like to express my sincere gratitude to my co-supervisor Prof. Dorian Haskard for such helpful supervisions and direction and for giving me the opportunity to perform my PhD dissertation at both the Kennedy Institute and at the National Heart and Lung Institute at Hammersmith Hospital.

I also thank Dr Tonia Vincent for playing an integral part in the inception of this project.

I am grateful to numerous colleagues at the Kennedy Institute, in particular to Leigh Madden for assistance with laboratory work, to Dr Ann Sandison and Mr David Essex for assistance with histology on mouse paws.

I would to thank the Kennedy Institute of Rheumatology Trustees for funding this work.

Finally I thank my wife for her continued patience before, during (and hopefully after) this project.

CHAPTER 1

1 INTRODUCTION

Musculoskeletal disorders such as rheumatoid arthritis (RA) and osteoarthritis (OA) are a common cause of pain and disability. Despite the introduction of novel biological therapies that target tumour necrosis factor-α (TNFα) in RA, a significant proportion of patients do not respond positively to treatment. In addition, the pattern of disease in patients may change over time, and alternative therapy may be required at different times. *In vivo* molecular imaging techniques are therefore of paramount importance for elucidating pathogenesis and quantifying the effects of therapy at the preclinical stage in animal models of disease. The significant potential for translating these techniques into patients with arthritis and other inflammatory diseases also holds future promise.

This thesis examines the potential of *in vivo* optical imaging by targeting fluorescently labelled anti-E-selectin monoclonal antibody to localise endothelial activation in inflamed tissues *in vivo*. The study aimed to demonstrate that this approach is a sensitive, specific and quantifiable preclinical molecular imaging technique for inflammatory models of RA, and further examined whether it can be used to delineate the specific effects of targeted biological therapy.

1.1 Rheumatoid Arthritis

RA is a chronic systemic inflammatory disease, primarily characterized by inflamed synovial tissue in multiple joints leading to localized destruction of cartilage and bone (Figure 1-1). It is a severe disabling disease that affects approximately 1% of the population on a worldwide basis (Feldmann, Brennan et al. 1996). The early diagnosis of RA is made problematic by heterogeneity in its clinical presentation and lack of sufficiently specific and sensitive laboratory tests. Conventional imaging strategies such as plain X-ray imaging are widely used to assess disease, and to measure progression and response to treatment (Guillemin, Billot et al. 2005). Because X-rays rely on relatively late features such as bone erosion and joint space narrowing, these may only show any significant changes after many months from disease onset (van der Heijde, van Leeuwen et al. 1995). Sensitive and specific methods of imaging are required for the detection of early inflammatory changes to the synovium in patients with arthritis and for monitoring treatment. Greater joint damage at baseline is

associated with poorer physical function and less improvement after treatment underlying the importance of early detection and intervention to slow the progression of joint destruction (Breedveld, Han et al. 2005). Magnetic resonance imaging (MRI) can directly visualize the bone and soft tissues in three dimensions and has the potential to measure inflammatory activity and joint destruction. Synovitis volume, bone marrow oedema and bone erosions are all potentially suitable for serial measurement (Hodgson, O'Connor et al. 2008), but none of these scoring systems is yet in routine clinical practice. Ultrasound and bone scintigraphy are other useful techniques for assessing RA. Ultrasound is useful for rapidly assessing multiple joints and is well established in the clinical assessment of synovitis and tenosynovitis; it may be combined with power Doppler ultrasound to provide further information on disease activity (Taylor, Steuer et al. 2004). Bone scintigraphy has been used for many years to detect inflammatory arthritis, but while it is a relatively sensitive technique it lacks specificity, has poor anatomical resolution and cannot accurately detect erosions (Weiss, Maxfield et al. 1965). Information on the character of the initial destructive events in RA is limited, since the affected structures are not directly accessible in early disease and because the above techniques do not offer insight into the cellular and molecular processes involved early in the cause of disease pathogenesis.

Significant advances in understanding the underlying aetiology of RA have been made. These point to a predominant role for major histocompatibility complex (MHC) class II dependent immune activation. This association has been brought to the fore by powerful evidence for antibody reactivity to proteins modified by citrullination (Klareskog, Ronnelid et al. 2008). Epidemiological and genetic studies of RA in relation to anti-citrulline immunity have demonstrated significant differences in subsets of patients with and without the presence of antibodies to citrullinated protein antigens (ACPA). Antibodies to citrullinated proteins can be found in approximately 60% of RA patients but only in 2% of the normal population making them highly specific for RA (Schellekens, Visser et al. 2000; Vincent, Nogueira et al. 2002; van Gaalen, Linn-Rasker et al. 2004). The occurrence of ACPA is closely linked to the HLA-DRB1 shared epitope alleles (Klareskog, Stolt et al. 2006). In addition to the previously established risk posed by smoking (Silman, Newman et al. 1996), there are further associations between those who are HLA-DRB1 positive and a close

segregation with those who are anti-cyclic citrullinated peptide antibody positive (Klareskog, Stolt et al. 2006). A recent study has demonstrated citrullinated α-enolase as a potential disease specific autoantigen in RA, although it remains unclear as to how antibodies to a ubiquitously expressed enzyme such as α-enolase may cause inflammation localised to the joints and other organs (Mahdi, Fisher et al. 2009).

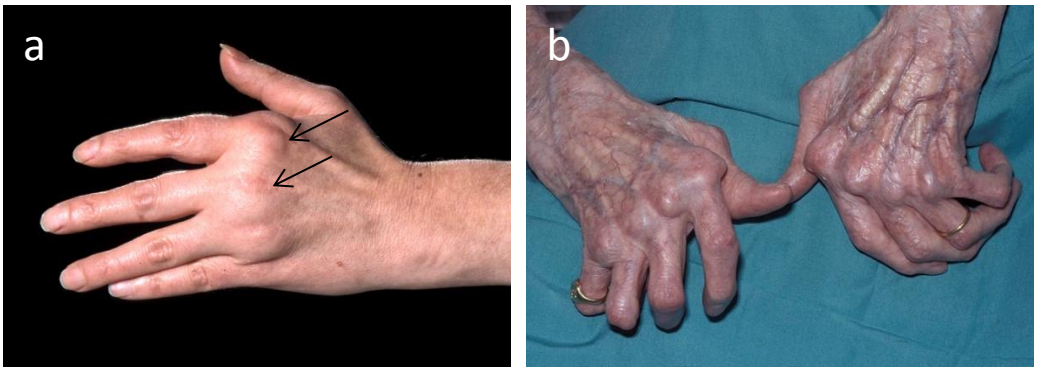

Figure 1-1 Progressive joint destruction in Rheumatoid Arthritis

Rheumatoid arthritis is characterised by progressive joint destruction. Panel a) demonstrates severe synovitis around metacarpal-phalangeal joints (arrowed) leading to progressive joint irreversible joint deformity and loss of joint function. Panel b): Late stage changes in RA showing severe joint deformity.

As our understanding of the molecular basis of RA improves, it has become possible to develop more sophisticated and sensitive techniques for imaging disease and detecting pathological change at an early stage. In particular, molecular imaging may also provide insight into disease mechanisms and elucidate the mode of action of therapeutic agents. *In vivo* imaging in the animal model is therefore of vital importance in developing these techniques helping to both understand the mechanism of action of novel therapies, as well as validating their use in ameliorating arthritis by developing reproducible objective measures of scoring disease activity and monitoring disease activity *in vivo*.

1.1.1 RA: Chronic Inflammation of The Synovium

Rheumatoid synovium is characterized by hyperplasia of the synovial lining layer and marked infiltration by lymphocytes, macrophages and plasma cells. Locally produced inflammatory mediators and the subsequent up regulation of adhesion molecules at sites of inflammation are pivotal to RA pathogenesis (Tak, Taylor et al. 1996). These are discussed in the following sections.

1.1.1.1 Histopathological changes to synovial architecture in RA

Normal synovium is a highly vascular tissue that protects the joint, and provides oxygen, and nutrients to the synovial tissue, and to the relatively avascular cartilage (FitzGerald and Bresnihan 1995). The normal synovium consists of an intimal lining, which is composed of macrophage- and fibroblast-like cells that are loosely associated without a definite underlying basement membrane, and a relatively acellular sublining, which merges with the joint capsule and contains loose connective tissue containing fibroblasts, macrophages, adipocytes, and vascular endothelial cells (EC) (Buch and Emery 2002). Synovial fibroblasts synthesise hyaluronic acid, the major component of the synovial fluid, and express vascular cell adhesion molecule (VCAM)-1, which distinguishes them from normal fibroblasts (FitzGerald and Bresnihan 1995). Synovial macrophages are phagocytic cells that help to clear debris from the joint space and act as sentinels for microbial encounters (Noss and Brenner 2008). In RA, the synovium is altered to a thickened and invasively growing tissue several cell layers thick, which covers and erodes the adjacent cartilage, bone and tendon. Histologically, the inflamed synovium shows pronounced angiogenesis, cellular hyperplasia, and influx of inflammatory cells (Lee and Weinblatt 2001). This is demonstrated in Figure 1-2.

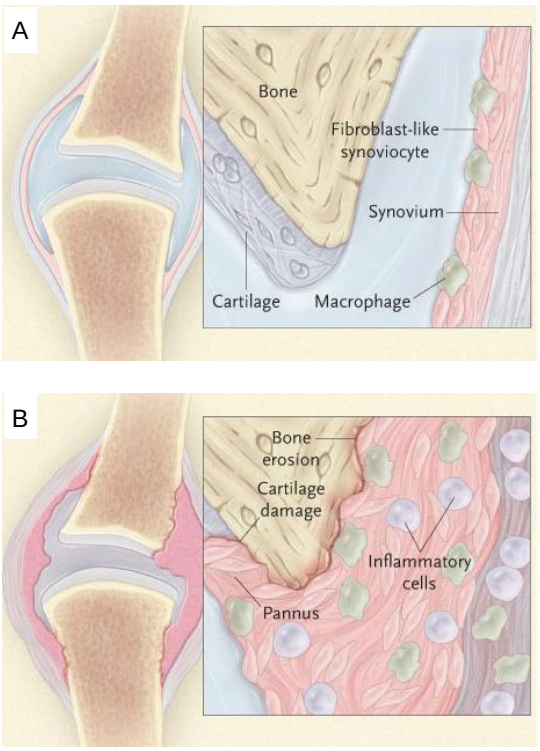

Figure 1-2 Comparison of normal and arthritic joint architecture in rheumatoid arthritis

The normal synovium (A), contains a lining layer that consists of macrophages and fibroblast-like synoviocytes. In the inflamed arthritic joint (B), there is an increase in the number of cells in the synovial-lining layer, infiltration of the synovium with inflammatory cells, development of bone erosions, and the establishment of pannus (granulation) tissue that invades the joint irreversibly changing its architecture (Lipsky 2007).

1.1.1.2 Cellular and soluble mediators of joint damage in RA

There are both cellular and soluble mediators of joint damage: antigen activated CD4+ T cells stimulate monocytes, macrophages and synovial fibroblasts to produce key cytokines and matrix metalloproteinases through cell surface signalling as well as through the release of soluble mediators that include TNFα (Choy and Panayi 2001). Cytokines are local protein mediators that are involved in almost all biological processes, including cell growth and activation, inflammation, immunity and differentiation. The synovial fluid is rich in many of cytokines, some of which also have immunoregulatory roles (Feldmann, Brennan et al. 1996; Choy and Panayi 2001). The central role of TNFα and its evolution to being a key mediator, that when blocked, could abrogate arthritis is discussed below. With further advances in understanding the immunopathology of RA and other autoimmune diseases have

come specific therapeutic targets that have in turn highlighted the effects of blocking particular cellular or molecular pathways. The role of B cells in RA pathology for example evolved in part by the clinical improvements seen in RA patients receiving B-cell depleting therapies such as rituximab, an anti-CD20 antibody, as discussed below.

1.1.2 Targeted Therapeutic Approaches for the Treatment of RA

A number of different agents that have broad ranging effects on the immune system are used to treat patients with RA. Conventional therapy includes the administration of anti-inflammatory drugs followed by disease modifying anti-rheumatic drugs (DMARDs). While traditionally these were used sequentially, evidence then supported their use in combination (O'Dell, Haire et al. 1996). However analysis of cytokine mRNA and protein in RA revealed that many proinflammatory cytokines such as TNFα, interleukin (IL)-1, IL-6, IL-8 and granulocyte-macrophage colony-stimulating factor (GM-CSF) were present in all patients regardless of therapy (Feldmann, Brennan et al. 1996). It was initially demonstrated that blockade of TNFα downregulated IL-1(Brennan, Chantry et al. 1989) and subsequently GM-CSF, IL-6, IL-8, half of the chemokines tested and many active molecules such as matrix metalloproteinases (Haworth, Brennan et al. 1991; Butler, Maini et al. 1995). From these observations evolved the first targeted drug that was shown to be successful for treating collagen induced arthritis (CIA) (Williams, Feldmann et al. 1992), providing the rationale for the clinical development of anti-TNF therapy (Maini, Breedveld et al. 1998). TNFα was therefore the first cytokine to be fully validated as a therapeutic target for RA. In 1993 this led to a clinical study of the therapeutic efficacy of a chimeric IgG_1 monoclonal antibody (infliximab) in RA (Elliott, Maini et al. 1993) with a randomised double blind placebo controlled trial performed in in the following year (Elliott, Maini et al. 1994). The development of TNFα inhibitors have revolutionised the management of RA, since they unequivocally reduce disease activity in the majority of patients treated (Weinblatt, Kremer et al. 1999; Lipsky, van der Heijde et al. 2000; Feldmann and Maini 2003; Weinblatt, Keystone et al. 2003; Keystone, Heijde et al. 2008; Keystone, Genovese et al. 2009; Smolen, Landewe et al. 2009). Different approaches for engineering proteins to block TNF have been developed (Isaacs 2009). These include a chimeric IgG1 monoclonal antibody (infliximab), monoclonal antibodies (MoAb)with fully human amino acid sequences

produced by phage display (adalimumab) or from mice transgenic for the human immunoglobulin locus (golimumab), an engineered P75 TNFRII dimer with a fully human amino acid sequence linked to the Fc portion of human IgG_1 (etanercept) (Moreland, Baumgartner et al. 1997; Moreland, Schiff et al. 1999; Moreland, McCabe et al. 2000); and a pegylated Fab' fragment that lacks an Fc portion (certolizumab). These agents vary in their mechanisms of action, to block free and membrane bound TNF, induction of apoptosis, antibody and complement dependent cell lysis and effects on secretion of pro-inflammatory cytokines from TNF-producing cells. Despite the differences in structure of these agents, broadly similar favourable outcomes are reported. This underscores the tenant that TNFα has a central role the network of molecular and cellular events in the pathogenesis of RA. (Tracey, Klareskog et al. 2008).

Cytokines other than TNFα have also been validated as therapeutic targets. These include IL-1 which is targeted by anakinra, a recombinant form of naturally occurring IL-1 receptor antagonist (IL-1ra) (Bresnihan, Alvaro-Gracia et al. 1998); however this has shown limited efficacy in RA even in combination with methotrexate (Cohen, Hurd et al. 2002). IL-6 has shown significant promise as a therapeutic target for the treatment of RA, and anti-IL-6 receptor antibody tocilizumab has been given approval for the treatment of moderate to severe RA in Europe (Maini, Taylor et al. 2006; Genovese, McKay et al. 2008; Smolen, Beaulieu et al. 2008). Another approach is to target cells producing the pro-inflammatory cytokines. Strong evidence for a critical role for B-cells in the immunopathogenesis of RA came from an open label study of Rituximab in combination with cyclophosphamide and corticosteroids (Edwards and Cambridge 2001). Rituximab is a genetically engineered chimeric anti-CD20 MoAb that is approved for the treatment of relapsed or refractory, low grade or follicular CD20+ B-cell non-Hodgkin's lymphoma. CD20 is a B-cell surface antigen that is expressed only on pre-B and mature B cells. It is not present on stem cells and is lost before differentiation of B cells into plasma cells. Therefore rituximab causes a selective transient depletion of the CD20+ B-cell subpopulation. The clinical efficacy of rituximab was confirmed in a multicentre randomised double blind controlled study in patients with active RA. This showed that rituximab provided significant improvement in disease (Edwards, Szczepanski et al. 2004). Despite the ongoing success of rituximab, other observations have supported a central role for T-cells in

the pathogenesis of RA. These include the induction of an inflammatory arthritis by transfer of CD4+ T cells from patients with RA when they were transferred into severe combined immunodeficient mice (Mima, Saeki et al. 1995). Clinically, drug therapy designed to interrupt T-cell activation via a co-stimulation pathway has been shown to be effective in RA. Abatacept is a recombinant fusion protein that blocks the co-stimulatory signal mediated by the CD28-CD80/86 pathway which is required for T-cell activation (Buch, Vital et al. 2008). Other targeted approaches have been directed to the treatment of RA. These include blocking angiogenesis. Vascular endothelial growth factor (VEGF) blockade in mice has been shown to be highly effective (Miotla, Maciewicz et al. 2000; Sumariwalla, Cao et al. 2003) and this is discussed further in Section 1.2.3.

1.2 The Vascular Endothelium: An Interface for the Interaction between Cytokines and Cell Surface Receptors

The activated endothelium is central to the initial and ongoing recruitment of inflammatory cells to sites of inflammation and it has long been recognized that endothelial activation plays a pivotal role during inflammatory responses. The endothelial adhesion and transendothelial migration of leukocytes is a well regulated sequence of events that involves a multitude of adhesion molecules and chemokines. Primarily selectins, integrins and members of the immunoglobulin superfamily of adhesion receptors are involved in leukocyte 'tethering', 'rolling', activation and transmigration (Sections 1.2.1 and 1.2.2). Vascular permeability and damage also occur through other mechanisms at all stages of the arthritic process. EC secrete several vasodilatory mediators including nitric oxide, prostacyclin (PGI2), platelet activating factor, histamine and others (Szekanecz and Koch 2008). The vascular permeability changes occurring in RA are described in Section 1.2.4. The neoangenic process that both occurs as a result of these vascular changes and is ultimately the cause of abnormal vascularity in RA is described in Section 1.2.3.

1.2.1 The Adhesion Cascade: A Complex Multistep Process

Leukocyte rolling, adhesion and transmigration through the activated endothelium were all described as early as the 19th century, when it was demonstrated that leucocytes extravasted through the lining of blood vessels in response to injury. The work of Julius Friedrich Cohnheim focused on the mechanisms involved in the

extravasation of leukocytes from the blood vessels in the inflamed mesentery of the frog. This work described time dependent alterations, namely dilatation of the arteries and veins, adhesion of colourless cells to the EC and their subsequent transmigration from capillaries and venules into the interstitial space (Cohnheim 1889). The physiological trafficking of lymphocytes through high endothelial venules of lymphoid organs was demonstrated in 1969 by Ford and Gowans (Ford and Gowans 1969). It was subsequently demonstrated that leukocytes could physically adhere to lymph node high endothelial venules within frozen sections (Stamper and Woodruff 1976). L-Selectin was then discovered as a leukocyte adhesion molecule mediating this interaction (Gallatin, Weissman et al. 1983). Following the primary culture of human umbilical vein EC (Jaffe, Nachman et al. 1973) work centered on the notion that EC are subject to different activation states influenced by proinflammatory cytokines that could render them more adhesive for leukocytes. This led to the identification of endothelial surface molecules responsible for this interaction including E-selectin (Bevilacqua, Pober et al. 1985). As adhesion molecules were progressively discovered that were involved in the leukocyte-EC interactions they were classified into families based on molecular structure and function (Bevilacqua, Butcher et al. 1991). Leukocyte extravasation was shown to be a step by step process of initial tethering, rolling along the endothelial surface (mediated largely by selectins and their ligands), arrest and firm adhesion (mediated by integrins and their ligands) and finally transmigration across the endothelium. This sequence is termed the adhesion cascade as shown in Figure 1-3. This is reviewed comprehensively in (Ley and Kansas 2004)).

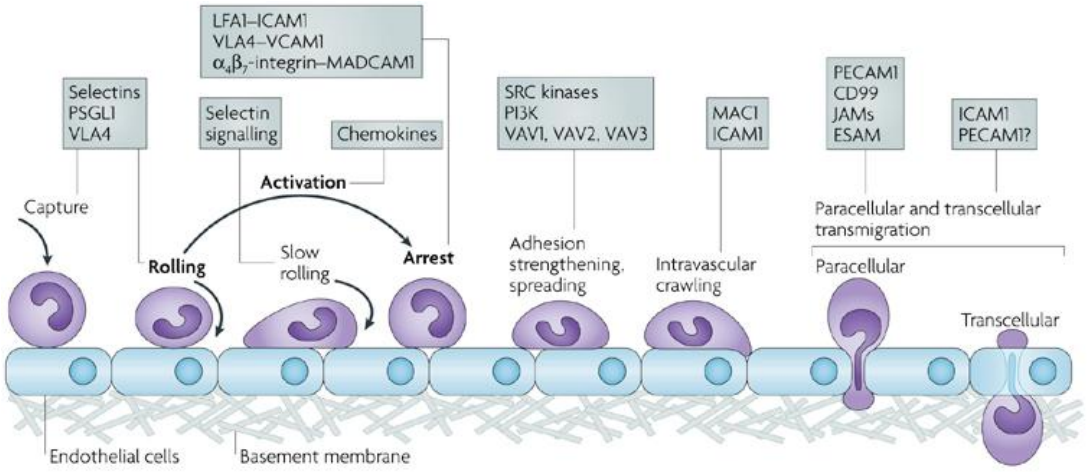

Figure 1-3 Key steps in the adhesion cascade

Important steps in leukocyte adhesion are: *rolling*, which is mediated by selectins, *activation*, which is mediated by chemokines, and *arrest*, which is mediated by integrins. Key molecules involved in each step are indicated in boxes. ESAM, endothelial cell-selective adhesion molecule; ICAM1, intercellular adhesion molecule 1; JAM, junctional adhesion molecule; LFA1, lymphocyte function-associated antigen 1 (also known as αLβ2-integrin); MAC1, macrophage antigen 1; MAdCAM1, mucosal vascular addressin cell-adhesion molecule 1; PSGL1, P-selectin glycoprotein ligand 1; PECAM1, platelet/endothelial-cell adhesion molecule 1; PI3K, phosphoinositide 3-kinase; VCAM1, vascular cell-adhesion molecule 1; VLA4, very late antigen 4 (also known as α4β1-integrin) (Ley and Kansas 2004).

1.2.2 E-Selectin: A Pivotal Endothelial Cell Adhesion Molecule for Leukocytes

E-selectin is expressed on the luminal surface of vascular EC in response to inflammatory stimuli including TNFα and IL-1 (Pober, Gimbrone et al. 1986; Wellicome, Thornhill et al. 1990). It acts as an adhesion molecule for the recruitment of circulating leukocytes into tissues during inflammatory responses (Springer 1990; Butcher 1991). As part of a complex multistep process, selectins promote the initial attachment (tethering) and subsequent moving (rolling) of leukocytes where they become activated as a result of locally produced chemokines (Springer 1994).

The primary sequences of three independently studied cell surface glycoproteins found on endothelium, platelets and leukocytes were first published in 1989 (Bevilacqua, Stengelin et al. 1989; Johnston, Cook et al. 1989; Lasky, Singer et al. 1989; Siegelman, van de Rijn et al. 1989). The term selectin highlights the presence of the lectin domain and the selectivity and function of these molecules. The selectin is prefixed by the cell type on which it was originally identified: E-selectin (endothelium), P-Selectin (platelets) and L-Selectin (lymphocytes) (Bevilacqua, Butcher et al. 1991).

L-selectin was first found as the murine lymph node homing receptor or MEL-14 antigen, defined by the MEL 14 MoAb which blocked the binding of lymphocytes to lymph node high endothelial venules in lymph node tissue (Gallatin, Weissman et al. 1983). Later, L-selectin was also found on neutrophil granulocytes and monocytes and was found to be generally involved in leukocyte entry in sites of inflammation. E-selectin was also found by a MoAb approach during the search for cytokine inducible surface proteins on EC that would mediate the binding of EC (Bevilacqua, Pober et al. 1987). P-selectin was originally found as a membrane protein in platelet storage granules that was of unknown function that was also later detected in EC (Hsu-Lin, Berman et al. 1984).

The selectins were found to contain 3 common protein domains. The NH2 terminus of each selectin is formed by a 120-amino acid domain which has homology with the lectin domain of the C-type animal lectins (Drickamer 1988). This is followed by a 35-40 amino acid repeated sequence similar that was first found in epidermal growth factor (EGF). The six cysteines in this element are located at equivalent positions to form ‘EGF repeats’. The single EGF element is followed by a varying number of

repetitive elements each about 60 amino acids long, resembling motifs found in complement regulatory proteins. All 3 selectins are anchored in the cell membrane by a single transmembrane region which is followed by a short cytoplasmic tail (Somers, Tang et al. 2000). A truncated recombinant form of E-selectin containing only the lectin domain and the EGF repeat has been crystallized, with the 3-dimensional structure determined (Graves, Crowther et al. 1994).

The ligands of selectins are mainly proteins that are posttranslationally modified by specific oligosaccharides which define physiological function (Varki 1994). The primary bases of adhesion are relatively weak calcium dependent interactions between the lectin domain and glycan ligands on apposing cells (Somers, Tang et al. 2000). Selectins and their specific ligands are also known to mediate signal transduction, besides having a direct role in leukocyte capturing (Crockett-Torabi 1998). Selectin ligands are carbohydrate-containing molecules and a variety of glycosyltransferases that have a role in their biosynthesis have been identified. These contribute to the formation of the sialyl lewis x structure on P-selectin glycoprotein ligand-1 (PSGL-1). Although E-selectin can bind PSGL-1, it does not appear to be the main E-selectin ligand and other ligands remain poorly defined (Ley and Kansas 2004). The inducible acquisition of selectin ligands is a key component in mediating T-cell recruitment to extra-lymphoid sites.

1.2.2.1 E-selectin expression during the inflammatory response

E-selectin is transcriptionally induced on EC by cytokines such as IL-1, TNFα and by bacterial lipopolysacharide. Early work demonstrated that surface expression of the protein on cultured human EC reached maximal levels 4-6 hours after stimulation and rapidly declined to basal levels after another 12-16 hours (Pober, Lapierre et al. 1987; Wellicome, Thornhill et al. 1990). Similar expression kinetics were also shown on mouse endothelioma cell lines, with maximal cell surface expression at 4 hours when stimulated with TNFα (Weller, Isenmann et al. 1992; Hahne, Jager et al. 1993).

Acute and chronic disease states, in various animal models and different tissue sites have demonstrated differing kinetics for E-selectin expression. The role of E-selectin in leukocyte accumulation *in vivo* has been studied extensively in the pig (Binns, Licence et al. 1992; Binns, Licence et al. 1996; Binns, Whyte et al. 1996), demonstrating that in pig skin there is constitutive expression of E-selectin (not seen

in the mouse as described below), as well as early upregulation of E-selectin levels. These earlier studies demonstrating the dependence of leukocytes on E-selectin for trafficking into inflamed tissue as well as the early recognition of their interdependence on other factors for localization and transmigration.

By contrast, in the murine contact hypersensitivity model where luminal endothelial selectin expression was quantified via radiolabelled administration of MoAb, persistence of both E- and P-selectin upregulation has been demonstrated (Harari, McHale et al. 1999). In this model the kinetics of selectin expression demonstrated both an early phase of upregulation peaking at 4-6 hours as well as a later phase at 24-48 hours. The early upregulation was distinguished by being dose dependent and postulated to be due to an 'irritant' response to the effect of administering oxazolone, with the later phase antigen specific and dependent on prior sensitization.

1.2.2.2 E-selectin imaging in animal models of inflammatory disease

The initial studies of labelled cell entry *in vivo* (Binns, Licence et al. 1992) and immunohistology were followed by labelling, anti-E-selectin MoAb with indium 111 or technetium 99m. Intravenously injected 111In-labelled anti-E-selectin MoAb (1.2B6) was taken up into inflammatory sites within pig skin stimulated with IL-1, TNFα or phytohemagglutinin (PHA), correlating with leukocyte accumulation and endothelial expression of E-selectin observable immunohistologically (Keelan, Harrison et al. 1994; Whyte, Haskard et al. 1994). This was further confirmed by showing that radiolabelled anti-E-selectin MoAb 1.2B6 whole molecule can be used to image localized endothelial activation in a porcine arthritis model induced by the intrarticular injection of PHA (Keelan, Licence et al. 1994). Because of the potential clinical complications with the use of a whole molecule MoAb due to non-specific Fc-mediated reactions, radiolabelled F(Ab)2 fragments were also shown to demonstrate the *in vivo* expression of E-selectin on synovial endothelium during the evolution of crystal induced arthritis in the porcine model, again using a radiolabelled antibody fragment (Chapman, Jamar et al. 1994). E-selectin expression on activated vascular endothelium has also been evaluated using MRI in an *in vivo* mouse model (Reynolds, Larkman et al. 2006). This study utilized the conjugation of ultra small superparamagnetic iron oxide nanoparticles as a contrast agent on an oxazolone induced contact hypersensitivity model and effectively depicted activated vascular endothelium in murine inflammation *in vivo* with MRI. A further example is the use

of NanoSPECT/CT imaging in the SCID mouse engrafted with human synovial tissue,using a radiolabelled anti-E-selectin antibody to give quantifiable 3D images of E-selectin targeted signal following stimulation with TNFα (Garrood, Blades et al. 2009)

1.2.2.3 E-selectin expression in RA

The endothelium in human RA synovium is known to express E-selectin (Corkill, Kirkham et al. 1991). Specific expression has been demonstrated in venules and capillaries in inflamed synovia of patients with RA but not by other cell types or by normal synovium (Koch, Burrows et al. 1991; Kriegsmann, Keyszer et al. 1995). The endothelial expression and serum levels of E-selectin and its downregulation have also been demonstrated in patients with RA treated with anti-TNF therapy (Paleolog, Hunt et al. 1996; Tak, Taylor et al. 1996). These clinical data highlighted the key importance of TNFα in the inflammatory cascade, with its blockade down-regulating cytokine inducible adhesion molecules including E-selectin as well as VCAM-1 and being associated with a reduction in synovial infiltration.

It has previously been shown that EC induced to express E-selectin by stimulation with cytokines (TNFα and IL-1) peaked in their expression at 4-6 hours and that by 24 hours the molecule was no longer detectable on the cell surface (Pober, Bevilacqua et al. 1986; Wellicome, Thornhill et al. 1990). This raises the possibility that a proportion of E-selectin may be shed from the EC surface. This was confirmed in a later study showing that EC in culture shed a small proportion of the total E-selectin that they synthesize into the culture medium (Newman, Beall et al. 1993). These investigators also showed that the soluble form of E-selectin is detectable in the serum of normal individuals, suggesting a constitutive production in the vasculature. This study also confirmed in small sample sizes elevated levels of soluble E-selectin in patients with septic shock. Deactivation of vascular endothelium by anti-TNFα antibody in patients with RA has also been shown to decrease serum E-selectin levels, with the earliest detectable changes on days 1-3 after anti-TNFα infusion. There was also a significant correlation between the decrease in serum levels of E-selectin and observable clinical benefit compared with those patients who failed to show a beneficial response to anti-TNFα (Paleolog, Hunt et al. 1996) The possible *in vivo* role of soluble adhesion molecules remain unclear although immobilized VCAM-1

and E-selectin have been found to support the binding of human leukocytes and leukocyte cell lines (Lobb, Chi-Rosso et al. 1991; Lobb, Chi-Rosso et al. 1991; Wellicome, Kapahi et al. 1993). Soluble E-selectin is chemotactic for monocytes (Kumar, Hosaka et al. 2001) and neutrophils (Lo, Lee et al. 1991) and increases β2 integrin mediated adhesion (Lo, Lee et al. 1991; Ruchaud-Sparagano, Drost et al. 1998; Ruchaud-Sparagano, Walker et al. 2000). Soluble E-selectin and VCAM-1 have also been demonstrated to promote angiogenesis in rat cornea and induce chemotaxis of human EC (Koch, Halloran et al. 1995). The levels of circulating E-selectin have been measured prospectively in patients with early RA over a five year period demonstrating that soluble E-selectin levels could be correlated with other markers of inflammation as well as showing an association with the degree of joint damage (Kuuliala, Eberhardt et al. 2002). The circulating soluble E-selectin levels in this study, however, were almost within the normal range compared to healthy control subjects, with other studies confirming similar results (Carson, Beall et al. 1994; Blann, Herrick et al. 1995; Voskuyl, Martin et al. 1995; Veale, Maple et al. 1998). It is postulated that even levels within the normal range may have a role in chronic inflammation and have been shown to occur for example in patients with clinically relevant atherosclerosis (Frijns, Kappelle et al. 1997; Fassbender, Bertsch et al. 1999).

1.2.3 Angiogenesis is Central to Promoting and Maintaining RA

The development of the vascular system is one of earliest events that occur during embryogenesis. Two different processes contribute to the formation of blood vessels: vasculogenesis and angiogenesis. The former refers to the *de novo* formation of vessels from progenitor cells whereas the latter is due to the formation of capillaries from pre-existing vessels (Carmeliet 2000). There are a number of pathological conditions where neovessel formation is a key factor in disease pathogenesis. These include cancer, retinopathy and RA (Carmeliet 2003). In extensive histological studies Fassbender et al concluded that one of the earliest and most striking changes in the rheumatoid synovium occurred in the microvasculature. The development of pannus tissue was seen to occur in three stages: synovial lining hyperplasia, pannus formation accompanied by the in-growth of a new vascular network, and further consolidation of the pannus leading to a relatively avascular fibrotic tissue (Fassbender and Simmling-Annefeld 1983). It is therefore widely accepted that angiogenesis is central to both promoting and maintaining RA (Weber and De Bandt 2000). The increased

tissue mass, increased endothelial surface area and disrupted architecture of pathological new vessels are all associated with increased expression of cytokines such as TNFα, transforming growth factor (TGF)-β as well as angiogenic factors such as VEGF which are highly upregulated in the diseased synovium and peripheral blood of RA patients (Fava, Olsen et al. 1994; Koch, Harlow et al. 1994; Paleolog, Young et al. 1998; Ballara, Taylor et al. 2001). Other pro-angiogenic factors expressed in RA include fibroblast growth factors (FGF) and platelet derived growth factor (PDGF) (Sano, Forough et al. 1990; Remmers, Sano et al. 1991; Remmers, Sano et al. 1991; Sano, Engleka et al. 1993).

VEGF is a growth factor that binds to heparin in the extracellular matrix and plays a central role in neovascularisation. Raised serum VEGF levels have been shown to be associated with destructive change in inflammatory arthritis with serum VEGF levels significantly higher in patients with early RA than in patients with self limiting arthritis. This implicates VEGF in the persistence of inflammatory arthritis and supports the hypothesis that expansion of synovial vasculature is important for the development of joint destruction in RA (Ballara, Taylor et al. 2001). Although it is generally accepted that angiogenesis plays a central role in the pathogenesis of RA, it is still debatable, whether the synovial vascular density is actually increased, decreased or unaltered at various stages of disease. Histological analysis of blood vessels in synovial membrane biopsy specimens revealed that tissue obtained from patients with early RA (disease duration less than three years), who had clinical and histological evident knee synovitis, were characterized by prominent vascular proliferation and an increase in the number of blood vessels per area (390 vessels/mm^2) as compared to postmortem control samples (270 vessels/mm^2) (FitzGerald, Soden et al. 1991). Examination of the synovial microvasculature in patients with chronic RA (mean disease duration 15 years) demonstrated that synovial capillaries are distributed more deeply in the rheumatoid synovium. Further, these patients exhibited a diminished capillary density within the synovium compared with normal controls, providing an anatomic explanation for chronic hypoxia in the rheumatoid synovium (Stevens, Blake et al. 1991). This observation further suggests that either natural vessel regression takes place, or synovial tissue growth outpaces neovessel formation, (although treatments might have influenced the synovial vessel density in this study as described in a more recent study below). Nevertheless, these

findings suggests that the synovial microvasculature in RA is reorganised, leading to reduced vascular densities adjacent to the joint space and increased vascular densities in the deeper synovium (Walsh 1999). Other studies demonstrate that the rate of neovascularisation seems to be increased in RA as demonstrated by immunohistological assessment of the synovial microvessel density using the expression of vascular markers CD31 or von Willebrand factor (vWf) in the synovium of arthritic joints (Giatromanolaki, Sivridis et al. 2001; Paleolog 2002). The number of synovial blood vessels has been found to correlate with synovial cell hyperplasia, mononuclear cell infiltration and indices of joint tenderness (Rooney, Condell et al. 1988). More recent evidence has also suggested that immature blood vessels are selectively depleted in response to anti-TNF therapy. Synovial arthroscopic biopsies were taken from RA, OA and normal control patients and analysed by double labelling of the endothelium and pericytes/smooth vessel mural cells to identify and quantify mature/immature blood vessels. In this study, a longitudinal analysis was also performed in 25 patients with active disease rebiopsied after TNFα therapy. This demonstrated that the density of immature but not mature blood vessels were depleted by anti-TNFα therapy (Izquierdo, Canete et al. 2009). Taken together these studies demonstrate that pathological neovascularisation occurs in RA but its phenotype may change over the time course of disease.

Collagen induced arthritis (CIA) is a mouse model of RA that has been used extensively to assess neovascular changes and determine the effects of vascular targeted therapy (Peacock, Banquerigo et al. 1992; Oliver, Banquerigo et al. 1994; Oliver and Brahn 1996). The latter study demonstrated that CIA can be suppressed by the addition of an angiogenesis inhibitor (AGM-1470) in combination with cyclosporine. Treatment with a soluble VEGF receptor has also been demonstrated to reduce disease severity in murine collagen induced arthritis by decreasing both VEGF levels, and bone and cartilage destruction as assessed by histology. A study in CIA has demonstrated that treatment with a soluble form of the Flt-1 VEGF receptor type 1 (sFlt-1) which was polyethylene glycol (PEG) linked significantly reduced both clinical score and paw swelling, compared with untreated or control treated animals. This study also demonstrated that the amount of VEGF increased as arthritis progressed and positively correlated with both clinical score and paw swelling (Miotla, Maciewicz et al. 2000). A further study has also demonstrated that adenoviral

delivery of Flt-1 abrogates disease activity in murine CIA. The effect of sFlt-1 expression on signs of disease was paralleled by reduced joint destruction and decreased expression of the vascular marker vWf. This study concluded that the actions of sFlt-1 were likely to be mediated by reduced synovial neovascularization, supporting the concept that VEGF blockade may be an effective therapeutic adjunct for the treatment of RA. Clinically, the most widely used drug that directly targets the vasculature is bevacizumab – a humanised MoAb that recognises and blocks vascular endothelial growth factor A (VEGF-A) (Los, Roodhart et al. 2007). This drug is used for the treatment of advanced stage metastatic malignancy of the GI tract, lung and breast. A further PEGylated anti-VEGF compound, pegaptanib, is licensed for the treatment of age related macular degeneration. Trials of VEGF inhibitors for the treatment of rheumatoid arthritis have thus far not generated a drug which is in routine clinical practice.

The epidermal growth factor (EGF) ligand/receptor family has also been postulated to play a role in RA pathogenesis (Shiozawa, Shiozawa et al. 1989; Kusada, Otsuka et al. 1993). The human epidermal growth factor receptor family (EGFR; also known as ErbB and human epidermal growth factor receptor, HER) belongs to the receptor tyrosine kinase (RTK) superfamily. The RTKs are well validated targets for cancer therapy but may also have broad therapeutic potential across a range of autoimmune and inflammatory conditions. The first approved RTK therapeutic Herceptin™ (trastuzumab, Genentech) is a MoAb that targets HER-2 and has been highly effective for the treatment of receptor positive breast cancer (Baselga, Tripathy et al. 1996).

The EGFR includes four members (HER-1/ErbB1, HER-2/ErbB2, HER-3/ErbB3 and HER-4/ErbB4). The gene symbol, ErbB, is derived from the name of a viral oncogene to which these receptors are homologous: Erythroblastic Leukemia Viral Oncogene. Insufficient ErbB signalling in humans is associated with the development of neurodegenerative diseases, such as multiple sclerosis and Alzheimer's disease. In mice, loss of signalling by any member of the ErbB family results in embryonic lethality with defects in organs including the lungs, skin, heart and brain. Excessive ErbB signalling is associated with the development of a wide variety of solid tumours. ErbB-1 and ErbB-2 are found in many human cancers and their excessive signalling may be critical factors in the development and malignancy of these tumours (Bublil and Yarden 2007). The EGFR are bound by a large family of ligands including EGF,

transforming growth factor-α (TGF-α), heparin-binding EGF like growth factor (HB-EGF), amphiregulin (AR), betacellulin (BTC), epiregulin (EPR), epigen (EPG), and neuregulins (NRG or heregulins) (Riese and Stern 1998). Ligand binding induces the formation of homo- or heterodimers between the receptors and, depending on the type of dimer formed, transphosphorylation of intracellular regions occurs and leads to the activation of numerous downstream signalling pathways. These include the many components of the mitogen activated protein kinase (MAPK) cascade, the phosphoinositide 3-kinase pathway and the phospholipase C pathway, resulting in cell proliferation, repair, survival and differentiation (Yarden and Sliwkowski 2001; Jorissen, Walker et al. 2003; Shepard, Brdlik et al. 2008; Huang, Brdlik et al. 2009).

Mutations that lead to the dysregulation of the HER proteins and their ligands have been discovered in many different types of cancers and malignant proliferation (Mendelsohn and Baselga 2003; Hynes and Lane 2005). Most notable examples of relevance clinically include the finding that HER-2 is over expressed in a proportion of patients with breast cancer. This led to the development of the drug trastuzumab, a MoAb that targets the extracellular domain of HER-2. This is approved for the adjuvant treatment of HER-2-overexpressing, node-positive or node-negative breast cancer (Slamon, Leyland-Jones et al. 2001). In contrast, cetuximab (Erbitux™, Merck, Germany) is a MoAb that targets HER-1, and is used for metastatic colorectal cancer and head and neck malignancies. Several others targeting HER-1, HER-2 and HER-3 are currently in development (Johnston, Navaratnam et al. 2006). However, resistance to agents that target single HER can occur due to compensation by or up-regulation of other HER family members (Huang, Brdlik et al. 2009). Furthermore, homodimerisation and heterodimerisation among members of the HER/ErbB family of receptors has been described, thus complicating therapies directed against a single HER receptor (Olayioye, Neve et al. 2000).

A number of studies suggest that EGFR family signalling may have a role in the development of RA. For example, Hallbeck *et al* have demonstrated that one of the primary ligands for the EGFR, TGF-α has increased mRNA and levels of protein expression in RA synovial tissue. Interestingly, in this study, TGF-α was present in knee synovial fluid samples of RA patients and levels were significantly higher compared to post-traumatic control samples (Hallbeck, Walz et al. 2005). High levels of another EGFR ligand, EGF, in synovial fluid samples of RA patients have also

been demonstrated (Kusada, Otsuka et al. 1993). Expression of HER-2/ErbB2 in the synovium of RA patients has further been described (Satoh, Kikuchi et al. 2001; Hallbeck, Walz et al. 2005). However, another study reported the expression of AR, but not of EGF, ERG, EPG, BTC, NRG1 or HB-EGF at the mRNA level in RA when compared to OA tissue, but the reason for the discrepancy between this report and other studies is unclear (Yamane, Ishida et al. 2008). The functional significance of the EGF/EGFR pathway in RA is also at present unknown. Activation of EGFR signalling may contribute to hyperplasia of the arthritic synovium, which is a major pathological feature of RA that precedes clinical presentation and prevails throughout the disease (Mor, Abramson et al. 2005). In support of this, trastuzumab, which binds the HER-2/ErbB2 receptor, and the tyrosine kinase inhibitors genistein and imatinib, have been shown to inhibit RA synovial cell growth (Satoh, Kikuchi et al. 2001; Kameda, Ishigami et al. 2006). EGF, when combined with pro-inflammatory mediators including TNFα and IL-1, increased expression by RA fibroblasts of matrix metalloproteinases such as MMP-1, MMP-3 and MMP-13, as well as release of IL-6 (Huber, Kunzler et al. 2008). Since EGF and these cytokines are all expressed in RA synovium, these findings suggest that EGF may synergise with other cytokines in RA. Moreover, these responses were abrogated by a small molecule inhibitor of HER-2/ErbB2. A recent study also reported that EGF stimulated ERK1/2 MAPK and NFκB pathways to stimulate cycoloxygenase-2 and prostaglandin E_2 (Nah, Won et al. 2009). EGFR over-expression may also contribute to RA progression by increasing angiogenesis through the production of pro-angiogenic factors such as vascular endothelial growth factor, IL-8 and basic fibroblast growth factor (Schreiber, Winkler et al. 1986; Goldman, Kim et al. 1993; Kumar and Yarmand-Bagheri 2001; Ravindranath, Wion et al. 2001). Angiogenesis is significantly increased in RA and results in the infiltration of inflammatory cells into the synovium, thus accelerating disease (Paleolog 2009). A treatment modality that inhibits both synovial hyperplasia and angiogenesis would be an attractive option in the immunotherapy of RA.

The highly unique compound RB200 is a bispecific ligand trap, composed of full length extracellular domains of HER-1 and HER-3 EGF receptor. Due to its pan-HER specificity, RB200 inhibits responses mediated by HER-1, HER-2 and HER-3 *in vitro* and *in vivo*.

The potential of utilising an antagonist (RB200) that targets all members of the EGF receptor family is discussed further in section 5.1.2.

1.2.4 Increased Vessel Permeability in RA: Cause or Consequence?

Multiple factors influence the leakage of substances from blood vessels. The major physiological mechanisms include the luminal surface area, permeability of the vessel wall and concentration of driving forces (hydrostatic and osmotic gradients) as well as the blood flow across the endothelium (Michel and Curry 1999; Bates, Heald et al. 2001). Early pathological studies identified vasodilation and increased vessel permeability from biopsies of arthritic joints (Kulka, Bocking et al. 1955; Schumacher and Kitridou 1972). As the vascular permeability increases this leads to plasma extravasation, oedema formation and swelling of the joint. This is mediated by a number of pro-inflammatory agents with evidence for an early neurogenic component. The contribution of sensory efferents and sympathetic afferents to joint injury and thus a possible neurogenic component for joint swelling has been investigated by examining the effect of nerve transection which was shown to reduce hyperalgesia, swelling and joint destruction in a rat arthritis model (Levine, Dardick et al. 1986). Earlier work demonstrated a role for substance P which belongs to the tachykinin neuropeptide family (Walsh, Mapp et al. 1992). Substance P is a potent mediator of increased microvascular permeability in species that include the mouse, through its action on postcapillary EC. Substance P induced oedema formation has been investigated by the use of knockout mice (Cao, Gerard et al. 1999). This model was also used to show that substance P also has a potent effect on cellular accumulation including neutrophil accumulation (Cao, Pinter et al. 2000). Other models have been used to dissect the role of substance P has in both acute and chronic inflammation of the footpad in NK receptor knockout mice. A study by Kidd et al examined the effect of intense inflammation produced by the intraplantar administration of *Mycobacterium Tuberculosis* (Kidd, Inglis et al. 2003). This demonstrated changes in mechanical hyperalgesia, soft tissue swelling and histological scores were significantly reduced in animals with selective NK-1 receptor deletion but that these responses were not seen at early time points. A further study by Keeble and collegues (Keeble, Blades et al. 2005) has demonstrated increased plasma extravasation from 18-72 hours in an inflammatory model of arthritis generated by the intra-articular administration of complete Freund’s adjuvant (CFA) into the murine

knee. It is also likely that many of these substances have peripheral actions that are mediated by pathways centred on the regulation endothelial nitric oxide synthetase (eNOS). These pathways have been further elucidated since the pioneering experiments of Furchgott and Zawadzki into the biological actions of nitric oxide for which they were awarded the Nobel prize in 1998 (Furchgott and Zawadzki 1980). The direct effect of substance P on nitric oxide release was investigated in rheumatoid synoviocytes and also in WT and NK1 knockout mice again following injection of *Mycobacterium Tuberculosis* into the mouse paw. This demonstrated that substance P induces NO in both rheumatoid synoviocytes and experimental models of inflammation with comparable effects to both TNFα and IL-1β (O'Shaughnessy, Vetsika et al. 2006).

Pathologic neoangiogenic vessels also have increased leakiness compared with normal vessels. This effect is well documented in neoangiogenic tumour tissue and is thought to also occur in RA due to increased blood perfusion and vascular permeability as part of both the ongoing inflammatory process and disordered architecture of new vessels. This may lead to as much as a forty fold increase in macroglobulin permeability in the inflamed joint (Levick 1981; Andersson, Johansson et al. 1998). Other evidence also suggests that local vascular permeability may be an early immune complex driven, vasoactive amine dependent process. The mechanisms underlying organ specific autoimmune disease are incompletely understood and it remains unclear how or whether autoantibodies can cause inflammation preferentially in certain tissues. It is recognised that there is a loss of immune tolerance relating to endogenous and exogenous antigens. Local vascular permeability may play an early significant role in this process (Pitzalis and Garrood 2006). Binstadt and colleagues have demonstrated by using intravital imaging that following the transfer of arthritogenic antibodies from K/BxN mice macromolecular vasopermeability is localised to sites that would be expected to develop arthritis in normal mice. (Mice expressing the KRN T cell receptor transgene and the MHC class II molecule A(g7) (K/BxN mice) develop severe inflammatory arthritis, and serum from these mice causes similar arthritis in a wide range of mouse strains, owing to pathogenic autoantibodies to glucose-6-phosphate isomerase (GPI)). This study also suggested an important function for histamine and serotonin in immune mediated vascular leak.

These vasoactive amines are well known to cause the formation of large gaps between EC, particularly in post capillary venules (Binstadt, Patel et al. 2006).

A number of approaches have been employed to make use of changes in vascular permeability by altering the pharmacokinetics of systemically administered compounds in order to improve their therapeutic index. One possibility is the direct conjugation of a drug to another larger molecule. An example of this is conjugation to polyethelene glycol. This approach has been successfully deployed for a number of drugs in routine clinical use such as the PEGylated forms of interferon-α and doxorubicin for the treatment of hepatitis C and breast cancer respectively (Harris and Chess 2003). In RA this approach has demonstrated improved localisation to sites of inflammation: A recent study has demonstrated increased levels of fluorescence in inflamed paws with a fluorescently labelled PEGylated anti-TNFα agent compared to non-PEGylated TNFα inhibitors (Palframan, Airey et al. 2009). It was postulated that this differential uptake may be due in part to the macromolecular structure of the PEGylated agent leading to greater diffusion into inflamed hyperpermeable tissue. Thus far however, it is not clear whether this confers any overall improved clinical efficacy compared to other ant-TNF agents (Kavanaugh, Smolen et al. 2009; Smolen, Landewe et al. 2009). Albumin-based drug delivery has also been investigated as a novel therapeutic approach for methotrexate use in RA. Large amounts of methotrexate are eliminated by the kidneys within a short period resulting in a short plasma half life and low drug concentration in the target tissue. Initial investigations in tumours have demonstrated that methotrexate albumin conjugates show superior accumulation in tumour bearing rat models (Stehle, Wunder et al. 1997). Methotrexate has been conjugated to human albumin (MTX-HSA) thereby taking advantage of increased extravasation, uptake and metabolism of albumin in inflamed synovial tissue. This method has demonstrated significantly increased levels of the conjugate in tissue (Wunder, Muller-Ladner et al. 2003), and in a further study the effectiveness of MTX-HSA in CIA was shown to be superior to MTX alone and that this effect in part was due to the local accumulation of the conjugate in inflamed tissue.

1.3 *In Vivo* Molecular Imaging Approaches in Arthritis

In vivo imaging of specific cells or molecules using non invasive methods helps to provide visualisation and quantification of specific molecular changes over time, shedding light on local and systemic mechanisms involved in acute and chronic inflammation, such as those described in preceding sections. It may also provide real time monitoring of cellular and molecular events involved in disease pathogenesis as well as provide specific quantification of the effect of novel therapies. Various imaging modalities are available such as CT, ultrasound, MRI and nuclear imaging methods such as single photon emission computed tomography (SPECT) and positron emission tomography (PET). These methods differ with respect to spatial resolution, ability to produce three dimensional images, depth limit, and sensitivity, the possibility of quantification and availability of imaging agents that can be coupled to specific molecular perturbations. Techniques that are in routine clinical use such radiography, CT and Ultrasound can provide high resolution images at the anatomical level whereas anatomical detail provided by molecular imaging techniques may be lacking. It can therefore be helpful to combine or co-register images to produce both functional imaging with anatomical localisation. (Weissleder and Mahmood 2001; Herschman 2003; Massoud and Gambhir 2003; Wunder, Straub et al. 2005). Conventional imaging techniques such as radiography can detect contrast but large amounts are required at the target site. The adverse effects of ionising radiation can then become restrictive, especially if imaging at multiple time points is required. Ultrasound has successfully been deployed to give information about blood flow using colour duplex sonography (Taylor, Steuer et al. 2004) but is a dynamic study that may be difficult to quantify at different time points. Targeted contrast agents for MR imaging have been developed. This includes using an iron oxide particle attached to E-selectin (Reynolds, Larkman et al. 2006). This approach can be advantageous as both anatomical and molecular information can be acquired simultaneously. Nuclear imaging methods are highly sensitive and can provide detailed quantitative information, but have greater limits regarding spatial resolution. Enhanced glucose metabolism has been successfully imaged by 18F-fluorodeoxyglucose PET imaging (Herschman 2003; Roivainen, Parkkola et al. 2003; Beckers, Ribbens et al. 2004; Beckers, Jeukens et al. 2006). Clinically, conventional imaging techniques such as technetium scanning act as surrogate measures of local blood flow and increased

permeability. The oldest radiopharmaceutical proposed for imaging inflammation is Gallium-67 citrate and this remains an established technique for imaging pulmonary and musculoskeletal inflammation especially in sarcoidosis. (Although interestingly this particular agent appears to bind directly to transferrin which then binds to activated leucocytes) (Oyen, Boerman et al. 1996). Other examples of so called non targeted approaches include radioloabelled liposomes, dextran, nanocolloid and HIg ((Dams, Oyen et al. 2000; Adams, Al Attia et al. 2001; Arzu Gencoglu, Aras et al. 2003; Kaya, Tuna et al. 2004). Other specific molecular targeting techniques have been developed but can be affected by the non-specific localization of agents to inflamed tissues. An example includes ^{123}I-labelled IL-1ra that did not show increased localisation compared to radiolabelled albumin (Barrera, van der Laken et al. 2000). It would appear in this study that, at the doses of labelled IL-1ra used, the most substantial effect was for local changes to reflect non-specific trafficking of the molecule due to local permeability changes in areas of inflammation. The therapeutic efficacy of IL-1ra in RA requires repeated administration of the cytokine at 1000-fold the doses used in the above imaging study, so it may be that higher doses were required to generate a specific component to the imaging compared to radiolabelled albumin. However, increasing the dose of imaging agent to that level would lead to unacceptable levels of radiation. The scintographic detection of radiolabelled TNF MoAb has also been investigated. This demonstrated a specific component to 99mTc labelled anti-TNF MoAb since uptake radiolabelled signal could be abrogated by 25% when excess anti-TNF was coadministered (Barrera, Oyen et al. 2003). This suggests that 75% of the signal is non-specific accumulation of labelled tracer at sites of inflammation. Interestingly, in RA, other workers have demonstrated that 99mTc-anti-CD3 scintigraphy can be used to differentiate between autoimmune rheumatic diseases and strongly correlates with clinical findings for patients with RA (Lopes, de Azevedo et al.). The therapeutic potential of anti-CD3 MoAb has been demonstrated in collagen induced arthritis, as discussed in Section 1.4.1. E-selectin has also been demonstrated to be an excellent target for specific targeting of activated endothelium and this is discussed in the following section. Having a molecular imaging strategy and a novel therapy directed against that imaging target may be an effective away of monitoring the effect of therapy.

1.3.1 E-Selectin: An Excellent Target for Molecular Imaging in RA

Scintigraphy utilizing a ^{99m}Tc-anti-E-selectin-Fab has been used to successfully image synovitis in patients with RA, in this case demonstrating improved specificity compared to a conventional tracer for bone and joint ^{99m}Tc-oxidronate (Tc-HDP), with particular specificity for targeting active joint inflammation (Jamar, Houssiau et al. 2002). Tc-HDP displays abnormal uptake over both currently inflamed and chronically damaged joints and is very sensitive for the detection of joint and subchondral bone abnormalities (Desaulniers, Fuks et al. 1974; Helfgott, Rosenthall et al. 1982), but it cannot distinguish accurately between actively and chronically inflamed joints (Fogelman 1980). The absence of signal uptake in normal joints by E-selectin targeted imaging described above allows for markedly improved detection of active joint disease in RA as shown in Figure 1-4. The MoAb described in this study is of murine origin, which raises the possibility of host immunogenicity. However the small amounts of MoAb required for imaging and also the use of the Fab fragment devoid of Fc portions, which are thought to be responsible for immunisation may reduce the likelihood of a human anti mouse antibody (HAMA) response. In this study patients were not tested for a HAMA response, but some were imaged again with ^{99m}Tc-anti-E-selectin-Fab 2-4 months later with no detectable change in the biodistribution of labelled antibody. In a previous study of fourteen patients with RA that received ^{111}In-labeled $F(ab')_2$ fragment of E-selectin HAMA responses were measured by ELISA comparing blood samples taken pre and post (14 days) immunisation. No HAMA were detectable following injection.

The endothelial expression and serum levels of E-selectin and its downregulation have also been demonstrated in patients with RA treated with anti-TNF therapy (Paleolog, Hunt et al. 1996; Tak, Taylor et al. 1996). This clinical data highlighted the key importance of TNFα in the inflammatory cascade, and that its blockade down-regulates cytokine inducible adhesion molecules including E-selectin (as well as VCAM-1) and is associated with a reduction in synovial infiltration. Hence E-selectin may be a very effective way of monitoring specific responses to TNF blockade in RA.

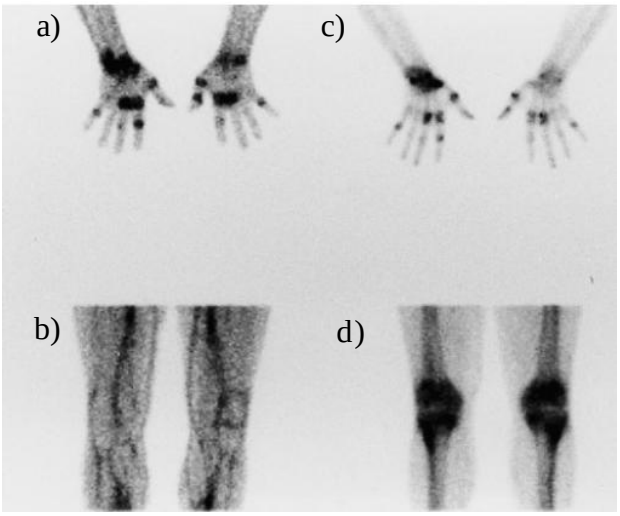

Figure 1-4 Comparison of ^{99m}Tc-1.2B6-Fab and ^{99m}Tc-HDP radiolabelled imaging in RA

Images obtained 4hrs after injection of Tc-1.2B6 Fab (a,b) and Tc-HDP (c,d) in two patients with RA. Demonstrating focal uptake in inflamed joints and less bone and subchondral uptake for the MoAb compared to conventional Tc –HDP scanning (Jamar, Houssiau et al. 2002).

1.3.2 In Vivo Fluorescence Imaging And Optical Imaging

In vivo molecular optical imaging has significant potential to delineate and measure at the macroscopic level *in vivo* biologic processes that are occurring at the cellular and molecular level (Biswal, Resnick et al. 2007). Optical imaging has already been developed for *in vitro* and *ex vivo* applications in molecular and cellular biology (e.g. fluorescence confocal microscopy), but is still at an early stage of development as a whole animal *in vivo* imaging technique, particularly in the context of arthritis. Both sensitivity and spatial resolution remain incompletely defined (Weissleder and Pittet 2008). The future however, holds considerable promise for non invasive visualisation of specific molecular targets which can be synergised with other imaging modalities such CT or MRI.

1.3.2.1 Principles of fluorescent imaging

Fluorescence is the excitation of a molecule (fluorophore) by light to a higher energy state, and its subsequent decay, resulting in emission of light at a higher wavelength. The difference between the emission and excitation wavelengths is termed the Stokes Shift, after Sir George Stokes who first described fluorescence in 1852. Some small

biological molecules (e.g. Nicotinamide adenine dinucleotide (NADH) and tryptophan) and proteins (e.g. phycoerythrin or green fluorescent protein (GFP)) are naturally fluorescent (intrinsic fluorophores), whereas extrinsic fluorophores are derived from many common dye families, such as xanthenes, cyanine and coumarin derivatives. Extrinsic fluorophores may be attached to proteins of interest by chemical modification of specific functional groups such as amino, carboxyl or thiol groups.

Fluorescence is visualised by excitation at an appropriate wavelength and capture of the emitted photons usually by a charge coupled detector (CCD). Advances in CCD design have enabled accurate detection of low levels of light. CCDs are constructed of thin silicon crystal sheets that operate by converting light photons into a tiny charge that can be measured and converted into a digital signal. Older CCD cameras had problems with noise from thermal energy turning into electrical signal (Spibey, Jackson et al. 2001). Thermal energy is dramatically reduced if the chip is adequately cooled. Early fluorescence imaging in animals was invasive, with intravital microscopy being the commonest tool. In contrast, fluorescence reflectance imaging allows non invasive *in vivo* real time images of the whole animal to be taken. However, images from a planar CCD are two dimensional and therefore lack tissue depth information. The high degree of absorption and scattering of light by biological samples limits the penetration of both the excitation and resulting emission signal (Mahmood and Weissleder 2003). Studies have suggested that fluorescent signals may be reduced by up to ten-fold per cm of depth, although this will vary with tissue type, wavelength and dye brightness (Contag, Contag et al. 1995). Accurate image acquisition may also be improved by either combining multiple images from different CCDs or by rotating a single CCD (Chen, Tung et al. 2002) in a tomographic manner allowing regions of interest to be visualised in a 3-dimensional plane. The use of tomography and early photon detection may also be a way of increasing signal specificity (Ntziachristos, Ripoll et al. 2005; Niedre, de Kleine et al. 2008).

In addition to the absorption and scattering of light (Mahmood and Weissleder 2003), biological samples autofluoresce at the wavelengths used for traditional extrinsic dye families (300-500 nm). Newer dyes better suited for *in vivo* studies fluoresce at higher wavelengths, close to the infra-red range (700-900 nm) as demonstrated in Figure 1-5. Examples include members of the Cyanine series of dyes from GE Healthcare and some of the Alexa Fluor series of dyes from Invitrogen. The intrinsically fluorescent

protein, GFP has a peak emission wavelength of 509nm and is therefore subject to significant autofluorescence from surrounding tissue if used for *in vivo* fluorescent imaging. However, several mutants of the monomeric red fluorescent protein that fluoresce at wavelengths above 600 nm have been produced (Tsien 2009). These have been used in a study by Winnard PT *et al*., where cancer cells labelled with the Tomato fluorescent protein was more readily detected compared with the same cells labelled with GFP (Winnard, Kluth et al. 2006). Advances in CCD technology and use of near infrared fluophores (NIRFs) will therefore allow for better image resolution. This has the potential to provide non-invasive imaging of molecular targets, and physiological process *in vivo*. *In vivo* fluorescence imaging also has several important advantages over other imaging techniques; there is no exposure to harmful radiation, it is relatively cheap, and images can be acquired rapidly (Massoud and Gambhir 2003). The following Table 1-2 is a summary of different molecular reporter technologies.

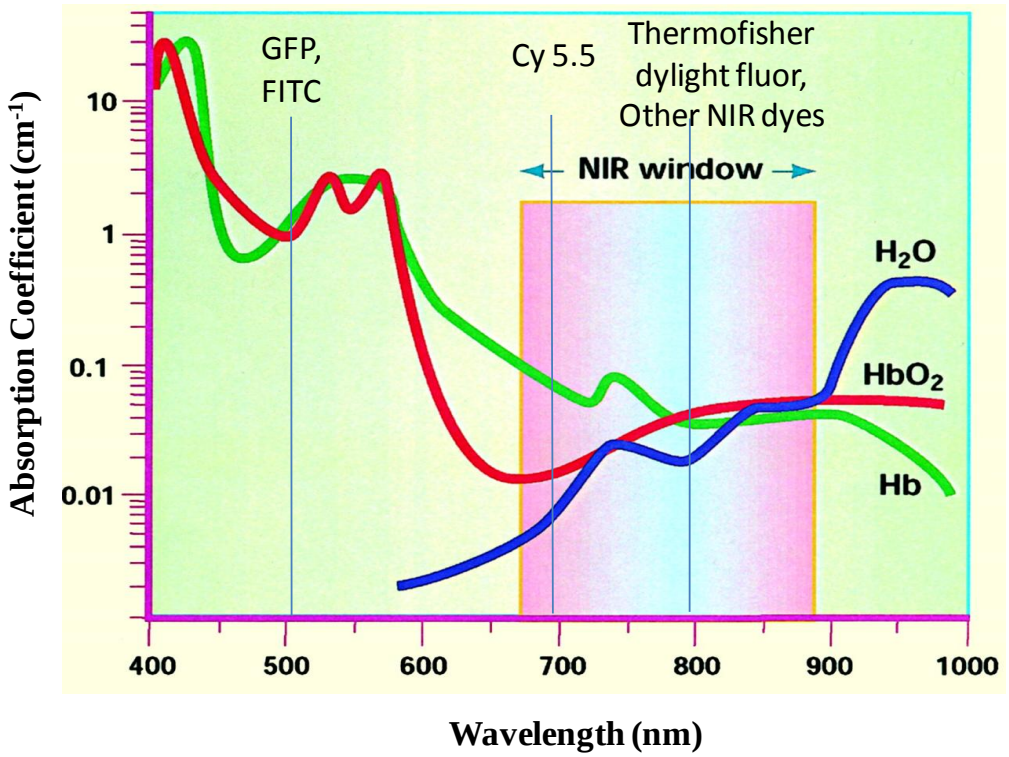

Figure 1-5 Absorption of light *versus* wavelength: tissue autofluorescence

Figure demonstrates the absorption spectra of water, deoxygenated and oxygenated haemoglobin as well as the emission spectral wavelength of some commonly used fluorescent dyes adapted from (Mahmood and Weissleder 2003). (GFP –green fluorescent protein, FITC- fluorescein isothiocyanate, Cy5.5 cyanine 5.5)

Table 1-1 Summary of fluorescence molecular reporter technologies

Technique	Description	Advantages	Disadvantages
Molecular Techniques	Non-specific dye tracking	Significant signal increase at sites of inflammation	Non-specific tracking not reflecting underlying molecular pathway
	Antibody based targets	Multitude of potential antibody targets	No signal amplification Non-specific antibody tracking
	Activatable probes	Continuous signal amplification Reduced or no fluorescence if not cleaved	Possible probe activation in non target areas, less spatial resolution
	Quantum dots (inorganic nanoparticle based probes	Photostable, intense luminosity, narrow emission/excitation wavelengths reduces background light scattering	Larger than traditional fluorophores Potential for long term toxicity
Transgenic Fluorescent protein expression	Fluorescence reporter proteins e.g. GFP	Direct visualisation of gene expression	Limited/no likelihood of use in humans Lower wavelength proteins most frequently used therefore increased tissue autofluorescence although higher wavelengths becoming available
	Bioluminescence	Ability to report on gene expression for lifetime of animal	Highly sensitive imaging equipment and long exposure times required for signal quantification

1.3.2.2 Potential molecular approaches for in vivo fluorescence imaging

Optical imaging of small animal cancer models has been the focus of a significant proportion of optical imaging investigations (Adams, Ke et al. 2007; Kovar, Simpson et al. 2007). A wide variety of targeted optical probes have been described in the literature. Targets have included cell surface receptors, metabolic pathways, hormone receptors, apoptotic markers and enzymatic activities (Kelloff, Krohn et al. 2005). The following section highlights some instructive examples of how imaging in this field has evolved and how these are likely to inform the use of fluorescent imaging in other diseases, including RA and OA. A summary of potential targets for optical imaging is included in Table 1-2

1.3.2.2.1 Targeted approaches for dye deposition

Antibodies directed against cell surface molecules which are over-expressed in cancer cells can be tagged by fluorophores. This targets the fluorescence to the diseased tissue. For example, specific antibody targeted resolution of tumours raised in a mouse model was achieved using Cy5.5 labelled tumour targeting antibodies (Ballou, Fisher et al. 1995). In a similar way tumour growth and neoplastic progression have been quantified using a label attached to epidermal growth factor (Kovar, Johnson et al. 2006). Other antibodies that have been used to target fluorescent signals include those against growth factor receptors (Koyama, Hama et al. 2007; Rosenthal, Kulbersh et al. 2007; Sampath, Kwon et al. 2007; Xu, Baidoo et al. 2007; Gleysteen, Newman et al. 2008; Withrow, Newman et al. 2008), cancer embryonic antigen (Fidarova, El-Emir et al. 2008; Gleysteen, Newman et al. 2008; Kaushal, McElroy et al. 2008; Lisy, Goermar et al. 2008; Newman, Gleysteen et al. 2008; McElroy, Hayashi et al. 2009) and cell surface receptors (Newman, Gleysteen et al. 2008; McElroy, Hayashi et al. 2009; Zou, Xu et al. 2009).

To minimise background signal, viable cancer cells have been imaged *in vivo* by a combinatorial approach of tagging antibodies with pH-activatable probes. These probes are activated after cellular internalisation by sensing the pH change in the lysosome (pH 5-6, compared to 7.4 of the cytoplasm). This was used in conjuction with the MoAb trastuzumab, which targets the human epidermal growth factor receptor type 2. Upon internalisation via the endosomal-lysosomal degradation

pathway, the probe is activated in the acidic environment yielding increased tumour specific/background signal (Urano, Asanuma et al. 2009).

1.3.2.2.2 Protease activity probes

The detection of proteolytic enzyme activity by compounds that have come to be called activity based probes (ABPs) has become an expanding avenue of tumour detection, particularly of those that are metastasizing. Activity based probes consist of dye and a quencher attached to opposite ends of a peptide linker. When the peptide sequence is cleaved by the targeted protease the fluorophore is separated from its quencher thereby increasing the fluorescent signal. This also allows the possibility of signal amplification when the probe is continuously cleaved as shown in

Figure 1-6. These compounds broadly target two families of protease activity. These are cathepsin activity (Joyce, Baruch et al. 2004; Figueiredo, Alencar et al. 2006; Blum, von Degenfeld et al. 2007; Melancon, Wang et al. 2007; Gounaris, Tung et al. 2008; Blum, Weimer et al. 2009; Sheth, Upadhyay et al. 2009) and the matrix metalloproteinase activity (Scherer, VanSaun et al. 2008). Apart from cancer, these ABPs have also been used to look at proteolytic activity in myocardial infarction (Chen, Tung et al. 2005) and atherosclerosis (Chen, Tung et al. 2002; Deguchi, Aikawa et al. 2006).

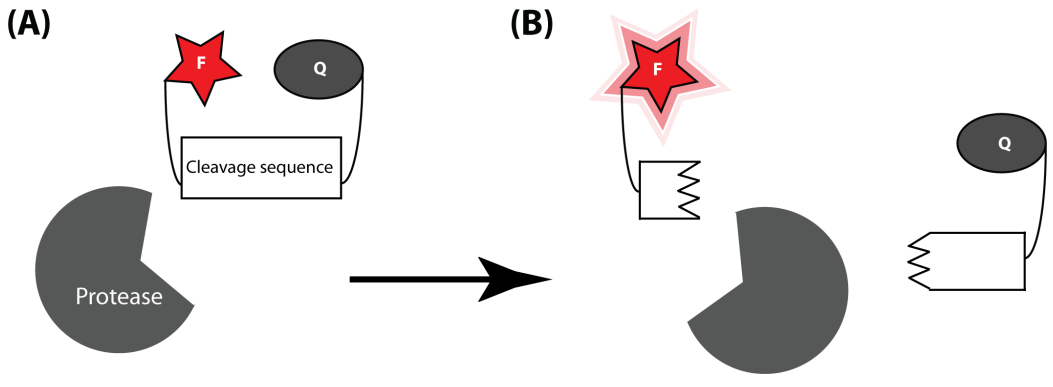

Figure 1-6 Principle of activity based probe showing quenched unquenched state

Activity based probe in quenched (A) and unquenched (B) state. Following cleavage of the target peptide sequence, fluorescence is increased. Fluorescence may be targeted to the protease using chemistry directed against the active site. F-fluorophore, Q-quencher.

One problem of this technique is that following protease activity diffusion of the cleaved ABP from the protease will occur. A method to keep the signal in close vicinity is to utilise polycationic (negatively charged) sequences that are taken up by cells. These have been termed cell penetrating peptides. In the absence of proteases their association with the cell surface is prevented by a polyanionic (positively charged) sequence that binds to the cationic sequence. The polyanionic sequence also contains a quencher which prevents fluorescence. The two sequences are linked by a peptide with a specific protease cleavage site. Upon cleavage by tissue proteases, the two strands separate, causing release of the fluorescent probe (now unquenched) and uptake by the cell (Jiang, Olson et al. 2004).

1.3.2.2.3 Bioluminescence

Bioluminescence is the conversion of chemical energy to light in living organisms. The luciferase enzymatic system is the most commonly found biological process to achieve this conversion. The enzymes in this pathway convert the luciferin substrate in the presence of several co-factors and adenosine triphosphate to generate oxyluciferin and light (Wilson and Hastings 1998). Bioluminescence has been most widely used in reporter gene assays, where the promoters of genes under study have been linked to the luciferase gene, and the resultant light is a direct measure of promoter activity.

The luciferase enzyme needs to be transfected into cells, limiting its use to animal models or transgenic animals. Its expression however, can be tightly controlled when linked to the appropriate promoter. The most commonly used luciferase enzyme system used comes from the firefly. The emission maximum of the firefly system is at 578 nm at 25^{o}C *in vitro*, but shifts to 612 nm at 37^{o}C (Zhao, Doyle et al. 2005), which may be troublesome for use *in vivo* due to the high levels of tissue absorption. Mutation of another luciferase from *Luciola cruciata* has allowed a shift in the emission maximum from 560nm to 613 nm and 605 nm, allowing a greater diversity of colours (Nakatsu, Ichiyama et al. 2006). This raises the possibility of obtaining further mutants that operate in the NIR spectrum. The luciferin substrate also needs to be delivered to where the enzyme is expressed, which may restrict the visualisation of certain organs. Use of different substrates with different pharmacokinetic profiles will also yield different dynamics of light production (Bhaumik and Gambhir 2002).

1.3.3 Fluorescent Imaging in Arthritis

Rheumatoid synovium is characterized by hyperplasia of the synovial lining layer and marked infiltration by lymphocytes, macrophages and plasma cells. Locally produced inflammatory mediators and the subsequent up-regulation of adhesion molecules at sites of inflammation are pivotal to RA pathogenesis (Tak, Taylor et al. 1996). Sensitive and specific methods of imaging are required for the detection of early inflammatory changes to the synovium in patients with arthritis and for monitoring response to treatment. *In vivo* imaging in the animal model is of vital importance in developing these techniques. Novel therapies can be better evaluated using sensitive, reproducible imaging of disease activity that reflects underlying molecular changes.

1.3.3.1.1 Invasive *In Vivo* Optical Imaging

Intravital fluorescence microscopy in inflammatory arthritis was first performed in 1993. This technique allows measurement of microhaemodynamic parameters as well as leukocyte EC interactions (Menger and Lehr 1993). Blood vessel diameter (Veihelmann, Szczesny et al. 1998; Veihelmann, Harris et al. 1999) and capillary density (Schmitt-Sody, Landes et al. 2003) were measured in the synovial microcirculation of the mouse knee joint following surgical exposure of the area of interest. The inhibitory effect of recombinant anti-leukoproteinase, a physiological inhibitor of granulocyte serine proteases on blocking the interactions of leukocytes on the endothelial lining was investigated by microscopic imaging of leukocyte rolling and adhesion *in vivo* (Sehnert, Gierer et al. 2006). A limitation of this technique is the need to expose surgically the area for direct microscopy.

1.3.3.1.2 Non- targeted imaging in animal models of arthritis

Disordered new vessels have increased vascular leakiness to macromolecules compared to normal vessels (Levick 1981) This is discussed in Section 1.2.4. Due to these local permeability changes non-specific dye deposition was used to visualise the arthritic joint *in vivo*. Enhanced localised deposition of free dye (not bound to a disease specific antibody or other target) in the arthritic joints of animals with induced arthritis has been examined in several studies. The NIR fluorophore Cy5.5 was visualised in arthritic knee joints following induction of antigen induced arthritis in mice (Hansch, Frey et al. 2004). This demonstrated an approximate 1.5 fold increase in signal in arthritic compared to non arthritic joints. Two other NIR dyes were

evaluated in a murine *Borrelia*-induced Lyme arthritis model (Fischer, Gemeinhardt et al. 2006). These techniques rely on the generalised increased blood perfusion and 'vascular leakiness' that are recognised to be present around the inflamed joint (Andersson, Johansson et al. 1998). This may lead to as much as a forty fold increase in macroglobulin permeability in the inflamed joint (Levick 1981). In such cases native dye most likely accumulates in the inflamed synovial membrane following phagocytosis by activated macrophages. Another study has demonstrated increased levels of fluorescence in inflamed paws with a fluorescently labelled PEGylated anti-TNFα agent compared to a non-PEGylated TNFα inhibitor (Palframan, Airey et al. 2009). There is also a recognised non-specific autofluorescence change in the absorption emission spectra of inflamed tissue (Hansch, Sauner et al. 2003), although this phenomenon is likely to be more limited at wavelengths in the NIR spectrum.

1.3.3.1.3 Targeting of specific molecular changes in arthritis

In vivo targeting of specific molecules that have been identified as being key components in the inflammatory cascade may help to increase specificity in assessing disease activity levels and differentiating subsets of arthritis.

Specific deposition of dye in the arthritic joint of antigen-induced arthritic mice has been achieved by targeting macrophages with Cy5.5 labelled anti-F4/80 antigen. The F4/80 antigen is expressed on the macrophages when they accumulate in inflamed joints (Hansch, Frey et al. 2004). There was however, a small increase in signal in the uninflamed contralateral knee joints as well as increased uptake in inflamed knee joints with the Cy5.5 labelled isotype control antibody. A similar study targeting folate receptors on activated macrophages, demonstrated a 2.3-fold increase in signal in inflamed compared to uninflamed joints (Chen, Mahmood et al. 2005). This increase was greater than that obtained following injection of free dye. Arthritis has also been detected with allogeneic leukocytes that were labelled *ex vivo* with fluorescent dye and re injected into arthritic mice (Simon, Daldrup-Link et al. 2006). Treatment with steroid reduced the signal intensity obtained. However, the degree of quantitative analysis was hampered by a relatively small change in signal intensity compared to the background signal.

1.3.3.2 Activity-Based Probes in Arthritis

Amplification of fluorescent signal at the site of inflammation using protease activatable probes may hold significant promise for *in vivo* imaging of arthritis, especially of OA, as local perturbations in proteolytic activity may be comparatively small. Cathepsins have been associated with arthritis and bone degeneration (Lang, Horler et al. 2000). A cathepsin B activatable NIR fluorescent probe was used in a mouse model of osteoarthritis and showed a 3-fold difference in signal intensity between normal and osteoarthritic joints (Bhaumik and Gambhir 2002; Lai, Chang et al. 2004). This particular probe has also been applied to tumour detection (Weissleder, Tung et al. 1999) as well as the localisation of atherosclerotic plaques *in vivo* (Chen, Tung et al. 2002). A similar probe was used to demonstrate that Methotrexate could abrogate some of the increased signal found in arthritic joints (Wunder, Tung et al. 2004). A further study also demonstrated that specific signal could be reduced and correlated with a decrease in clinical disease indices such as redness and measurable paw swelling (Izmailova, Paz et al. 2007). However, these studies did not examine whether an uncleavable form of peptide demonstrated similar signal or whether any specific inhibitor of the protease could prevent cleavage in the arthritic joint.

Table 1-2 Comparison of optical imaging techniques

Technique	Description	Resolution	Depth	Time	Advantages	Disadvantages
Intravital microscopy	Imaging technique based on fluorescence microscopy adapted for *in vivo* use	1µm	<400-800µm	Minutes to hours	Quantification of individual cellular changes	Invasive microscopic technique
Fluorescence Reflectance Imaging (FRI)	Non invasive whole body imaging, obtaining two-dimensional planar images	2-3mm	<1cm	Seconds to minutes	Comparatively low cost, images rapidly acquired. May have significant use for detecting peripheral arthritis	Signal quantification challenging Limited depth resolution
Fluorescence Molecular Tomography (FMT)	Non invasive imaging, obtaining three-dimensional mapping of fluorescent signal	1mm	<10cm	Minutes to hours	3 dimensional imaging, able to limit effects of light scattering by analysing images from multiple angles	Longer acquisition times for whole body imaging. Single animal able to be imaged at a time
Bioluminescence imaging	Non invasive imaging, signal detected as a result of luciferase expression	2-3mm	<10cm	Minutes	Ability to report on gene expression for lifetime of animal	Genetic modification of host required Limited quantification of signal

1.4 Animal Models of RA and Inflammation

1.4.1 Collagen Induced Arthritis: A Well Validated Pre Clinical Model of RA

Animal models of arthritis are of paramount importance as experimental tools for many aspects of research including the evaluation of novel therapies, searching for markers of disease progression and evaluating novel imaging techniques, such as those described in preceding sections. RA and other inflammatory joint disorders remain an important target for drug development and animal models of arthritis have been widely used in testing novel therapies. CIA is an animal model of RA, in which disease is induced in genetically susceptible mice with type II bovine collagen. This technique was first described in rats in 1977 (Trentham, Townes et al. 1977), and subsequently established in mice (Courtenay, Dallman et al. 1980). Type II collagen is a major constituent protein of cartilage in the diarthrodial joints, the predominant site of inflammation in RA (Myers, Rosloniec et al. 1997). Intradermal immunisation of genetic susceptible mouse strains, mainly DBA/1 or B10RIII mice, with bovine type II collagen (CII) emulsified in CFA triggers an autoimmune response to mouse CII that leads to inflammatory arthritis. Susceptibility to collagen-induced arthritis is associated with MHC class II genes, although non-MHC genes also play a role. Both B- and T-lymphocytes are important in the pathogenesis of collagen-induced arthritis. Histologically, hallmarks of both CIA and RA are infiltration of the subsynovial tissue by inflammatory cells, synovial hyperplasia, angiogenesis as well as erosion of cartilage and bone by a pannus-like tissue (Trentham, Townes et al. 1977; Wooley, Luthera et al. 1981; Lee and Weinblatt 2001). Heterologous (e.g. bovine or chicken) CII is used for the immunisation. Arthritis tends to follow an acute, self-limiting disease course. The arthritis starts approximately three to four weeks after immunisation, usually in a limited number of joints and gradually spreads to multiple joints (Holmdahl, Bockermann et al. 2002). In mice, immunisation with bovine, chicken, or rat type II collagen usually leads to a relatively acute form of arthritis. By contrast, immunisation with murine collagen results in a more chronic disease. This difference may be due to the extent to which the immune response is targeted at self collagen, as opposed to the collagen used for immunisation (Holmdahl, Jansson et al 1986; Holmdahl, Andersson et al 1989). CIA been widely used to study mechanisms involved in the arthritic process and to identify potential new therapies for RA. Pro-inflammatory cytokines, such as TNFα and IL-1β are expressed in the arthritic joints

of both murine CIA and RA. A number of studies initially focussed on the effects of TNFα blockade during the induction phase of CIA (Piguet, Grau et al. 1992; Thorbecke, Shah et al. 1992) subsequently the effect of anti-TNFα treatment in mice with established CIA was demonstrated. This showed that in mice treated with intraperitoneal injection of anti-TNFα MoAb there was a dose dependent reduction in the severity of arthritis and that joints were protected from erosive changes (Williams, Feldmann et al. 1992). While CIA is well validated it does have some unique components to disease pathogenesis and has classically been a strain dependent model of arthritis, with H-2^q and H-2^r stains in DBA/1 mice showing the greatest degree of susceptibility. One issue, for example is that the T-cell proliferative response to type II collagen in immunised DBA/1 mice peaks a significant amount of time before the onset of arthritis and is in decline by the time of disease onset and that the disease course is generally relatively acute, peaking at 4 to 5 weeks following immunisation and then gradually resolving. For this reason a protocol for the induction of arthritis in C57BL/6 mice utilising chicken type II collagen has been developed (Inglis, Simelyte et al. 2008). The development of arthritis in this model is associated with a very strong T-cell response to collagen that remains elevated for up to 3 months post immunisation (Inglis, Criado et al. 2007). Interestingly this disease also has other differences in phenotype with less swelling and a more gradual increase in clinical score, with a later (6-8 weeks after onset) more significant inflammatory cell infiltration compared to DBA/1 mice. A further limitation of the classic CIA model in DBA/1 mice is that most transgenic and knockout strains of mice are on a C57BL/6 background (H-2^b) hence the further usefulness of having a reliable method of arthritis induction in BL/6 mice.

Animal models of arthritis provide a vital ongoing test bed for developing novel molecular targets for the future treatment of inflammatory disease. For example, several possible inhibitors of angiogenesis, including soluble VEGFR1, have been shown to reduce disease severity in CIA (Miotla, Maciewicz et al 2000; Afuwape, Feldmann et al 2003; Sumariwalla, Cao et al 2003). More recently it has been demonstrated that anti-CD3 therapy is highly effective for the treatment of CIA with the capacity to generate antiarthritic CD8+ Treg cells and expand the relative numbers of CD4+ Treg cells (Notley, McCann et al.). These examples demonstrate the requirement for both an effective animal model of RA and the need for targeted

molecular therapy that can be monitored *in vivo* and in the future translated from the animal model into human studies.

1.4.2 Acute Models of Inflammation

In addition to models of arthritis such as CIA, a number of different models that induce acute paw oedema in mice or rats have been developed. Initial studies focused on examining the nocioceptive and inflammatory alterations in rodents and subsequently on evaluating the efficacy and mechanism of action of compounds such as anti-inflammatory drugs. Rat paw oedema was first characterised using carageenin induced inflammation. Carageenan derived from red algae produces a local inflammation following local injection (Winter, Risley et al. 1962; Di Rosa 1971; Di Rosa 1971; Di Rosa, Papadimitriou et al. 1971). It was demonstrated that carrageenan intraplantar injection in rats produces a monophasic oedematous response in the rat paw that is accompanied by inflammatory cell migration, marked nocioceptive alterations and increased NO levels (Salvemini, Wang et al. 1996). In this study rat paw oedema was found to be maximal by six hours and remained elevated by 10 hours and could be abrogated by constitutive and inducible nitric oxide synthetase inhibitors with concomitant decreases in neutrophil infiltration. This group have examined in more detail the participation of TNFα in the inflammatory and nocioceptive responses evoked by carrageenan injected into the mouse paw. The intraplantar injection of carrageenan (300μg) confirmed a marked and biphasic paw oedema with peaks at 6 hours and 72 hours with significant increases in myeloperoxidase activity that peaked at 6 hours in C57/BL6 mice. All of this activity was significantly abrogated in TNFα p55 receptor knockout mice. The systemic administration of anti-TNFα antibody produced similar decreases in paw oedema, allodynia and myeloperoxidase (MPO) activity. Interestingly the inflammatory responses of carreegenan were also abrogated when mice were previously treated with the preferential inhibitor of TNFα synthesis thalidomide. Another study has examined the role of neutrophil migration in carreegenan induced paw oedema determined by MPO staining by examining the effect of fucoidin an inhibitor of neutrophil rolling that binds L-selectin (Cunha, Verri et al. 2008). Another technique has been to inject zymosan into the mouse paw (Keystone, Schorlemmer et al. 1977; Gado and Gigler 1991). Zymosan is a component of the bacterial cell wall that induces an intense inflammatory response (Lundberg and Arfors 1983). This model has again been used

to test the short term efficacy of anti inflammatory compounds. Gado and Gigler injected 0.1ml of a 2% suspension of zymosan into the rat paw. This caused a 90% increase in paw volume, with a biphasic time course. The paw swelling reached a maximum 45 minutes after injection with a second peak of swelling after 6 hours. Zymosan has also been used as an acute model of arthritis to examine the effects of Tenascin C, an endogenous activator of Toll like receptor 4, that has been found to be essential for maintaining inflammation in arthritic disease (Midwood, Sacre et al. 2009). In this model rapid paw swelling was reached after 24 hours, maintained for 24 hours, with swelling still seen at 4 days with histological evidence of arthritis demonstrating cellular infiltration and cartilage loss. Injection of TNFα into the hind paw of the rat has also been utilised to demonstrate the role of TNFα in the development of acute inflammatory hyperalgesia (Cunha, Poole et al. 1992). This study used doses of TNFα between 0.0025 and 2.5pg in 100µl of vehicle. Paw swelling was not measured in this study. A subsequent study by Woolf and colleagues again in rats examined the role of TNFα in contributing to inflammatory sensory hypersensitivity by inducing IL-1β and nerve growth factor (NGF)(Woolf, Allchorne et al. 1997). This study by comparison, used much higher doses of TNFα (50-500ng). This demonstrated that IL-1 and NGF were TNFα dependent at early (6 hours) but not late (24 hours) time points, but again paw swelling was not measured in this study. A further study by Campos and colleagues examined the relationship between pretreatment with TNFα and injection of bradykinin (Campos, Souza et al. 1998). This study used a dose of 5ng per paw of TNFα as a pretreatment which in itself did not cause significant increases in paw volume. Subsequent injection of bradykinin did cause significant increases in paw swelling suggesting that the prior injection of cytokines IL-1β or TNFα into the rat paw resulted in a rapid onset and significant upregulation of B_1 receptors, characterised by marked and dose dependent oedema formation in response to further injection of bradykinin. Colleagues at The Kennedy Institute of Rheumatology have demonstrated that TNFα induces hyperalgesia and neutrophil migration as measured by the myeloperxidase assay following injection of 20ng of TNFα in 10µl of vehicle in the paws of C57Bl/6 mice. While the injection of higher doses of TNFα was noted to cause swelling the complete dose dependence of TNFα on paw swelling had not been fully delineated. They have however shown that IL-17 induced hyperalgesia was dependent on neutrophil migration and that TNFα

induced paw swelling could be abrogated in p55 TNF receptor knockout animals. These effects could also be blocked by the prior administration of fucoidin (unpublished observations).

1.5 Hypothesis and Objectives

The targeting of E-selectin on activated vascular endothelium has previously been well validated in both animal and human studies. My hypothesis was that fluorescent imaging utilising E-selectin as a target holds significant potential as a non invasive, *in vivo* molecular imaging technique in murine arthritis.

My objectives were to:

1. To establish proof-of-principle imaging of joints of mice with inflammatory arthritis using fluorescently labelled anti-E-selectin *in vivo*
2. To apply fluorescence imaging to investigate the *in vivo* mode of action of vascular-targeted therapies in murine inflammatory arthritis. In particular to determine the treatment response and changes in E-selectin targeted fluorescent imaging following administration of a novel EGF receptor antagonist (RB200) in CIA.

CHAPTER 2

2 MATERIALS AND METHODS

2.1 Chemical Components

If not otherwise specified, chemicals were obtained from VWR International Ltd (Lutterworth, UK), Sigma Aldrich (Dorset, UK) or Merck Chemicals Ltd (Nottingham, UK) in analytical grade quality.

2.2 Cell Lines

Hybridoma cell lines expressing rat anti-mouse E-selectin IgG2a MoAb (MES-1) and rat IgG2a isotype control antibody against dinitrophenol (DNP) were kind gifts from Dr Derek Brown (UCB, Slough, UK) and Professor David Gray (University of Edinburgh). The method used for cell culture is described in Section 2.4.1.

2.3 Fluorescence Reflectance Imaging Device

Optical imaging experiments were performed using a fluorescence reflectance imaging (FRI) device (Kodak *In-vivo* Multispectral System FX Pro). This utilizes a 175W Xenon illumination source coupled to an automated multi-wavelength series of excitation filters with a range of 390-770nm and emission filters between 480-830nm. This allows a wide range of fluorescent dyes of varying wavelengths to be tested. Fluorescence emission is captured using a monochrome interlined cooled CCD with a pixel density of 2048x2048 pixels (Figure 2-1). Image acquisition and analysis has been performed using proprietary Kodak software (version 5.0).

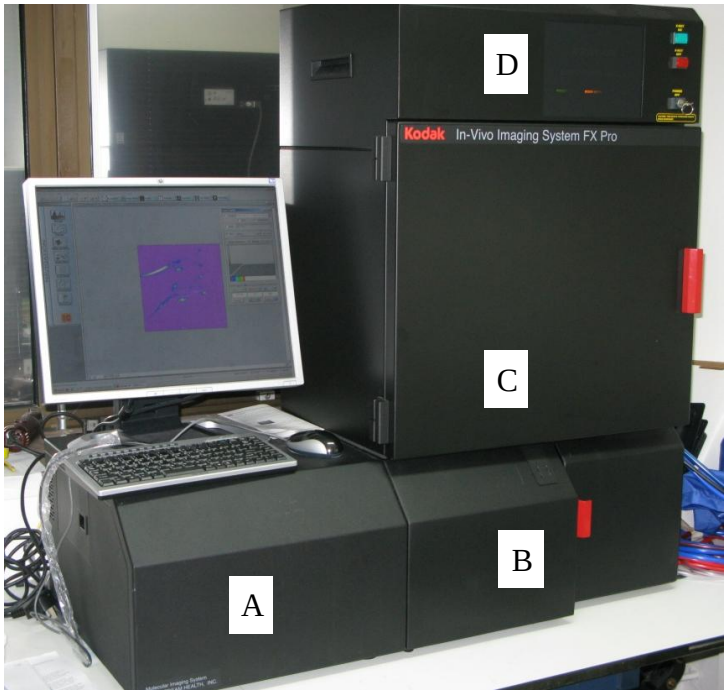

Figure 2-1 Fluorescence Reflectance Imaging: Kodak *In Vivo* Imaging System FX Pro

The above photograph describes the experimental set up described in the text. A) Light source and excitation filters. B) Emission filters and CCD C) Animal chamber and anaesthetic apparatus D) X-ray device.

2.4 Production of Anti-E-Selectin and Anti-DNP Isotype Control Antibodies

2.4.1 Cell Culture for Anti-E-Selectin and Anti-DNP Antibodies

Cell lines were cultured in RPMI media (Sigma Aldrich, St Louis, USA) containing heat-inactivated 10% foetal calf serum (FCS) (Invitrogen, Renfrew, UK), 100U/ml penicillin, 50μg/ml streptomycin and 4.5g/l L-glutamine (Sigma-Aldrich, Poole, UK). The hybridoma was divided and culture media added. The colony was expanded to as many 175cm^2 flasks as were required. Cells were grown to confluency and divided into equal volumes of media every 1-2 days. After appropriate growth, the cells were left in an incubator without feeding and allowed to die off (cells shrivelled and media yellow). I aimed for 25-50% viability before aiming to spin down. Cell death was assessed by counting the proportion of live and dead cells following application of Trypan Blue stain (0.1ml of 0.4%). By maintaining uniform cell viability this ensured similar batches of antibody yield from sequential cultures as demonstrated in Figure

2-2. This demonstrates the mean cell viability and total protein yields for 3 sequential cell cultures demonstrating consistent protein yield. The cells and supernatant were then collected and spun at 4,000rpm for 15 minutes to get rid of cell debris.

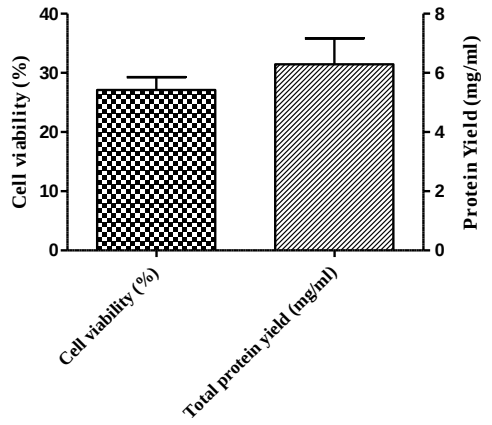

Figure 2-2 Cell viability and yield of anti-DNP antibody

Graph demonstrating the mean cell viability prior to antibody harvest and mean total protein yield of DNP antibody following purification from the cultured hybridoma cell line after 3 sequential cultures. Similar results were obtained for E-selectin antibody.

2.4.2 Affinity Purification of Cultured Antibodies

Affinity purification utilises specific non-covalent binding interactions between ligand and target molecules. The target molecules to be purified are added to a solid support allowing them to bind by their specific affinity to the immobilized ligand molecules. The non-bound components are then washed away and the captured target molecules eluted from the ligand molecules using buffer conditions that disrupt the affinity interaction.

The collected supernatant from hybdridoma cultures was initially pre-cleared on sepharose beads to remove non-specifically sticky proteins. 5 mls of 80% sepharose 4B was placed into a glass chromatography column and equilibrated with phosphate buffered saline (PBS). The supernatant was then applied to the column using a peristaltic pump at a flow rate of 1 to 5mls/min. The sepharose 4B beads were then discarded. The pre-cleared supernatant was then applied to a protein G column (3 mls of 80% slurry placed in column and equilibrated with 10x gel bead volume of PBS). The pre-cleared supernatant was then applied at a flow rate of 1.5mls/min. The column was then washed with 5x gel bed volume (12 mls) of PBS to remove any unbound proteins from the column. The last 1 ml wash fraction was analysed by

measuring the absorbance at 280nm (A280) to ensure all non-bound proteins were removed, with the spectrophotometer set at zero using the same PBS used to wash the column. If the A280 was >0.05 then the wash step was repeated until the A280 was <0.05.

Antibodies were then eluted with 5x gel bed volume (i.e. 12 mls) of Glycine-HCl pH 2 in a tube containing 200µl of 1M tris(hydroxymethyl)aminomethane (Tris) pH 8.8 per ml of eluent. This acts to neutralize the antibodies preventing degradation/inactivation at high pH. The last 1 ml of eluent was analysed at A280 to ensure all bound antibodies have been eluted (spec: zero with mixture made up of 1 ml Glycine-HCl pH 2 added to 200µl 1M Tris pH 8.8 mixture, aim A280 <0.05). The elution was repeated with one further gel bed volume of Glycine-HCl pH 2 until all bound antibodies were eluted. All antibodies were pooled together and the yield determined at A280 (spec: zero with mixture made up of 2 x 2.4 mls PBS added to 3x 2.4 mls Glycine-HCl pH 2 and 2.4 mls 1M Tris pH 8.8). A VivaSpin® (Sartorius, Aubagne, France) device with molecular weight cut-off 50,000 or 100,000, buffer exchanged with PBS was utilized to concentrate the purified antibodies. The protein G column was washed with 10x gel bed volume (24 mls) of Glycine-HCl pH 2.

2.4.3 Measurement of Antibody Concentration Following Production and Purification to Ensure Accurate Quantification for Labelling and Imaging

The concentration of purified antibody was calculated by measuring absorbance at 280nm at the end of the purification process. More accurate protein concentration measurements were also made using the Pierce BCA protein assay kit (Thermofisher, Loughborough, UK). This method utilises the reduction of Cu^{2+} to Cu^{1+} by protein in an alkaline medium. The subsequent detection of Cu^{1+} can then be made by using a colourmetric reagent, bicinchoninic acid (BCA), the resultant complex showing strong absorbance at 562nm. This was utilised to accurately determine the amount of protein required for each individual labelling reaction; ensuring optimum conditions for labelling and for optimising the dye/protein ratio and standardising protein concentrations between target and control antibodies, in turn ensuring that comparable amounts are used when injecting under *in vivo* conditions. 25µl of standard or unknown sample was loaded onto duplicate wells of a 96 well polystyrene plate. 200µl of the working reagent, comprising of a 50:1 mixture of BCA reagent A:B were

added to the individual wells and the plate covered and incubated at 37ºC for 30 minutes. Absorbance measurement was performed at 540nm using a plate reader and the protein concentrations within test samples were calculated by Ascent software (Version 2.6, Thermo Labsystems) using the 9 point standard curve as a reference.

2.4.4 Determination of Antibody Purity by SDS PAGE Prior to Labelling

The purity of anti-E-selectin and anti-DNP antibodies obtained from cell culture was determined using sodium dodecyl sulfate polyacrylamide gel electrophoresis (SDS PAGE; NuPAGE Novex Bis-Tris Mini Gel, Invitrogen, Paisley, UK). This is a technique used to separate proteins according to their electrophoretic mobility. The preparation of samples, running buffer, gel loading and running conditions were performed according the manufacturer's protocol. 10µl of the sample (either DNP or E-selectin antibody at a concentration of 50µg/ml) was combined with 2.5µl of loading buffer and 2µl of reducing agent (either NUPAGE sample reducing agent, Invitrogen, Paisley, UK or Beta-Mercaptoethanol (2µl of 10mM solution)) and made up to a total volume of 20µl with deionised water. Samples were then heated at 70ºC for 10 minutes. Samples were loaded onto the gel and the gel chambers loaded with running buffer. Electrophoresis was run at a constant 150V for 1 hour. A protein standard molecular weight marker was used to determine the molecular weight of component parts. 0.2% Coomasie brilliant blue stain was applied for 60 minutes. The gel was destained, by placing in 100 mls 30% methanol. This was replaced with fresh destain solution every half an hour for 1-2 hours. Mass spectrophotometry was performed following excision of gel fragments (Waters Micromass Xevo QTof, Milford, Massachusetts, USA) (courtesy of Dr Robin Wait, Kennedy Institute of Rheumatology).

2.4.5 Fluorescent Labelling of Anti E-Selectin and Control Antibodies

Fluorescent labelling is the process of attaching a fluorophore to another molecule such as a protein or nucleic acid. Generally, this is accomplished by using a reactive derivative of the fluorophore that can selectively bind to a functional group on the target molecule. Common reactive groups include amine reactive isothiocyanate derivatives such as FITC and TRITC (derivatives of fluorescein and rhodamine) amine reactive succinimidyl esters such as NHS-fluorescein, and sulfhydryl reactive maleimide activated fluors such as fluorescein-5-maleimide. Reaction of any of these

reactive dyes with another molecule results in a stable covalent bond formed between a fluorophore and a labelled molecule.

Following a fluorescent labelling reaction, it is necessary to remove any non reacted fluorophore from the labelled target molecule. This can be accomplished by size exclusion chromatography, taking advantage of the size difference between fluorophore and labelled protein, nucleic acid, etc. Fluorophores may interact with the separation matrix and reduce the efficiency of separation. For this reason, specialized dye removal columns that account for the hydrophobic properties of fluorescent dyes are sometimes used. Reactive fluorescent dyes are available from many sources. They can be obtained with different reactive groups for attachment to various functional groups within the target molecule. They are also available in labelling kits that contain all the components to carry out a labelling reaction. Various proprietary fluorescein derivatives have been developed to increase signal intensity, photostability or with different attachment groups to bind a variety of different molecules. The most common reactive group present for antibody labelling is an active NHS ester reactive group that will couple to primary amines forming stable conjugates. Three different proprietary NIR dye antibody labelling kits were assessed when performing preliminary *in vivo* imaging experiments. The Thermofisher DyLight 750nm dye labelling kit was selected for further *in vivo* imaging experiments because it had an efficient and reproducible conjugation reaction, confirmed effective removal of free dye and was relatively inexpensive.

2.4.5.1 Techniques of fluorescent labelling

Anti-E-selectin and anti-DNP antibodies were prepared for conjugation according to manufacturer's instructions. The protocol used for fluorescent labelling of antibody for *in vivo* experiments is also included in more detail in Appendix 2.2. 1mg of protein (either anti-E-selectin or anti-DNP antibody) was used for labelling at a concentration of 2 mg/ml. The correct concentration of protein was achieved by adding labelling buffer. This was made by diluting Borate Buffer (0.67M) to 0.05M in PBS: 75 µl of Borate Buffer (0.67M) was added to 925 µl of PBS. 0.5 mls of the prepared protein was added to the vial of DyLight Fluorophore reagent and vortexed gently. The reaction mixture was then incubated for 60 minutes at room temperature protected from light. The samples were then mixed with purification resin and then centrifuged for 45 seconds at ~1,000 × g to remove the storage solution.

2.4.5.2 Measurement of the fluorescent labelling reaction

Following protein labelling and purification it is necessary to measure the fluorophore to protein ratio. This can be calculated by measuring absorbance ratios using a spectrophotometer. Quantification of protein: dye conjugation is essential for predicting the amount of probe necessary to gain adequate signal intensity in an experiment and for controlling signal intensity between experiments. While a greater number of fluorescent molecules per target molecule may increase specific signal intensity, over labelling can cause quenching as a result of fluorescent emissions from one dye molecule being absorbed by neighbouring dye molecules. Over labelling may also cause loss of biological activity of a molecule or decreased solubility. By contrast under labelling will lead to a weakened fluorescent signal and a weakened fluorescent probe.

2.4.5.2.1 Quantification of fluorophore labelling

The principles of absorbance are outlined below:

The ratio of the radiant power (P) transmitted to the radiant power incident (Po) on the sample is called the transmittance, T:

Absorbance (A) is defined as the log of the reciprocal of transmittance:

$A = -\log T = \log (1/T)$

In a spectrophotometer the transmittance and absorbance of a sample depends on the molar concentration (c), light path length in centimetres (L) and molar absorptivity (ε) for the dissolved substance at the specified wavelength (λ) (Dean 1992).

$A \lambda = \varepsilon c L$

Beer's Law states that molar absorbtivity is a constant (and the absorbance is proportional to the concentration) for a given substance dissolved in a given solute measured at a given concentration. Molar absorptivities are therefore called *molar absorption co-efficients* or *molar extinction co-efficients.* Transmittance and absorbance are unitless and therefore the units for molar absorptivity cancel with units of measure in concentration and light path and have units of M^{-1} cm^{-1}. Therefore, with a 1cm cuvette:

$A \lambda = \varepsilon c L = \varepsilon c$ when L=1cm

While there is no single correct molar extinction co-efficient for a complex molecules such as immunoglobulins, it is possible to calculate these for the published literature (Gill and von Hippel 1989). Differences in buffer type, pH etc can all have an effect. Most immunoglobulins have protein extinction co-efficients (ε percent) in the range of 12-15. Therefore in typical antibody solutions it has been assumed $A280^{1\%}$ = 14 or $A280^{0.1\%}$ = A280 1mg/ml = 1.4 For a typical IgG, with molecular weight 150,000, this value corresponds to a molar extinction co-efficient (ε) equal to 210,000 $M^{-1}cm^{-1}$

2.4.5.2.2 Procedure for determining the dye:protein ratio

The maximum absorbance of the fluorescent dye molecule is described to an extent by its extinction co-efficient (ε). Amax is the absorbance (A) of a dye solution measured at the wavelength maximum (λmax). Together the Amax and (ε) may be used to calculate the molar concentration of dye in a sample. Standard absorbance at 280nm (A280) is used to determine the protein concentration in a sample. However because fluorescent dyes also absorb at 280nm a correction factor must be used to adjust for the amount of A280 contributed by the dye. The correction factor (CF) equals the A280 of the dye divided by its Amax. In practice this number will be very small when dyes are used that are in the NIR range (where there will be minimal effect from the dye on the A280 value) (Gill and von Hippel 1989; Pace, Vajdos et al. 1995).

Following removal of excess dye from the sample by dialysis as described in the protocol the absorbance was measured at 280nm using a spectrophotometer (Perkin Elmer lambda Bio 20, Massachusetts, USA) with a 1cm light path.

Absorbance of the protein dye conjugate was then measured at the λmax for the dye molecule. Calculation of protein molarity and degree of labelling was measured using the following parameters:

Parameters for determining dye/protein ratio

E	protein molar extinction co-efficient (for IgG ~ 210,000 $M^{-1}cm^{-1}$)
A_{max}	Absorbance of a dye solution at the maximum wavelength λmax for the dye molecule
CF	correction factor - any absorbance at A_{280} caused by the dye
Dilution Factor	The extent to which the dye:protein sample has been diluted for absorbance measurement.
ε	molar extinction co-efficient of fluorescent dye

Critical values for Thermoscientific Pierce fluorescent dye at 750nm wavelength:

Wavelength maximum (λmax)	Extinction co-efficient (ε)	Correction Factor
753nm	220,000 $M^{-1}cm^{-1}$	0.0200

Dye/protein ratio calculation

$$Protein\ Concentration\ (M) = \frac{\mathrm{A280} - (\mathrm{AMax} \times \mathrm{CF})}{\mathrm{E\ (protein)}} \text{ X dilution}$$

$$Moles\ of\ dye\ per\ mole\ of\ protein = \frac{\mathrm{Amax\ of\ labelled\ protein}}{\varepsilon \times \mathrm{protein\ conc\ (M)}} \text{ X dilution f}$$

The sample was dialysed to ensure that no free dye following dye protein conjugation was present in the sample this is considered to be especially important because free dye can be visualised as having tracked to sites of inflammation (Hansch, Frey et al. 2004). 50µl of sample was diluted in 450µl of PBS and placed into a 10,000MW cut-off dialysis cassette (Pierce Slide-A-Lyzer 10K cut-off cat no 66380) and placed in 3l of 1x PBS for 4 hours. 3l of PBS was buffer exchanged after 4 hours and then left for 12 hours in a cold room. The sample was removed from the cassette and absorbance was remeasured at A280 and the Amax of the dye to determine whether there had been any change in the dye-protein ratio.

2.4.6 Measurement of The Immunoreactivity of DNP and E-Selectin Antibodies Pre and Post Labelling by ELISA

Enzyme linked immunoabsorbent assay (ELISA) is an immunoassay frequently applied to determine the concentration of a specific protein in a sample. The method of sandwich ELISA makes use of two antibodies that bind to epitopes that do not overlap on the antigen of interest. During the first step, a highly purified antibody (capture antibody) is non-covalently adsorbed onto plastic microtiter plates creating a solid phase. Excess antibody is removed by washing and samples are applied to the plate. Diluted standard samples of the antigen are employed to constitute a standard curve for calculation of the antigen concentration in tissue samples. The immobilized antibodies serve to specifically capture soluble proteins present in unknown samples. After washing away unbound sample, the captured antigens are detected by biotin-conjugated antibody (detection antibody) that binds to a second epitope on the antigen. Streptavidin-labelled horseradish peroxidase (HRP) binds to the biotin which is linked to the detection antibody. Following the addition of a chromogenic substrate, the absorbance of coloured product generated by the bound, enzyme-linked detection reagents is measured spectrophotometrically on an ELISA plate reader at an appropriate optical density (OD).

ELISA was performed to confirm the immunoreactivity of anti-E-selectin antibody before and after conjugation. Following each step the ELISA plate was washed with 0.1% PBS/Tween. The plate was coated with 100µl of recombinant mouse E-selectin at a concentration of 3µg/ml (recombinant mouse E-selectin, CD62E, Fc chimera, R&D Systems, Minneapolis, USA). The plate was covered and left overnight. Wells were then blocked with 200µl of 2% BSA/PBS and incubated for 1-2 hours at room

temperature on a rotating platform. 100µl of either anti-DNP or E-selectin antibody was added at a concentration of 2ng/ml and the plate left for 1hr at room temperature. This was followed by the addition of 100µl of biotinylated rabbit anti-rat IgGa at a concentration of 0.5µg/ml (Vector, Burlingame, CA, USA) and left for a further hour. 0.5µg/ml of streptavidin conjugated to horseradish peroxidase (HRP; R&D Systems, Minneapolis, USA) was left for a maximum of 1 hour. 100µl of 3,3',5,5'-tetramethylbenzidine (TMB) (KPL, Gaithersburg, USA) was used as substrate (equal volumes of substrates A and B). 50µl of stop solution (2M H_2S0_4) was then added resulting in a colour change from turquoise to yellow. The reaction was then read at 450nm on a Multiskan Plate Reader (Thermoscientific, Loughborough, UK). Binding was quantified using a standard curve of rat anti-mouse E-selectin IgG2a MoAb (R&D Systems, Minneapolis, USA). This was calculated by the accompanying computer software Ascent, version 2.6 (Thermoscientific, Waltham, MA, USA).

2.4.7 Endothelial PY4.1 Cell Culture

The endothelial cell line (EC) used in this study was PY4.1, a mouse EC line derived from hemangiomas induced by the expression of the polyoma early region in transgenic mice. Cells were a kind gift from Dr Victoria Bautch, University of North Carolina, Chapel Hill, USA. The cells retain EC properties such as a characteristic cobblestone appearance at confluency, contact-inhibited growth, and active uptake of acetylated low density lipoprotein. Expression analysis shows that the cells express both the polyoma transgene and the von Willebrand factor, an EC marker. These properties confirm the endothelial nature of this cell line (Dubois, Kolpack et al. 1991; RayChaudhury, Frazier et al. 1994). In addition PY4.1 cells stimulated with TNFα demonstrate increased lymphocyte binding, following upregulation of cytokines (Heyward, Dubois-Stringfellow et al. 1995). Cells were maintained in Dulbecco's modified eagles medium (DMEM) (ATCC, Teddington, UK) supplemented with 10% FCS (Gibco, Invitrogen, Paisley, UK) and 100 U/ml penicillin and 0.1 mg/ml streptomycin (PAA, Yeovil, UK) as recommended by ATCC. The cell line was maintained in a humidified incubator at 37°C and 5% CO_2.

(a)

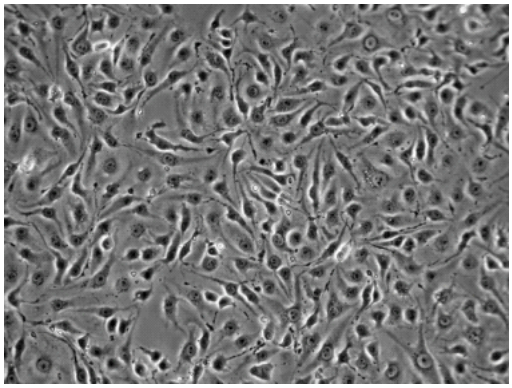

(b)

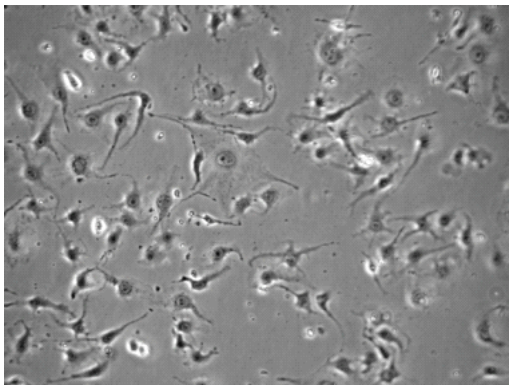

Figure 2-3 Phase contrast images of the PY4.1 endothelial cell line

Representative images of PY4.1 cells showing a confluent monolayer, panel (a) and a sub-confluent monolayer of cells panel (b) (Magnification x40).

2.4.7.1 Measurement of reactivity for anti-E-selectin and anti-DNP antibodies to endothelial cells before and after stimulation with TNFα

PY4.1 cells were plated out at 90% confluency into 30mm^2 well tissue culture plates, and allowed to adhere overnight and reach full confluency. Cells were checked under a microscope to insure a confluent monolayer had been reached. Cells were stimulated with Murine TNFα (PeproTech, Inc, Rocky Hill NJ, USA) for 5 hours, to induce expression of E-selectin. Murine TNFα was diluted in serum-free DMEM medium. Cells were incubated at 37°C and 5% CO_2. After stimulation cells were carefully washed with serum free medium and then fixed for 6 minutes with 4% paraformaldehyde (PFA)/PBS. The cells were washed with PBS/2%BSA three times, care being taken not to disturb the monolayer. To prevent non-specific binding the cells were incubated over night at 4°C in 2%BSA/PBS on a rocking platform. Cells were washed three times with PBS/2% BSA. Cells were then incubated on a shaking platform for 1 hour with anti-E-selectin or anti-DNP or no antibody as a control. Cells were then washed three times with PBS/2% BSA. Cells were then incubated on a

shaking platform for 1 hour with biotinylated rabbit anti-rat IgGa (Vector, Burlingame, CA, USA) at a concentration of 0.5μg/ml. Cells were washed three times with PBS/2% BSA. Streptavidin HRP (R&D Systems, Minneapolis, MN USA) diluted 1:400 was added to the plates and incubated for 45 minutes on a shaking platform. Cells were washed three times with PBS/2% BSA. TMB substrate and TMB substrate B (KPL, Gaithersburg, Maryland, USA) mixed together in equal volumes were then added to the plate and blue colour allowed to develop. Acid Stop solution (2M H_2SO_4) was added to terminate the reaction and change the plate contents to yellow so that colouration could be read on a plate reader at 450nm.

For fluorescence imaging, cells were plated at 90% confluence onto Lab-Tek Flaskette glass slides (Nalge Nunc, New York, USA), followed by stimulation in the absence or presence of TNFα for 5 hours. Following blocking overnight, cells were incubated with anti-DNP or anti-E-selectin antibodies at a concentration of 2μg/ml. Cells were washed and incubated with biotinylated rabbit anti-rat IgGa (Vector, Burlingame, CA, USA; 0.5μg/ml) for 1 hour, followed by streptavidin Alexa Fluor 488 (0.1μg/ml; Invitrogen, Renfrew, UK). Cells were mounted using VectaShield Mounting Medium with DAPI nuclear counterstain (Vector Laboratories Inc, Burlingame, CA, USA) and images were acquired on a Nikon T2000u microscope, (Nikon, Belmont, CA, USA).

2.5 Animal Models of Inflammation for *In Vivo* Imaging Experiments

2.5.1 Laboratory Animal Care and Regulatory Approval

Male DBA/1-Ola/Hsd mice (H-2q) aged 8-12 weeks were purchased from Harlan Laboratories UK (Blackthorn, Bicester, UK) for the collagen induced arthritis model. Male C57BL/6J ($H\text{-}2^b$) mice aged 6 weeks were purchased for the TNFα induced paw oedema model. Mice were housed in groups of 6, and were maintained at 21°C ± 2°C on a 12-hour light/dark cycle with food and water *ad libitum*. They were maintained under standard conditions at the Biological Service Unit (BSU) of the Kennedy Institute of Rheumatology. All studies were performed in accordance with the UK Animals (Scientific Procedures) Act 1986 regulations for the handling and use of laboratory animals and performed under PPL 70/6533: Identifying and targeting mediators of inflammation.

2.5.2 Collagen Induced Arthritis

The most widely used mouse model to study RA is collagen-induced arthritis (CIA). Type II collagen-induced arthritis was first described in rats in 1977 (Trentham, Townes et al. 1977), and subsequently established in mice (Courtenay, Dallman et al. 1980) as described in Section 1.4.1.

2.5.2.1 Purification of type II collagen

Experimental arthritis can be induced in susceptible mouse strains by immunisation with either heterologous (e.g. bovine, chicken) or homologous type II collagen. Type II collagen is the most abundant collagen found in hyaline cartilage (e.g. in synovial joints, sternum, respiratory tract), comprising 80-90% of the total collagen content. For all experiments, type II collagen was purified from bovine articular cartilage, obtained from the femoral heads of 2-3 month old calves, following the method originally performed by Miller (Miller 1972) and adapted from (Inglis, Simelyte et al. 2008).

The bovine articular cartilage were powdered using a liquid nitrogen freezer-mill (Spex Industries Inc, Metuchen, NJ, USA). To remove proteoglycans, 5 volumes of 4M guanidine hydrochloride in 0.05M Tris (pH 7.5) were added to the powdered cartilage and left stirring over night at 4°C. The cartilage was pelleted at 12,000 rpm for 1 hour at 4ºC. The insoluble residue was washed 2-3 times by stirring in 0.5M acetic acid followed by centrifugation. The pellet was then washed in 20 volumes of 0.5M acetic acid to eliminate the remaining guanidine. The pH was adjusted to pH 2.8 using 70% formic acid. 1g of pepsin was added for every 20g of cartilage (wet weight). This was left stirring for 48 hours at 4ºC. The sample was then centrifuged and the supernatant retained. To precipitate type II collagen from the supernatant NaCl (powder) was added gradually with stirring to produce a final concentration of 0.89 M. This was left to equilibrate overnight at 4ºC and then centrifuged at 14,000g for 1 hour at 4ºC. The pellet dissolved in 0.1M acetic acid. The residual pepsin was inactivated by dialysing against 0.02M Na_2PO_4 (pH 9.4). This was then centrifuged and then the pellet redissolved in 0.5M acetic acid. Finally this was dialysed exhaustively (at least 10 changes of solution) against 10 litres acetic acid (0.5M). The collagen was freeze-dryed and stored in a dessicator at 4°C or -20°C. For immunization, collagen was dissolved at 4 mg/ml in 0.1M acetic acid overnight.

2.5.2.2 Induction of arthritis

To induce arthritis in male DBA/1 mice, animals were administered a combination of Isofluorane (4%) and Oxygen (1l/min) by a gaseous anaesthetic delivery device (Vetech, UK) and shaved at the base of the tail. In-house prepared bovine type II collagen as described above was emulsified with an equal volume of complete Freund's adjuvant (CFA; DIFCO, Detroit, MI, USA). Each mouse received an intradermal injection of 200 µg bovine type II collagen (bCII) emulsified in CFA into the base of their tail.

2.5.2.3 Evaluation of arthritis

In order to determine onset and development of arthritis in the acute CIA models, mice were examined daily 14 days following immunisation. Arthritis was characterised by evaluation of joint properties and inflammation of surrounding tissues. Disease onset was considered as the day that paw swelling or erythema in the paws could be observed. The disease severity was recorded for each paw daily using the following scoring system based on the visual signs of arthritis: 0 = normal paw, 1 = mild swelling and/or erythema of the joint or individual digits; 2 = moderate swelling and erythema, 3 = moderate swelling and erythema accompanied with joint rigidity. An arthritis score (range 0 - 12) was assigned to each mouse by summing up the score of each paw. For clinical monitoring of CIA development in conjunction with the arthritis score, paw swelling was assessed by measuring the diameter of the hind paws using microcallipers (Röhm BG Ltd, Kingston-upon-Thames, UK).

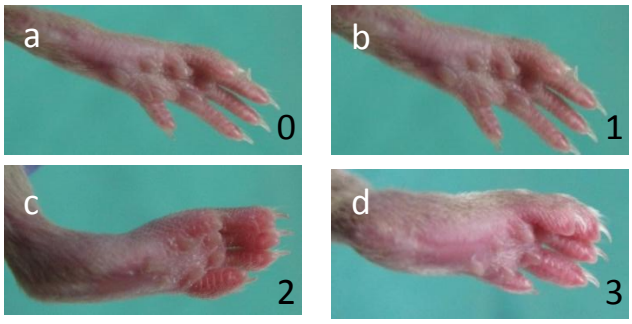

Figure 2-4 Representative clinical scores of mice with CIA

Panel (a) Normal hind paw (clinical score 0). (b) Hindpaw with mild swelling (clinical score 1). (c) Hindpaw with pronounced oedematous swelling (clinical score 2). (d) Hindpaw with ankylosis (joint fusion) (clinical score 3).

2.5.2.4 Protocols for determining effect of therapy in CIA

2.5.2.4.1 Effect of etanercept in CIA

Disease was induced in 40 male DBA/1 mice (12 weeks old) as described in Section 2.5.2.2. Human TNF type II receptor fusion protein (etanercept) (Wyeth Pharmaceuticals, Taplow, UK) was administered intraperitoneally (i.p.) (100μg) on days 1, 4, and 7 following the onset of arthritis in treatment groups (n=8 per group for either anti-E-selectin or anti-DNP-antibody injected groups). Mice were selected for imaging either with matched clinical score or at day 10 following arthritis onset and were transferred to the optical imaging device and anaesthetised as per the protocol in Section 2.7.

2.5.2.4.2 Effect of RB200, an EGF receptor construct, in CIA

Disease was induced in 60 male DBA/1 mice (12 weeks old) as described in Section 2.5.2.2. Rb200 (gift from Dr Michael Shepard, Halozyme Therapeutics, San diego, USA) was administered (i.p.) on day of disease onset (day 1), and then on days 4 and 7 of disease, at a dose of 0.5mg/kg or 10mg/kg, with equal volumes of PBS equivalent to etanercept given to control animals (N=6 per group. Etanercept was given (i.p.) on the day of disease onset (day 1), and then on days 4 and 7, at a dose of 1mg/kg or 5mg/kg, (equivalent to either 20 or 100μg per animal respectively) with an equal volume of PBS equivalent to Rb200 in control animals. Combination treatment of 0.5mg/kg Rb200 plus 1mg/kg etanercept was given i.p. on day of disease onset (day 1), and then on days 4 and 7. Arthritis assessed by paw swelling or as clinical scores

based on all 4 paws. Fluorescence imaging *in vivo* was performed on day 10, animals were injected with anti-mouse E-selectin MoAb labelled with Thermofisher DyLight 750nm near infrared probe (excitation/emission spectra 752nm/778nm respectively). *In vivo* imaging studies were undertaken at 2-24 hours following intravenous (i.v.) injection of labelled antibody using a near infrared optical *in vivo* imaging system, as described in Section 2.7.

2.5.3 TNFα Induced Paw Oedema

Paw swelling was induced by the intraplantar injection into the right hind paw of recombinant murine TNFα (5-50ng) (PeproTech Inc, London, UK). This was administered in a vehicle of 1% mouse plasma diluted in PBS. For administration of TNFα into the paw anaesthesia was induced with a combination of isofluorane (2-4%) and oxygen (1-2l/min) using a gaseous anaesthetic delivery system as described in Section 2.7. Animal groups (n=5) were then either injected with Anti-E-selectin or DNP antibody labelled with DyLight 750nm (i.v) (5-50µg/200µl). Paw thickness was measured with microcalipers (Röhm BG Ltd, Kingston-upon-Thames, UK) or *in vivo* optical imaging was performed at 2, 8 and 24 hours as per the protocol described in Section 2.7.

2.5.3.1 Protocols for determining effect of therapy in TNFα induced paw oedema

2.5.3.1.1 Effect of etanercept in TNFα induced paw inflammation

Human TNF type II receptor fusion protein (100µg) (etanercept) (Wyeth Pharmaceuticals, Taplow, UK) was administered intraperitoneally (i.p.) 12 and 4 hours prior to injection of dye labelled antibodies and induction of paw swelling. Animal groups (n=5) were then either injected with anti-E-selectin or DNP antibody labelled with DyLight 750nm i.v. (5µg/200µl). This was followed by gaseous induction of anaesthesia. Paw swelling was then induced by recombinant murine TNFα intra-plantar injection into the right hind paw as described above. Measurements of paw thickness were taken at sequential time points or *in vivo* optical imaging was performed at 2, 8 and 24 hours as per the protocol described in Section 2.7.

2.6 Histopathological Evaluation of Arthritis

2.6.1 Haematoxylin and Eosin (H&E) Specimen Preparation

At the end of an experiment, paws were dissected post-mortem and fixed overnight at 4ºC in 1% phosphate buffered PFA. Paws were then decalcified in a 0.3M EDTA solution for 12-14 days. Placing the slides in standard histology cassettes and an excess of EDTA ensured an adequate volume and circulation of the decalcificant. Decalcificant was intermittently manually agitated and changed on two occasions. In order to further facilitate the decalcification process, paws were sagitally divided to

the proximal metatarsal joint. X-ray analysis performed between days 7 and 14 to monitor the progress of decalcification was performed to ensure that decalcification was complete so that cutting can be optimized as shown in Figure 2-5. Decalcification of the inflamed mouse paws is necessary for subsequent cutting of the specimens. If calcified bone remains in the tissue it will splinter and fracture when cut on the microtome. Tissue blocks were sectioned to 4 μm thicknesses using a microtome. The tissue sections were allowed to adhere onto Snowcoat X-tra glass microscope slides (Surgipath, Peterborough, UK) and stained using Mayer's modification of Harris haematoxylin and eosin method. Used with a mordant, haematoxylin stains nuclei blue. Eosin is used to counterstain other cellular components red-pink. For the staining, tissue sections were first deparaffinised in xylene and re-hydrated in absolute alcohol. After washing in distilled water, sections were stained in Harris haematoxylin solution for 3 minutes. Excess stain was washed away with water, and the staining differentiated in 1% acid alcohol for 30 seconds. Following washing in water, sections were dipped into 0.2% ammonia water for 30 seconds for blueing the haematoxylin dye. Sections were washed in water and counterstained in eosin solution for 30 seconds. Slides were washed with water, dehydrated through 95% and absolute alcohol. Before the tissue sections were mounted with xylene based mounting medium, they were cleared with xylene. The stained sections were assessed microscopically to evaluate arthritic changes in the tibia tarsus joint (TTJ), metatarsophalangeal joint, proximal phalangeal joint (PPJ) and the distal phalangeal joint (DPJ). Images were captured with a digital camera (ProgRes CF Scan, Jenoptik, Jena, Germany) connected to an Olympus BH-2 microscope (Olympus, Tokyo, Japan) and analysed using (ProgRes Capture Pro camera control software, version 2.11 Jenoptik, Germany).

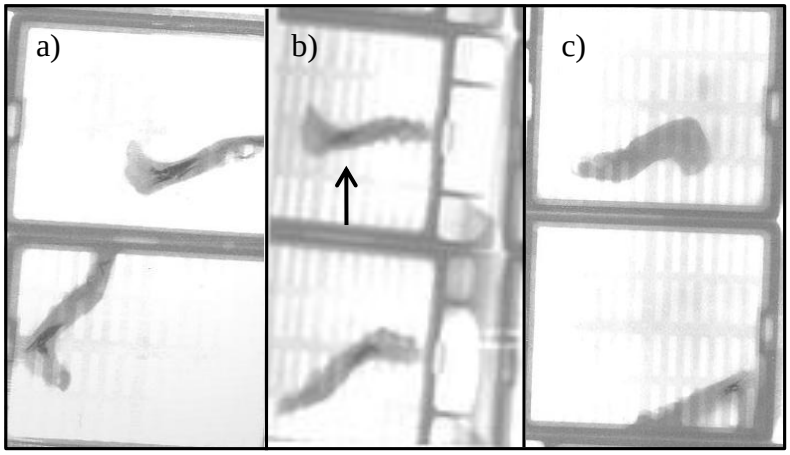

Figure 2-5 Decalcification of mouse paws

X-ray analysis of mouse paws at days 7, 9 and 14 (panels a,b,c) to monitor the progress of decalcification. X-ray analysis at 7 days shows significant areas of calcification (arrow) within the tarsal bones of the mouse paw that had resolved by day 14 (c).

2.6.2 Immunohistochemistry for Vascular Markers of Inflammation

In preliminary studies, arthritic mouse paw sections were utilized to examine the expression of E-selectin. These were used to determine an optimum protocol for i) fixation, and ii) decalcification to optimize antigen preservation. Prior experience with these techniques has shown that preservation of antigenicity has been very difficult to maintain during the fixation and decalcification process. My work in this area has enabled the formulation of a novel and reproducible protocol for subsequent time-course experiments facilitating reproducible immunohistochemistry for analysis of paw sections in the CIA model. The following conclusions were reached regarding fixation: Frozen, unfixed specimens demonstrated positive staining with anti-E-selectin antibody compared to a negative control (no primary antibody), but there was poor overall preservation of tissue architecture. Fixation with formaldehyde did not preserve of antigenicity. Antigenicity was preserved with the use of 1% PFA in frozen sections. Antigenicity was not preserved in paraffin embedded sections.

Following decalcification as described above, tissue blocks were mounted onto a cork disc embedded in an optimum cutting temperature glycol resin, snap frozen in isopentane suspended in a bath of liquid nitrogen, cut to a width of 4µm on a cryostat

(Leica CM 1900) with a tungsten carbide blade, picked up onto glass microscope slides (Menzel-glaser superfrost plus) and finally specimens were bonded onto the slides by heating in an oven for 2 hours at 37°C. (Initial specimens demonstrated poor adherence to the slide, but fixed specimens which were heat bonded onto specialised slides for frozen sections showed improved adherence). The complete protocol for preparation of specimens is shown in Appendix 2.1. Briefly, slides were blocked with 10% normal rat serum (Vector, Peterborough, UK) before addition of anti-E-selectin or anti-DNP antibodies (10µg/ml) or anti- CD31 (MEC 13.3; BD Pharmingen, Oxford, UK) (diluted 1:400), followed by 0.5µg/ml biotinylated rabbit anti-rat antibody (Vector, Peterborough, UK), avidin-biotin-peroxidase complexes and 3,3'-diaminobenzidine (Vector, Peterborough, UK) solution. Finally slides were counterstained with Harris Haematoxylin (Sigma-Aldrich, Poole, UK).

2.6.3 Detection Of *In Vivo* Injected E-Selectin Antibody by Immunohistochemistry In *Ex Vivo* Specimens

In order to determine whether i.v. injected E-selectin tracks to the inflamed synovium of the arthritic joint where E-selectin expression has been demonstrated histologically, mice with severe arthritis (>day 10) were injected with 50ug of either anti-E-selectin or anti-DNP antibody (n=3) per group at time points of 1,4 and 24 hours. Following injection the mice were sacrificed and paws were then fixed and prepared (as described in Section 2.6.2 in paraformaldehyde, decalcified in EDTA and snap frozen in the same way as for previous optimized specimen preparation. For the staining protocol slides were blocked with 10% normal rat serum (Vector, Peterborough, UK) followed by 0.5µg/ml biotinylated rabbit anti-rat antibody (Vector, Peterborough, UK), avidin-biotin-peroxidase complexes and 3,3'-diaminobenzidine (Vector, Peterborough, UK) solution. Finally slides were counterstained with Harris Haematoxylin (Sigma-Aldrich, Poole, UK).

2.7 *In Vivo* Optical Imaging

The following relates to general details regarding preparation of mice for *in vivo* imaging and principles of image capture. An appropriate anaesthetic regime using isofluorane has been utilized to ensure mice can be imaged *in vivo* for multiple time points and prolonged periods. The anaesthetic circuit for the Kodak imager has been redesigned for effective and safe anaesthetic use. It was necessary to design and build

an oxygen/gas delivery circuit that effectively balances administration of anaesthetic gases as well as safely scavenged used or excess anaesthetic gas. The circuit is housed within the pre-existing imaging box and is capable of regulating the supply of anaesthetic gas for up to three animals. It is also capable of providing a warm air supply for prolonged anaesthesia as demonstrated in the following Figure 2-6.

a)

b)

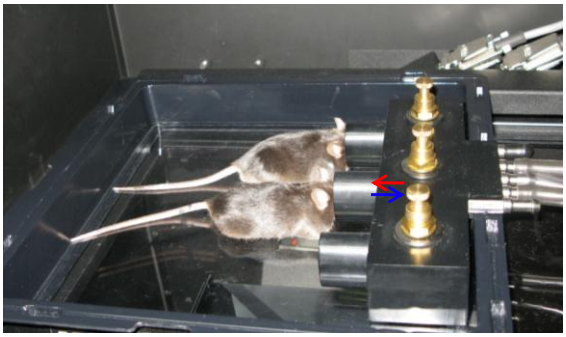

Figure 2-6 Anaesthetic device for small animal imaging

Images of prototype design for (a) anaesthetic housing and (b) animals anesthetised prior to fluorescent imaging. Isofluorane and Oxygen is delivered and scavenged via nose cones (as indicated by arrows). Multiple animals (n=3) animals can be imaged at any one time point and positioning of animals can be reproduced for sequential imaging studies.

Mice were injected with either control or anti-E-selectin antibody conjugated with Thermofisher DyLight 750 NIR dye (5-50 µg) via the tail vein. For imaging they were then anaesthetised with a mixture of isofluorane (2-3%) and Oxygen (2-4l/min). Optical imaging was performed using the Kodak Multispectral FX Pro fluorescence reflectance imaging device (Carestream Molecular Imaging, Rochester, USA) as described above. Filters for excitation and emission were set to 730nm and 770nm

respectively. An identical imaging protocol (exposure time: 60 seconds, 4x binning, f-stop: 2.51, field of view: 158.5, focal plane: 9.4mm) was maintained for all images. When required comparative X-ray images were taken using the following image settings: (exposure time: 20 seconds, 4xbinning, f-stop: 2.51 field of view: 158.5, focal plane 9.4mm)

Images were analysed using the Kodak Molecular Imaging software program (Version 5.0, Carestream Molecular Imaging, Rochester, USA). A region of interest (ROI) created by an automated tool was determined around the inflamed or control paw. Mean ROI signal intensities are expressed as arbitrary fluorescent signal intensity units. Fluorescence gray scale images were artificially coloured for depiction purposes according to a colour scale set to the highest and lowest levels of mean fluorescence intensity (red and purple indicate maximum and minimum light intensity respectively). The fluorescence images were co-registered onto X-ray images taken concurrently, when anatomical localisation was required.

2.7.1 Determination of Optimum Excitation/Emission Wavelength of Fluorescent Dye for Excitation for *In Vivo* Imaging by Measurement of Autofluorescence

To determine the peak levels of autofluorescence a live DBA/1 mouse was anaesthetised and imaged according to protocols described in Section 2.7. Images were taken at sequential excitation wavelengths between 390-770nm, and the resulting Autofluorescence emitted read between 535-830nm, using the Kodak *In Vivo* FX Pro imaging system.

2.8 Statistical Analysis

Results were expressed as mean ± SEM. Data were analysed using, 1- and 2-way analysis of variance (ANOVA) with Bonferroni post-hoc analysis, or Students t-test. P-values of less than 0.05 were considered to be statistically significant. Data were analysed using GraphPad Prism 5.0 (Graph Pad Software, CA, USA).

Appendices

Appendix 2.1 Staining protocol for E-selectin, CD-31, and DNP antibodies

1. Slides placed in 37°C oven for two hours to optimize adhesion to the slide
2. Fix in acetone for 5 minutes
3. Air dry slides for ½ min. DO NOT LET SLIDES DRY AFTER THIS STEP.
4. Wash in PBS/TBS gently tip off and discard (subsequently referred to as 'wash')
5. Block with 10% normal serum/PBS/TBS for 60 minutes at room temperature (RT). Normal serum is the serum of the species that the secondary biotinylated antibody is raised in. Use heat-inactivated serum, in this case rabbit serum.
6. Wash
7. Block with Avidin solution undiluted for 15 minutes at RT in moist chamber (Vector Blocking Kit- Catalog No. SP2001).
8. Wash
9. Block with biotin solution undiluted for 15 minutes at RT in moist chamber (Vector Blocking Kit).
10. Wash
11. Add primary antibody (200µl per slide) (working antibody concentration of 10µg/ml) Incubate for 45 minutes at RT in moist chamber.
12. Wash in PBS for 5 min.
13. Incubate with secondary antibody (rabbit-anti rat) biotinylated for 40 minutes at RT in a moist chamber. Dilute this antibody 1:100 with PBS/TBS to which normal serum from the species that the tissue is from has been added at 2%.
14. (When working with mouse tissue, make sure that the secondary antibody is not absorbed against rabbit because you get more unspecific staining for unknown reasons).
15. Prepare the ABC complexes at this stage. Use Vector's ABC-Elite-Standard Kit for Peroxidase (Vector Catal. No. PK6100). To 100µl of PBS add 1 µl solution A (Avidin) from the kit and mix well. Then quickly add 1µl of solution B (Biotin-Peroxidase) from the kit and mix well. Let stand 30 minutes for the complexes to form and it is ready to be used. If it stands a little longer it is OK but not less than ½ hour. MAKE SURE TO USE DIFFERENT PIPETTE TIPS FOR SOLUTION A and SOLUTION B.
16. Wash
17. Inactivate slides for endogenous peroxidase by incubating them for 15 minutes in 0.3% hydrogen peroxide/PBS/TBS at RT.
18. Wash
19. Incubate with the ABC complexes prepared for 40 minutes at RT in a moist chamber.
20. Prepare Vector DAB: As per kit (4 drops buffer, 8 drops DAB, 4 drops hydrogen peroxide substrate in 10mls distilled water)
21. Wash
22. Incubate in DAB solution for 4 minutes

23. Wash in PBS for 5 min.
24. Counterstain with Harris Haematoxylin for 1minute, differentiate in i) 0.5% acid/alcohol ii)wash tap water until nuclei blue
25. Dehydrate in graded alcohol baths (automated) – 70%/90%/absolute/absolute
26. Clear with 3 baths of xylene
27. Slides mounted with surgipath coverslips and pertex xylene based mountant on Leica CV5000 automated coverslipper
28. Personal protective clothing and safety equipment to be used throughout all procedures.

Appendix 2.2 Procedure for Labelling Proteins with DyLight Fluorophores (Thermofisher technologies)

A. Protein Preparation

Note: When labelling with the DyLight 594 Kit, prepare the protein in PBS. If the Borate Buffer has precipitated during storage, solubilize it by warming and vortexing the vial.

1. The optimal labelling buffer is 50 mM sodium borate, pH 8.5 (please see note above). For best results use 1 mg of protein at ~2 mg/ml. Prepare the protein as follows:

Proteins Lyophilized in PBS: Just before use, prepare the labelling buffer by diluting the Borate Buffer (0.67 M) to 0.05 M in PBS or ultrapure water. Prepare only enough labelling buffer required for the reaction (for example, to prepare 1 ml, add 75 µl of Borate Buffer (0.67 M) to 925 µl of ultrapure water or PBS). Reconstitute 1 mg of protein with 0.5 ml of labelling buffer.

Proteins in PBS Solution: Add 40 µl of the Borate Buffer (0.67 M) to 0.5 ml of 2 mg/ml protein in PBS. If the protein is > 2 mg/ml, adjust the concentration to 2 mg/ml with labelling buffer (for example, 0.05 M sodium borate − see the above bullet point: Proteins Lyophilized in PBS).

Proteins in Other Buffers: Protein must not be in a buffer containing ammonium ions or primary amines (for example, Tris or glycine). If necessary, replace buffer with 50 mM sodium borate (Product No. 28384), pH 8.5 by dialysis or buffer exchange.

B. Protein Labelling

1. Tap the bottom of the DyLight Reagent vial against a hard surface to ensure the dye is in the bottom of the tube. Add 0.5 mls of the prepared protein to the vial of DyLight Reagent and vortex gently or invert 10 times.
2. Briefly centrifuge the vial to collect the sample in the bottom of the tube.
3. Incubate the reaction mixture for 60 minutes at room temperature protected from light.

C. Protein Purification

1. Place two spin columns in two microcentrifuge collection tubes.
2. Mix the Purification Resin to ensure uniform suspension and add 400 µl of the suspension into both spin columns. Centrifuge for 45 seconds at ~1,000 × g to remove the storage solution. Discard the used collection tubes and place the columns in new collection tubes.
3. Add 250-270 µl of the labelling reaction to each spin column and mix the sample with the resin by pipetting up and down or briefly vortexing.

4. Centrifuge columns for 45 seconds at ~1,000 × *g* to collect the purified proteins. Combine the samples from both columns (~0.5 mls total). Discard the used columns.
5. Store the labeled protein protected from light at 4°C for up to one month. Alternatively, store labeled protein in single-use aliquots at -20°C. Avoid repeated freeze/thaw cycles. If the final concentration of conjugate is < 1 mg/ml, add a stabilizing agent, such as bovine serum albumin at 1-10 mg/ml.

CHAPTER 3

3 ANTIBODY CHARACTERISATION AND LABELLING

3.1 Introduction

A potential molecular target for fluorescent labelling and subsequent imaging in *in vivo* models of inflammation is E-selectin (ELAM-1). It is a 115kDa glycoprotein induced on EC in response to pro-inflammatory cytokines involved in RA such as IL-1β and TNFα (Pober, Gimbrone et al. 1986; Wellicome, Thornhill et al. 1990). As part of a complex multistep process, selectins promote the initial attachment (tethering) and subsequent moving (rolling) of leukocytes on endothelium, where they become activated as a result of locally produced chemokines (Springer 1994). Locally produced inflammatory mediators and the subsequent up-regulation of adhesion molecules at sites of inflammation are key factors in RA pathogenesis (Tak, Taylor et al. 1996). The vascular endothelium acts as an interface for the interaction between cytokines and cell surface receptors, promoting the recruitment of circulating leucocytes to sites of inflammation. The endothelium in RA synovium has been demonstrated to express E-selectin (Corkill, Kirkham et al. 1991). Selectin:ligand interactions are one of the first to occur during recruitment of circulating leucocytes to sites of inflammation. E-selectin has previously been investigated as a molecule for tracking inflammation. Scintigraphy utilizing a radiolabelled anti-E-selectin antibody has also been used to successfully image synovitis in patients with RA, with a 99m Tc-anti-E-selectin-Fab demonstrating improved specificity compared to a conventional tracer for bone and joint inflammation, 99mTc-oxidronate (Chapman, Jamar et al. 1996; Jamar, Chapman et al. 1997; Jamar, Houssiau et al. 2002). This study also demonstrated particular specificity for targeting active joint inflammation (Jamar, Houssiau et al. 2002). Decreased endothelial expression and reduced serum levels of E-selectin have also been demonstrated in patients with RA treated with anti-TNF therapy (Paleolog, Hunt et al. 1996; Tak, Taylor et al. 1996).

Production of functional, uniform E-selectin antibody was a key objective of the early work of this project. The work in this chapter aimed to ensure that E-selectin antibody which was produced from cell culture could bind to both E-selectin and to TNFα-stimulated EC, after labelling with fluorophore. Furthermore, selection of dye in the near infra red (NIR) range also has been demonstrated in other studies to be at an

optimal wavelength to delineate specific signal in the animal model. My objective was therefore to confirm this in the live animals to be used for both a model of acute inflammation, namely the TNFα paw injection model, and for CIA, a chronic model of inflammatory arthritis.

Determining and demonstrating that a reproducible labelling technique was also of paramount importance prior to commencing *in vivo* imaging experiments. Prior studies have clearly demonstrated that free dye can track to sites of inflammation due to increased vessel permeability and this is discussed in detail in introductory section 1.2.4. Confirmation that free dye had been removed from labelled anti-E-selectin and isotype control preparations is therefore presented.

Image acquisition and the parameters for digital imaging are also explored. Image acquisition has been developed in keeping with proprietary protocols for imaging fluorescent agents with differing emission and excitation spectra as per the manufacturers' guidance.

Recording a digital image involves determining an appropriate focal length for imaging at particular wavelengths as well as calibrating the camera for artefact due to lens refraction. Image capture time may be varied according to brightness of fluorescent emission and size of region of interest. Pixel binning may be required to increase the sensitivity of image capture. Pixel binning involves the summation of detected signal from more than one pixel to one central pixel effectively decreasing the resolution of the image. Changing the aperture (*f-stop*) of the camera is another way of either allowing more or less light through the lens and hence to the sensor. Allowing more light utilizes a larger surface of lens and hence there is likely to be more distortion of light from the lens edges, with the converse being true if the less light and the central portion of the lens is used. For *in vivo* imaging experiments a simple protocol has been developed so that both exposure time, pixel binning, focal length, aperture, and field of view are kept constant so that images can be compared accurately. The parameters of image processing are therefore examined, to ensure a reliable method of data collection is employed. A technique was developed to provide quantification of digital signal from fluorescent images. This was so that signal intensity between selected areas could be determined and longitudinal comparisons made of fluorescence signal over time.

3.2 Objectives

i. To demonstrate the adequate production from cell culture of functional uniform, anti-E-selectin and matched isotype anti-DNP control antibodies

ii. To ensure that anti-E-selectin antibody could bind to both E-selectin and to TNFα–stimulated EC before and after labelling with fluorophore

iii. To determine a reproducible fluorescent dye labelling technique with satisfactory dye:protein ratios and with exclusion of free dye from the sample

iv. To demonstrate that imaging in the NIR spectrum optimises target fluorescent signal intensity

v. To delineate the parameters of image quantification from the digital imaging device

3.3 Results

3.3.1 Determining Purity of Antibody By SDS PAGE Prior to Labelling

The purity of anti-E-selectin and anti-DNP antibodies obtained from cell culture was determined using sodium dodecyl sulfate polyacrylamide gel electrophoresis (SDS PAGE). This demonstrated that both anti-E-selectin antibody and control anti-DNP antibody show major bands at 100-150kDa (G9 and G10 respectively), and at approximately 50kDa (H5 and H6) and 25kDa (H9 and H10) as demonstrated in Figure 3-1a. These are most likely to correspond to immunoglobulin heavy and light chain fragments. Analysis of the bands was then performed by mass spectroscopy. This confirmed the identity of the major bands (Figure 3-2). The minor bands are likely to be albumin (F9 and F10), that had been carried over from the purification process. It is possible to generate other sizes of immunoglobulin fragments if cell culture conditions are not carefully regulated. This may in turn have implications for the efficiency of antibody labelling and hence ability of the labelled antibody to target E-selectin expression on activated EC *in vivo.* If for example there were significant amounts of albumin contaminating the sample, this could non-specifically track to sites of inflammation due to local permeability changes.

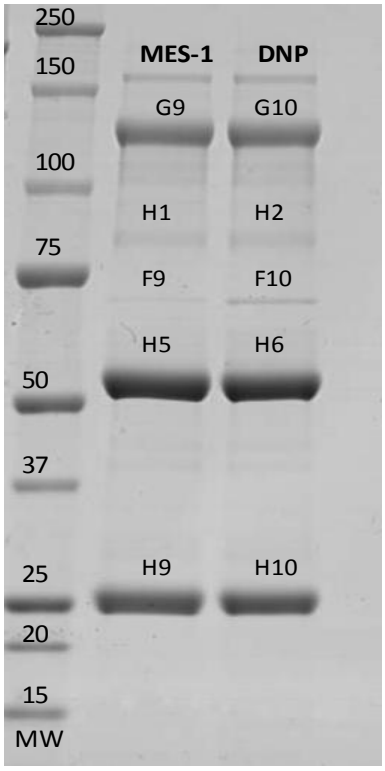

Figure 3-1 Purity of anti-E-selectin and anti-DNP antibodies produced from cell culture

Purity of antibodies was confirmed by gel protein electrophoresis (NuPAGE Novex Bis-Tris Mini Gel, Invitrogen, Renfrew, UK) followed by Coomasie stain. The left hand section of the gel is a molecular weight standard (MW), with subsequent lanes for anti-E-selectin antibody and anti-DNP antibody respectively. The following Figure 3-2 demonstrates the corresponding mass spectometry readouts for the various gel bands.

F9	gi|229552 albumin
F10	ALBU_BOVIN Serum albumin precursor
F11	ALBU_BOVIN Serum albumin precursor
F12	ALBU_BOVIN Serum albumin precursor
G1	gi|148744106 IGL@ protein/ gi|108750 Ig heavy chain precursor
G2	gi|108750 Ig heavy chain precursor/Keratin
G3	gi|108750 Ig heavy chain precursor/ gi|148744106 IGL@ protein
G4	gi|108750 Ig heavy chain precursor/ gi|148744106 IGL@ protein
G5	Unidentified
G6	Unidentified
G7	gi|108750 Ig heavy chain precursor
G8	Keratin
G9	gi|108750 Ig heavy chain precursor/ gi|110132 Ig heavy chain V region
G10	gi|108750 Ig heavy chain precursor/ gi|110132 Ig heavy chain V region
G11	gi|108750 Ig heavy chain precursor/ gi|3834651 immunoglobulin heavy chain variable region
G12	gi|108750 Ig heavy chain precursor/ gi|110132 Ig heavy chain V region
H1	gi|108750 Ig heavy chain precursor/ gi|148744106 IGL@ protein
H2	gi|108750 Ig heavy chain precursor/ gi|148744106 IGL@ protein
H3	gi|148744106 IGL@ protein
H4	gi|108750 Ig heavy chain precursor
H5	gi|108750 Ig heavy chain precursor/ gi|3834651 immunoglobulin heavy chain variable region/ gi|121052 Ig gamma-2A chain C region/ gi|114673589 PREDICTED: hypothetical protein [Pan troglodytes]?
H6	gi|108750 Ig heavy chain precursor/ gi|114147714 immunoglobulin heavy chain variable region
H7	gi|108750 Ig heavy chain precursor
H8	gi|108750 Ig heavy chain precursor/ gi|420178 Ig mu chain V region
H9	gi|86438072 Vl1a protein/ gi|52367058 immunoglobulin kappa light chain constant region
H10	gi|86438072 Vl1a protein/ gi|148744106 IGL@ protein
H11	gi|86438072 Vl1a protein/ gi|148744106 IGL@ protein/ gi|52367058 immunoglobulin kappa light chain constant region
H12	gi|86438072 Vl1a protein/ gi|148744106 IGL@ protein/ gi|115545495 IGK protein

Figure 3-2 Summary of immunoglobulin components identified by mass spectroscopy

Sections of gel were cut out from gel protein electrophoresis (NuPAGE Novex Bis-Tris Mini Gel, Invitrogen, Renfrew, UK) The corresponding mass spectrometry (Waters Micromass Xevo QTof, Milford, Massachusetts, USA) readouts for the various gel bands as shown in Figure 3-1 are displayed.

3.3.2 Imaging in the Near Infrared Spectrum Leads to Reduced Levels of Autofluorescence in A Live Mouse

This preliminary investigation was performed to ensure that imaging in the NIR was optimal in order to decrease levels of autofluorescence in the live strain of mouse chosen for *in vivo* experiments. This would then maximise measurable signal from targeted fluorescence to sites of inflammation compared to background signal (i.e. increase signal specificity). A healthy DBA/1 mouse was anaesthetised and imaged at sequential emission and excitation wavelengths from 400-800nm. This confirmed that peak autofluorescence levels were measured at lower wavelengths (500-60nm) with minimal autofluorescence in the NIR range (700 to 800nm). A representative example of imaging at both low (below the NIR range) and higher wavelengths (within the NIR range) is demonstrated in Figure 3-3 (a) and (b) respectively. A graph of autofluorescence throughout the range of wavelengths from 400 to 800nm is shown in Figure 3-4. This confirmed that fluorophores working in the yellow hashed area would not be subject to the autofluorescence interference that is measured at lower wavelengths. The following sections detail the *in vitro* and *in vivo* characterisation of anti-E-selectin and control antibodies labelled with NIR fluorescent dye.

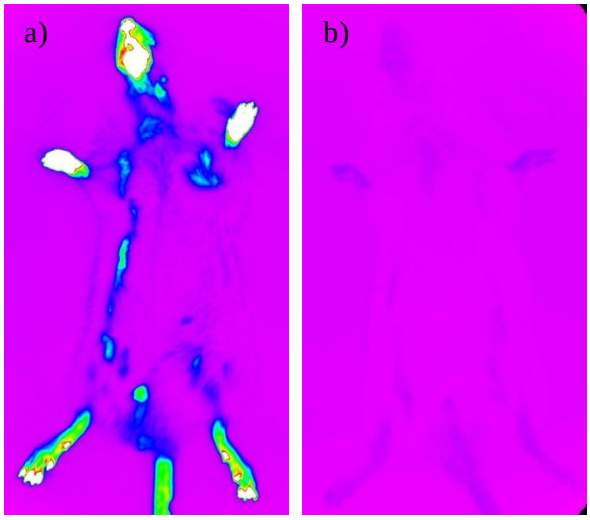

Figure 3-3 Visual representation of autofluorescence from a live DBA/1 mouse

A live DBA/1 mouse was anaesthetised and images obtained of (a) autofluorescent emission (535nm) following light excitation at (390nm) and (b) autofluorescent emission within the autofluorescent range (730nm) following excitation (750nm), using the Kodak *In Vivo* FX Pro imaging system.

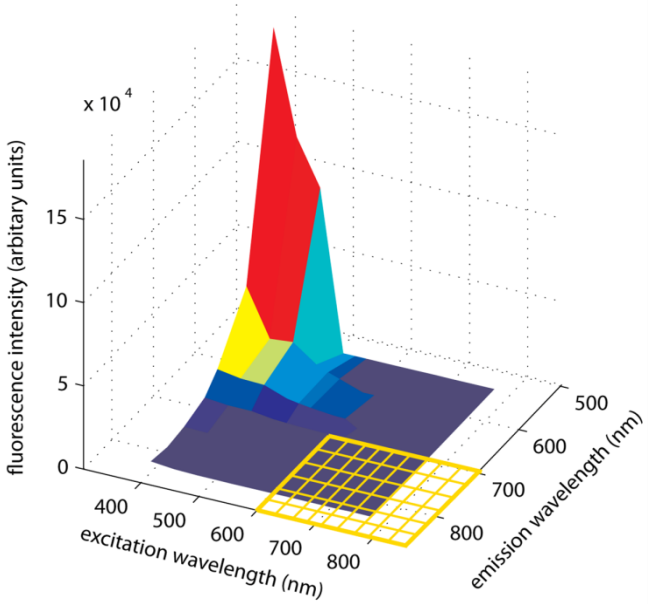

Figure 3-4 Autofluorescence in a live DBA/1 mouse

A live DBA/1 mouse was anaesthetised and images obtained of autofluorescent emission (535-830nm) following light excitation between 390-770 nm, and the resulting autofluorescence read between 535-830 nm, using the Kodak *In Vivo* FX Pro imaging system.

3.3.3 Dye/Protein Binding: Ratio of Absorbance At 280 And 750nm

Following conjugation of antibodies to the Thermofisher Dylight 750nm fluorochrome as detailed in Section 2.4.5, it was necessary to firstly ensure that there was absorbance corresponding to the peak absorbance/fluorescence of the dye at 750nm (i.e. within the NIR range required for *in vivo* imaging). Secondly, it was important to determine that the dye-protein ratio was within the range to allow adequate emission of the dye for *in vivo* imaging. Over-labelling of the dye can cause quenching of fluorescent signal because one fluorescent molecule will absorb light from an adjacent one, this is termed auto quenching. Thirdly, I aimed to test the reliability of consecutive labelling reactions to ensure that control and anti-E-selectin antibodies were comparably labelled. This was to ensure that there could be accurate quantification of fluorescent signal in relation to known antibody concentration for *in vivo* imaging experiments. Furthermore, this ensured there could be a comparison between experiments conducted with batches of antibody from labelling reactions performed at different time points. Following labelling it is recognised that over time there is a relative decrease in fluorophore intensity following excitation. The rate of this degradation was not measured in the present study, but rather fresh batches of antibody were made and tested for dye protein ratios and the efficacy of antibody binding quantified by ELISA as described below. Relative absorbance was measured at a range of wavelengths from 220nm to 800nm, as shown in Figure 3-5a to determine the A280 and Amax of the protein/dye conjugate at 750nm. Dye:protein ratios were 1.65 and 1.93 mols of dye per mol of protein for anti-E-selectin and anti-DNP antibodies respectively as measured for three separate labelling reactions, based on the ratio between the absorbance at 750nm and 280nm (Figure 3-5b). I found some degree of variation in the use of absorbance calculations to measure either protein concentration (A280) or to measure the absorbance of fluorophores at higher wavelength following conjugation with antibody. In order to ensure that an accurate amount of antibody was both used for fluorophore labelling and then subsequently injected during *in vivo* experiments, a BCA protein assay was used to determine accurate protein concentration measurements prior to labelling.

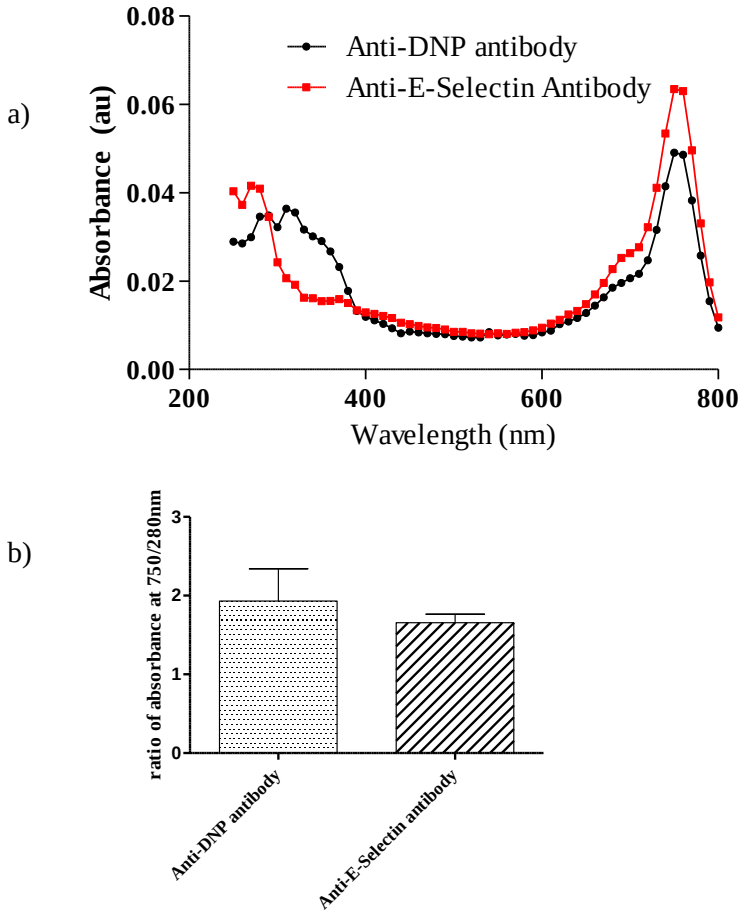

Figure 3-5 Dye protein binding: ratio of absorbance at 280nm and 750nm

Panel (a) shows typical absorbance spectra of both anti-E-selectin and anti-DNP Thermofisher Dylight 750nm dye labelled antibodies at wavelengths from 200 to 800nm, showing comparable absorbance and relative ratio of absorbance at 280nm *versus* the peak of dye absorbance at 750nm. Panel (b) demonstrates that the absorbance ratios (ratio of absorbance at 750nm/280nm) have remained consistent over three labelling reactions.

Further purification steps were also undertaken to ensure that the above measurements did not include absorbance from dye at 750nm that was unbound to antibody (i.e. that the labelling reaction had not been complete and there was free dye in the sample). This is especially important because it is recognised that free dye may track to sites of both acute and chronic inflammation due to changes in vascular permeability (as discussed in Section 1.2.4). Specimen samples were dialysed against PBS. Figure 3-6 illustrates that pre- and post-dialysis samples exhibit comparable absorbance characteristics. This suggests that excess free dye was not contributing to the small difference in absorbance between DNP and E-selectin antibodies observed in Figure

3-5, and that there was not free dye in the samples. Further absorbance spectroscopy on the dialysate also confirmed no absorbance (i.e. no free dye had been dialysed from the sample). In a separate preliminary experiment both samples were also subjected to further centrifugation using a molecular weight cut-off spin column and this also confirmed that there was no fluorescence in the lysate, confirming that all dye in the sample was bound to antibody and could therefore not pass through the spin column (data not shown).

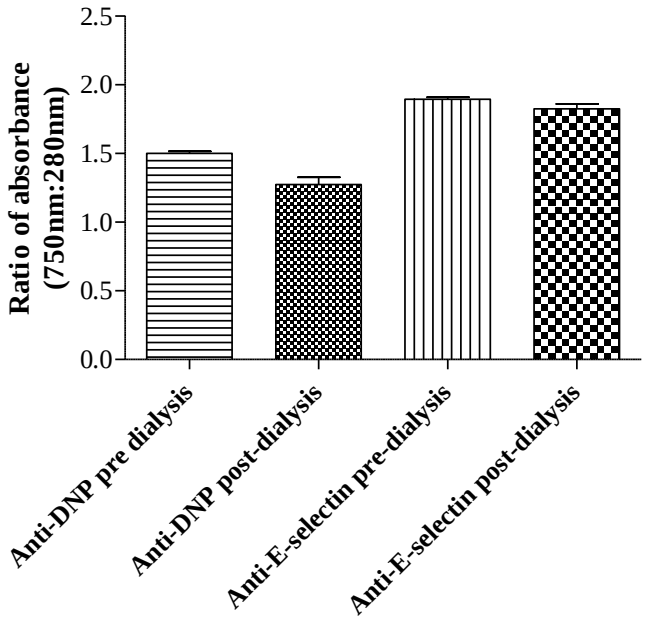

Figure 3-6 Dye protein ratio following dialysis

The absorbance of both anti-E-selectin and anti-DNP Thermofisher Dylight 750nm dye labelled antibodies were measured before and after dialysis.

Taken together these experiments have demonstrated that using a commercially well validated labelling technique for antibody conjugation to a NIR fluorophore had taken place effectively with a satisfactory number of dye molecules per antibody and that free dye had been removed effectively from the sample.

3.3.4 Characterisation of Anti-E-Selectin Antibody Binding

3.3.4.1 ELISA following fluorophore conjugation

The specificity of dye labelled anti-E-selectin antibody binding to E-selectin coated ELISA plates was subsequently assessed. This was to ensure that fluorophore conjugation had not altered the binding properties of the anti-E-selectin antibody. This was compared to that of a commercially available anti-E-selectin antibody as demonstrated in Figure 3-7. There were slight increases in binding efficacy following conjugation. This might be due to small differences in the calculated concentration of the dye antibody conjugate following conjugation. Secondly, there may also be a small contribution from the fluorophore to the optical reading taken at the end of the ELISA, which was not corrected for during the calculation of binding efficacy for the dye antibody conjugate. The contribution from the fluorophore is likely to very small, as confirmed from the minimal relative absorbance at 450nm from the conjugate demonstrated in Figure 3-5. Furthermore this experiment confirmed that control anti-DNP antibody failed to bind recombinant murine E-selectin. This process was also repeated on further batches of antibody to confirm similar levels of immunoreactivity of cultured antibodies prior to use for *in vivo* imaging experiments. This ensured that the antibody production technique had produced antibody of consistent efficacy and that there had not been any degradation of antibody efficacy following storage after production.

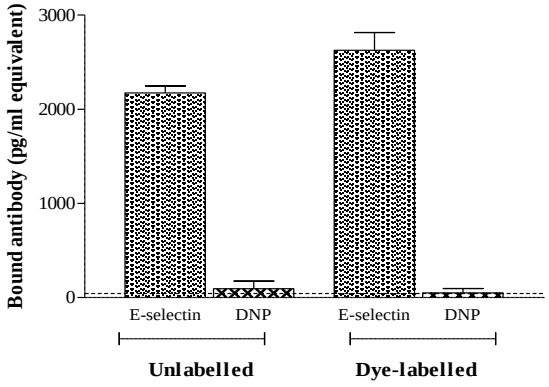

Figure 3-7 Anti-E-selectin antibody binding before and after fluorophore labelling

Anti-E-selectin or isotype control (anti-DNP) antibodies were added at a concentration of 2ng/ml to plates pre-coated with recombinant mouse E-selectin (3µg/ml). Binding was compared before and after labelling with Dylight 750 nm near infrared fluorophore, and quantified using a standard curve of commercial anti-mouse E-selectin antibody. Dashed line shows PBS (background control).

3.3.4.2 Binding to mouse PY4.1 endothelial cell line following TNFα stimulation

To confirm that anti-E-selectin antibody bound effectively to activated endothelium, as a pre-requisite to *in vivo* imaging studies in models of inflammation, murine PY4.1 EC were incubated in the absence or presence of TNFα. This experiment showed that anti-DNP antibody did not bind to activated PY4.1 cells, in contrast to anti-E-selectin antibody, which demonstrated significantly increased binding following TNFα treatment of PY4.1 as shown in Figure 3-8

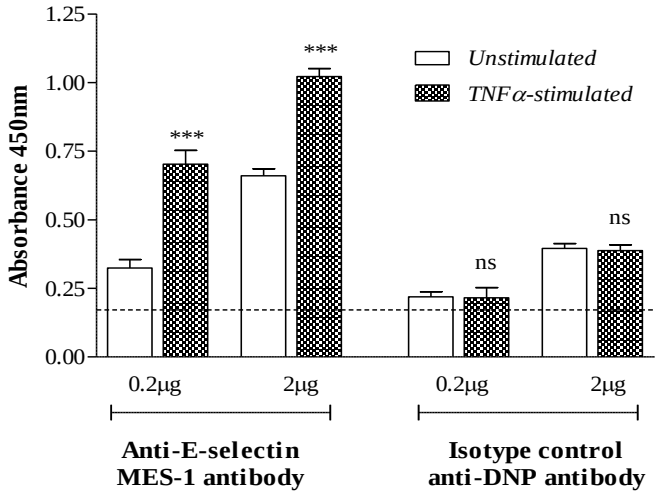

Figure 3-8 Anti-E-selectin binding to endothelial cells following stimulation with TNFα

Mouse PY4.1 endothelial cells were stimulated in the absence or presence of recombinant murine TNFα (10ng/ml for 5 hours). Cells were incubated with either anti-E-selectin or isotype control (anti-DNP) antibodies (0.2μg/ml and 2μg/ml) and binding was quantified colourimetrically. Dashed line shows binding of secondary antibody only. Data are mean ± SD, and were analysed by 1-way ANOVA *versus* unstimulated PY4.1 cells: *** $p<0.001$, ns = not significant.

The effect of increasing the TNFα dose on anti-E-selectin antibody binding to stimulated EC is shown in Figure 3-9. At the two doses used here there was no difference in the binding of anti-E-selectin. Other experiments with lower doses of TNFα stimulation, for both the same and longer periods (5 and 24 hours) did not demonstrate increased binding of anti-E-selectin antibody (not shown)

It is interesting to note that there was a degree of anti-E-selectin antibody binding to unstimulated cells. The cell culture is not serum starved and therefore increased levels of cytokine expression (which might stimulate E-selectin) maybe expected. Equally it is possible that PY4,1 cells express E-selectin 'constitutively'.

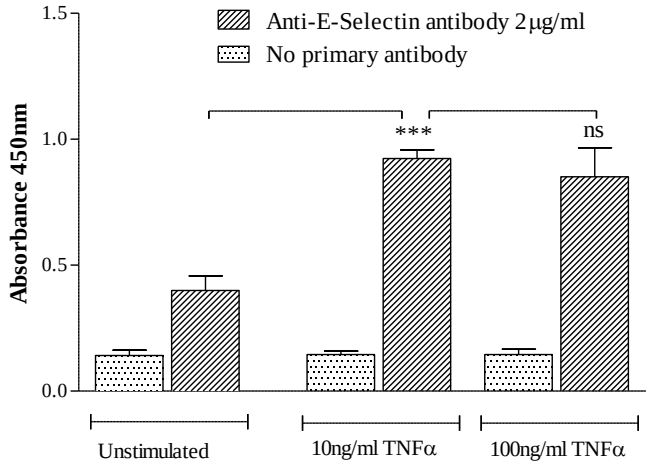

Figure 3-9 Comparison of E-selectin binding at different doses of TNFα

Mouse PY4.1 endothelial cells were stimulated in the presence of recombinant murine TNFα (10ng/ml or 100ng/ml for 5 hours). Cells were incubated with either anti-E-selectin antibody (2μg/ml) and binding was quantified colourimetrically. Data are mean ± SD, and were analysed by 1-way ANOVA *versus* unstimulated PY4.1 cells: *** $p<0.001$, ns = not significant.

Images of EC following stimulation with TNFα and binding of anti-E-selectin antibody were also taken. This was achieved by applying an Alexa Fluor® 488 streptavidin conjugate following application of the biotinylated rabbit anti-rat secondary antibody. A DAPI nuclear counterstain was used to delineate individual cells as demonstrated in Figure 3-10.

.

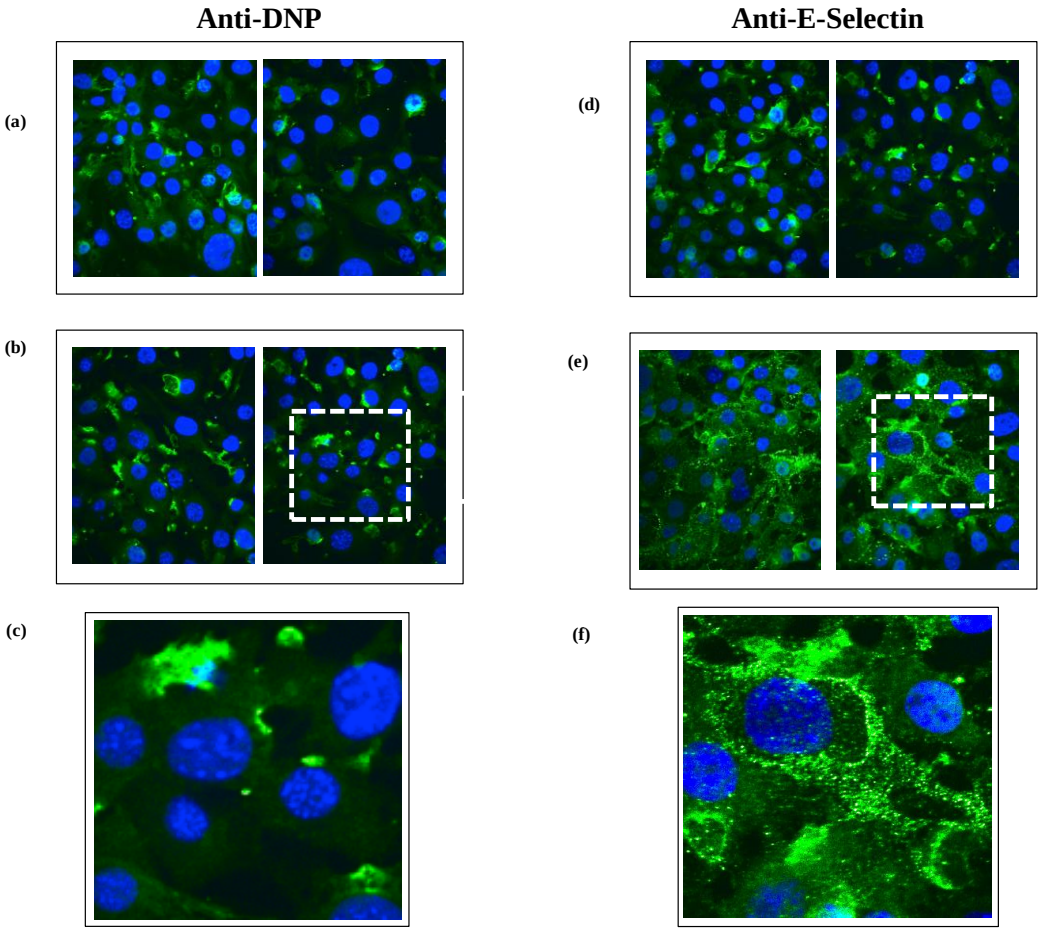

Figure 3-10 Fluorescent imaging of endothelial cells expressing E-selectin

Representative fluorescence images of either anti-DNP or anti-E-selectin stained PY4.1 cells incubated in the absence (a,c) or presence (b,d and c,e) of TNFα followed by secondary detection with biotinylated rabbit anti-rat IgGa and then by streptavidin Alexa Fluor 488 with DAPI nuclear counter stain. Magnified images of anti-DNP (c) and anti-selectin (f) antibody stained cells as demonstrated by hashed boxes.

3.3.5 Visualisation and quantification of Fluorescent Signal Using Fluorescent Reflectance Imaging

Preliminary experiments were performed using the Kodak fluorescence reflectance imaging device. This was firstly to understand clearly the visual representation of fluorescent signal following acquisition of a digital image and, secondly, ensure accurate quantification of fluorescent emission from the dye antibody conjugate to enable meaningful analysis of *in vivo* fluorescence imaging. This would also determine the detection limits of the device for differentiating between control and targeted fluorescent antibody signal. This was undertaken by imaging a 96 well plate with serial dilutions of both dye labelled antibodies (unbound to any particular target antigen). Identical settings were used for imaging (exposure time: 60 seconds, 4x binning, f-stop: 2.51, field of view: 158.5mm, focal plane: 9.4mm). Visual representation of the image is demonstrated in Figure 3-11.

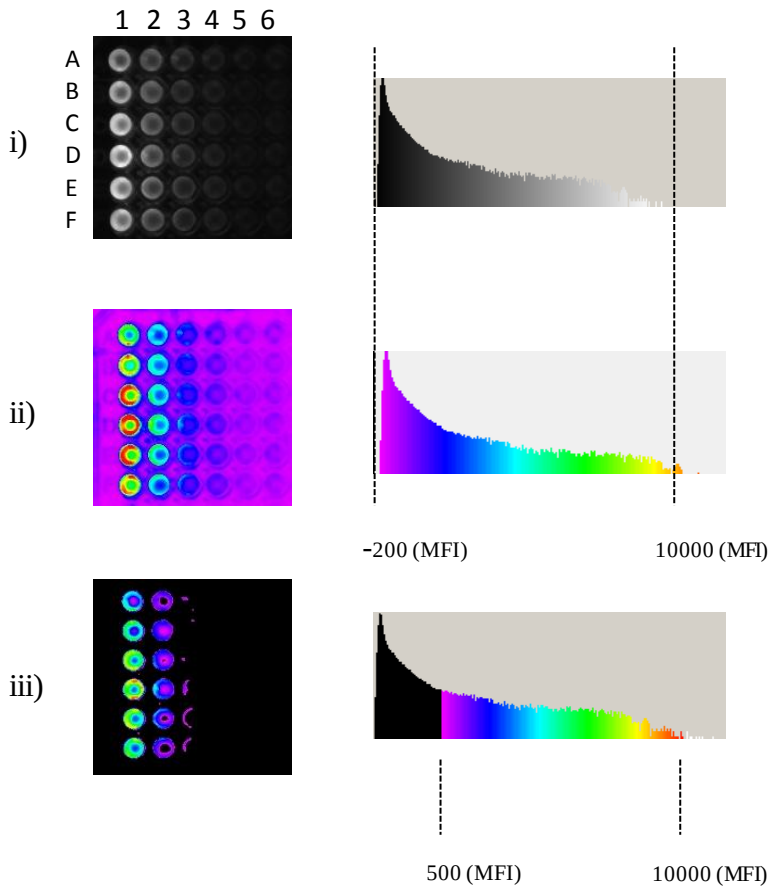

Figure 3-11 Visualisation of fluorescent signal using fluorescent reflectance imaging

Figure demonstrates the fluorescent image obtained after placing a 96 well plate containing dye labelled E-selectin (wells A-C) or DNP (wells D-F) antibody conjugate in 1:2 serial dilutions with a highest concentration of 12.5µg/ml and lowest of 0.2µg/ml (1-6). The same plate is shown in panels (i-iii) but the image settings have been changed. Panel i) is a grayscale image, ii) following application of a colour wheel and iii) demonstrating the effect of narrowing the range of colour used to depict different fluorescence intensities. The following imaging protocol was used: (exposure time: 60 seconds, 4x binning, f-stop: 2.51, field of view: 158.5, focal plane: 9.4mm). Fluorescence gray scale images were artificially coloured for depiction purposes according to a colour scale set to the highest and lowest levels of mean fluorescence intensity (red and purple indicate maximum and minimum light intensity respectively). MFI=Mean fluorescence intensity.

The fluorescence of the anti-E-selectin and DNP dye labelled conjugate relative to the concentration of antibody using the Kodak fluorescence reflectance imaging device was then determined by measuring the mean fluorescence intensity (MFI) of each well taken from the digital images depicted in Figure 3-11. It is important to note that the underlying measurement of MFI expressed as arbitrary units will remain constant. This is irrespective of whether the image had been adjusted for either grayscale or colour, or whether the colour wheel has been changed to represent a narrower range of mean fluorescence intensity as depicted in Figure 3-11(iii).

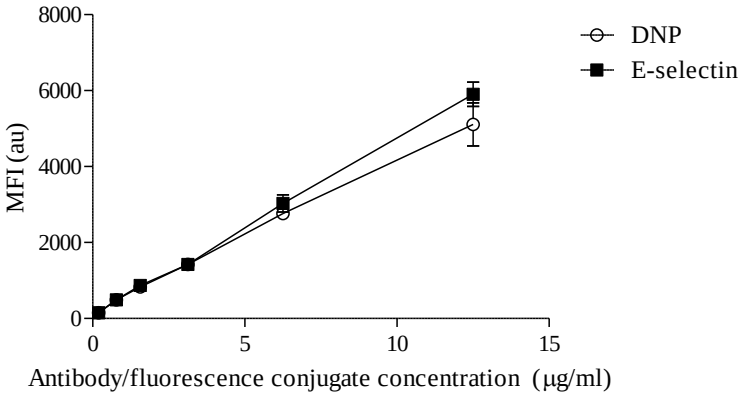

Figure 3-12 Quantification of fluorescent signal using fluorescent reflectance imaging

Figure demonstrates results of quantifying fluorescent images obtained after placing a 96 well plate containing dye labelled anti-E-selectin or control antibody diluted in serial 1:2 dilutions with a highest concentration of 12.5µg/ml and lowest of 0.2µg/ml. This shows a linear relationship for both samples taken under the following settings: (Exposure time: 60 seconds, 4x binning, f-stop: 2.51, field of view: 158.5, focal plane: 9.4mm). Regions of fluorescence were quantified by taking a mean fluorescence signal level from a circular area around each well.

The above figure demonstrates that the concentration of dye antibody conjugate *versus* MFI was identical for both anti-DNP and E-selectin antibodies and that there was a linear relationship between the concentration of either dye antibody conjugate and emitted MFI following excitation at 730nm and measured emission at 770nm. This data also delineates a threshold for detection of fluorophore dye/antibody conjugate with the current image settings. The minimal concentration of antibody/fluorescence conjugate used is 19.53ng/ml and this returned a MFI signal of 148.1 arbitrary units (au). This is well within the range of error for mapping

fluorescent images, particularly in the inflamed mouse paw as discussed in Section 3.3.6. Care was therefore taken to ensure that the parameters for imaging were kept constant for future experiments *in vivo* imaging experiments for accurate comparison of datasets.

3.3.6 Mapping Fluorescence Levels in Paw Inflammation: Using A ROI Tool to Accurately Quantify Signal

Following the *in vitro* studies described above, a technique was required that could reliably sample and quantify the degree of fluorescent signal within mouse paws *in vivo*. Selecting a circular region of interest is an appropriate technique for quantifying signal from a fixed, uniform source of emission such as from an ELISA plate as depicted in Figure 3-12. Signal from an irregular, variably sized paw where signal may be homogenous may require a different technique. Placement of a circular region of interest (ROI) could either under or over estimate fluorescence signal intensity depending on positioning and may also be affected by bias. Sequential circular, fixed regions of interest were compared to applying regions of interest using a mapping tool (Figure 3-13(i)). The latter technique maps a line to the point of maximal difference between an area of increased signal intensity and lower levels as depicted in Figure 3-13(ii), in mice injected with TNFα into the right paw. When quantifying signal the intensity of light emission from each pixel can either be expressed as a mean or net amount (with background levels of fluorescence subtracted). Figure 3-13(iii) demonstrates that both mean and net scores return a similar distribution of signal when taking a region of interest of the whole paw for analysis. While there may be, a degree of variable signal throughout a mouse paw due to increases in signal from isolated areas of E-selectin expression due vascular activation the overall value for each paw has been used. The resolution of fluorescent imaging device may not be sufficient to delineate changes in specific areas of the mouse joint such as individual metatarsal joints which measure ~0.1mm. In addition since there is no method to determine the depth of tissue from which fluorescent signal is emitted from accurate comparisons between groups would be problematic.

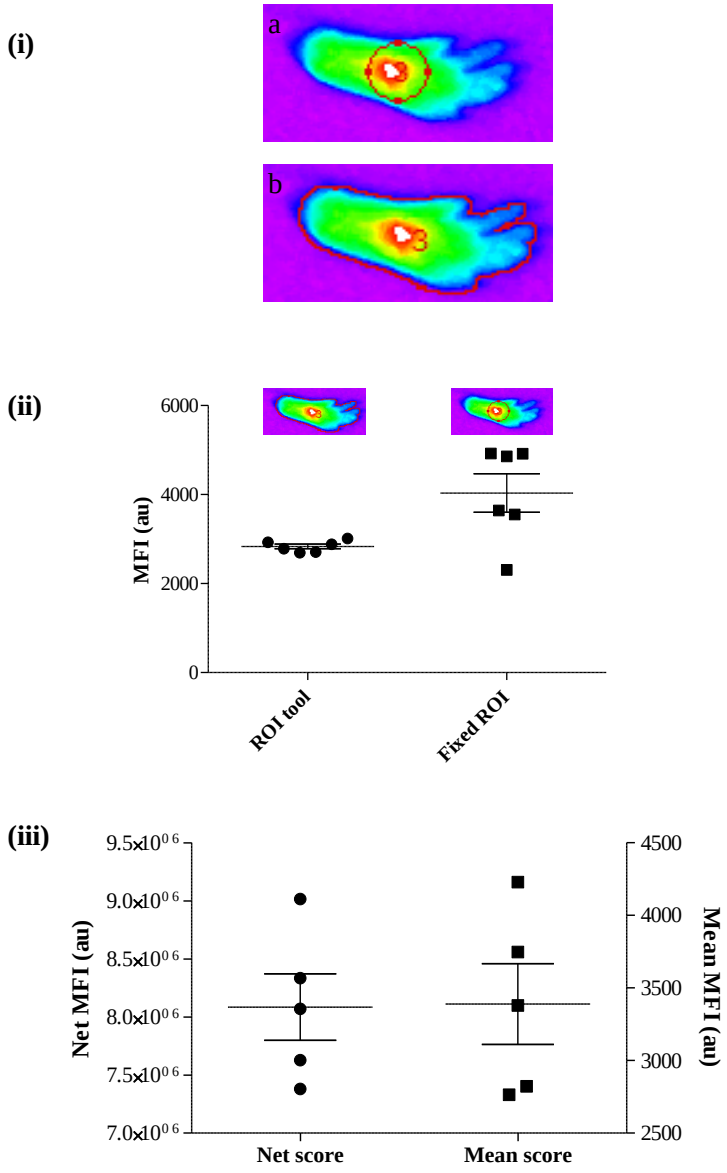

Figure 3-13 Techniques for mapping fluorescent intensity levels in paw inflammation

Representative images taken following injection of anti-E-selectin antibodies labelled with Dylight 750 nm Near Infra Red fluorophore (50µg i.v.). Paw swelling was induced by the intraplantar injection of murine TNFα (50ng) into the right paw. Panel (i) depicts images of measuring pixel intensity by a fixed circular ROI (a) and using an automated mapping tool (b). All readings were taken from a single inflamed paw. Panel (ii) shows the quantification of mean fluorescence intensity by using either the ROI tool or by using a fixed ROI. (iii) Mean and Net scores are represented from 5 mice with inflamed paws at 8 hours following injection of TNFα into the footpad. The mean score is calculated by taking the mean of the fluorescent signal returned from all pixels within the ROI. The net score is the total of the fluorescent signal returned from all pixels intensity signal with a mean of the ROI perimeter subtracted. Mean ± SEM are indicated.

3.4 Discussion

My objectives in this chapter were to demonstrate that both anti-E-selectin and DNP isotype control antibodies can be reproducibly produced from cell culture. My second objective was ensure that that labelling with a NIR dye had resulted in satisfactory dye to target ratios and that free dye has been removed from the resulting conjugate. I have ascertained that anti-E-selectin antibody can bind to both E-selectin and to TNFα stimulated EC. Finally the parameters and potential method of quantifying fluorescent images have been explored. NIR imaging at wavelengths of 700-800nm in a DBA/1 mouse model is optimal to ensure auto fluorescent signal returned from tissue is minimised. The increase in signal seen at lower wavelengths is due to fluorescent emission from primarily deoxygenated and oxygenated haemoglobin (Weissleder and Ntziachristos 2003). This observation has important implications for assessing the overall sensitivity of FRI to delineate a specific molecular target. Higher background autofluorescence levels would significantly decrease the sensitivity of the system (i.e. the ability to detect a minimal amount of fluorescence signal returned from a specific molecular target).

I have confirmed that a NIR fluorophore can be bound to both anti-DNP and E-selectin antibodies reproducibly and that an appropriate ratio of fluorophore to antibody can be achieved. This is vital to ensure that the bound fluorescently labelled antibody will return adequate brightness following illumination for it to emit signal that can be detected externally by the fluorescent reflectance imaging device. Over-labelling of the antibody can cause auto quenching of the conjugate and hence decrease fluorescence levels. While it is clearly paramount that the optical conjugate is as bright as possible it is also interesting to note that it appears from the images of EC that anti-E-selectin antibody is rapidly internalised and can be visualised within the cells as discrete areas of increased fluorescence. If for example the conjugate was internalised and then the fluorophore could be engineered to dissociate from the target molecule the fluorescent signal would then increase and this could be an effective way of localising the fluorophore to its intended location. This has been explored by labelling a monoclonal antibody target with up to 7 fluorophores that were then found to dissociate following binding, thereby increasing fluorescence at the intended target (Ogawa, Regino et al. 2009). Anti-E-selectin labelled fluorescence labelling does not affect epitope recognition.

It was then necessary to ensure that the conjugation process had not affected the binding of antibody for its intended molecular target. This was confirmed by both ELISA and a cell based assay of EC that had been stimulated with TNFα. This system also helped to confirm the time course of E-selectin expression following stimulation with TNFα. This is of relevance particularly when investigating the parameters of E-selectin expression following injection of TNFα into the mouse footpad. The time course of E-selectin expression also reflects that seen by previous investigators when E-selectin is induced on EC in response to pro-inflammatory cytokines involved in RA such as interleukin (IL)-1β and TNFα (Pober, Gimbrone et al. 1986; Wellicome, Thornhill et al. 1990). The analysis of pixel intensities returned from digitised images and from labelled E-selectin and DNP antibodies demonstrates a linear relationship between antibody/fluorophore concentration and Mean fluorescence intensity. The ability to understand clearly both the composition of a digital image and how it may be quantified, with a reproducible measuring technique was clearly vital for performing quantification when undertaking *in vivo* imaging experiments.

The following chapter details how an acute model of inflammation may be used to determine the parameters of targeted *in vivo* fluorescent imaging. The effects of TNFα injection into the paw are investigated. Increased E-selectin expression is demonstrated by immunohistochemistry, and the use of *in vivo* fluorescent imaging to detect specific E-selectin targeted signal is investigated.

CHAPTER 4

4 RESULTS: ESTABLISHING AN ACUTE MODEL OF INFLAMMATION FOR *IN VIVO* FLUORESCENCE IMAGING

4.1 Introduction

In the previous chapter I demonstrated that E-selectin could be targeted by anti-E-selectin antibody following its conjugation to a NIR fluorophore. Following the *ex vivo* fluorescence imaging described in Section 3.3.5, my subsequent aim was to use this conjugate to quantify E-selectin expression by detecting NIR fluorescence *in vivo.* Fluorescence imaging has been used previously to detect arthritis and the ability of fluorescence imaging to detect both non-specific uptake of dye to sites of inflammation (Hansch, Frey et al. 2004) and also detect antigen targeted dye deposition (Hansch, Frey et al. 2004; Chen, Mahmood et al. 2005) is discussed in Section 3.3.6. These studies have unpinned the potential use of fluorochrome imaging in the NIR for the detection of inflammatory changes in experimental arthritis.

An acute model of inflammation was required for *in vivo* imaging studies to determine whether E-selectin could be detected early in the inflammatory response, prior to exploring the parameters of fluorescence imaging in murine CIA, which is a complex model of arthritis characterised by significant heterogeneity in time of onset, incidence and disease severity. Therefore, while setting up novel imaging equipment and determining the parameters of imaging *in vivo*, an acute model of inflammation would best serve this purpose. This would also ensure that appropriate numbers of animals could be used for controls, experiments could be performed quickly and efficiently, whilst also minimising animal redundancy because incidence would be 100%. In my preliminary work (not described in this thesis), I investigated the effect of zymosan injections into the mouse paw. This technique is recognised to produce an acute, intense inflammatory reaction with severe joint swelling. Prior work by Gado and Gigler has investigated this model to explore the parameters of pain pathways. The development of these models is discussed in Section 1.4.2. In their experiment, the rat paw was injected with 0.1ml of a 2% suspension of zymosan and this caused a 90% increase in paw volume (Gado and Gigler 1991). My preliminary qualitative findings also confirmed that animals develop an intense degree of paw oedema. I therefore considered that the modulation of an inflammatory model by a single

cytokine may generate a less complex inflammatory process that did not lead to such significant levels of oedema. Since TNFα is a central regulator in CIA as well as in RA, I explored whether this cytokine could be used to develop an acute inflammatory response. The role of TNFα in CIA was primarily demonstrated by investigating the effect of TNFα blockade. The abrogation of arthritis in this animal model provided the pre-clinical data demonstrating that blockade of TNFα was a viable therapeutic target for patients with RA (Williams, Inglis et al. 2005). TNFα injections into the footpad have also been used to investigate mechanisms of hyperalgesia. Prior work on this model is discussed in the introductory Section 1.4.2.

TNFα, IL-1 and bacterial lipopolysaccharide all transcriptionally induce the expression of E-selectin, an adhesion molecule expressed in RA and the target of the antibody characterised in Chapter 3. Work on human endothelioma cell lines has shown expression of the protein to reach maximal levels 4-6 hours after stimulation with TNF with a decline to basal levels at 12-16 hours (Pober, Lapierre et al. 1987; Wellicome, Thornhill et al. 1990). Similar expression kinetics were also shown on mouse endothelioma cell lines, with maximal cell surface expression at 4 hours when stimulated with TNFα (Weller, Isenmann et al. 1992; Hahne, Jager et al. 1993). Furthermore, my own results described in Chapter 3 have shown that TNFα upregulates E-selectin expression in mouse PY4.1 endothelial cells. This therefore confirms that the expression kinetics of E-selectin are well suited to investigation with an acute inflammatory model.

A well validated target antibody, labelled to a NIR fluorophore with confirmed binding to recombinant E-selectin and to E-selectin expressed on TNFα-stimulated EC, as well an isotype control antibody, were both now ready. These could be tested in an acute model of inflammation to explore the parameters of *in vivo* imaging, as described in Chapter 3. My objective was therefore to investigate the specificity of localised antibody binding *versus* non-specific trafficking to sites of inflammation. By utilising the above target and control antibody I aimed to delineate the **sensitivity** of the system (differences between background autofluorescence and dye-labelled antibody generated signal intensity); and the **specificity** of binding (differences between anti-E-selectin *versus* anti-DNP generated fluorescent signal intensity).

Finally, a number of different anti-TNFα MoAbs have now been shown in clinical trials to be effective in patients with severe RA. This mode of therapy for RA is discussed in Section 1.1.2. In addition to chimeric or humanised monoclonal antibodies that are in clinical use for TNF blockade in RA, various TNF receptor based biologics have also been tested and shown to be effective. The most significant of these in current clinical use is etanercept, a dimeric TNF receptor type II-Fc fusion protein (Moreland, Baumgartner et al. 1997). I have investigated the use of this drug to prevent TNFα-induced paw swelling and have shown that this can also be detected by E-selectin targeted *in vivo* fluorescent imaging, thereby validating this as an *in vivo* molecular imaging technique.

4.2 Objectives

i. To develop a cytokine-mediated acute model of inflammation that has a 100% incidence, an acute time course, is dose dependent and reproducible

ii. To demonstrate that TNFα injection into the paw causes increased E-selectin expression that can be detected by immunohistochemistry

iii. To investigate whether TNFα injection into the paw causes increased E-selectin expression that can be detected *in vivo* by fluorescently labelled anti-E-selectin antibody

4.3 Results

4.3.1 The TNFα–Induced Model of Acute Paw Inflammation

Acute paw swelling caused by local injection of TNFα was developed as a reproducible acute model of paw inflammation *in vivo*. This was a prelude to exploring the parameters of *in vivo* fluorescence imaging. While this model has been used to investigate the mechanism of pain, and while paw swelling has been recognised to be caused by TNFα (Cunha, Poole et al. 1992; Woolf, Allchorne et al. 1997; Campos, Souza et al. 1998), further delineation of the TNFα-induced response was required to ensure that it was an acute, reproducible, dose dependent model of inflammation where increased E-selectin expression could be demonstrated. A representative example of paw swelling induced by the intraplantar injection of TNFα is demonstrated in Figure 4-1.

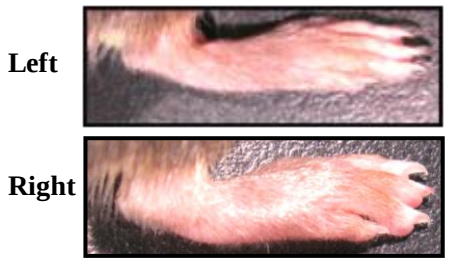

Figure 4-1 Representative example of paw swelling following the intraplantar injection of TNFα

Paw swelling was induced by intraplantar injection of murine TNFα 50ng into the right mouse paw in C57/BL6 mice. A representative image of the right mouse paw at peak paw swelling (4-6 hours) is demonstrated. The uninflamed, contralateral, left, uninjected paw is also shown.

This figure demonstrates that following TNFα injection the paw is uniformly oedematous. Paw swelling was evident on both dorsal and plantar surfaces. Following a 50ng injection of TNFα, at the 4 hour time-point the mean paw thickness would be expected to increase by a mean of 0.4mm from 2.1mm to 2.5mm – an increase of 19.1% (n=5 animals).

4.3.1.1 Measurement of acute paw swelling induced by TNFα: a dose dependent transient increase in paw thickness

Injection of between 5 and 100ng of TNFα into the mouse right foot-pad produced a transient dose-dependent right paw swelling that peaked at 4-6 hours post-injection and resolved within 24 hours, with a 100% incidence, thereby reducing animal redundancy. Paw swelling was assessed by measuring the maximal thickness between the dorsal and planter surfaces of the paw using microcalipers and calculating the change in thickness for each inflamed paw as demonstrated in Figure 4-2. This experiment confirmed that injection of an identical quantity (10µl) of vehicle (PBS with 1% mouse serum) did not produce any swelling of the mouse paw. Following injection of TNFα (50ng), there was also no evidence of swelling in the contralateral left paw (LP); this is investigated in more detail in Figure 4-3. By 24 hours following injection of TNFα, visible paw swelling had resolved and there was no difference in paw thickness compared to time 0. In separate experiments I have also confirmed that there were no secondary or biphasic increases in paw swelling at later time-points (not shown).

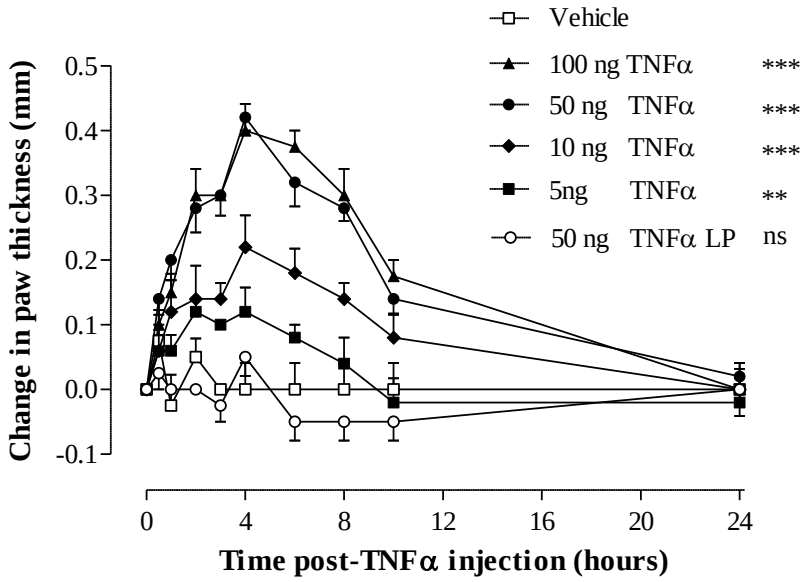

Figure 4-2 TNFα induced paw model: paw swelling is dependent on the dose of TNFα

Transient paw oedema was induced by intraplantar injection of mouse TNFα (5-100ng) into the right paw of C57/BL6 mice (n=4-5 per group). Vehicle (PBS) injected-mice were used as a control. Paw thickness of the contralateral left paws (LP) of animals injected with TNFα (50ng) are also shown. Data were analysed by 2-way ANOVA *versus* vehicle: ** $p<0.01$, *** $p<0.001$, ns=not significant.

I also investigated whether there were any systemic effects following injection of TNFα into the right paw, by determining whether there was any contralateral paw swelling. At doses of up to 50ng of TNFα, no swelling of the left uninjected (contralateral) paw occurred (also shown in the experiment illustrated in Figure 4-2), although there was transient contralateral paw swelling when 100ng of TNFα was injected. However, this effect was not statistically significant when compared to vehicle-injected mice. This is demonstrated in Figure 4-3, and suggests that this concentration of locally injected TNFα was having a systemic effect. For future experiments it was important to select a dose of TNFα that did not produce changes in contralateral paw thickness since this paw serves as an internal control for measuring mean fluorescence signal as described in the following sections. Subsequent studies for *in vivo* imaging therefore all utilised 50ng TNFα to induce paw swelling.

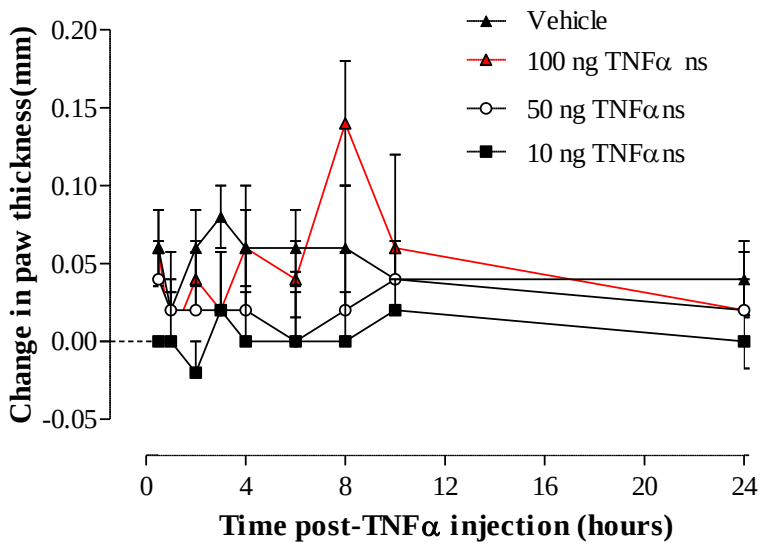

Figure 4-3 Demonstration of systemic action of TNFα following injection

Transient paw oedema was induced by intraplantar injection of mouse TNFα (5-100ng) into the right paw of C57/BL6 mice (n=5 per group). Vehicle (PBS) injected-mice were used as a control. Paw thickness of the contralateral left paws (LP) of animals is shown. Data were analysed by 2 way ANOVA *versus* vehicle: ns=not significant.

To confirm that anti-E-selectin antibody did not have any effect on paw swelling following the injection of TNFα (as a pre-requisite to imaging studies), animals were pre-injected intra-venously (i.v.) with different quantities of either anti-E-selectin or DNP antibodies. The data in Figure 4-4a demonstrate that anti-E-selectin antibody does not have a measurable effect on paw thickness at doses of either 5 or 50μg, given by i.v. injection 1 hour prior to the subsequent intraplantar injection of TNFα. Similar data were obtained for anti-DNP antibody (Figure 4-4b).

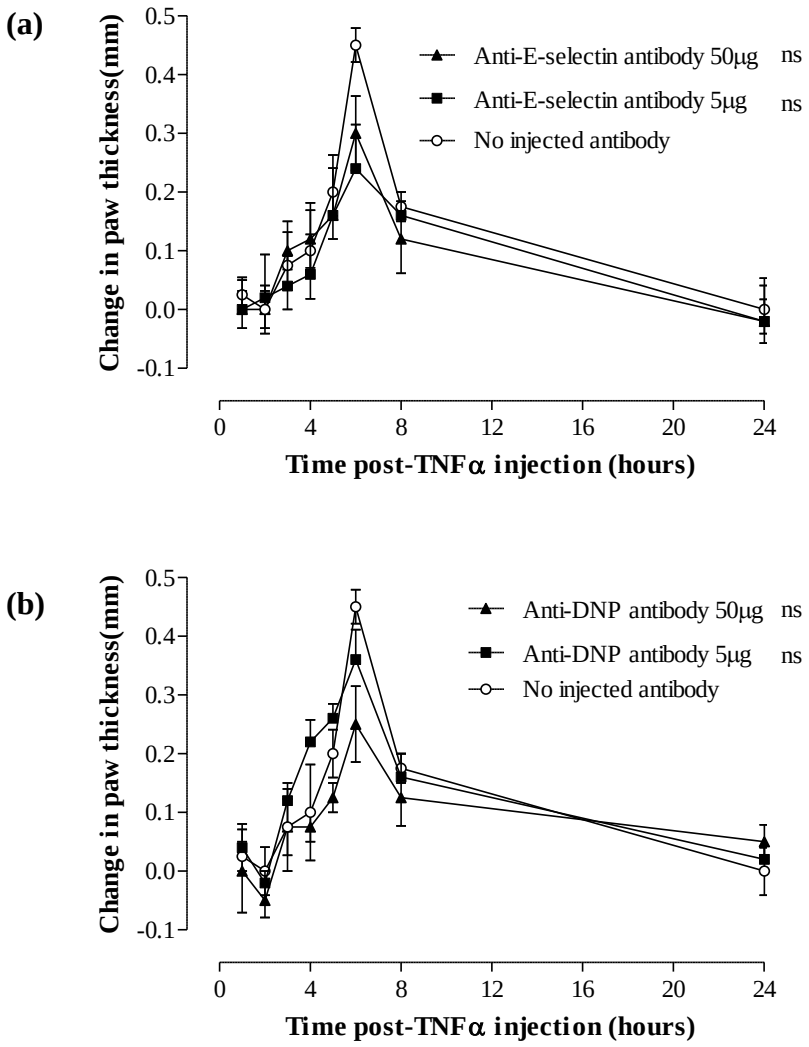

Figure 4-4 Effect of pre-injection of anti-E-selectin on TNFα induced paw swelling

Paw swelling was induced by the intraplantar injection of murine TNFα 50ng into C57/BL6 mice (n=4-5 per group). Mice had been pre-injected with anti-E-selectin antibody (a) or anti-DNP antibody (b) at doses of 5 or 50μg (i.v.) 1 hour prior to the induction of paw swelling using TNFα. Graph demonstrates mean change in paw thickness over time. Data were analysed by 2-way ANOVA *versus* animals not injected with antibody: ns=not significant.

4.3.2 Histological Changes in TNFα-Induced Paw Inflammation Model

Histological specimens were also taken at various time-points following the induction of inflammation by injection of TNFα into the footpad, to study the time-course of inflammation and potentially E-selectin expression. Figure 4-5 shows that 4 hours after TNFα injection, there is a marked inflammatory infiltrate in the footpad, but this had resolved by 24 hours.

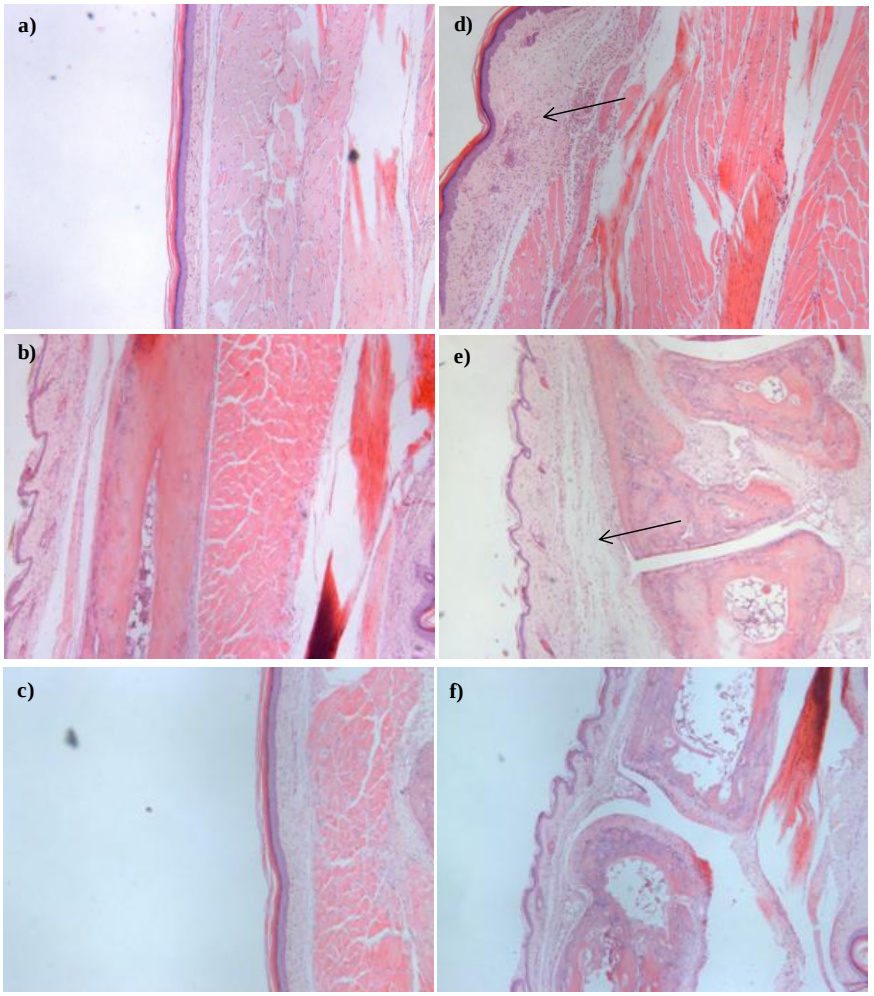

Figure 4-5 Comparison of paw inflammation in TNF injected and PBS injected mouse paws following injection

C57/BL6 mice were injected with 50ng TNFα into the right paw d,e) or uninjected left paw a,b). Paw sections were stained using haematoxylin and eosin. Images were taken at x20 magnification. These representative images demonstrate that there is no paw inflammation or cellular infiltrate at the base of the footpad at 4 hours in the left paw (a,b), whereas TNFα induced an inflammatory infiltrate in the right paw, as indicated with arrow (d,e). No inflammation was detected in the right paw at 24 hours following TNFα injection (c,f).

Further specimens were taken at early (2 hours), mid (6 hours) and late 72 (hours) time-points to confirm that there was both an influx of inflammatory cells and that there was subsequent resolution (data not shown).

E-selectin expression in the paw oedema model was then explored. This is shown in Figure 4-6. This demonstrates that increased binding of anti-E-selectin antibody can be detected at 4 hours following injection of TNFα into the footpad. Increased antibody binding is localised to areas where there has been substantial inflammatory infiltrate. This is likely to represent increased E-selectin antibody binding to sites of increased E-selectin expression in microvessels where the endothelium is activated due to the local injection of TNFα.

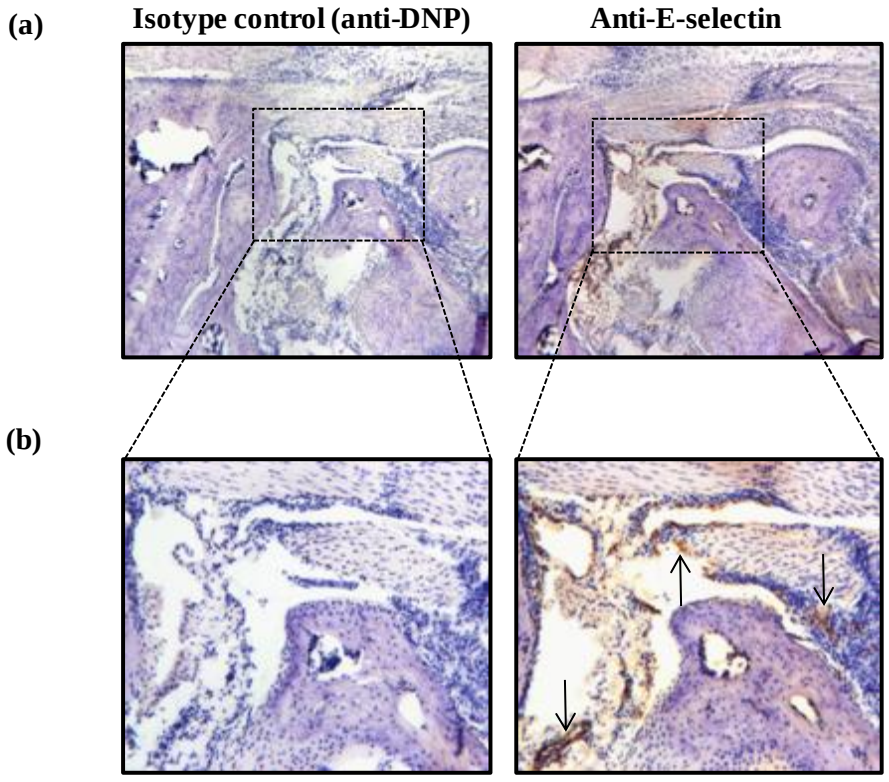

Figure 4-6 E-selectin expression in the TNFα-induced paw oedema model

Representative histological images of paws harvested 4 hours following induction of paw oedema by intraplantar injection of TNFα (50ng) in C57/BL6 mice. Serial sections were stained with either anti-E-selectin antibody or isotype control antibody (anti-DNP). Immunostained sections were counter-stained with haematoxylin. Images show the metatarsal joints of mouse paws. (a) Original magnification x 40, with further magnification depicted in (b). Increased staining at sites of inflammation is shown by arrows.

4.3.3 E-Selectin Targeted Fluorescence Imaging *In Vivo*: Quantifying Endothelial Activation *In Vivo* In TNFα-Induced Paw Oedema

Having established TNFα-induced paw swelling as a reliable and reproducible model of paw inflammation, characterised by expression of E-selectin and by neutrophil infiltration, my study then aimed to investigate anti-E-selectin antibody trafficking *in vivo*. To study NIR fluorescently labelled anti-E-selectin antibody trafficking *in vivo*, images were obtained at different times following injection of NIR fluorophore labelled anti E-selectin antibody followed by induction of paw swelling with 50ng TNFα, and compared with the signal obtained from isotype control anti-DNP antibody. Visual representation of the changes in fluorescence signal intensity was obtained by applying a colour wheel graded to signal intensity (Figure 4-7). These images suggest that E-selectin antibody localised selectively to the TNFα-injected right paw to a greater extent than control antibody, particularly at early time-points after TNFα injection.

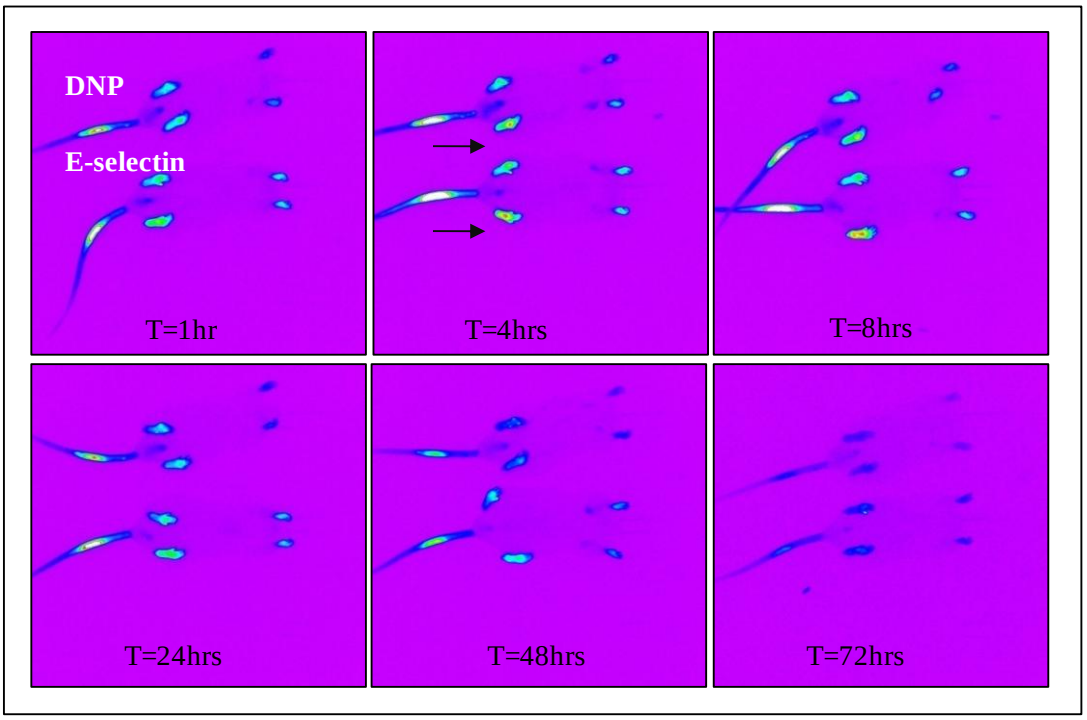

Figure 4-7 TNFα-induced paw swelling can be detected by E-selectin targeted NIR fluorescent imaging

Following injection of either anti-E-selectin or anti-DNP antibodies labelled with Dylight 750 nm Near Infra Red (NIR) fluorophore (50μg, i.v.), paw swelling was induced by intraplantar injection of murine TNFα (50ng) into the right paw (indicated by arrow) of C57/BL6 mice. Fluorescence images were obtained at different time-points post-injection of TNFα and are shown from representative anti-E-selectin and anti-DNP-injected mice.

The following Figure 4-8 shows the fluorescent changes obtained from imaging at the 8 hour time-point. This is to demonstrate in closer detail the fluorescent image obtained from a mouse injected with either NIR fluorophore labelled anti-DNP antibody or anti-E-selectin targeted antibody. Figure 4-8b also shows the method for demarcating a region of interest around the mouse paw. The Mean Fluorescence Intensity (MFI) could then be calculated. The technique for this is detailed in Section 3.3.6. Animals were then kept in the same batches and placed in the same order for imaging throughout the time course of experiment, so that imaging time-points were kept as accurate as possible.

(a)

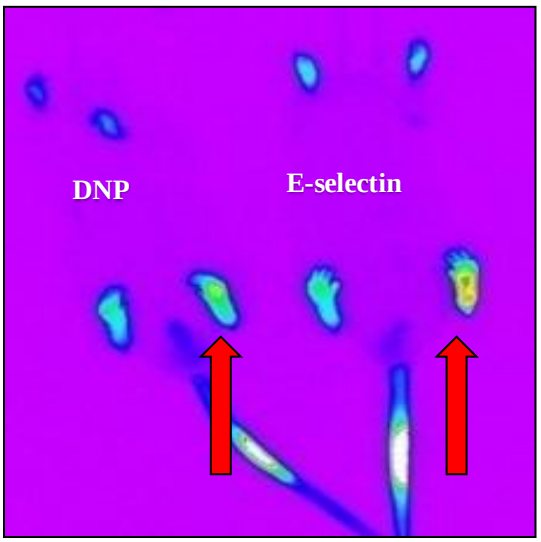

(b)

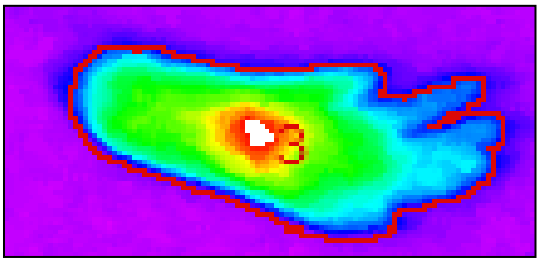

Figure 4-8 Demonstration of fluorescence images at the 8 hour time-point following injection of TNFα

Following injection of either anti-E-selectin or anti-DNP antibodies labelled with Dylight 750 nm NIR fluorophore (50µg, i.v.), paw swelling was induced by intraplantar injection of murine TNFα (50ng) into the right paw (indicated by arrows) of C57/BL6 mice (a). Panel (b) demonstrates the regions of interest taken from a representative mouse paw to determine levels of fluorescence.

Quantification of fluorescence intensity levels from regions of interest (ROI) of inflamed paws showed the dynamic changes of anti-E-selectin and anti DNP antibody signal in eight animals injected with either target or control dye-labelled antibody and then imaged in pairs. The signal in the right paws (RP) from both groups peaked 6-8 hours after injection and had largely returned to baseline at 72 hours following injection of antibody (Figure 4-9). Fluorescence signal was higher for anti-E-selectin-injected animals than for anti-DNP-injected mice. Furthermore, fluorescence signal was lower in the contralateral left paws (LP; not injected with TNFα) than in the RP for both anti-E-selectin and anti-DNP antibody-injected mice.

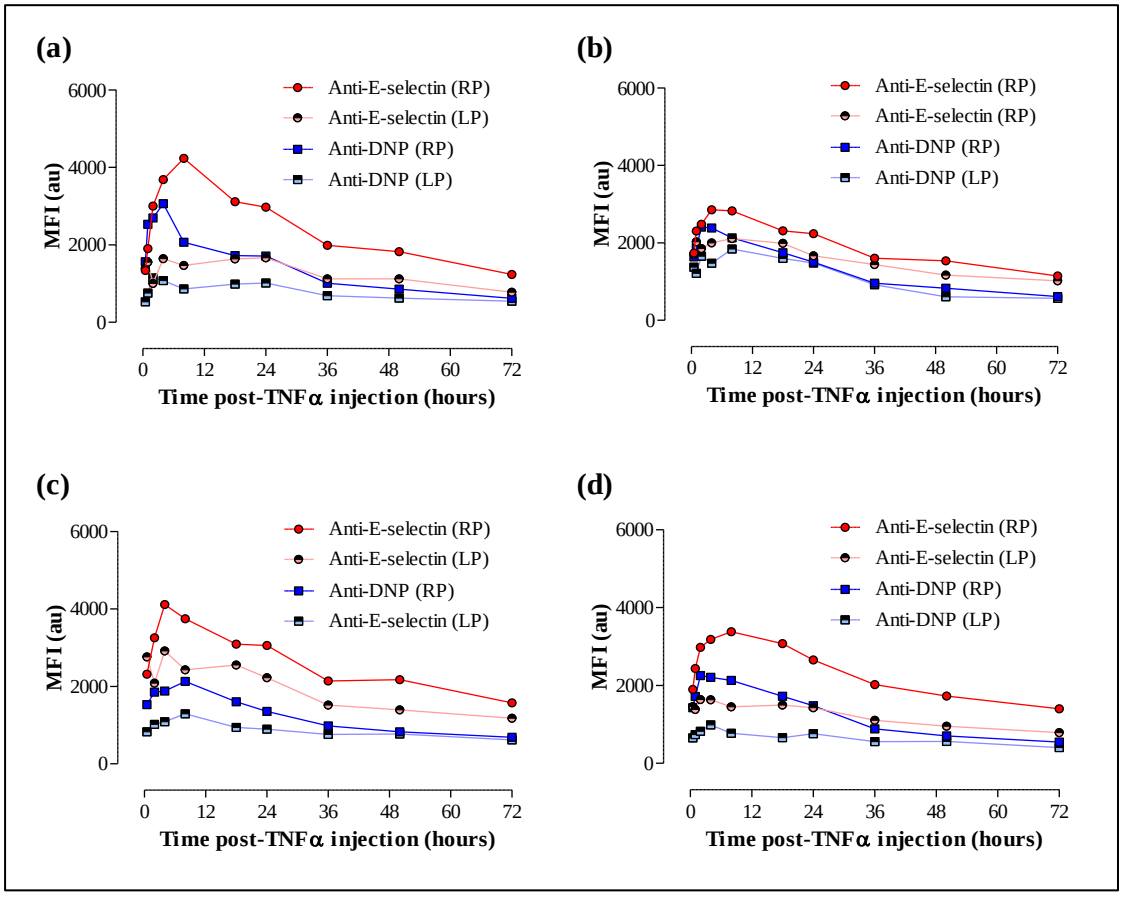

Figure 4-9 Quantification of E-selectin targeted NIR fluorescence in the TNFα-induced paw swelling model

Following injection of either anti-E-selectin or anti-DNP antibodies labelled with Dylight 750 nm NIR fluorophore (50µg, i.v.), paw swelling was induced by intraplantar injection of murine TNFα (50ng) into the right paw (RP) of C57/BL6 mice. Fluorescence images were analysed at different time-points post-injection of TNFα for pairs of anti-E-selectin and anti-DNP-injected mice. Mean Fluorescence Intensity (MFI) measurements in injected RP and contralateral left paws (LP) for 4 individual pairs of mice are shown in panels (a-d).

The mean fluorescence signal from all mice was then analysed, this is shown in Figure 4-10. These data show that there were significant differences ($p<0.001$) between the anti-E-selectin and anti-DNP antibody injected animals in terms of the fluorescence signal in the TNFα-injected right paws (Figure 4-10a). There were also significant differences between the anti-E-selectin and anti-DNP antibody injected animals in the contralateral left paws (LP; $p<0.001$), and in animals that were injected with dye-labelled antibody but did not receive any intraplantar injection of TNFα ($p<0.001$; Figure 4-10b). Further analysis of the control groups for this experiment is outlined in the next paragraph.

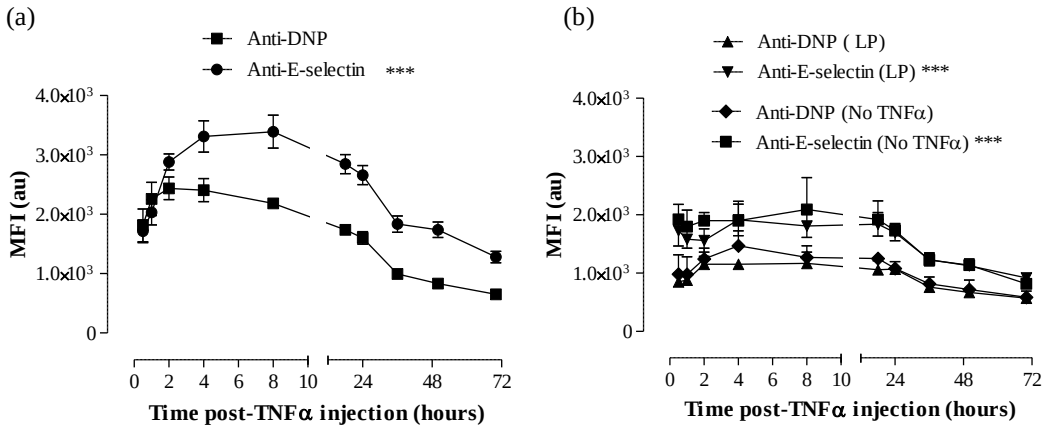

Figure 4-10 Quantification of E-selectin targeted NIR fluorescent imaging over time

Following injection of either anti-E-selectin or anti-DNP antibodies labelled with Dylight 750 nm NIR fluorophore (50μg, i.v.), paw swelling was induced by the intraplantar injection of murine TNFα (50ng) into the right paw of C57/BL6 mice. Panel (a) demonstrates right paw (RP) mean fluorescence intensity (MFI) at different time-points post-injection (n=5 per group). Panel (b) demonstrates the fluorescent signal returned from the contralateral left paws (LP) and also from paws of animals uninjected with TNFα (n=5 per group). Data were analysed by 2-way ANOVA comparing anti-DNP *versus* anti-E-selectin-injected mice: *** $p<0.001$.

Because there were differences between anti-E-selectin and anti-DNP injected animals (Figure 4-10b), I therefore considered how to account for this in order to make meaningful comparisons between anti-E-selectin targeted signal and the signal in animals injected with anti-DNP control antibody. To resolve these differences, the MFI of the control uninjected left paw (LP) was subtracted from each inflamed right paw (RP). This is demonstrated in Figure 4-11. This shows that there is a significant increase in E-selectin targeted signal relative to anti-DNP injected animals. This also demonstrates that the mean fold difference in corrected signal intensity of E-selectin to DNP is 1.72 at the 8 hour time point. This was the maximal fold difference for this experiment: the fold difference at 2 and 24 hours was 1.15 and 1.51 respectively.

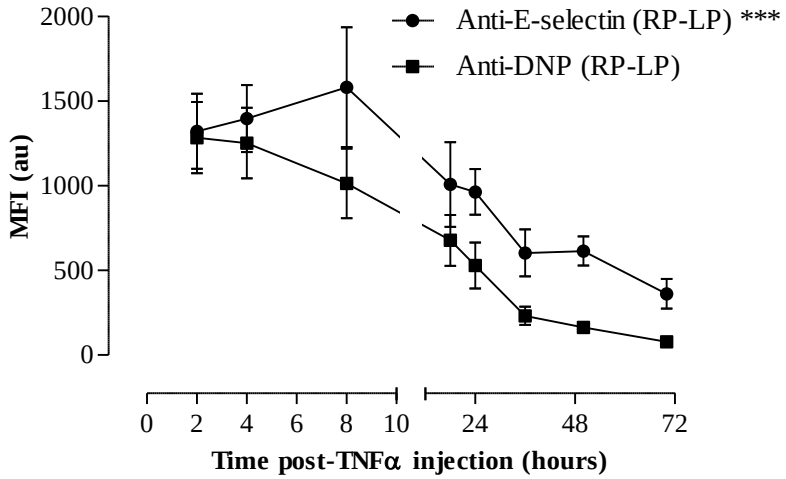

Figure 4-11 Mean fluorescence intensity following subtraction of control paw

Following injection of either anti-E-selectin or anti-DNP antibodies labelled with Dylight 750 nm NIR fluorophore (50μg, i.v.), paw swelling was induced by the intraplantar injection of murine TNFα (50ng) into the right paw (RP) of C57/BL6 mice (n=5 per group). The mean fluorescence intensity (MFI) of the left (uninflamed) paw (LP) has been subtracted from the MFI for each RP for each animal. Data were analysed by 2-way ANOVA: *** $p<0.001$.

Other methods of correcting for the difference in signal were considered. These included using an alternative vascular site on the mouse such as the snout so that this could serve as an internal reference. A redesign of the anaesthetic equipment resulted in this being technically difficult because the snout was contained within the anaesthetic nose cone. Another method was also considered. This was to subtract the values of fluorescent signal from earlier time-points. However these points are subject to significant variability in signal intensity. This is because of the short time period between injection of antibody and imaging may be different between injected groups

and initial clearance of dye may be more variable between animals. The *in vivo* parameters of these very early time-points may be technically more challenging to investigate since animals would effectively need to be continuously anaesthetised for imaging.

4.3.4 Reduction in Injected Antibody Dose Increases Signal Specificity

Further experiments were then performed to determine in more detail the effect of injected antibody dose on specificity for E-selectin and to assess further the measurement of signal in animals uninjected with TNFα. MFI was measured in both injected right paws and contralateral left paws of animals injected with different doses of antibodies (Figure 4-12a). Decreasing the dose of injected antibody from 50μg to 5μg increased the ratio of anti-E-selectin:anti-DNP signal from 1.15-fold to 2.13-fold(Figure 4-12b-c). Since injection of 5μg of antibody demonstrated optimal specificity for E-selectin targeted binding, this antibody dose was subsequently used for *in vivo* fluorescence imaging studies.

Interestingly there were small differences between fluorescent signal from anti-E-selectin and anti-DNP injected mice in the control (left) paws (Figure 4-12a) or between anti-E-selectin and anti-DNP fluorescent signal in animals not injected with TNFα in this series of experiments (not shown). This may be because of small differences in the labelling reaction, or antibody concentrations used in the first experiment. This was despite the prior attempts to generate similarly labelled anti-E-selectin and anti-DNP antibody concentrations and fluorophore ratios. In practice the calculation of dye/protein ratios by measuring absorbance at 280nm and at the peak absorbance of the fluorophore are subject to some variation and therefore may not compare to the degree of fluorescence following *in vivo* injection of the dye-labelled antibody conjugate.

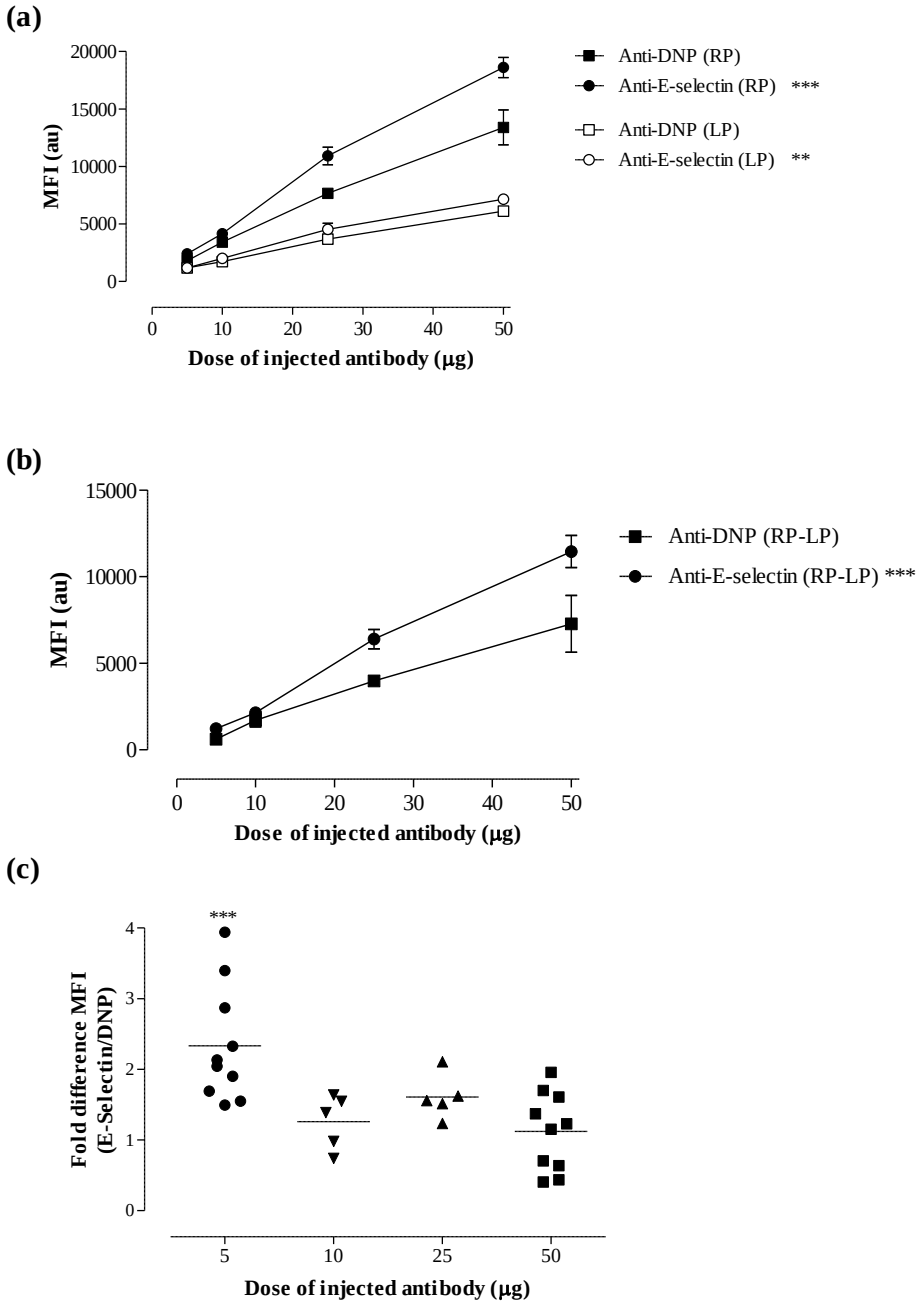

Figure 4-12 Effect of antibody concentration on target specificity

Following injection of either anti-E-selectin or anti-DNP antibodies labelled with Dylight 750 nm NIR fluorophore at doses of 5µg to 50µg i.v., paw swelling was induced in C57/BL6 mice by the intraplantar injection of murine TNFα. MFI has been quantified at the 8 hour time-point. (a) Data from right injected (RP) and left uninjected (LP) paws are shown (n=5-10 per group). Data are mean ± SEM, and were analysed by 2-way ANOVA *versus* anti-DNP injected animals: *** $p<0.001$. (b) Fluorescence levels from uninflamed paws (LP) were subtracted. Data are mean ± SEM, and were analysed by 2-way ANOVA *versus* anti-DNP injected animals: *** $p<0.001$. (c) Fold difference of E-selectin antibody MFI compared to control anti DNP antibody. Bars indicate mean values, and data were analysed by 1-way ANOVA with Bonferroni post-hoc correction *versus* 50µg antibody: *** $p<0.001$.

These experiments therefore suggested that 5μg of dye labelled antibody was optimal and subsequent studies utilised this dose. Figure 4-13a represents the results of an experiment designed to look more closely at both E-selectin targeted and control groups following injection of 5μg of dye-labelled control or anti-E-selectin antibody. This figure demonstrates that there is increased signal returned from anti-E-selectin antibody-injected animals (relative to anti-DNP-injected animals) at 2, 8 and 24 hours in the TNFα-injected right paws (RP) with only minor differences between control (left) paws (LP). Figure 4-13b demonstrates further detail of the signal at the 8 hour time-point from either left paws, or from animals that did not receive an injection of TNFα or those injected with the same volume of PBS and 1% mouse plasma into the right paw. The mean fluorescent signal following injection of either anti DNP or E-selectin antibody for control groups (either LP, no injection of TNFα or injection of PBS vehicle) is demonstrated. This shows that are no significant differences between the MFI returned from these groups at this time-point. Other time-points showed similar findings with regard to background signal. I was therefore able to subtract a mean background level of fluorescence from the mean of the left paw signal intensity to leave the specific signal (minus background) from control antibody or anti-E-selectin injected right paws at 8 hours following the intraplantar injection of TNFα. This is demonstrated in Figure 4-13c. The small levels of residual signal for the left paws represent the minor degrees of variation between injected animals following subtraction of the mean background signal.

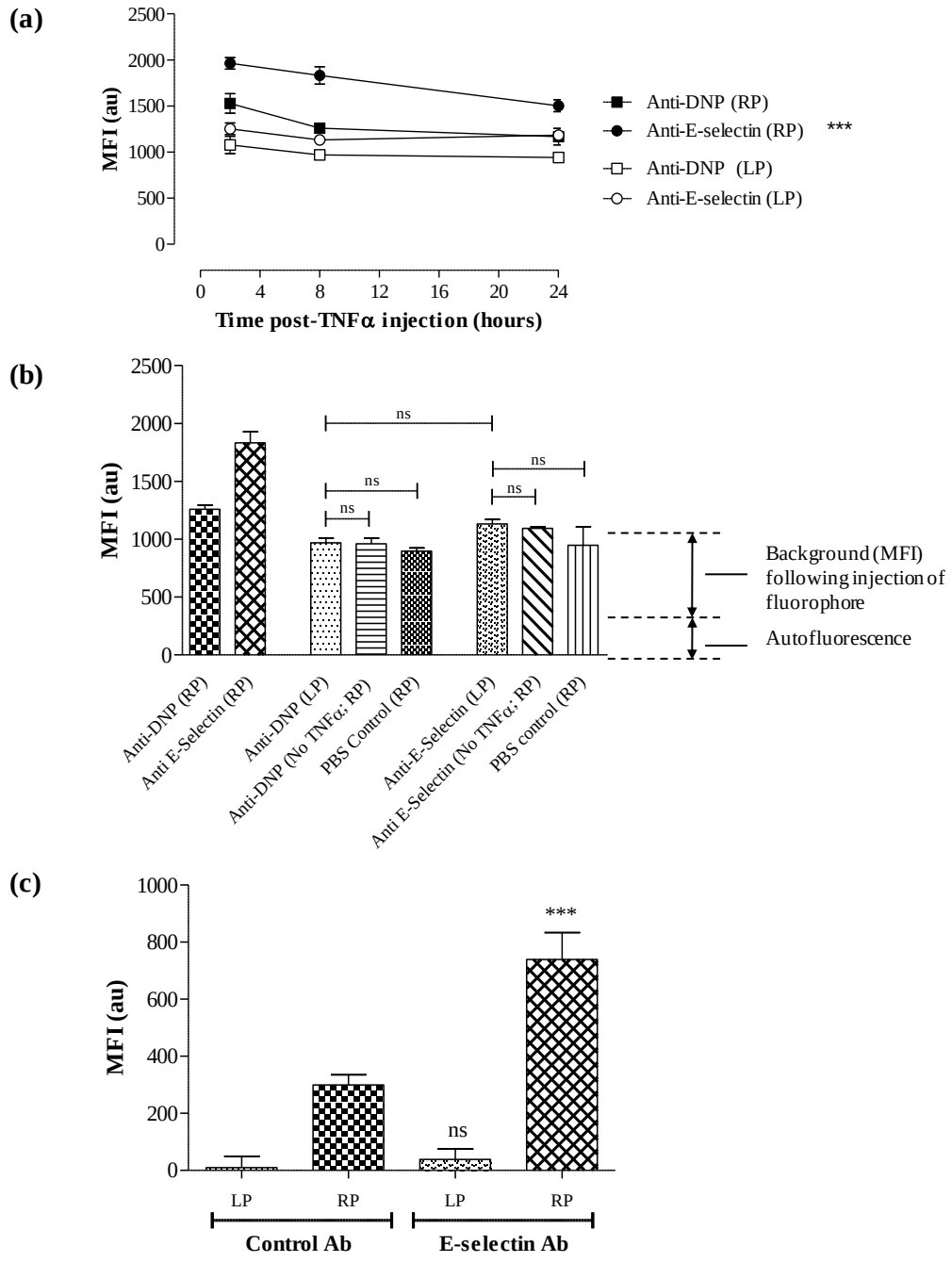

Figure 4-13 Mean fluorescence intensity: increased specificity at 5µg antibody

Following injection of either anti-E-selectin or anti-DNP antibodies labelled with Dylight 750 nm NIR fluorophore at a dose of 5µg i.v., paw swelling was induced by intraplantar injection of 50ng murine TNFα in C57/BL6 mice (n=4-6). Mean fluorescence signal (MFI) was measured between 2 and 24 hours (a). (b) Mean fluorescence signal (MFI) quantified at the 8 hour time-point is shown for right injected (RP) and uninjected (LP), as well as for uninjected (RP) controls (no TNFα or PBS control) to highlight the relative contribution of both autofluorescence and background mean fluorescence intensity. (c) The mean background intensity from control and anti-E-selectin targeted animals was subtracted. Data are mean ± SEM, and were analysed by 1-way ANOVA with Bonferroni post-hoc correction *versus* control antibody: *** $p<0.001$, ns=not significant.

The following Figure 4-14 demonstrates the relationship between the digital fluorescence images obtained and the quantitation of MFI. Figure 4-14a demonstrates a close-up detail of the fluorescence obtained at t=8 hours following injection of dye-labelled antibodies. The gradation in the colour wheel applied to signal intensity in the left hand figure is set over the range of mean fluorescence intensity as indicated in the right hand graph. Figure 4-14b shows how the mean background (mean left paw MFI for each group) fluorescence can be subtracted from the digital image by narrowing the range over which the gradation of colour represents MFI. In addition this image has also been overlaid onto a digital X-ray of the mouse taken at the same time point. In Figure 4-14c the MFI returned from control animals (injected with anti-DNP fluorescent labelled antibody) has also been subtracted. The threshold of the colour wheel has been set above calculated mean background MFI for injection of control antibody into TNFα injected paws. This image therefore represents the specific signal from anti-E-selectin targeted binding at 8 hours following induction of inflammation by injection of TNFα into the mouse paw.

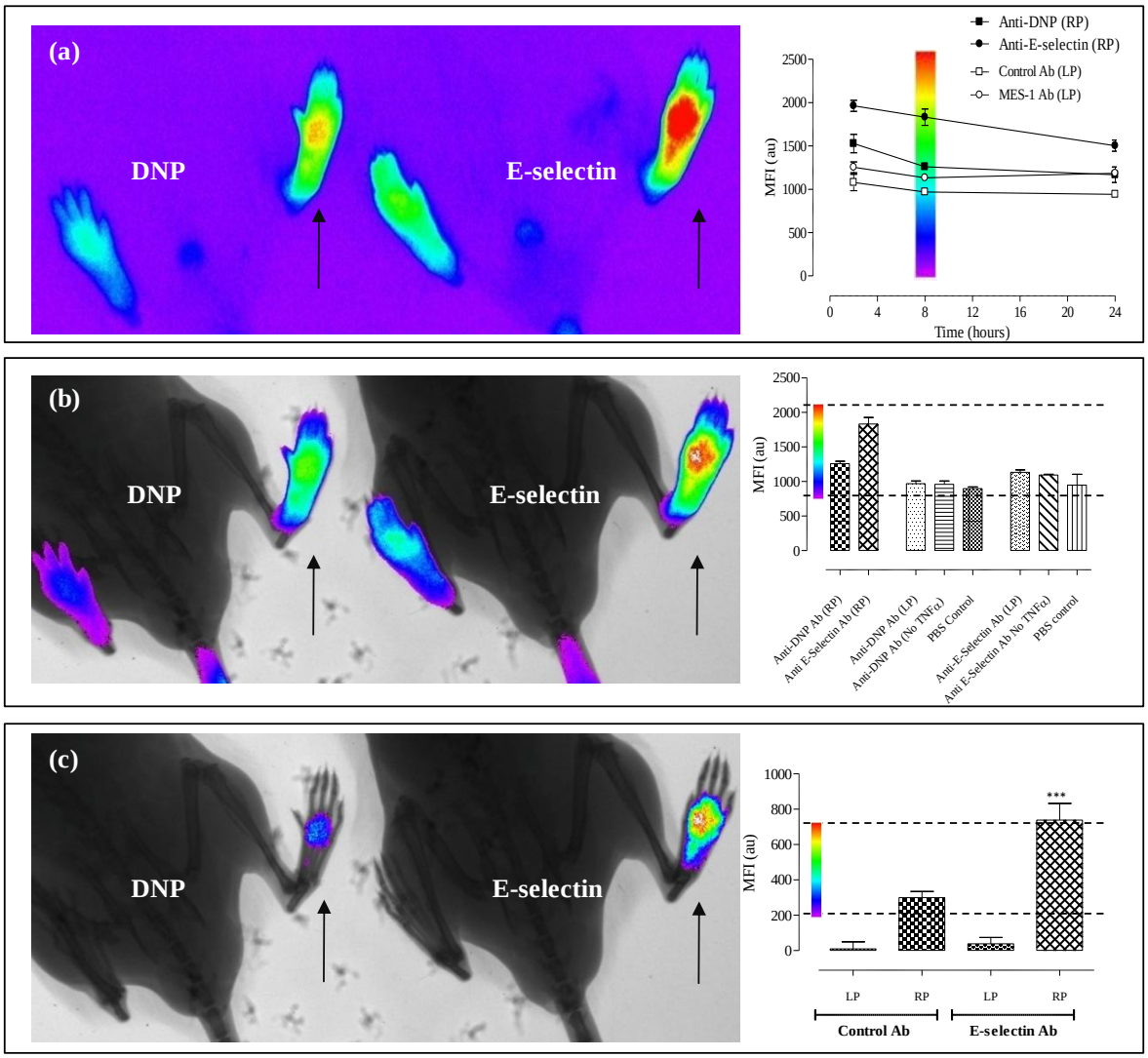

Figure 4-14 Specific anti-E-selectin targeted fluorescent signal co-registered with X-ray imaging

Following injection of either anti-E-selectin or anti-DNP antibodies labelled with Dylight 750 nm NIR fluorophore at a dose of 5µg i.v., paw swelling was induced by intraplantar injection of murine TNFα in C57/BL6 mice (n=4-6). Mean fluorescence signal (MFI) was measured between 2 and 24 hours (a). (b) Mean fluorescence signal (MFI) quantified at the 8 hour time-point is shown for different groups of mice. (c) The mean background intensity (mean MFI of LP data) from control and anti-E-selectin targeted animals was subtracted. In the left hand panel the corresponding fluorescent image overlaid onto a coregistered X-ray. The colour wheel to depict signal intensity has been adjusted to the range as shown on the graph (a,b,c).

4.3.5 E-Selectin Targeted Signal Can Be Abrogated By TNF Receptor Blockade

The purpose of this part of the study was to determine the effect of etanercept on TNFα-induced paw swelling, to further confirm the dependence of paw swelling on TNFα activity. Etanercept is an engineered TNFRII dimer with a fully human amino acid sequence linked to the Fc portion of human IgG_1. It has been effective in the abrogation of disease in CIA (Piguet, Grau et al. 1992; Wooley, Dutcher et al. 1993). It is in clinical use for the treatment of RA patients not responsive to conventional DMARDs (Moreland, Baumgartner et al. 1997; Moreland, Schiff et al. 1999). Firstly the effect of etanercept on TNFα-induced paw swelling by measuring paw thickness was investigated; this is demonstrated in Figure 4-15. This figure shows that the pre-treatment by etanercept (100μg, i.p.) 12 hours prior to induction of paw swelling with TNFα significantly abrogated the measured change in paw thickness. Indeed the paw thickness in animals which received TNFα plus etanercept was not significantly different from the left paw thickness of TNFα-injected mice. Similar results were obtained when etanercept was administered 4 hours prior to intraplantar injection of TNFα (not shown).

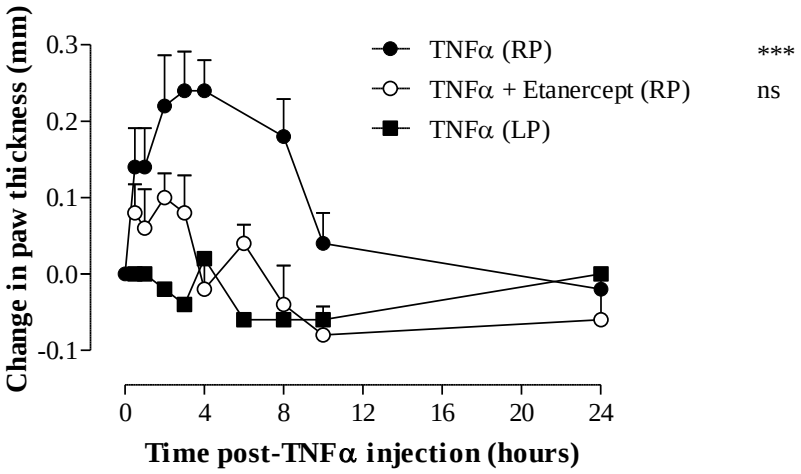

Figure 4-15 Etanercept abrogates TNFα-induced paw swelling

Paw swelling was induced by the intraplantar injection of murine TNFα (50ng) in C57/BL6 mice, which received a prior injection of soluble human TNFRII (100μg, i.p.) 12 hours before TNFα injection. Change in paw thickness over time was measured. Data are mean ± SEM (n=5 per group) and were analysed by 2-way ANOVA *versus* the contralateral left paw (LP) thickness of animals treated with TNFα alone: *** $p<0.001$, ns=not significant.

I therefore investigated whether E-selectin targeted fluorescent imaging was also capable of detecting this change. Animals were pre-treated with etanercept and then imaged at 2, 8 and 24 hours following induction of paw swelling by the intraplantar injection of TNFα. This is demonstrated in Figure 4-16, which shows that there was a significant 61.1% reduction in E-selectin targeted signal compared to control antibody signal. This demonstrates the considerable efficacy of etanercept in abrogating TNF dependent inflammation. There was also a reduction in the MFI of animals injected with dye-labelled control antibody but this did not reach statistical significance. This suggests that the E-selectin specific component to the fluorescent signal is reduced to a greater degree than the reduction in non-specific targeting of antibody to sites of inflammation. Since there is a significant reduction in paw swelling it would be expected that non-specific antibody uptake would also decrease. It is well recognised there is also a reduction in the non-specific trafficking of antibody into the site of inflammation due to changes in vascular permeability that occur at sites of inflammation, as discussed in Section 1.2.4.

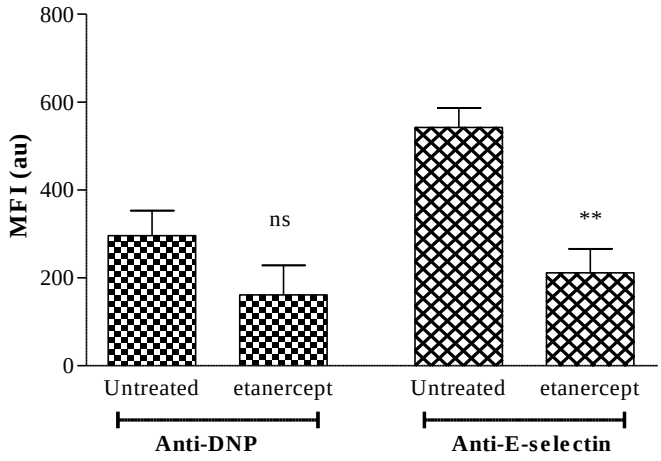

Figure 4-16 Etanercept abrogates E-selectin specific signal in inflamed paws

Following injection of either anti-E-selectin or anti-DNP antibodies labelled with Dylight 750 nm NIR fluorophore (5μg i.v.), paw swelling was induced by intraplantar injection of murine TNFα (50ng) in C57/BL6 mice. The effect of treatment using soluble human TNFRII (100μg, i.p.) 12 hours prior to TNFα injection is demonstrated. Mean fluorescence intensity (MFI) was measured at 8 hours. Mean background fluorescence levels from uninflamed left paws (LP) were subtracted. Data are mean ± SEM, and were analysed by 1-way ANOVA with Bonferroni post-hoc test *versus* untreated animals: ** $p<0.01$, ns=not significant.

4.4 Discussion

In this chapter my objectives were initially to develop an acute model of inflammation and to demonstrate E-selectin expression early in the time course of inflammation by immunohistochemistry. The model was then used to determine the parameters of E-selectin targeted *in vivo* imaging and to quantify E-selectin expression over the time course of inflammation. Induction of acute paw inflammation by the intraplantar injection of TNFα has been utilised successfully for this purpose. I have further been able to demonstrate that *in vivo* fluorescence imaging of E-selectin is a sensitive, specific and quantifiable method of detecting endothelial activation in an acute inflammatory model. The final objective was to determine the effect of a therapeutic intervention in abrogating paw swelling following injection of TNFα. This too has been demonstrated and the effect of this on targeted imaging has been quantified. This demonstrated that there was a significant decrease in E-selectin targeted imaging following pre-treatment with the soluble TNF receptor antagonist etanercept. Acute paw swelling caused by local injection of TNFα was initially investigated as a reproducible acute model of paw inflammation *in vivo*. The expression of E-selectin was then investigated by immunohistochemistry. In order to measure cytokines or other molecules in whole joints, sectioning of bone is required. This was technically difficult to perform on a cryostat as the small bones in a mouse paw will often splinter disrupting the architecture of histological specimens. Work was therefore undertaken to refine this technique. Some investigators have reported the detection of cytokines (IL-1β and RANKL) in paraffin fixed decalcified joint (Romas, Sims et al. 2002; Lubberts, Koenders et al. 2004) but the ability to detect many other cytokines will be lost following paraffin sectioning. Techniques have been developed at the Kennedy Institute for decalcifying tissue sections and then performing fresh frozen sectioning (Marinova-Mutafchieva, Williams et al. 1997; Gabay, Marinova-Mutafchieva et al. 2001). I therefore needed to develop a protocol for immunohistochemistry that ensured whole paw specimens could be processed and E-selectin expression demonstrated in the TNFα induced paw model. Measurements of paw thickness following TNFα injection confirmed that the change in paw thickness over time is reproducibly dependent on the dose TNFα. Immunohistochemistry demonstrated the expression of E-selectin following at early time points following the injection of TNFα. The application of immunohistochemistry techniques developed in this model

could then also be used to investigate the *in vivo* expression of E-selectin in CIA. Application of antibodies labelled with NIR fluorophore in the TNFα-induced paw model, allowed measurement of levels of signal from uninflamed paws to determine signal sensitivity (E-selectin antibody signal *versus* background), whereas comparing control antibody injected groups to those injected with anti-E-selectin antibody determined signal specificity (anti-E-selectin *versus* anti-DNP antibodies). Subtracting background signal (mean signal intensity of uninflamed left paws) from the signal obtained from inflamed right paws ensured variations due to injection differences were excluded. The time course of anti-E-selectin antibody binding over 6-8 hours in this model is in keeping with previously found kinetics for E-selectin expression *in vivo* (Harari, McHale et al. 1999). Labelling anti-E-selectin antibody with a fluorophore in the NIR range was key to the success of *in vivo* imaging. This ensured specific signal from inflamed paws was not subject to the significant autofluorescence that occurs when imaging at lower wavelengths. So that following imaging the system was able to detect E-selectin specific signal in difference to the signal returned from control antibody. The optimum wavelength for imaging was determined when a DBA/1 mouse was imaged at different wavelengths below and within the NIR as demonstrated in Section 3.3.2. This has also been recognised by others to be a significant determinant for the ability of fluorescent imaging to delineate target signal (Fischer, Gemeinhardt et al. 2006; Weissleder and Pittet 2008). The facility to co-register images with digital X-ray imaging of the target region further helped delineate anatomical localisation of fluorescence signal.

A reason for increased signal in the anti-E-selectin antibody-injected groups could be due to systemic E-selectin expression due to a generalised effect from the intraplantar injection of TNFα. Particularly since there was a small effect on paw thickness at higher (100ng) doses of TNFα and there may therefore be a low level of E-selectin expression at doses lower then 100ng. However in the control animals that received intravenous injection of dye-labelled antibodies but no intraplantar injection of TNFα there were still differences between anti-E-selectin and DNP fluorescence signals. This may indicate that there are differences in the amount of injected antibody or that the degree of fluorophore labelling was different between the groups. Interestingly, this difference was not demonstrated when making a comparison between fluorescence intensity by measuring the fluorescence from serial dilutions of dye-

labelled antibodies *in vitro* as shown in Section 3.3.5. Another possibility is that there was a small degree of constitutive E-selectin expression accounting for the increased anti-E-selectin targeted signal. E-selectin expression *in vivo* has been characterised in the pig following injection of either IL-1 or TNFα and constitutive expression of E-selectin in the skin demonstrated by immunohistochemistry in this model (Keelan, Licence et al. 1994). In initial experiments one significant limiting technical factor was performing multiple i.v. injections within a short time period so that animals were grouped for accurate analysis at both early, mid and late time-points. Although it may be possible to stagger the imaging time points this would also be technically challenging. Hence a significant additional component to this early work was establishing efficient procedures for preparation, injection and imaging of animals.

In this study I also explored the possibility of whether E-selectin antibody had any therapeutic effect in the TNFα-induced paw inflammation model. Pre-injection of anti E-selectin antibody at varying doses did not have any effect on TNFα-induced paw swelling. Targeting E-selectin may expected to inhibit the interactions between leukocytes, platelets and EC within the vascular compartment, leaving tissue leukocyte interactions intact. Some studies using E-selectin antagonists in humans examining the effect of targeted selectin therapy on reperfusion injury have been promising (Lefer 2000). However a carbohydrate based on Sialyl-Lewis X had no effect in patients undergoing angioplasty for ischaemia reperfusion injury (Harari, Marshall et al. 2001; Marshall and Haskard 2002). Intravenous administration of the CDP850 humanised anti-E-selectin antibody reduced levels of soluble E-selectin in plasma and of E-selectin in psoriatic plaques of patients of patients with psoriasis, but did not affect overall clinical outcomes (Bhushan, Bleiker et al. 2002). This may be explained in part by a degree of redundancy with regard to circulating leukocyte attachment to the activated endothelium in humans and animal models. Furthermore as both E- and P-selectin recognise PSGL-1 there may also be redundancy in ligand recognition (Moore 1998). It remains possible that inhibitors of selectin function may emerge that have higher affinity for selectins than sialyl-Lewis X analogues. For example a recombinant soluble antagonist of PSGL-1, rPSGL-Ig has shown promise as a cardioprotective agent by improving postischaemic flow following ischaemia reperfusion injury in pigs (Hansen, Kumar et al. 2004). The therapeutic potential of the rPSGL-1 was also demonstrated in established CIA in DBA/1 mice (Sumariwalla, Malfait et al. 2004).

The following chapter aimed to translate the refined techniques and observations from the TNFα-induced paw oedema model into the CIA model, where paw swelling and clinical score is known to be heterogeneous and subjective. Murine heterologous CIA has several similarities with RA, including synovitis, pannus formation, erosion of cartilage and bone, fibrosis and joint rigidity (Holmdahl, Jansson et al. 1986; Holmdahl, Andersson et al. 1989). Therefore a clear understanding of specific *versus* non-specific fluorescent signal was required to delineate the relative effects of each in CIA.

CHAPTER 5

5 RESULTS: QUANTITATIVE E-SELECTIN TARGETED FLUORESCENT IMAGING OF CIA

5.1 Introduction

The work described in the previous chapters generated important information about how to optimise *in vivo* optical imaging so that E-selectin targeted fluorescent signalling could be utilised in a mouse model of acute inflammation *in vivo*. In this chapter, I aimed to translate the studies in the TNFα-induced paw swelling model into an effective method of imaging activated endothelium in CIA by targeting E-selectin expression. I also aimed to demonstrate how it can be used as a molecular imaging technique to delineate the effects of therapy in CIA. Taken together with my findings in the previous chapter this would validate *in vivo* visualisation of a fluorescently labelled MoAb detecting endothelial activation as a precise, quantifiable pre-clinical molecular imaging technique for murine arthritis.

5.1.1 Collagen Induced Arthritis

CIA is a clinically heterogeneous disease induced in genetically susceptible mice by the intradermal injection of type II bovine collagen (CII). This is discussed in Section 1.4.1. In the present chapter the histological hallmarks of CIA and their relationship to E-selectin expression *ex vivo* are investigated. The histological features of CIA are not dissimilar from RA. In CIA there is infiltration of subsynovial tissue by inflammatory cells, synovial hyperplasia, angiogenesis and erosion of cartilage by bone, all of which occur in RA (Trentham, Townes et al. 1977; Wooley, Luthera et al. 1981; Lee and Weinblatt 2001). B- and T-lymphocytes are both involved in the pathogenesis of CIA with a peak T-cell response occurring around the time of disease onset. Although T-cells play a role in the autoimmune response in CIA, B-cells and auto-antibodies against CII appear to be the primary effector mechanism in this model. The requirement for T-cells in this model is further supported by the fact that only mice with a certain MHC class II molecule are susceptible to CIA. CD4+ T-cells can be detected in the synovial tissue of CIA mice (Marinova-Mutafchieva, Williams et al. 2000). However, transferring CIA with CD4+ T-cells has proven to be difficult (Taurog, Kerwar et al. 1985) and anti-CD4 treatment T-cell directed therapy of established CIA has relatively little impact on inflammatory processes in the joint (Marinova-Mutafchieva, Williams et al. 2000). The onset of CIA is characterised by

high titres of anti-CII antibodies, which bind to the joint cartilage and activate the complement cascade (Williams, Jones et al. 1998). In contrast to the transfer of CII-reactive T-cells, passively transferred IgG anti-CII antibodies induces a severe arthritis in naïve mice (Holmdahl, Jansson et al. 1990). The importance of B-cells has further been shown by the fact that B-cell deficient mice are protected from CIA (Svensson, Jirholt et al. 1998).

Pro-inflammatory cytokines such as TNFα are crucial in the regulation of joint inflammation and tissue destruction in arthritis. The administration of TNFα has been shown to accelerate severity of CIA in rats (Brahn, Peacock et al. 1992). In contrast, disease is inhibited when mice are treated with anti-TNF antibody (Williams, Feldmann et al. 1992). The expression of EC surface markers, however, has not been extensively studied in CIA. One study has made a comparison of the E-selectin expression at the mRNA and protein level in different murine models of inflammation. E-selectin expression was determined both at the mRNA level using RT-PCR and at the protein level using immunohistochemistry (Everts, Asgeirsdottir et al. 2003). CIA was induced by injection of bovine collagen intradermally and mice were given a booster of collagen at day 21. Signs of arthritis were not detected until day 28. Mice were then sacrificed at either day 28, day 30, day 35 or day 43 to generate knee specimens with either no, mild, moderate or severe arthritis respectively. Hence this model differs from the CIA experiments I have described in this chapter, being more chronic in nature. These workers did find that E-selectin mRNA levels in synovial biopsies from the knee specimens were increased in mild, moderate and severely diseased animals compared to those without any macroscopic signs of inflammation. Interestingly, these workers were less successful in demonstrating positive staining of E-selectin by immunohistochemistry in inflamed tissue. They noted occasional E-selectin expression detectable by immunohistochemistry in severe inflamed tissue at day 43 post immunisation but not at other times in mild and moderate disease.

A number of prior studies have investigated fluorescent imaging in animal models of arthritis to detect both targeted and non-specific signal change in arthritis. A Cy5.5-labeled antibody against macrophages was used successfully to label inflammatory changes in experimental arthritis. Between 2 and 72 hours, arthritic knee joints showed significantly higher fluorescence levels compared with contralateral joints. In

this study it appeared that following injection Cy5.5 bound mainly to albumin with microscopy confirming Cy5.5 deposition in the synovial membrane it also appeared that macrophages actively phagocytosed Cy5.5 following uptake to inflamed areas that had occurred most likely as a result of non-specific trafficking due to enhanced vascular permeability (Hansch, Frey et al. 2004). The same investigators targeted the F4/80 antigen on macrophages by conjugating the Cy5.5 fluorochrome to anti-F4/80 antibody and demonstrated that signal in inflamed joints was significantly higher than that generated by the isotype control labelled antibody. Simon *et al* evaluated whether optical imaging of reinjected leukocytes labelled *ex vivo* with an NIR dye could detect antigen induced arthritis (Simon, Daldrup-Link et al. 2006). This study showed that at 4 and 24 hours there was some significant accumulation in arthritic *versus* control knees. The targeting of arthritis by other mechanisms is also discussed in the introductory Section 1.3.3.2. No investigators thus far, however, have examined whether E-selectin can be utilised as a marker of endothelial activation in CIA and detected *in vivo* by utilising optical imaging of fluorescently labelled anti-E-selectin antibody, and this is addressed in the first part of this chapter.

The following Section gives background information about a novel therapeutic approach for CIA and how this may be tested in the CIA model using *in vivo* E-selectin targeted imaging, which forms the basis for the second part of this chapter.

5.1.2 RB200: A Novel EGFR Antagonist

In addition to utilising anti-E-selectin as technique to follow arthritis *in vivo*, it would be of interest to determine whether *in vivo* imaging can also be applied to study the effects of therapy in CIA. An antagonist (RB200) has been developed that targets all four members of the epidermal growth factor (EGF) receptor family. This is discussed further in section 1.2.3. Despite the success of conventional monoclonal antibody technology that usually targets a single molecule or receptor, there is often intricate cooperation amongst multiple signalling pathways or a number of closely related cell surface receptors that can lead to reduced efficacy. To circumvent this problem, a bi-specific ligand trap, RB200, composed of the full length extracellular domain of HER-1/ErbB1 and HER-3/ErbB3 fused with the Fc domain of human IgG1 has been designed (Sarup, Jin et al. 2008; Jin, Zhang et al. 2009). RB200 may therefore be expected to down-regulate responses mediated via all four HER subfamily members due to its broad pan-HER efficacy. RB200 has been shown to bind to both HER-

1/ErbB1 ligands (TGF-α, HB-EGF) and to HER-3/ErbB3 ligands (NRG1-α and NRG1-β3). Moreover, RB200 inhibited EGF- and NRG1-β1stimulated tyrosine phosphorylation of HER family proteins (HER-1, HER-2 and HER-3), and also showed potency in a variety of cell proliferation assays (Sarup, Jin et al. 2008). In addition RB200 has been shown to inhibit tumour growth *in vivo* in two human tumour xenograft (epidermoid carcinoma and non-small cell lung cancer) nude mouse models (Sarup, Jin et al. 2008). A representation of the structure of RB200 is demonstrated in the following Figure 5-1.

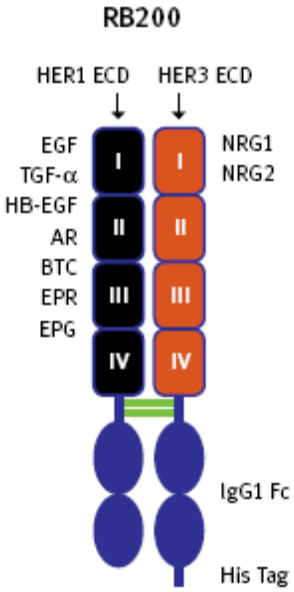

Figure 5-1 Representative structure and principle binding affinity of RB200

Figure demonstrates that RB200 is an Fc mediated heterodimer of native HER1 and HER3 ligand binding domains, retaining the specificity of both HER1 and HER3. (EGF = epidermal growth factor, TGF-α= transforming growth factor-α, HB-EGF = heparin-binding EGF like growth factor, AR = amphiregulin, BTC = betacellulin, EPR = epiregulin, EPG = epigen; HER-3/ErbB3 ligands: NRG-1 = neuregulin-1, NRG-3 = neuregulin-3.)

It was shown at the Kennedy Institute that adenoviral delivery of the human EGFR family inhibitor, Herstatin, significantly abrogated murine CIA (Sumariwalla, Jin et al. 2008). Herstatin is an N-terminally modified alternative splice variant of HER-2/ErbB2, retaining intron 8, resulting in the formation of an approximately 68kDa protein, which disrupts dimerisation and thus serves as a natural inhibitor of native HER-2/ErbB2, as well as HER-1/ErbB1and HER-3/ErbB3 (Doherty, Bond et al. 1999). Investigation of the role of IL-18 in upregulating angiogenic factors in RA tissue fibroblasts has demonstrated that downstream signalling pathways from phosphorylated tyrosine kinase domains of ErbB receptors induce angiogenic factors including VEGF via distinct mechanisms (Amin, Mansfield et al. 2007). This suggests that RTKs blockade may have significant effects on angiogenesis in RA. Engagement of HER receptors has been shown to increase the release of VEGF in malignancy (Petit, Rak et al. 1997; Konecny, Meng et al. 2004). Since homodimerisation and

heterodimerisation among members of the the ErbB family of receptors are known to occur agents that target multiple receptors are desirable. The dual kinase receptor lapatinib targets both EGFR and HER-2, and thus has been found to be more effective in the treatment of angiogenic proliferation in metastatic cancer (Diaz, Nguewa et al. ; Nahta, Yuan et al. 2007).

The efficacy of RB200 has been investigated previously. RB200 inhibited EGF- and NRG1-β1stimulated tyrosine phosphorylation of HER family proteins (HER-1, HER-2 and HER-3), and also showed potency in cell proliferation assays (Sarup, Jin et al. 2008). In addition RB200 has been shown to inhibit tumour growth *in vivo* in two human tumour xenograft (epidermoid carcinoma and non-small cell lung cancer) nude mouse models (Sarup, Jin et al. 2008). Prior work at the Kennedy institute has demonstrated the therapeutic efficacy of RB200 in abrogating CIA, demonstrating a significant effect on paw swelling, and clinical score. Immunohistochemical analysis also demonstrated reduced vascularity following analysis for CD31 staining (unpublished observations). In addition behavioural responses such as feeding, grooming, climbing were measured by an automated activity monitor. This demonstrated significant improvements following treatment with RB200 and there was also no evidence of adverse outcomes following treatment. Further experiments were therefore undertaken to determine whether there may be a synergistic effect between low dose RB200 and the TNF receptor blocker etanercept. This presented an opportunity to determine whether RB200 and etanercept either alone or in combination had significant effects on *in vivo* E-selectin targeted imaging in CIA.

5.2 Objectives

i. To determine the characteristics of CIA as a model of arthritis for *in vivo* fluorescence imaging
ii. To demonstrate that increased E-selectin expression can be detected by immunohistochemistry
iii. To investigate whether increased E-selectin expression can be detected *in vivo* by fluorescently labelled anti-E-selectin antibody
iv. To determine the effect of a novel therapeutic compound, RB200, on *in vivo* E-selectin targeted fluorescent imaging.

5.3 Results

5.3.1 Collagen Induced Arthritis

5.3.1.1 CIA in DBA/1 mice – clinical course of the disease

Immunisation of male DBA/1 mice with bovine type II collagen in complete Freund's adjuvant resulted in development of inflammatory arthritis. Disease onset and progression was monitored daily from 10 days after immunisation. This was to determine the time of onset of arthritis and to quantify the extent of oedema, erythema and deformity. Figure 5-2 is a representative graph of disease development. The first clinical signs of arthritis generally appeared at day 14 after collagen injection, with a mean onset of 25 days post primary immunisation. The severity of arthritis was represented as an arthritic index on a 0-3 scale. Each paw was graded and the sum of the scores obtained from all four paws was used as the arthritis score, resulting in a maximal possible score of 12 per mouse. In conjunction with the clinical score, hind paw swelling was measured. In my experiments, the incidence of arthritis varied between 50-80%. The reasons for variability in incidence are not known. Theories have included that mice have originated from different housing facilities, or they were kept in different cages or that the collagen preparations have variable efficacy depending on their purity. For imaging experiments the combined clinical score of the hind paws was used. Front paws were not assessed by fluorescence imaging. This is because of their small size, difficulty positioning for clear recording of signal and difficulty interpreting histological sections.

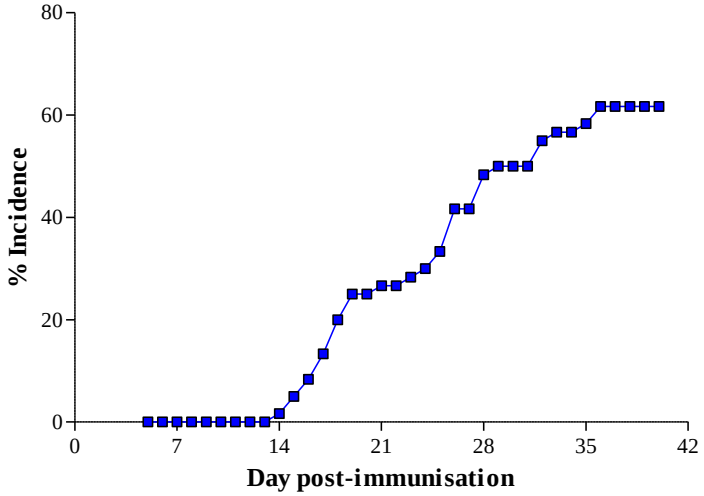

Figure 5-2 Incidence of arthritis following immunisation with bovine type II collagen

Graph demonstrates the typical incidence of a CIA experiment over time following immunisation of DBA/1 mice with bovine collagen. Mice were monitored daily to assess for disease onset.

The clinical onset of CIA was marked by rapidly increasing oedema and erythema of the paws and ankles/wrists of both hind and forelimbs, usually commencing in one limb and then often spreading into the other limbs. Later clinical characteristics of the disease (beyond day 8 of arthritis) included reduced oedema, as a result of gross joint deformation and total loss of joint mobility. As well as the incidence, the severity of the disease was extremely variable between experiments. A clinical score of 12 was rarely reached; more common was a clinical score of 2.5-6, with the disease involving one or two paws of the animal. A representative time course of arthritis progression determined by measuring clinical score and paw thickness is demonstrated in Figure 5-3. While there was progression and worsening of arthritis in the majority of animals over time, there was significant heterogeneity between animals at any particular time-point of arthritis. This is best highlighted in Figure 5-3b. Unlike the typical clinical course of RA, disease progression in CIA is often characterised by an asymmetrical rapidly progressive arthritis that leaves some paws apparently unaffected.

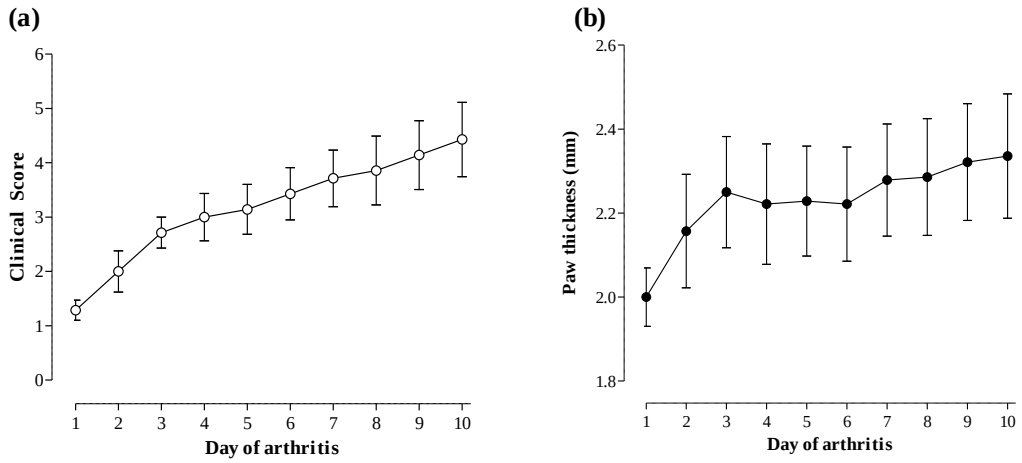

Figure 5-3 CIA: Time course of progression in DBA/1 mice

Graphs illustrate an example of a typical CIA experiment run in this study to demonstrate the disease course. Immunisation of DBA/1 mice with bovine CII induced joint inflammation with characteristic oedema and erythema. Mice with visual appearance of arthritis (redness and/or swelling of a paw) were monitored daily to observe disease progression. The inflammatory response was represented as paw thickness in mm and clinical score. Clinical score panel (a) correlated well with paw thickness panel (b). Data are expressed as means ± SEM (n = 11).

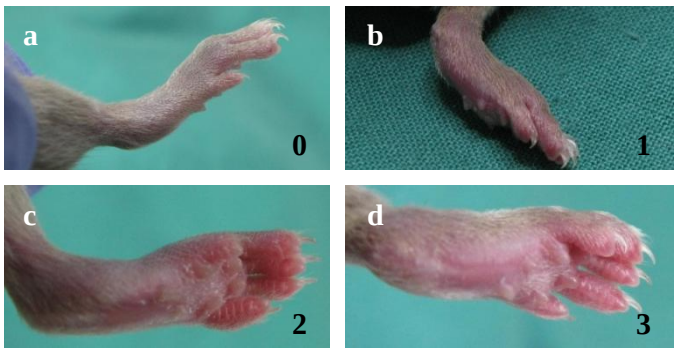

Figure 5-4 Representative clinical scores of mice with CIA

Panel (a) Normal hind paw (clinical score 0). (b) Hind paw with mild swelling (clinical score 1). (c) Hind paw with pronounced oedematous swelling (clinical score 2). (d) Hind paw with ankylosis (joint fusion) (clinical score 3).

Figure 5-4 demonstrates representative examples of clinical scoring for mice with CIA. The clinical score is based on a visual assessment of the overall appearance of the mouse paw. Since this scoring is subjective there can be differences between observers when making an assessment of the clinical score in CIA. This is especially the case with minimal mild (grade 1) paw swelling. This is further complicated by the occasional transient swelling of paws that can occur over 12-24 hours which has the appearance of early arthritis but then spontaneously resolves.

5.3.1.2 Histological analysis of CIA

Histological analysis was used to confirm the clinical assessments. Paws were harvested at various time-points and processed for histological evaluation. No clinical or histological evidence of arthritis was seen in control animals receiving CFA alone. Sections of healthy joints revealed well defined joint spaces, with the articular surface of bones covered with cartilage of uniform thickness and smooth surface. The histological examination of paws with collagen induced arthritis revealed a good correlation between the clinical and the histological findings. In paws judged to have mild arthritis, on histological analysis these demonstrated limited inflammatory cell infiltration in the superficial layers of the synovium. Sections of severely arthritic paws, however, exhibited widespread infiltration of inflammatory cells throughout the joint tissue, extensive proliferation and vascularisation of the synovium, as well as invasion and erosion of cartilage and subchondral bone by inflamed synovium, leading to complete disorganisation of the joint architecture and in some areas to the development of fibrous or bony ankylosis. Figure 5-5 demonstrates the typical histopathological features of a severely arthritic paw compared to a healthy paw. Areas where new vessel formation is suggested correspond to similar areas on specimens stained for CD31.

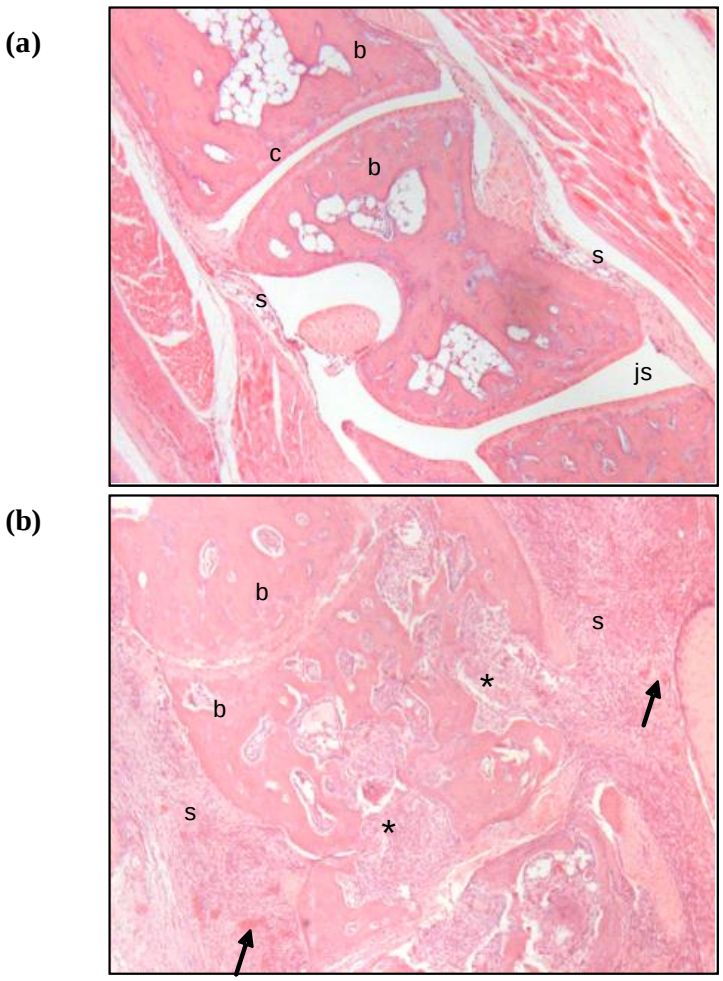

Figure 5-5 Histological characteristics of CIA

Representative sections of first metatarsal joints from a), healthy and b), arthritic mice stained with haematoxylin and eosin. Tissue was obtained on day 10 of arthritis. The healthy section demonstrates normal joint architecture without signs of inflammation or bone destruction. Synovial hyperplasia, inflammatory cell infiltration, loss of cartilage and bone are evident in the arthritic joint. (s) inflamed synovium, (*) inflamed synovium invasion into bone, arrows show synovial blood vessels; (b) bone; (c) cartilage; (s) synovium; (js) joint space, (original magnification x 40).

5.3.1.3 Immunohistochemistry to assess E-selectin expression and synovial vascularisation in CIA

To determine whether E-selectin is expressed in the inflamed synovium of mice with CIA, immunohistochemistry was performed. The technique used to preserve antigenicity was identical to that used to prepare specimens when examining E-selectin expression in the TNFα-induced paw inflammation model as presented in Section 4.3.2. Joint sections were obtained from the hind paw of an animal on day 5 following the onset of hind paw arthritis. Representative images are shown in Figure 5-6. These demonstrate that there was significant histological evidence of arthritis within the joint (Figure 5-6a,b) and that within areas of inflamed synovium there was positive staining for E-selectin as marked by the arrows (Figure 5-6d), but that there was no equivalent staining for microvessels in specimens stained with the isotype control antibody DNP (Figure 5-6c).

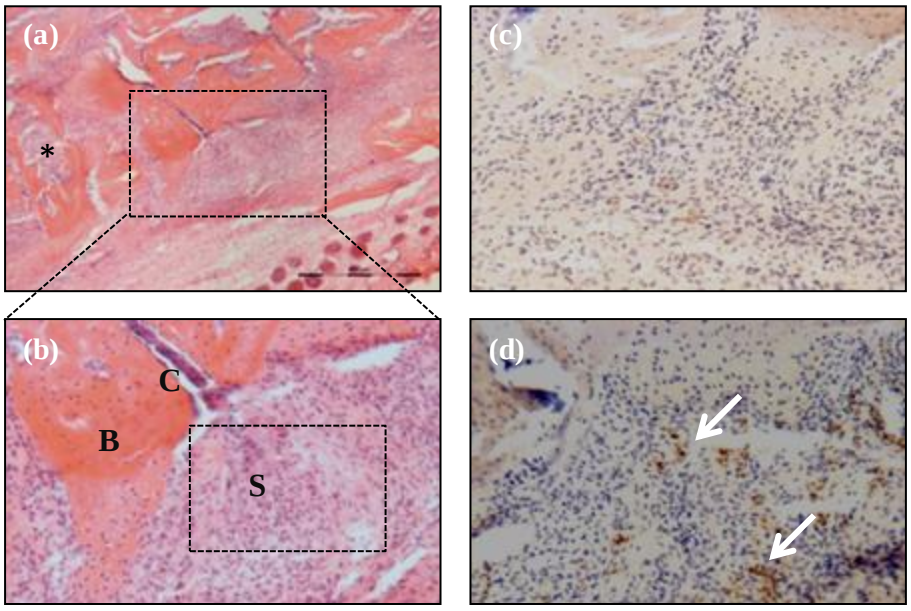

Figure 5-6 E-selectin is expressed in the inflamed synovium of mice with CIA

(a-c) Serial sections from a mouse paw with CIA (day 5) were stained using haematoxylin and eosin (a,b), or with either (c) isotype control antibody or (d) anti-E-selectin antibody (magnified from area in (b)). Arrows indicate brown precipitates demonstrating the presence of positive E-selectin binding in inflamed microvessels. (S=synovium, B=bone, C=cartilage, *=invading synovium). (scale bar 500μm)

Anti-E-selectin antibody binding to activated endothelium in inflamed synovium was compared to the staining pattern obtained by using an antibody directed to Platelet Endothelial Cell Adhesion Molecule 1 (PECAM-1/CD31). The staining process for CD31 also involved preparing cryosections following decalcification to preserve antigenicity as detailed in Section 2.6. The expression of CD31 by EC is well recognized for its use in detecting EC in tissue sections. CD31 is an immunoglobulin (Ig) superfamily member expressed on the surface of platelets and leukocytes, and is also concentrated at the lateral junctions of EC (van Mourik, Leeksma et al. 1985; Muller, Ratti et al. 1989; Albelda, Oliver et al. 1990). CD31 is composed of six extracellular Ig-domains, a transmembrane domain and a cytoplasmic domain. Its ligands include itself by homophilic interaction involving Ig-domain 1, and also αvβ3 integrin and cyclic ADP ribose hydrolase (CD38) by heterophilic interaction involving Ig-domains 1–3. Since its original cloning, much has been learned about the role of CD31 in mediating various cellular interactions. It has been implicated in various biological functions such as leukocyte transmigration, cell migration, angiogenesis, cell signalling and cell adhesion (Woodfin, Voisin et al. 2007).

The staining patterns for anti-E-selectin antibody and anti-CD31 antibody are shown in Figure 5-7. This figure demonstrates that both are targeted to the inflamed synovium where there is likely to be new vessel formation. Anti-E-selectin antibody bound specifically to smaller vessels within the inflamed synovium, whereas anti-CD31 antibody bound to both large and small vessels throughout the paw in both inflamed and uninflamed areas. The differential binding patterns for anti-E-selectin and anti-CD31 antibody are also demonstrated in Figure 5-9.

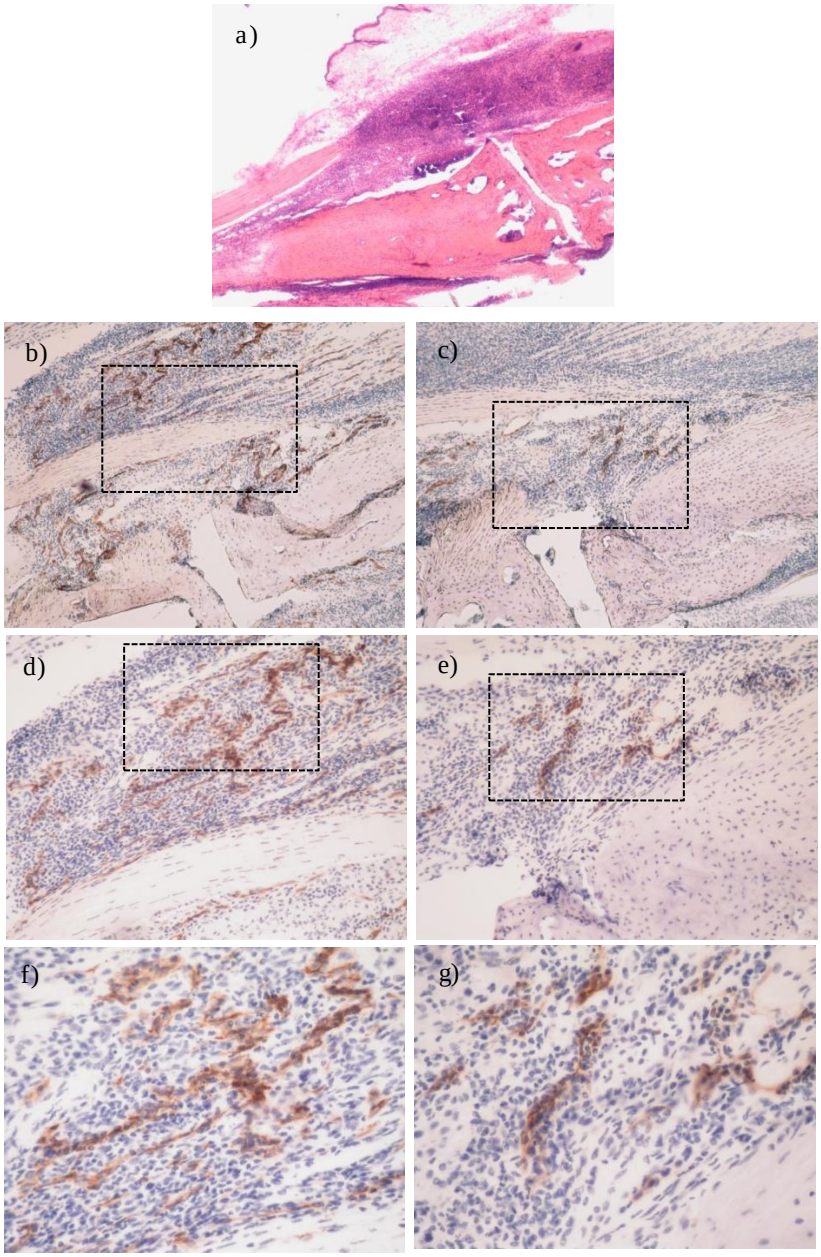

Figure 5-7 E-selectin expression in inflamed mouse synovium: comparison with CD31

Haematoxylin and eosin section of inflamed mouse metatarsal joint, taken from DBA/1 mouse with severe arthritis (a). Further serial sections were immunostained with anti-CD31 antibody (b, d, f) or anti-E-selectin antibody (c, e, g), and are shown at 50x (b, c), 100x (d, e) and 200x (f, g) magnification.

The following figure (Figure 5-8) demonstrates that in a mouse joint unaffected by arthritis (in immunised but non-arthritic animals) there was no histological evidence of arthritis. Haematoxylin and eosin stained tissue sections from this clinically healthy mouse displayed normal joint architecture without synovial hyperplasia or infiltrating leukocytes as well as intact cartilage and bone. There was no evidence of positive anti-E-selectin antibody staining. There was however evidence of CD31 positive staining in some of the vessels in the paw. These are histologically normal blood vessels that have a distinct lumen and larger diameter.

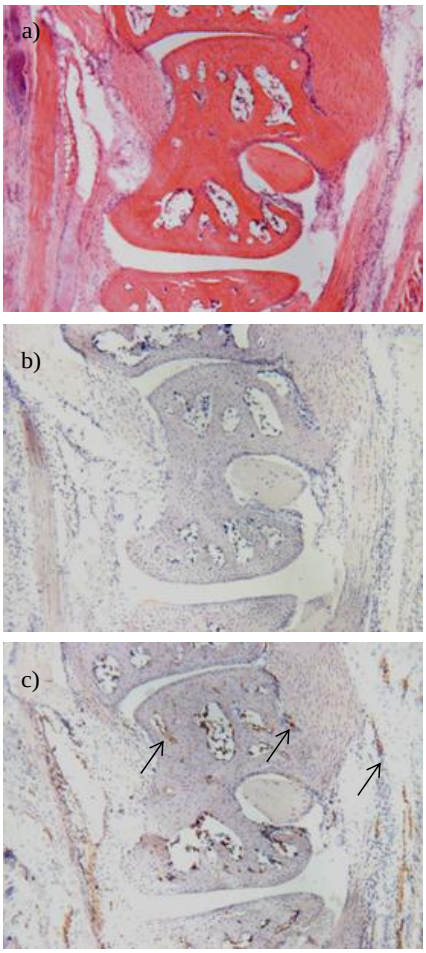

Figure 5-8 Comparison of anti-E-selectin and CD31 staining in non-arthritic mouse paw

Representative histological sections of paw tissue from a clinically healthy mouse that had been immunised with type II bovine collagen but did not develop arthritis. Images show the metatarsal joints of mouse paws. (a) Haematoxylin and eosin section (b) anti-E-selectin antibody-stained section. Brown precipitates indicate the presence of CD31 positive staining and are marked by the arrows in (c). (magnification x40).

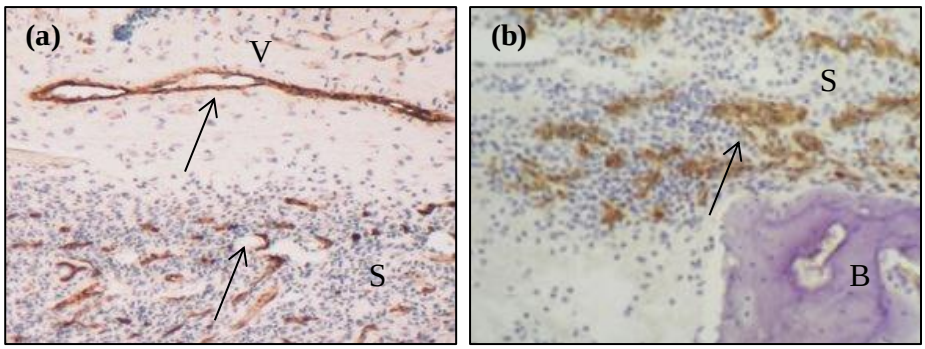

Figure 5-9 Differential binding of anti-E-selectin and anti-CD31 antibody

Representative figure of anti-CD31 (a) and anti-E-selectin antibody binding (b) from a DBA/1 mouse with severe (day 10) arthritis following immunisation with type II bovine collagen. Differential binding pattern in both figures is indicated by arrows. (S=synovium, B=bone, C=cartilage, V=vessel). x100 magnification.

Figure 5-9 represents the differential binding of anti-E-selectin and anti-CD31 antibody. This shows that anti-CD31 shows positive staining to both large and small vessels in the mouse paw, but that anti-E-selectin positive staining has a greater intensity of staining in small calibre vessels with areas of inflamed synovium.

E-selectin expression was further qualitatively assessed at early, mid and late time-points of arthritis. This is demonstrated in Figure 5-10. This confirms that there was E-selectin expression evident at days 1, 5 and 10 following the onset of arthritis. Qualitative comparisons of anti-E-selectin binding have been made at different time-points in arthritis, with the conclusion that there may be relatively more expression at earlier time-points (days 1-5 following onset of arthritis) compared to anti-CD31 but at later time-points (days 5-10 following onset of arthritis) there was relatively less anti-E selectin binding compared to CD31. Meaningful further quantification was not possible because of the limited number of available specimens with sufficiently preserved architecture. There was often considerable loss of tissue integrity and architecture following cryosectioning. This is one significant disadvantage of this technique. Frozen sections of demineralised bone are very brittle and quite often tissue damage occurred during preparation. Morphological analysis of demineralised cryosectioned bone tissue is not recommended due to difficulties in avoiding tissue artefacts at the sectioning procedure. For this reason only a few paw sections were available to compare from individual experiments.

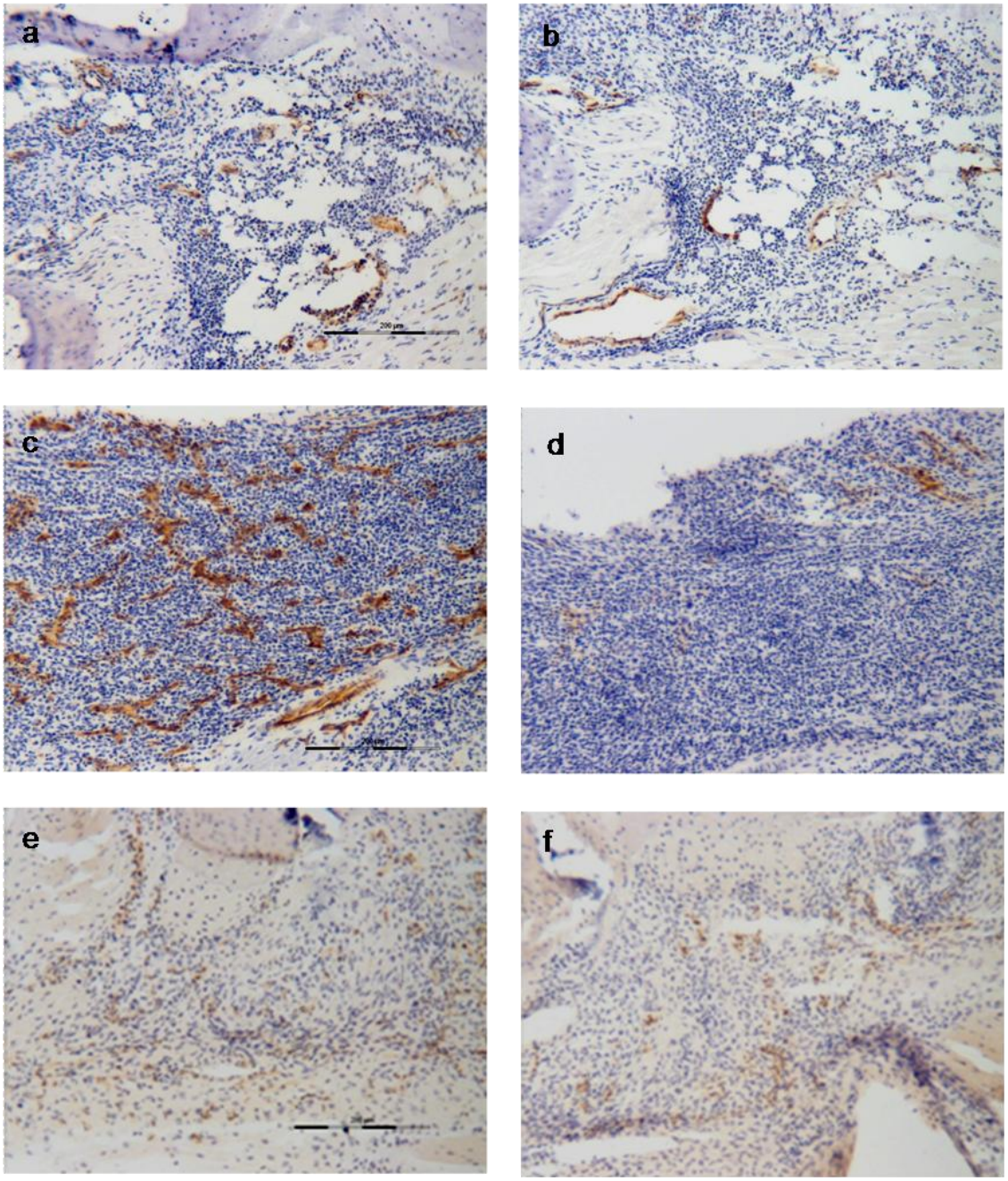

Figure 5-10 E-selectin is expressed at early, mid and late time-points in CIA

Serial sections at original x10 magnification showing anti-CD31 antibody staining (a,c,e) and anti-E-selectin antibody staining (b, d, f) at days 1 (a, b), 5 (c, d) and 10 (e, f) of arthritis. Scale bars on images a, c and e are shown at 200μm.

Increased binding of anti-E-selectin antibody had therefore been demonstrated in *ex vivo* mouse paws with arthritis following the onset of CIA. I next sought to determine whether following i.v. injection of anti-E-selectin antibody, *in vivo* binding to activated endothelium could be detected in *ex vivo* specimens by secondary antibody directed against the E-selectin antibody (anti-rat antibody). This is demonstrated in Figure 5-11.

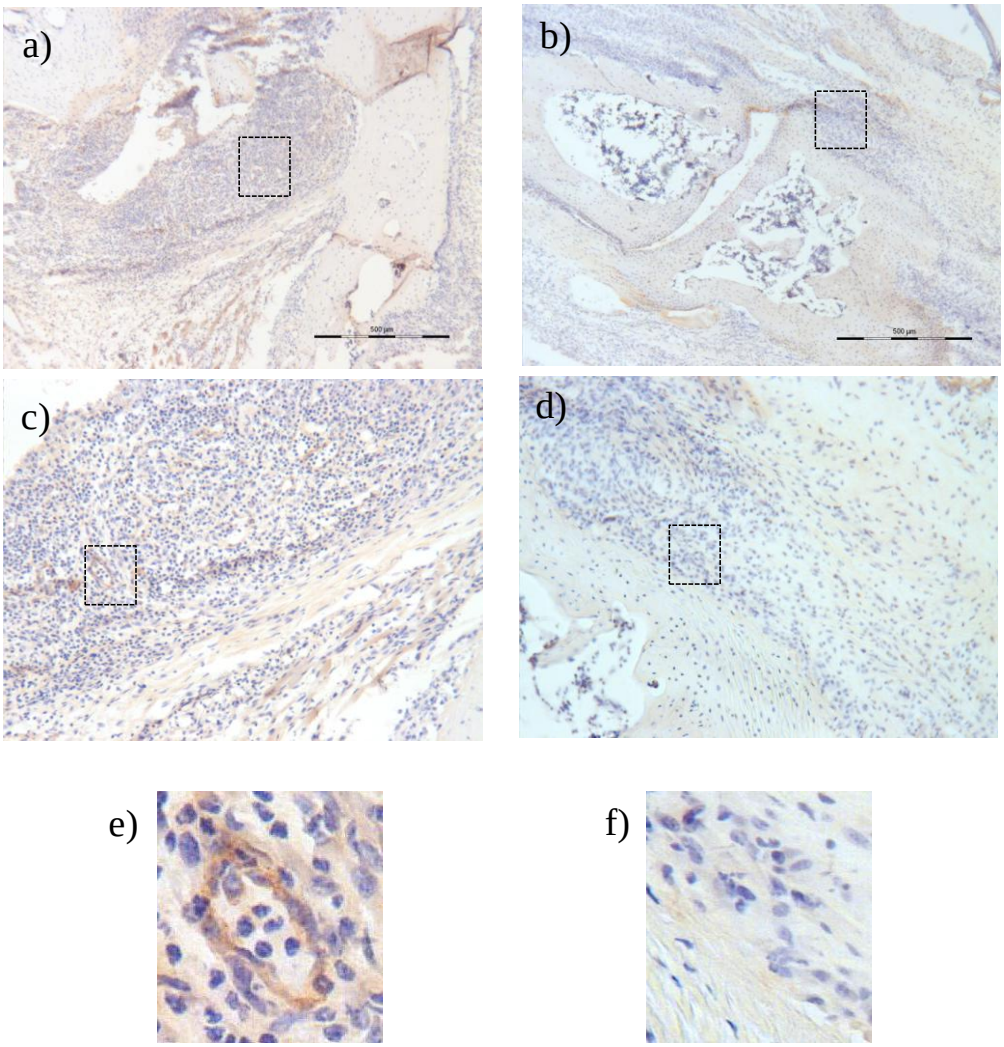

Figure 5-11 Anti-E-selectin antibody can be detected following i.v. injection in CIA

Sections of inflamed mouse metatarsal joint, taken from DBA/1 mouse with severe arthritis (>day 10 from onset). Mice were injected with E-selectin (a, c, e) or isotype control anti–DNP (b, d, e) and sacrificed after 4 hours. Scale bars show length of 500μm. Image (e) demonstrates small vessel staining with no similar staining shown in mouse injected with control antibody (f). Magnification scale bar in a) and b) 500μm.

The above figure shows that E-selectin antibody can be detected at sites of inflammation in specimens that have received an injection of antibody *in vivo.* There was no positive staining for the control DNP antibody. Anti- E-selectin antibody was detected at 4 hours following i.v. injection of antibody but not at 12 or 24 hours not shown). The absence of antibody detection at the other time-points cannot be taken solely as evidence that detection was maximal at 4 hours since there was poor preservation of specimens as described above and although there was a consistent difference between anti-E-selectin and anti-DNP antibody, staining of specimens was variable in intensity. Since *in vivo* imaging experiments took place over 24 hours this made concurrent *in vivo* fluorescent imaging and immunohistochemical studies not possible within the same experiment. Combined with variable morphology from frozen sections, matching of specimens from separate experiments was also not always possible.

5.3.2 E-Selectin Targeted Fluorescence Imaging *In Vivo*: Quantifying Endothelial Activation In Collagen Induced Arthritis

Having demonstrated E-selectin expression in mice with CIA by immunohistochemistry, the next part of the study aimed to assess E-selectin targeted fluorescence imaging *in vivo* in CIA. Arthritis was induced in DBA/1 mice by immunising with bovine type II collagen in CFA. Following the onset of arthritis animals were randomised into groups to receive either anti-DNP antibody or anti-E-selectin antibody. The following Figure 5-12 shows that there was significant heterogeneity in the clinical score (Figure 5-12a) and paw thickness (Figure 5-12b). In many animals either a right or left hind paw developed arthritis, hence there were significant numbers of animals with a hind paw that had no evidence of arthritis as measured by conventional scoring parameters at the time of injection.

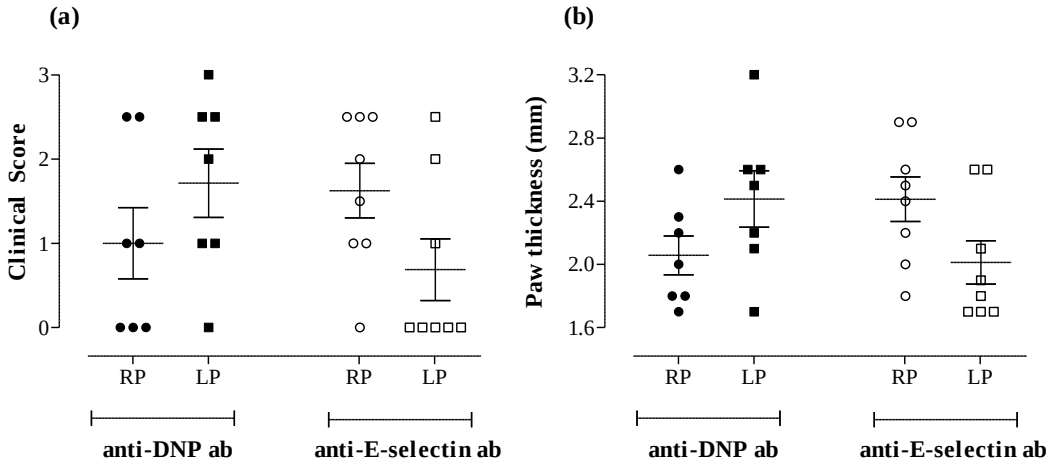

Figure 5-12 CIA: clinical score and paw thickness for correlation *in vivo* fluorescent imaging study

Graphs illustrate clinical score and paw thickness of all hind paws of DBA/1 mice with bovine collagen induced arthritis. Mice were randomised for injection with either anti-DNP or anti-E-selectin dye labelled antibody. Clinical score panel (a) and paw thickness (mm) panel (b) are shown at time of injection with dye labelled antibodies. RP-right paw; LP-left paw.

Mice with CIA were injected with either anti-E-selectin or anti-DNP antibodies labelled with Dylight 750 nm Near Infra Red fluorophore (5μg i.v.) and fluorescent images at different time-points post-injection were acquired. The following Figure 5-13 demonstrates the MFI of DBA/1 mice 5-10 days following onset of CIA. This shows that with more severe arthritis there is increased signal in both anti-DNP and anti-E-selectin antibody injected animals. Figure 5-13c shows that there appears to be increased signal in the inflamed mouse paws of the anti-E-selectin injected mouse compared to the anti-DNP control antibody injected animal. In this case both mice (anti-E-selectin and anti-DNP injected) have a comparable clinical score and paw diameter. However taken together the represented examples demonstrate substantial heterogeneity in clinical score and paw diameter. This correlates with the visual images of MFI from all animals. Figure 5-13d shows that there appear to be similar levels of signal returned from animals for both groups that have not been immunised with bovine collagen and received either anti-E-selectin or DNP antibody injections.

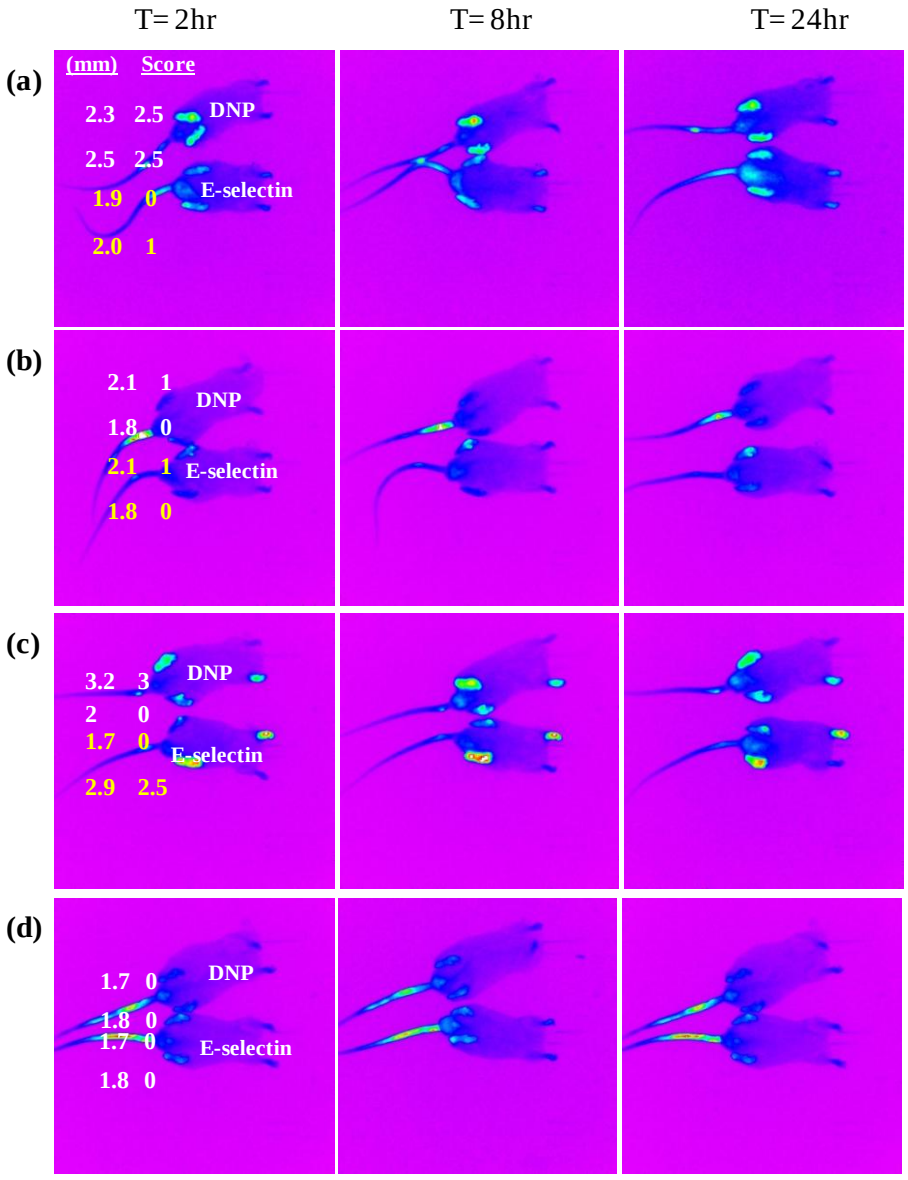

Figure 5-13 CIA can be detected by detected by E-selectin targeted fluorescent imaging

Following onset of arthritis induced with bovine collagen, DBA/1 mice with clinically distinct arthritis as assessed by clinical score and measurement of paw swelling were assigned into a group to receive either anti-E-selectin or anti-DNP antibodies labelled with Dylight 750 nm Near Infra Red fluorophore (5µg i.v.). Fluorescent images at different time-points post-injection following injection of labelled antibodies are shown from representative pairs of anti-E-selectin and anti-DNP injected mice with arthritis (a-c). The paw diameter (mm), and clinical score (score) are listed next to each paw for each animal. Panel (d) demonstrates fluorescent images of animals that had not received immunisation with bovine collagen.

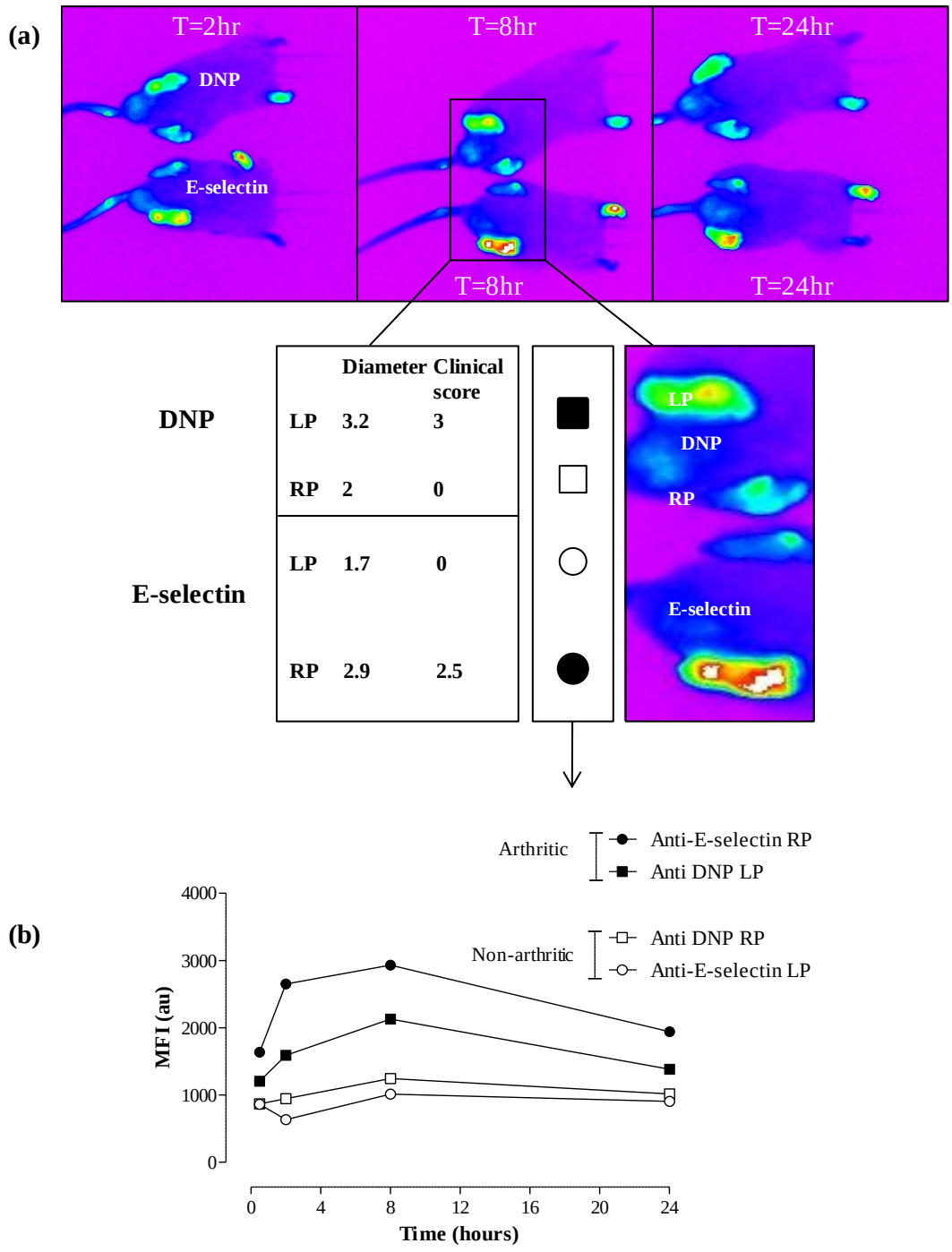

Figure 5-14 E-selectin targeted signal can be detected in collagen-induced arthritis

Following onset of arthritis induced with bovine collagen mice were injected with either anti-E-selectin or anti-DNP antibodies labelled with Dylight 750 nm Near Infra Red fluorophore (5µg i.v.). Representative images over a 24 hour period are shown in (a). Mean fluorescence intensity (MFI) scores of the hind paws and their relationship to the clinical score are shown in (b). The mean background of fluorescence intensity from control animals injected with either anti-E-selectin or anti-DNP antibody but not immunised with bovine collagen has been subtracted).

The above Figure 5-14 represents a closer detail of Figure 5-13c. This demonstrates the relationship between the coloured fluorescent image and MFI quantification from both the inflamed and uninflamed paws in mice injected with either anti-DNP control antibody or anti-E-selectin antibody. The technique for quantification of MFI was identical to the method utilised in Section 4.3.1 using the TNFα-induced paw oedema model.

Quantification of the MFI of mouse paws demonstrates that there are marked differences in signal intensity between inflamed and uninflamed paws and that there is a higher measured MFI returned from the inflamed/arthritic mouse paw following injection of anti-E-selectin antibody than for either the uninflamed paw or for a mouse with arthritis and injected with anti-DNP antibody. The diameter and clinical score (3.2mm and 3.0mm respectively) is greater for the anti-DNP injected mouse compared to the diameter and clinical score for the anti-E-selectin injected animal (2.9mm and 2.5mm respectively). Since all mouse paws may be affected with arthritis following immunisation with bovine collagen, then using an unaffected paw as an internal control based on a clinical score of 0 may not be accurate. This paw may have subclinical arthritis and hence an increased MFI or there may be increased E-selectin expression in pre-arthritic uninflamed paws in animals injected with bovine collagen. In this example however, there are relatively small differences between anti-DNP control and anti-E-selectin injected animals although there does appear to be some heterogeneity in the fluorescent signal returned from the left paw of the E-selectin injected animal that had been given a clinical score of 0 (Figure 5-14a).

Groups of animals with CIA as depicted in Figure 5-12 were then further matched for clinical score and paw thickness to ensure that meaningful comparisons could be made between control DNP and E-selectin dye labelled antibody injected animals. Only mouse paws with clinically distinct arthritis and a hind paw thickness ≥2.2mm were compared. The selection of this level of paw swelling represents a threshold for paw thickness where there is moderate to severe, clinically definite arthritis. Clinical scores in anti-DNP and anti-E-selectin antibody injected groups were 2.1 ± 0.3 and 2.1 ± 0.2 respectively (Pearson correlation coefficient = 0.85). Similarly, paw diameters in anti-DNP and anti-E-selectin antibody injected groups were 2.5 ± 0.3 and 2.6 ± 0.2 respectively (Pearson correlation coefficient = 0.66). The matched groups are demonstrated in the following Figure 5-15.

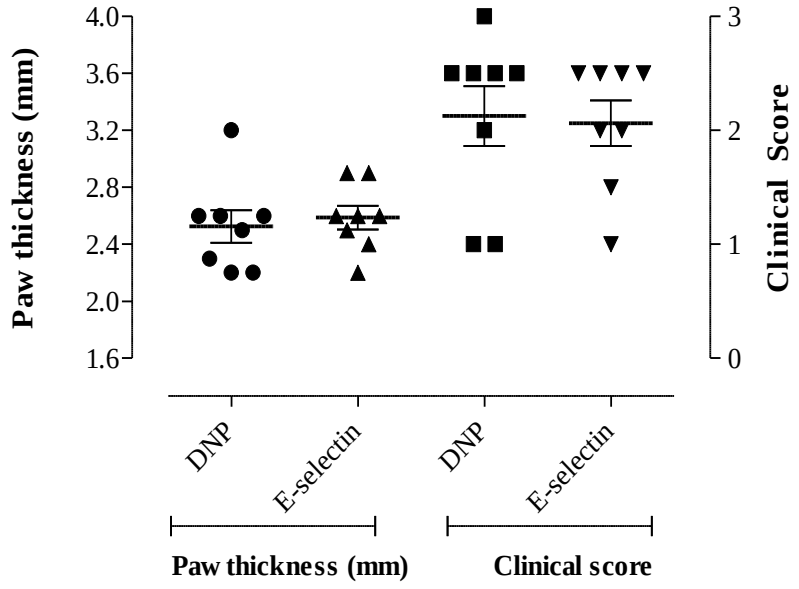

Figure 5-15 Matched clinical score and paw thickness for *in vivo* imaging of CIA

Figure represents the clinical score and paw thickness (mm) for either anti-DNP or anti-E-selectin dye labelled antibody injected DBA/1 mice with bovine CII induced joint inflammation with characteristic oedema and erythema at days 2-10 following onset of arthritis. Mice with a hind paw thickness of ≥2.2mm only were selected for comparison.

The following figure demonstrates the MFI from animals with a paw thickness of ≥2.2mm and having clinically definite arthritis as demonstrated in the above Figure 5-15. Healthy mice (not immunised with collagen) without arthritis were assessed for comparison. Significant differences were observed in the fluorescence intensity between healthy and arthritic animals injected with anti-E-selectin ($p<0.001$), and between arthritic animals injected with anti-E-selectin and anti-DNP ($p<0.001$). There were no significant differences between levels of MFI returned from healthy mice injected with either anti-DNP or anti-E-selectin injected antibody. For the subsequent analysis a mean background signal for both DNP and E-selectin injected animals was removed. The mean background signal was calculated from the mean signal returned from the paws of healthy animals (unimmunised with bovine collagen) injected with either anti-DNP or anti E-selectin antibody.

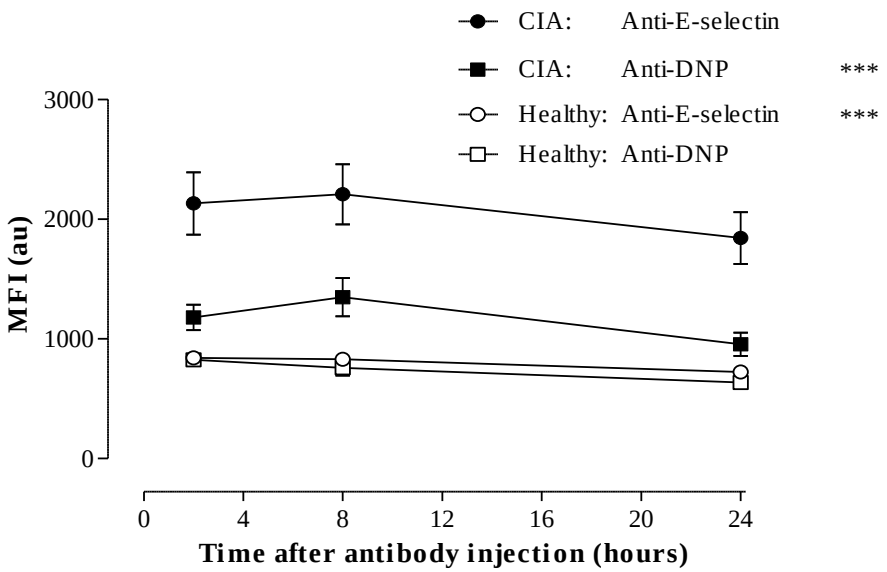

Figure 5-16 E-selectin targeted signal can be detected in collagen-induced arthritis

Following onset of arthritis induced with bovine collagen, mice with clinically distinct arthritis and paw thickness ≥2.2mm were injected with either anti-E-selectin or anti-DNP antibodies labelled with Dylight 750 nm Near Infra Red fluorophore (5µg i.v). Mean fluorescence intensity (MFI) scores for arthritic and healthy animals (non-immunised controls) are depicted. Data are mean ± SEM, and were analysed by 2-way ANOVA *versus* arthritic anti-E-selectin antibody-injected mice: *** $p<0.001$.

At the 8 hour time-point (after antibody injection) data demonstrate localisation of both antibodies to arthritic paws relative to non-arthritic paws, with a 2.34-fold increase in anti-E-selectin antibody fluorescence relative to DNP in inflamed paws ($p<0.01$). This is shown in Figure 5-17. Fluorescence signal following injection of anti-E-selectin antibody with subtraction of background signal (MFI of unimmunised mouse paw for anti-DNP and anti-E-selectin groups respectively) was combined with X-ray co-localisation. This demonstrated that areas of increased signal are often localised to the metatarsal heads and ankle joints. This corresponds with the increased levels of inflammation in these joints seen with immunohistochemistry. A representative example is shown in Figure 5-17b.

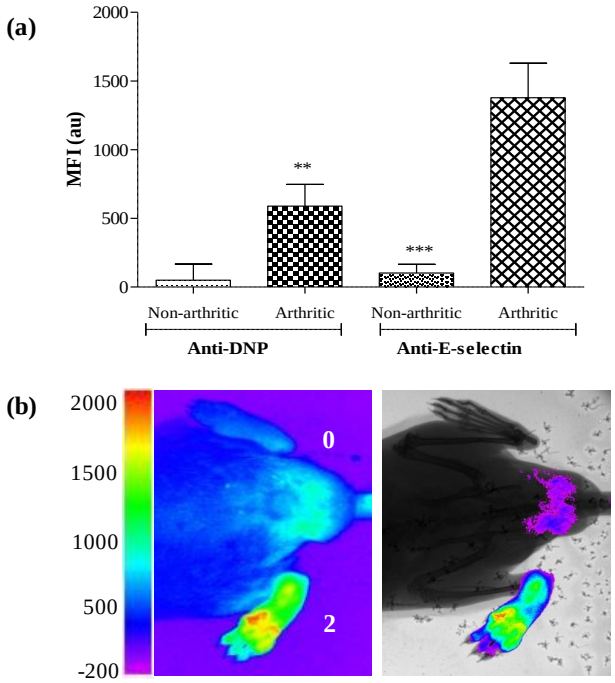

Figure 5-17 E-selectin specific signal can be anatomically co-registered with plain X-ray imaging in collagen-induced arthritis

Mice were injected with either anti-E-selectin or anti-DNP antibodies labelled with Dylight 750 nm Near Infra Red fluorophore (5µg i.v.). Panel (a) shows 8 hour time-point of mice with/without clinically definite arthritis and paw thickness ≥2.2mm. Background fluorescence levels from uninflamed paws of non-arthritic healthy mice for both anti-DNP and E-selectin animals have been subtracted. (b) Representative image of mouse with hind paw arthritis and corresponding image co-registered with X-ray following subtraction of background fluorescence. Clinical scores of imaged paws are shown. Data are mean ± SEM, and were analysed by 1-way ANOVA *versus* arthritic anti-E-selectin antibody injected mice: ** $p<0.01$, *** $p<0.001$.

The relationship between paw thickness and MFI in all mouse paws from animals where arthritis had been detected was also examined irrespective of whether they had reached a paw diameter of ≥2.2mm. Interestingly, in animals with CIA, both anti-DNP and anti-E-selectin antibody fluorescence correlated with disease severity assessed as paw swelling (Pearson correlation co-efficient = 0.8605 and 0.863 respectively; $p<0.001$). However, the anti-E-selectin antibody fluorescence was significantly different to that for anti-DNP (slopes 1676 ± 265.1 and 954.9 ± 160.7 MFI arbitrary units per mm respectively, $p<0.05$). This is demonstrated in Figure 5-18.

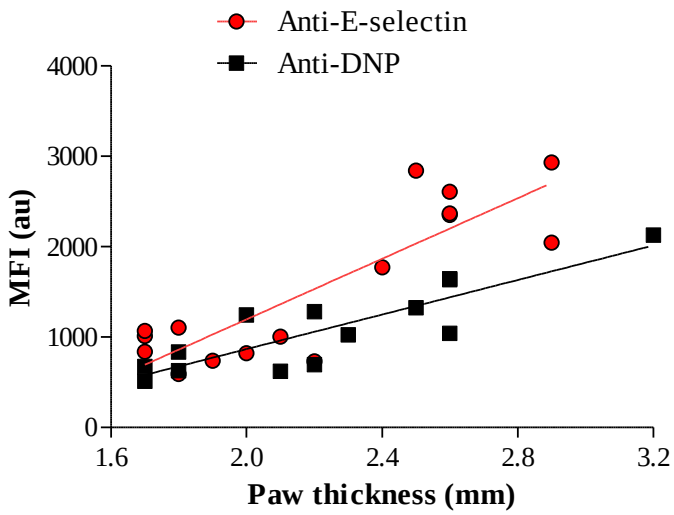

Figure 5-18 E-selectin fluorescent signal correlates with mean paw thickness

Mice were injected with either anti-E-selectin or anti-DNP antibodies labelled with Dylight 750 nm Near Infra Red fluorophore (5µg i.v.). At the 8 hour time-point the MFI of mice with/without arthritis was plotted against paw thickness. (Pearson correlation co-efficient = 0.8605 and 0.863 for anti-DNP and anti-E-selectin injected groups respectively; $p<0.001$).

5.3.2.1 E-selectin targeted signal detects subclinical arthritis

To analyse whether E-selectin targeted signal demonstrates increased sensitivity for detecting subclinical arthritis, fluorescent images of paws were selected for analysis from the above CIA experiment that had been given a clinical score of 0, but in mice that had developed arthritis in other paws. These images were compared to the paws of control animals that had not been immunised with collagen to induce CIA. A representative image of a mouse with hind paw arthritis in one paw but no obvious arthritis in the second contralateral paw is shown in Figure 5-19b. Joints with a clinical score of 0 but with increased E-selectin signal were seen in animals that had arthritis in other paws (Figure 5-19c). The mean signal returned from these animals was 924 ± 37 arbitrary units. This was significantly different ($p<0.01$) to the mean signal from paws of animals that had not been immunised for CIA (mean signal 795 ± 25). No significant differences were detected in the DNP signal returned from animals immunised for CIA (660 ± 43) compared to healthy controls (751 ± 46). Animals that had active arthritis in other paws were imaged, at between 5 and 10 days following arthritis onset (30-40 days following immunisation). The development of further arthritis in these paws would not be expected at this late stage of the experiment. Imaging also marked the endpoint of the experiment.

A further experiment was performed to examine whether anti-E-selectin targeted antibody signal was detectable prior to the onset of arthritis (data not shown). Following injection of dye labelled antibody, imaging was undertaken at days 14 and 21 following induction of arthritis. At day 14, none of the animals imaged had any detectable evidence of arthritis. None of the images showed any evidence of relative increased signal in any paws. At day 21, similarly, there were no animals where increased signal was visualised where arthritis was absent; i.e. this experiment did not demonstrate any predictive capability for detecting increased E-selectin expression prior to the onset of arthritis. Of the animals imaged at the day 14 time-point, 8 out of 10 in the anti-E-selectin antibody injected group developed arthritis and 6 out of 10 in the anti-DNP antibody treated group developed arthritis. They developed arthritis sequentially from days 16 and 18 respectively. At day 21, in the anti-E-selectin injected group, 6 animals had no evidence of arthritis and 3 of those went on to develop arthritis 2, 3 and 5 days following imaging. In the anti-DNP antibody treated group imaged at day 21, 6 animals had no evidence of arthritis and 2 of these

developed arthritis 3 and 6 days following imaging. Repeated injection of dye labelled antibody was not considered in this experiment due to the comparatively long half life of the antibody *in vivo* making detection of small differences in signal not possible.

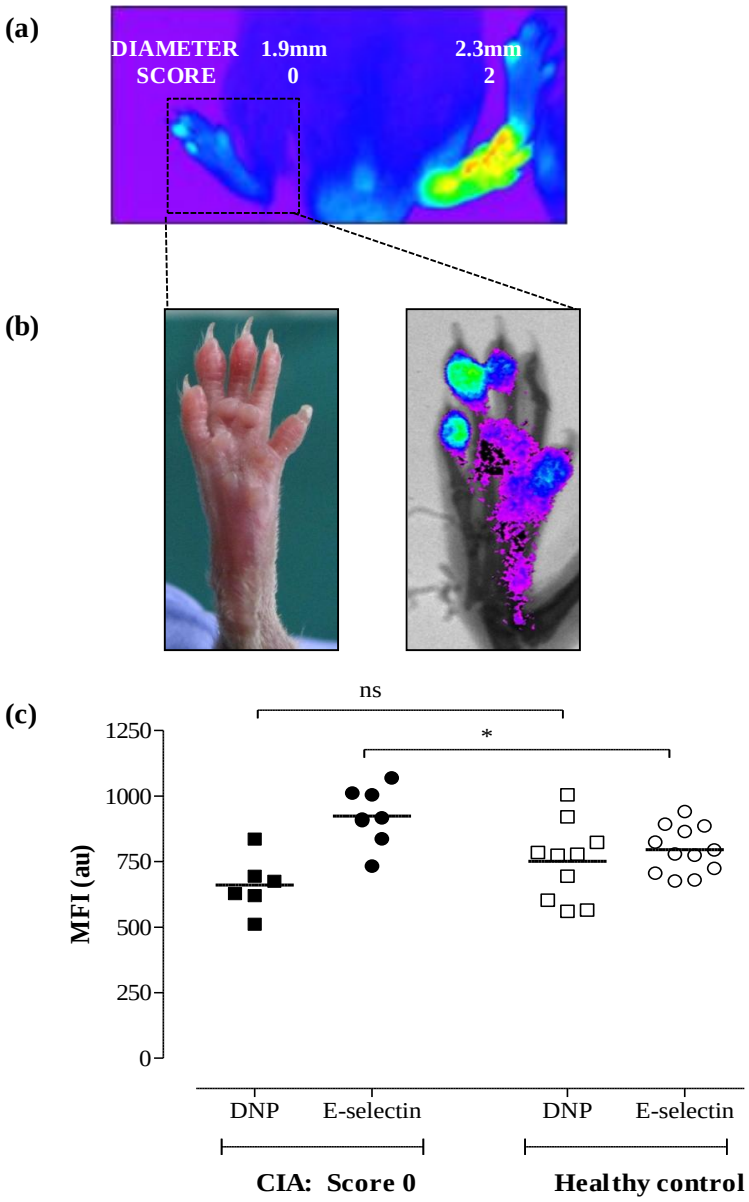

Figure 5-19 E-selectin targeted signal detects subclinical activation in CIA

Mice were injected with anti-E-selectin labelled with Dylight 750 nm Near Infra Red fluorophore (5µg i.v.). Paws were selected for analysis that had been given a clinical score of 0 in animals which had developed arthritis in other paws. These images were compared to the paws of age- and gender-matched control animals that had not been immunised with collagen to induce CIA. (a) Representative image of mouse with arthritis in 1 of 2 hind paws (clinical scores and paw diameters are shown). (b) Picture and fluorescence image with co-registered X-ray of paw without visible arthritis. (c) Quantification of the mean fluorescence intensity (MFI) from immunised and control groups at 8 hours. Line shows mean value, and data were analysed by 1-way ANOVA: $p<0.05$.

5.3.2.2 Etanercept abrogates fluorescent signal in CIA

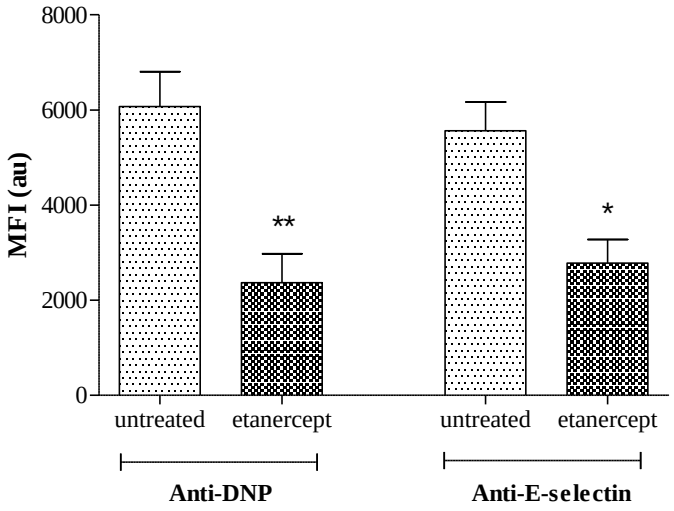

Figure 5-20 Etanercept abrogates fluorescent signal in CIA

Following onset of arthritis induced with bovine collagen, mice with clinically definite arthritis were either treated with etanercept (100μg i.p.) or left untreated. Groups were matched for clinical score and paw thickness, and injected with either anti-E-selectin or anti-DNP antibodies labelled with Dylight 750 nm Near Infra Red fluorophore (50μg i.v.). Data are mean ± SEM, and were analysed by 1-way ANOVA *versus* arthritic mice: * $p<0.05$, ** $p<0.01$.

Treatment with TNFα-Fc fusion protein (etanercept; 100μg i.p. on days 1, 4 and 7 following onset of arthritis) abrogated arthritis. The clinical score at day 10 following arthritis onset was 4.43 ± 0.69 in untreated mice, compared to 0.15 ± 0.34 in etanercept-treated mice ($p<0.05$ by t-test, n=6 per group). This correlated with a significant reduction in E-selectin targeted fluorescence signal. This is demonstrated in the above Figure 5-20. A similar decrease in fluorescence signal was observed in the anti-DNP injected group. There were no significant differences between the E-selectin and DNP etanercept-treated groups, and indeed between the E-selectin and DNP untreated groups.

5.3.3 Determining The Effect of The Human HER-1:HER-3 Epidermal Growth Factor Receptor Bispecific Ligand Trap on *In Vivo* E-selectin Targeted Fluorescent Imaging in CIA

Studies performed at the Kennedy Institute sought to determine whether RB200 had a therapeutic effect when used for the treatment of CIA. Initial experiments suggested favourable results, demonstrating that the potent human EGFR extracellular domain heterodimer RB200 abrogates CIA. This was determined by measuring the effects of RB200 on conventional outcome measures such as paw swelling and clinical score. Further experiments were performed to assess whether low dose RB200 and combined blockade by the etanercept would have additional therapeutic benefit. I therefore also sought to determine the effect that this combination treatment had on *in vivo* E-selectin targeted fluorescent imaging.

Disease was induced in 60 male DBA/1 mice (12 weeks old) as described in Section 2.5.2. RB200 (gift from Dr Michael Shepard, Halozyme Therapeutics, San Diego, USA) was administered intra-peritoneally (i.p.) on day of disease onset (day 1), and then on days 4 and 7 of disease, at a dose of 0.5mg/kg or 10mg/kg, with equal volumes of PBS equivalent to etanercept given to control animals (n=6 per group. (Prior experiments performed at the Kennedy Institute had demonstrated significant efficacy of RB200 at 10 mg/kg, minimal efficacy at 1mg/kg and no significant difference in disease severity of CIA at 0.1mg/kg, unpublished observations). Etanercept was given (i.p.) on the day of disease onset (day 1), and then on days 4 and 7, at a dose of 1mg/kg or 5mg/kg (equivalent to 20μg and 100μg per mouse respectively), with an equal volume of PBS equivalent to RB200 in control animals. (Similarly prior experiments had demonstrated significant abrogation of arthritis with 100μg (5mg/kg) of etanercept and minimal effect with 20μg (1mg/kg) of etanercept; Kennedy Institute, unpublished observations). Combination treatment of 0.5mg/kg RB200 plus 1mg/kg etanercept was given i.p. on day of disease onset (day 1), and then on days 4 and 7. Arthritis was assessed by paw swelling or as clinical scores based on all 4 paws. Fluorescence imaging *in vivo* was performed on day 10, animals were injected with anti-mouse E-selectin MoAb labelled with DyLight 750nm near infrared probe (excitation/emission spectra 752nm/778nm respectively). *In vivo* imaging studies were undertaken at 2, 8 and 24 hours following i.v. injection of NIR labelled anti-E-selectin antibody.

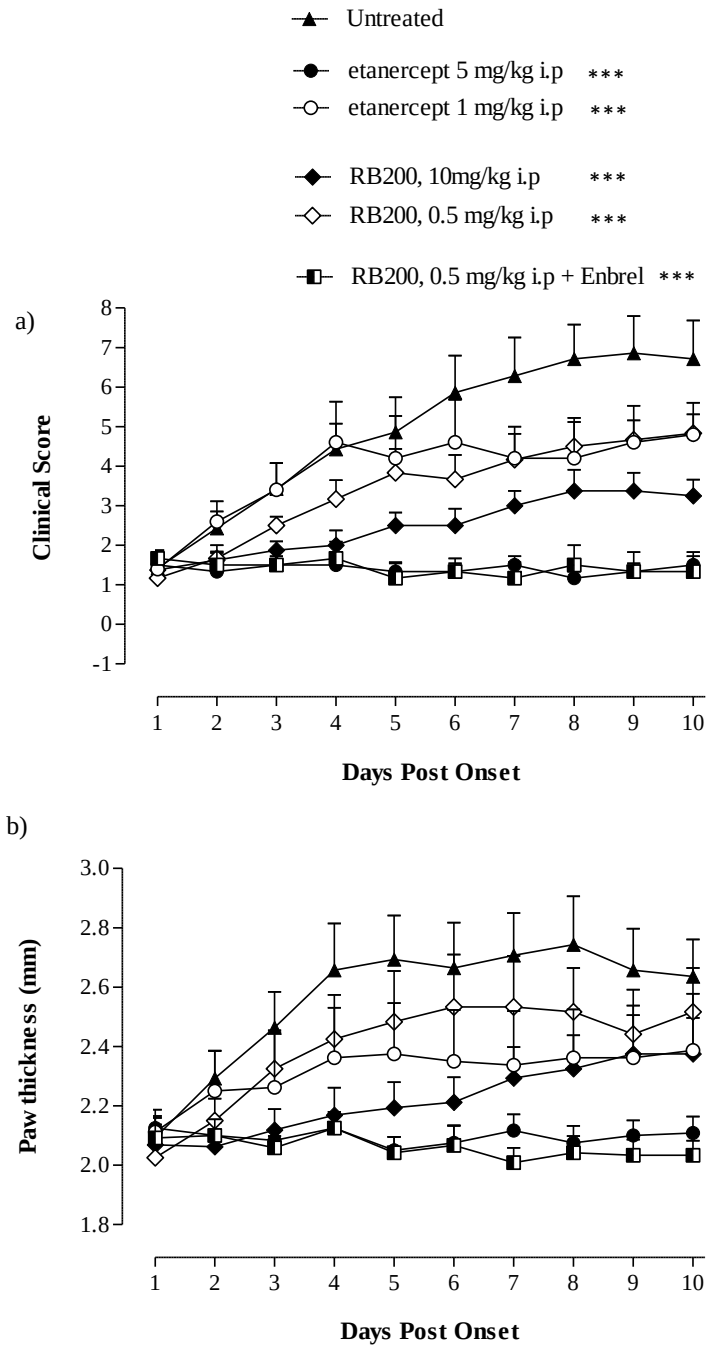

Figure 5-21 Low dose etanercept and RB200 exert a synergistic effect on clinical score and paw swelling in acute collagen-induced arthritis

Following onset of arthritis induced by bovine collagen, mice were treated i.p. on the day of disease onset (day 1), and then on days 4 and 7 of disease, with RB200 at a dose of either 0.5 (n=6) or 10mg/kg (n=8) or a combination of RB200 0.5mg/kg plus etanercept 1mg/kg (n=6). As controls, mice received 5mg/kg etanercept (100µg) i.p. (n=6) or 1mg/kg (20µg) i.p of etanercept (n=7) or an equivalent volume of PBS (n=7). (a) Clinical score was assessed. (b) Paw swelling was measured with callipers over a 10 day period, and data are both mean of the hind paws expressed as a difference from baseline. Results are expressed as mean ± SEM, and were analysed using 2-way ANOVA *versus* untreated mice: ***$p<0.001$.

The above figures demonstrate the effects of either RB200 or etanercept on disease in mice with established CIA. This shows that at high dose both etanercept (5mg/kg) and RB200 (10mg/kg) have a significant effect on both progression of clinical score and paw swelling. Similarly low dose etanercept (1mg/kg) and RB2000 (5mg/kg) ameliorates clinical score and paw swelling. The combination of RB200 and etanercept at low dose has a marked effect on both measures of disease activity in CIA. Indeed the RB200 and etanercept combination was significantly different to either low dose etanercept alone ($p<0.001$ for both clinical score and paw swelling) or low dose RB200 alone ($p<0.001$ for both clinical score and paw swelling).

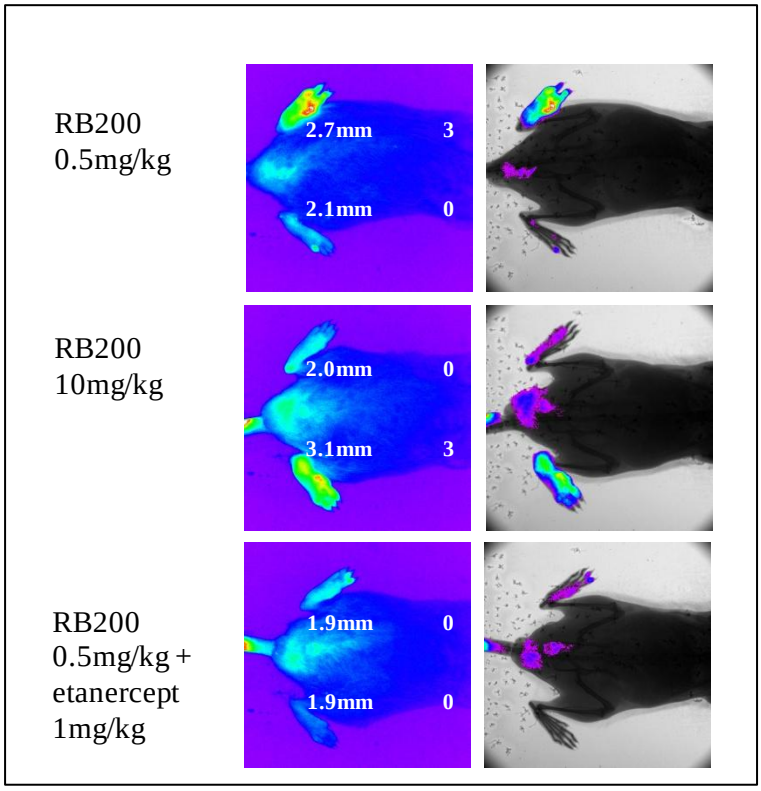

Figure 5-22 Low dose etanercept and RB200 exert a synergistic effect on E-selectin targeted *in vivo* fluorescent imaging in acute collagen-induced arthritis

Following onset of arthritis induced by bovine collagen, mice were treated i.p. on the day of disease onset (day 1), and then on days 4 and 7 of disease, with RB200 at a dose of 0.5 mg/kg or a combination of RB200 0.5mg/kg plus etanercept 1mg/kg. As controls, mice received 1mg/kg of etanercept or an equivalent volume of PBS. For imaging mice were injected with near infrared dye labelled anti-E-selectin antibody (5µg i.v.); images were obtained 8 hours following injection of the dye antibody conjugate. Left hand panel depicts mean fluorescent intensity of representative images following application of a colour wheel to depict signal intensity. Right hand panel demonstrates corresponding image co-registered with X-ray following subtraction of background fluorescence (mean signal intensity from animals not immunised for CIA).

Figure continued on next page.....

Figure 5.22 (continued)

Following onset of arthritis induced by bovine collagen, mice were treated i.p. on the day of disease onset (day 1), and then on days 4 and 7 of disease, with RB200 at a dose of 0.5 mg/kg or a combination of RB200 0.5mg/kg plus etanercept 1mg/kg. As controls, mice received 1mg/kg of etanercept or an equivalent volume of PBS. For imaging mice were injected with near infrared dye labelled anti-E-selectin antibody (5µg i.v.); images were obtained 8 hours following injection of the dye antibody conjugate. Left hand panel depicts mean fluorescent intensity of representative images following application of a colour wheel to depict signal intensity. Right hand panel demonstrates corresponding image co-registered with X-ray following subtraction of background fluorescence (mean signal intensity from animals not immunised for CIA).

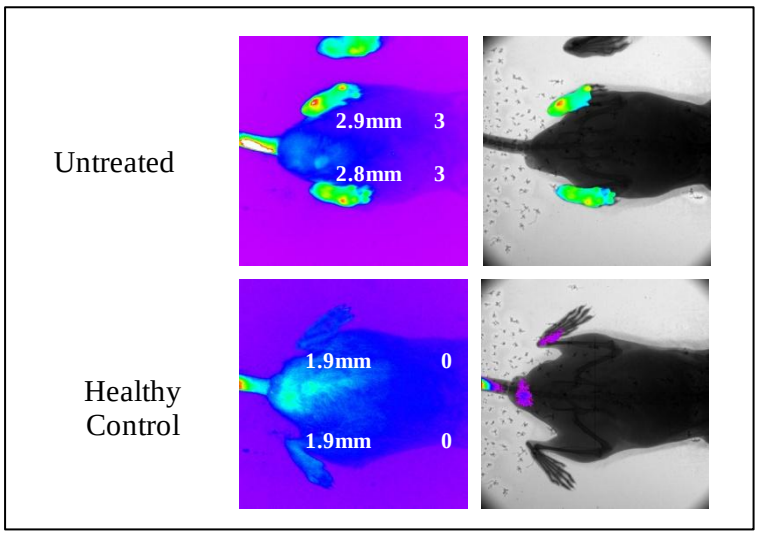

The above representative examples of fluorescent imaging demonstrate that the combination of low dose etanercept and RB200 apparently have a marked effect in decreasing the E-selectin targeted signal in animals with arthritis when compared with either treatment on its own. While both low dose etanercept (1mg/kg) and RB200 (0.5mg/kg) had some overall therapeutic efficacy on the total amount of arthritic disease in each animal, it was only with combination treatment that there was complete abrogation of fluorescent signal. Quantification of MFI over 24 hours in the different treatment groups is demonstrated below. This shows that combination treatment returns the E-selectin targeted MFI to the same levels as that seen in control animals that have not been immunised for CIA. Comparing the effect of anti-DNP and anti-E-selectin in the treatment groups would help to answer whether there is a differential effect of combination treatment on E-selectin specific signal. This was not possible in this experiment due to the sizes and diversity of treatment groups constraining the number of animals that could be imaged. The following Figure 5-23 demonstrates that the combination of low dose RB200 and etanercept have a significant additive effect on abrogation of E-selectin targeted fluorescent signal, when compared to either treatment administered in isolation. The mean fluorescence signal for each animal has been calculated by adding the mean fluorescence from both left and right hind paws. For the purposes of clarity mean fluorescent signal returned from animals treated with either high dose etanercept or RB200 have not been included on this graph, but are included in the following Figure 5-24. This figure demonstrates the mean signal returned from each paw of all animals in all treatment groups.

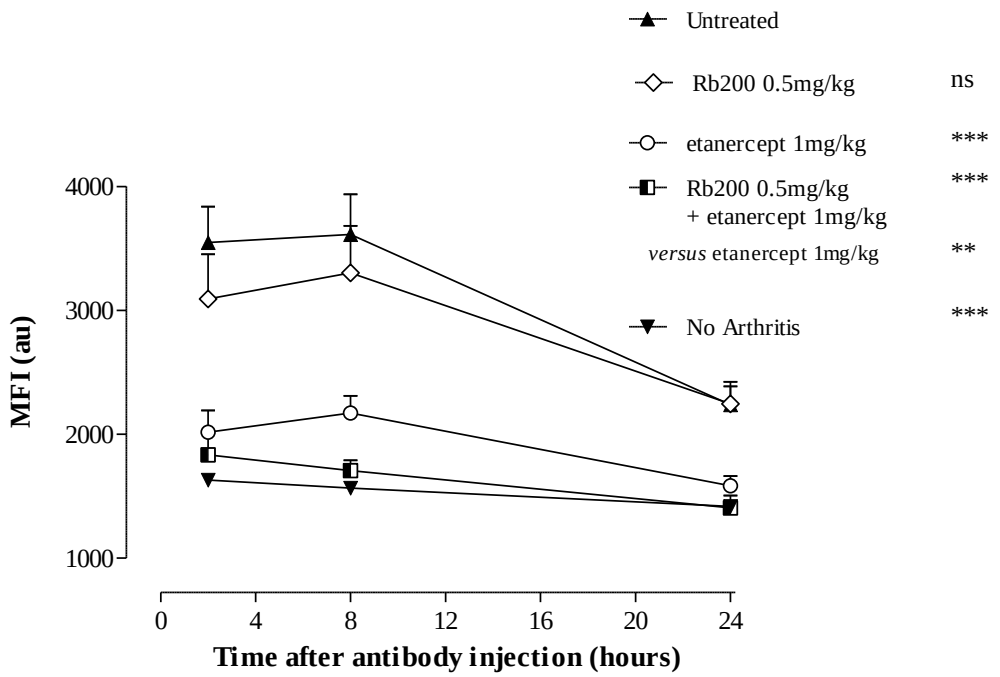

Figure 5-23 Low dose etanercept and RB200 exert a synergistic reduction in E-selectin targeted signal in acute collagen-induced arthritis

Following onset of arthritis induced by bovine collagen, mice were treated i.p. on the day of disease onset (day 1), and then on days 4 and 7 of disease, with RB200 at a dose of either 0.5 (n=6) or 10mg/kg (n=8) or a combination of RB200 0.5mg/kg plus etanercept 1mg/kg (n=6). As controls, mice received 5mg/kg etanercept (n=6) or 1mg/kg of etanercept (n=7) or an equivalent volume of PBS (n=7). For imaging mice were injected with near infrared dye labelled anti-E-selectin antibody (5µg i.v.); images were obtained at 2, 8 and 24 hours following injection of the dye antibody conjugate. Results are expressed as mean ± SEM of both hind paws, and were analysed using 2-way ANOVA *versus* untreated mice: ** $p<0.01$, ***$p<0.001$. An additional comparison between mice treated with RB200 0.5mg/kg plus etanercept 1mg/kg and etanercept 1mg/kg alone is also shown.

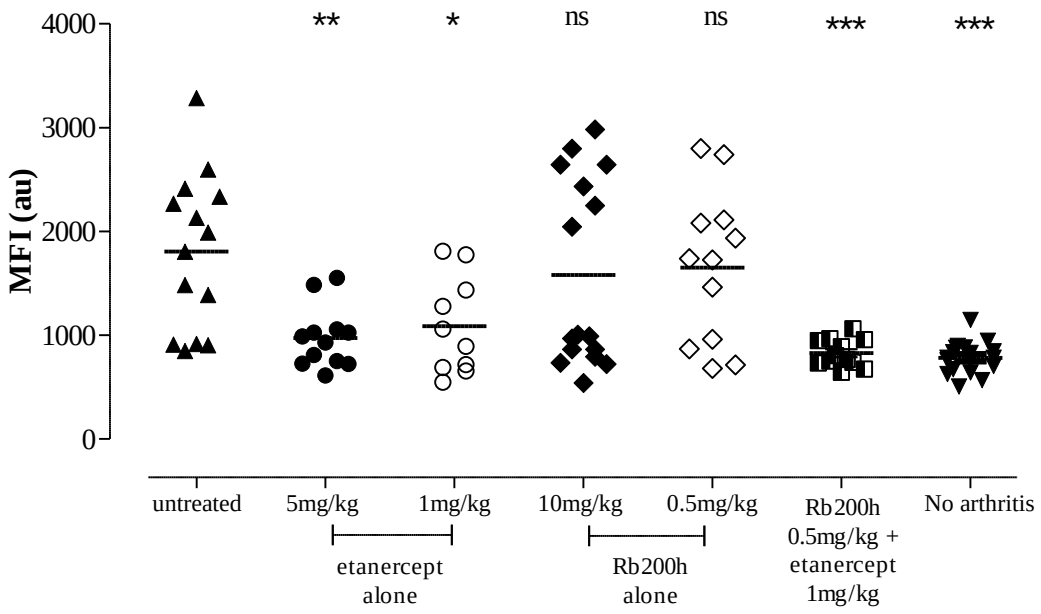

Figure 5-24 Low dose etanercept and RB200 exert a synergistic reduction in the incidence and severity of E-selectin targeted signal in acute collagen-induced arthritis

Following onset of arthritis induced by bovine collagen, mice were treated i.p. on the day of disease onset (day 1), and then on days 4 and 7 of disease, with RB200 at a dose of either 0.5 (n=6) or 10mg/kg (n=8) or a combination of RB200 0.5mg/kg plus etanercept 1mg/kg (n=6). As controls, mice received 5mg/kg etanercept (n=6) or 1mg/kg of etanercept (n=7) or an equivalent volume of PBS (n=7). For imaging mice were injected with near infrared dye labelled anti-E-selectin antibody (5µg i.v.); images were obtained at 8 hours following injection of the dye antibody conjugate. Data was analysed by 1-way ANOVA *versus* untreated mice (***$p<0.001$).

The MFI returned from each individual mouse paw from each treatment group at the 8 hour time-point is shown in Figure 5-24. This highlighted that the combination treatment results in a marked reduction in arthritis in all mouse paws. The mean fluorescent signal from other treatment groups showed that higher levels of signal are returned from a proportion of animal paws, suggesting that there remained elevated levels of inflammation in these groups. Further experiments with increased animal numbers would be required to delineate the additional benefit of combination treatment at differing relative doses.

5.4 Discussion

CIA is an animal model that has significant similarities to RA and is characterised by progressive joint swelling and destruction. In this chapter, I have established that during the course of CIA, E-selectin expression on activated endothelium can be detected by immunohistochemistry. I have then shown that NIR dye labelled anti-E-selectin antibody can be detected by fluorescent reflectance imaging in the inflamed paws of animals with CIA when compared to the uptake of NIR dye labelled isotype control antibody to similar sites of inflammation within the arthritic joint. Furthermore, subclinical levels of increased E-selectin signal are investigated. This is a novel method for detecting and quantifying the *in vivo* expression of E-selectin in CIA. Finally, I have demonstrated that NIR E-selectin targeted imaging can be used to investigate the effects of a novel therapy in CIA. This has quantified the effect of RB200 – a pan ligand EGFR trap - that demonstrated a significant synergistic blockade of E-selectin targeted fluorescent signal when used in combination with low dose etanercept.

CIA was induced by immunising male DBA/1 mice with heterologous (bovine) type II collagen. Clinical observations and measurements of both paw swelling and clinical score have confirmed that CIA followed a typical clinical course of disease in these experiments. Similarly, histological analysis also confirmed the presence of arthritis and progressive joint destruction with worsening severity of arthritis. Synovial vascularisation was also assessed by microscopic examination of tissue sections probed for both E-selectin and CD31 by immunohistochemistry. Angiogenesis, the formation of new blood vessels, is one of the earliest histolopathologic findings in RA and appears to be necessary for pannus development (Kimball and Gross 1991) and also plays an active role in inflammation as a source of both cytokine and protease activity due to the increased number of blood vessels and infiltrating cells brought in by these vessels (Colville-Nash and Scott 1992). The expanded vascular bed volume resulting from angiogenesis may be further expected to have ongoing expression of cytokines including E-selectin. This has been confirmed by the immunohistochemistry experiments described in this chapter that show increased CD31 expression within areas of invading inflamed synovium around the arthritic joint and in addition also demonstrated E-selectin expression within these areas. Analysis of the immunohistochemistry specimens demonstrated that not all specimens

or areas of inflamed tissue demonstrated E-selectin expression. This emphasizes the difficulty of analysing immunoreactivity of antigens expressed on the endothelial surface following the fixation process for mouse paws as described in Section 2.6. A previous study that investigated the expression of E-selectin CIA noted occasional E-selectin expression that may be due to underlying specimen preparation (Everts, Asgeirsdottir et al. 2003). However, analysis of E-selectin expression in different tissues in the pig following E-selectin staining showed most intense staining on the endothelium of arteries and veins of all sizes, with less expression on capillaries (Keelan, Licence et al. 1994). This observation indicates that there may be heterogeneity between the EC lining of different vessels in their capacity to respond to stimulation by inflammatory signals such as cytokines. They may therefore have a differing ability to react to leukocytes. Differences between the pattern of immunohistochemical staining for E-selectin expression and *in vivo* findings may occur for other reasons. A component of fluorescent signal in inflamed tissue may be due to the uptake of fluorescently labelled E-selectin antibody bound to soluble E-selectin. Evidence does support there being a pool of soluble E-selectin and this is discussed in Section 1.2.2.3. Attempts were made to further analyse the distribution of E-selectin in the inflamed paw with fluorescent microscopy following injection of NIR dye-labelled antibody. This however proved challenging since there were limitations to the filter sets that were available in the NIR range and following specimen preparation there were significant levels of autofluorescence in the heterogenous tissue of the inflamed paw. The co-registration of fluorescent signal with plain X-ray however, has helped to delineate increased *in vivo* signal around the ankle and metatarsal heads. This corresponded with the sites of maximal tissue damage observed on histological specimens. More detailed analysis of these changes using the current imaging and X-ray device would be limited by the resolution of digital images obtained. There are alternative macroscopic fluorescent imaging devices that have a higher level of resolution compared to the apparatus used for these experiments. For example, two photon-excitation microscopy is a fluorescence imaging technique that allows imaging of living tissue up to a depth of one millimeter (Denk, Strickler et al. 1990). Compared to a confocal microscope, photon detection is much more effective since even scattered photons contribute to the usable signal. A number of limitations of two-photon microscopy exist: the pulsed lasers needed for two-photon excitation are much more expensive then the constant wave (CW) lasers

used in confocal microscopy; the two-photon absorption spectrum of a molecule may vary significantly from its one-photon counterpart; and for very thin objects such as isolated cells, single-photon (confocal) microscopes can produce images with higher optical resolution due to their shorter excitation wavelengths. In light scattering tissue, on the other hand, the superior optical sectioning and light detection capabilities of the two-photon microscope result in better performance. It is therefore a technique that with appropriate adaptations may be well suited to imaging peripheral arthritis in animal models.

One of the significant challenges of this section of work was to ensure that there were sufficient animals within each comparator group so that levels of arthritis were closely matched for clinical score and paw swelling. The heterogeneity of CIA is a useful paradigm of RA, but this makes matching for changes in clinical score and paw thickness between groups of animals very challenging. My work in the previous chapter had shown that a significant component of the fluorescent targeting was due to the non-specific uptake of antibody to sites of inflammation. This occurs at sites where there is increased vessel permeability allowing leakage of macromolecules from the circulation into the inflamed area. The initial immunohistochemistry work in CIA had shown that E-selectin expression could be detected at both early, mid and late time-points during the course of arthritis. Overall analysis of the control and anti-E-selectin antibody targeted groups did also confirm that they were matched for duration of arthritis and the time of imaging. Nevertheless this did not give precise information about the time course of E-selectin expression during the evolution of arthritis in the CIA model. The heterogeneity of CIA is also reflected when analysing the fluorescent emission from both arthritic and non-arthritic paws in CIA. This showed that there is considerable variation in signal intensity, between animals and between paws in the same animal. This is reflected in Figure 5-20 - while there are significant differences between etanercept treated and untreated groups there were no differences between E-selectin and DNP targeted untreated groups. There are likely to be a number of reasons for this. The number of animals in each of the groups was comparatively small (n=3-4 per group) so that despite matching of groups for clinical score there was significant heterogeneity in signal. Also, this experiment was performed prior to the experiments detailed in Section 4.3.4 that showed an injection of 5μg dye labelled antibody had increased sensitivity for detecting differences in the

MFI between anti-DNP and anti-E-selectin dye labelled injected animals. Hence, in order to detect the E-selectin specific component of the fluorescent signal in CIA compared to trafficking of non targeted antibody, the number of animals was increased in each comparator group, the optimum dose of antibody was used and paws were closely matched for clinical score and the extent of paw swelling. By closely controlling for these parameters I have shown that E-selectin targeted signal can be detected during the evolution of arthritis in CIA in addition to the increases in signal from anti DNP injected antibody. This suggests that there is ongoing endothelial activation and E-selectin expression in the inflamed joint, in addition to changes in vascular permeability. Other workers have also recorded potential difficulties analysing data from CIA experiments due to low levels of incidence and disease heterogeneity. For example Palframan and colleagues did not generate enough data points to examine the distribution of fluorescently labelled certolizumab pegol at all stages of arthritis (Palframan, Airey et al. 2009) and paws were only analysed with a score of 2 which may significantly decrease the objectivity of comparisons between groups because of the subjective nature of clinical scoring.

The heterogeneity of CIA was also a particular challenge when attempting to determine whether E-selectin targeted imaging could be utilised as a predictor of arthritis onset in any given animal. Since the onset of arthritis may be at any time-point between 14-30 days following immunisation assessing at which time-point to image was problematic. Similarly, obtaining matched animals between groups when incidence of arthritis was variable was also challenging. Over a number of experiments it was also noted that at times a number of animals develop a transient arthritis that subsequently resolved. The reasons for this spontaneous regression or lack of arthritis progression are not understood. It may be possible that there is an imbalance between regulatory T-cell (Treg) numbers at various time-points during the evolution of arthritis. This supported by the finding that anti-CD3 therapy expands the number of CD4+ and CD8+ Treg cells and induces sustained amelioration of CIA (Notley, McCann et al.). Since it is possible to label anti-CD3 antibody one possibility would be to co-image animals following injection with two different fluorescently labelled targets such as anti-CD3 and anti-E-selectin antibody. These could be labelled with similar fluorophores but with sufficiently different excitation/emission wavelengths so that they could be discriminated *in vivo*. By injecting both antibodies

into the same animal it would be possible to measure their differing fluorescent emission over the time course of inflammation. It would also be of interest to investigate the early expression of E-selectin prior to the onset of arthritis further. This would obviously be of significant use clinically to determine appropriate targeted molecular therapy at an early stage in the evolution of arthritis. Further comparison regarding the change in anti-E-selectin *versus* anti-DNP dye labelled antibody signal changes over the time course of arthritis would also be of interest. This would provide information about *in vivo* dynamic changes in adhesion molecule expression compared to local permeability changes during the evolution of early arthritis.

Injection of dye labelled control antibody does also detect changes in paw thickness and paw oedema in CIA. There is a linear correlation between paw swelling and the MFI returned from inflamed joints. The trafficking of macromolecules to sites of inflammation due to increased vessel permeability has previously been recognised to take place at the inflamed joint and this is discussed in Section 1.2.4. The NIR fluorophore Cy5.5 was visualised in arthritic knee joints following induction of antigen induced arthritis in mice (Hansch, Frey et al. 2004) showing a 1.5 fold increase in signal in the inflamed knee joint. This is similar to the increase in anti-DNP antibody fluorescent signal - demonstrated at the 8 hour time-point in Figure 5-17. However it is at this time-point that there is a further 2.34 fold increase in anti-E-selectin targeted fluorescence signal which points to ongoing E-selectin expression on the activated endothelium in CIA. This suggests that there is continued recruitment of inflammatory cells to sites of inflammation in CIA during the progression of arthritis.

This study however, did demonstrate that E-selectin targeted signal can be detected in animals immunised for CIA with subclinical arthritis suggesting that even in animals without overt arthritis there is a background level of vascular activation. Closely correlating increased signal in these animals with underlying histological change, may help to determine whether there are underlying histological abnormalities in these paws or whether increased signal represents a general or systemic increase in E-selectin targeted signal. This may help to delineate be whether there has been complete abrogation of arthritis and vascular inflammation by targeted molecular therapy, or whether there was only amelioration of arthritis.

The effect of the fusion receptor protein etanercept on fluorescence imaging in CIA was also examined. In this experiment it was challenging to generate sufficient numbers in both treatment and control groups to adequately examine the differences between the reduction in isotype control (non-specific) fluorescent signal and the signal due to specific E-selectin targeting. In the previous chapter I demonstrated that E-selectin targeted imaging was significantly reduced by etanercept in the TNFα-induced paw inflammation model. Since there is likely to be a significant proportion E-selectin expression early in the course of this model then blockade of TNFα is likely to have a significant effect on the E-selectin specific component. However in the CIA model E-selectin expression is likely to be at a continuous but lower level over the chronic course of arthritis, hence etanercept may have a proportionately less significant effect on selectin *versus* non-specific dye trafficking.

The final section of work in this chapter examined the differential effect of the novel pan ligand EGFR blocker RB200 on both conventional clinical scoring and on E-selectin targeted *in vivo* optical imaging. In order to determine the effects of both etanercept and RB200 at high and low dose, as well as the two in combination at low dose and obtain matched groups, I examined their respective effects on E-selectin targeting only. The combination of low dose RB200 and etanercept completely abrogates arthritis by both measures. It is interesting to note that this includes complete abrogation of the fluorescent signal to a level seen in healthy controls. Cellular heterogeneity, redundancy of molecular pathways and effects of the microenvironment are all likely to contribute to the disease heterogeneity seen in CIA. This makes it unlikely that therapy directed at one abnormally activated signalling pathway is likely to be sufficient (Citri and Yarden 2006). Therefore combined blockade of functionally linked and relevant multiple targets has become an attractive therapeutic strategy. The implications of this are discussed further in Chapter 6

In summary in this chapter I have demonstrated that E-selectin targeted is a viable *in vivo* imaging technique in CIA with significant potential to investigate further the early molecular changes that occur in arthritis in the animal model. The combined approach of collectively targeting EGFR signalling, thereby inhibiting the potential for neoangenesis as well as blockade of the key cytokine TNFα that may be produced both prior and following EGFR activation represents an opportunity to switch off the molecular aberrations in CIA and prevent the evolution of arthritis. Deploying a novel

molecular *in vivo* fluorescence imaging technique by targeting the endothelial expression of E-selectin may also be a highly specific method of monitoring the effects of dual targeted therapy.

CHAPTER 6

6 GENERAL DISCUSSION

Expression of leukocyte adhesion molecules such as E-selectin on the surface of EC is one of the first steps in the evolution of chronic inflammation, which underlies the pathogenesis of disease states such as RA. The first objective of this study was to demonstrate the use of a fluorescently labelled monoclonal antibody against E-selectin to visualise endothelial activation by optical imaging in inflamed tissues *in vivo*. I have demonstrated that both E-selectin and DNP isotype control antibody can be reproducibly manufactured from cell culture and have ensured that labelling with a NIR dye was achieved reliably. The parameters of *in vivo* NIR imaging of arthritis have been explored so that specific and background signal from inflamed joints was determined. I have then demonstrated that E-selectin targeted *in vivo* optical imaging both in the TNFα-induced model of paw inflammation and in acute CIA is a sensitive, specific and quantifiable molecular imaging technique. My second objective was to determine whether the effects of novel vascular targeted therapy can be interrogated by utilising E-selectin targeted *in vivo* fluorescent imaging. The effects of RB200, a pan ligand EGFR trap, were investigated. NIR E-selectin targeted imaging was able to delineate clear differences between both E-selectin and RB200 treatment groups and to demonstrate the abrogation of arthritic E-selectin generated signal with the combination of low dose etanercept and RB200.

Developing a model of inflammation by injecting TNFα into the hind paw to generate acute inflammation was a key component of the success of this project. This technique has previously been utilised to demonstrate the role of TNFα in the development of acute inflammatory hyperalgesia (Cunha, Poole et al. 1992). The novel use of the TNFα-induced paw model was utilised as an *in vivo* platform for targeted fluorescence experiments. Disease onset was acute, incidence was 100%, animal redundancy was minimised and the TNFα dose-dependent inflammatory response was extremely reproducible. Furthermore imaging and anaesthetic protocols were developed and standardised, so that imaging could be performed safely on multiple animals at selected time points over 24 hours to investigate peak differences between control and target antibody injected groups. Labelling E-selectin with a fluorophore in the NIR range was also important for successful *in vivo* imaging. This ensured specific signal from inflamed paws was not subject to the significant

autofluorescence that occurs when imaging at lower wavelengths (Fischer, Gemeinhardt et al. 2006; Weissleder and Pittet 2008). Preliminary work demonstrated that at lower wavelengths autofluorescence would be a major limiting factor in detecting signal from a specific molecular target. Therefore imaging at higher wavelengths e.g. in the NIR range has helped to increase the sensitivity of optical *in vivo* imaging by decreasing background autofluorescence. The time course of NIR fluorophore-labelled anti-E-selectin antibody binding over 6-8 hours in this model is in keeping with previously found kinetics for E-selectin expression *in vivo* (Harari, McHale et al. 1999). Measuring levels of signal from uninflamed paws determined signal sensitivity (E-selectin antibody signal *versus* background), whereas comparing anti-DNP control antibody injected groups to those injected with anti-E-selectin antibody determined signal specificity. Subtracting background signal from uninflamed paws from the signal obtained from inflamed paws was one method of ensuring variations due to differences in injection volumes between animals were excluded. Furthermore this refined model allowed for a considerable reduction in the number of animals required for initial *in vivo* imaging techniques. Experiments could be designed and performed rapidly and the incidence of inflammation within each experiment was 100%. Consistent levels of paw swelling were also generated following injection of TNFα into the footpad and this further reduced the number of animals required. This adheres to the principles of good experimental practice for humane experimental techniques that have been instituted and developed for biomedical research in all specialties (Workman, Aboagye et al. 2010) This model also provided useful information about the differences between non-specific trafficking of dye labelled anti-DNP antibody compared to E-selectin targeted imaging. TNFα-driven acute inflammation by direct injection in the footpad is likely to cause vascular permeability changes by upregulating a number of local pro-inflammatory agents that lead to acute permeability changes in the vessels of the mouse paw. Interestingly, the TNFα paw injection model was originally developed for investigating pain pathways in the foot. This is described further in Section 1.4.2. Previous work on this and other similar models of acute inflammation in the footpad have demonstrated that there may well be a significant neurogenic component to local paw swelling. In particular the tachykinin neuropeptide substance P has been shown to be a potent mediator of microvascular permeability. This is discussed further in the introductory Section 1.2.4. It is therefore likely that both DNP and a proportion of E-

selectin labelled antibodies have similar initial trafficking into the inflamed mouse paw. Nevertheless, E-selectin upregulation (as demonstrated by immunohistochemistry) leads to additional targeting of anti-E-selectin labelled antibody as detected by fluorescence imaging. The differences between local or regionalised specificity of dye antibody trafficking *versus* EC specific targeting are of interest for both future molecular imaging as well as the potential for specific targeting of the inflamed synovium to enhance local delivery of novel therapeutics.

The observations from the TNFα-induced paw oedema model were then translated into the murine heterologous CIA model. This has several similarities with RA, including synovitis, pannus formation, erosion of cartilage and bone, fibrosis and joint rigidity (Holmdahl, Jansson et al. 1986; Holmdahl, Andersson et al. 1989). Despite much work in CIA focussing on disease pathways, the dynamic changes in leukocyte expression remain poorly defined. Immunohistochemistry to detect expression of antigens such as E-selectin, to inform on changes in leukocyte trafficking, can be challenging and difficult to quantify. Hence, for this project novel techniques for paw decalcification and specimen preparation were utilised to ensure that E-selectin and the vascular marker CD31 could be detected. This demonstrated that E-selectin could be detected at both early (day 2), mid (day 5), and late (day 10) of arthritis. When *in vivo* imaging was applied in the CIA model, with close matching of clinical groups for disease severity, E-selectin signal could be detected as early as 30 minutes and up to 24 hours following antibody injection with significant correlation between E-selectin and clinical score. In CIA, as was the case with the acute paw oedema model, the differences between specific and non-specific trafficking of either anti-DNP or anti-E-selectin dye labelled antibody are of interest. In the TNFα-induced model, early release of vasactive mediators following TNFα injection generates acute permeability change leading to both non-specific trafficking of antibody as well as increased anti-E-selectin antibody binding as discussed above. However in the CIA model, where arthritis is well established, there are also likely to be other factors as well as expression of vasoactive substances that lead to ongoing permeability changes. In established CIA the invading synovium is rich in neoangiogenic blood vessels that have disordered architecture and increased vascular permeability . This is likely to be similar to the permeability change that occurs in neoangiogenic tumour blood vessels (McDonald and Baluk 2002). Primarily, the increased leakiness of

pathologic neoangiogenic vessels compared to normal vessels, is therefore also likely to play an important role in generating fluorescent signal in established CIA. The initial investigations of E-selectin targeted *in vivo* optical imaging in CIA focussed on analysing whether specific signal can be achieved compared to isotype control antibody in animals with established arthritis. In these animals there does appear to be ongoing E-selectin expression that can be detected by E-selectin targeted optical imaging. However, I have also shown that there was increased E-selectin upregulation in non-arthritic paws in these animals with no significant increase in anti-DNP antibody targeted signal. This may suggest that there is either local or systemic ongoing vascular activation in CIA which does not lead to substantial local permeability change (since this change would be represented by increased levels of control antibody signal due to non-specific macromolecular leakage into the inflamed synovium). Further analysis of these groups including histological correlation would be required to verify that this *in vivo* imaging technique could be used to investigate the differences between E-selectin upregulation and permeability change during the course of CIA. Analysis of anti-E-selectin binding prior to disease onset would also provide important details about early vascular changes occurring during the inception of arthritis. The disease heterogeneity seen in CIA to a degree reflects the complex pattern of disease seen in RA, which is characterised by more complex patterns of joint involvement and relative sparing of some joints, such as the distal interphalangeal joints in the hands. The reasons for tissue specific differences in disease expression and vascular permeability in RA or indeed in the animal model have not been fully elucidated but could be addressed further with vascular targeted optical imaging. More recent investigations into the mechanisms that may underlie joint specific inflammation have indicated that there are tissue specific cell adhesion molecules and vascular ‘addressins’, in addition to chemokine-receptor interactions (Pitzalis and Garrood 2006). In addition other evidence suggests that arthritogenic antibody transfer from K/BxN mice causes local macromolecular vasopermeability (Binstadt, Patel et al. 2006). This is also discussed in Section 1.2.4 in relation to the general permeability changes that occur due to the realease of local vasoactive amines and due to the pathologic architecture of neoangenic vessels.

Few studies have investigated the changes in vascular permeability that occur in RA and other inflammatory diseases. One early study performed by Jayson and colleagues

in 1971 did analyse the rate of tissue fluid formation in the forearms of patients with RA, demonstrating that there were increases in the rate of oedema formation that was independent to pre-existing therapy (Jayson and Barks 1971). There are however clear differences between CIA and RA. Arthritis in the mouse paw occurs in association with oedema of the whole mouse paw – it is this change that is readily detected by fluorescent imaging where there is a linear correlation between paw swelling and mean fluorescent signal. In RA there may be localised joint swelling, but not swelling of the whole hand or foot. RA is also characterised by significant levels of bone marrow oedema that occurs at both early and established phases of disease. Longitudinal MRI analysis of bone marrow oedema in the wrists of patients with RA has been demonstrated to predict erosive progression (Palosaari, Vuotila et al. 2006). Bone marrow oedema (i.e. increased water content in the trabecular bone) can also be a non-specific and reversible finding that is frequently seen in patients following trauma and other conditions such as OA. Detecting differences between non-specific oedematous changes and those associated with progression to inflammatory joint disease would clearly be helpful. There are limitations to the current system since oedema from different tissues can only be viewed in two dimensions. But the facility to co-register images with digital X-rays of the target region further helped delineate anatomical localisation of fluorescence signal has been explored in this study. This helped to identify signal in specific areas such as around the ankle and forefoot joints. The ability to co-register images using different modalities such as optical and X-ray imaging is likely to be of significant use when using novel imaging platforms to detect underlying pathological molecular changes in arthritis. A multimodal nanoparticle contrast agent containing embedded luminophores and surface immobilised gadolinium chelates has been developed as a contrast agent for inflamed synovium in CIA (Kim, An et al. 2009). Multimodal imaging in a heterogeneous model such as CIA is likely to be of significant use so that accurate comparisons in individual animals can be made.

The detection of subclinical activation in CIA may be useful for other reasons. Firstly, it may be that this can be developed as a method of detecting very early arthritis. Interestingly this compares with similar findings when radiolabelled E-selectin was used to image endothelial activation in RA and found to image specifically some clinically silent joints (Chapman, Jamar et al. 1996). Secondly, the detection of

ongoing subclinical levels of endothelial activation in CIA may be of use in detecting the efficacy of therapy. As targeted therapy evolves to complete blockade of arthritis, there will be a need to ensure that disease activity has been completely abrogated. It is well recognised in RA, that vascular inflammation leads to worsening cardiovascular morbidity and mortality. Standardised mortality ratios for cardiovascular disease in RA range from 1.2 to 5 and cardiovascular death accounts for up to 50% of mortality with life expectancy reduced by 10-15 years (Sattar, McCarey et al. 2003). There is also a similar trend in patients with systemic lupus erythematosus and other connective tissue diseases with a marked increase in stroke and myocardial infarction reported (Esdaile, Abrahamowicz et al. 2001). This is supported by both epidemiological data and in addition there is strong evidence that systemic markers of inflammation independently predict coronary heart disease events in men and women without pre-existing heart disease (Sattar, McCarey et al. 2003). The suspected pathogenesis of atherosclerosis has evolved from a lipid deposition disorder to a focal chronic inflammatory disease with upregulation of macrophage activating cytokines such as TNFα, IL-1 and IL-6 (Pasceri and Yeh 1999). Hence, an *in vivo* imaging system that is able to target E-selectin expression on chronically activated endothelium and its abrogation by specific molecular therapy may be of considerable use in determining longer term responses to treatment. There are however limitations to the current system in this respect. Imaging has been possible in the relatively denuded mouse paw that is only a few millimetres thick, but attempts to imaging specific signal in other areas have been less successful. For example to image chronic inflammatory change in large vessels such as the aorta other tissue as well as mouse skin and fur would contribute to light scattering. The current imaging device would also lack resolution to detect signal change in specific vessels clearly. One solution may be to deploy alternative hardware devices that utilise tomographic techniques to generate images in multiple planes so that signal can be resolved at different depths in three dimensions. A recently published study utilised novel tomographic techniques to discriminate between DMARD and non-DMARD therapy in CIA. Although the tomographic technique allowed discrimination of different parts of the mouse paw, resolution may need to be improved further to delineate signal differences between large vessel walls and their lumen in CIA (Peterson, Labranche et al.).

Other studies also reflect similar kinetics for *in vivo* imaging of experimental arthritis with NIR fluorescence. Hansch *et al* examined early experimental arthritis with NIR fluorescence in a murine model of antigen induced arthritis; the target was the F4/80 antigen present on the surface of macrophages. This demonstrated that there were peak differences in signal intensity at 2-6 hours following antibody injection with a reduction in responses to baseline levels of fluorescence at 72 hours following injection of isotype control antibody with still some residual level of fluorescence from Cy5.5 target antibody (Hansch, Frey et al. 2004). Changes in the level of the F4/80 antigen as detected by immunohistochemistry were not measured in this experiment. A cathepsin B activateable NIR fluorescent probe was used in a mouse model of osteoarthritis and showed a 3-fold difference in signal intensity between normal and osteoarthritic joints (Bhaumik and Gambhir 2002; Lai, Chang et al. 2004). My study, however, is the first to target the endothelium by a specific molecular marker and to quantify the temporal changes of both isotype control and targeted antibody trafficking in two differing murine models of arthritis.

Using E-selectin targeted fluorescent imaging to test the action of the novel compound RB200 marked the second important objective of this study. This was firstly an opportunity to investigate the efficacy of this drug in CIA using a novel molecularly targeted *in vivo* imaging technique. Secondly this helped to delineate the possibilities for using a vascular targeted imaging technique to define the effects of therapy *in vivo*. This showed the additional abrogation of E-selectin targeted signal with combination therapy. Significant evidence points to a link between EGFR receptor blockade and downstream signalling pathways that lead to neoangiogenesis in the inflamed joint. Ligand binding to EGFRs causes autophosphorylation of the RTK domain and activation of a series of intracellular pathways leading to gene transcription. Therapeutic agents that target EGFR and/or ERBB2 generally induce cytostatic effects in vitro, and less frequently apoptosis (Baselga and Arteaga 2005; Mendelsohn and Baselga 2006). By contrast, *in vivo* data have shown that anti-EGFR therapy can induce tumour regression, an effect that might not be explained in full by inhibition of the tumour target (Hanahan and Folkman 1996). This discrepancy suggests that EGFR signalling affects both biological effects of the tumour cell and tumour-host interactions during angiogenesis. In addition direct angiogenic effects have been demonstrated in EGFR-expressing human microvascular EC which induce

tube formation in response to EGF or TGF-α signalling. These processes are prevented by the tyrosine kinase inhibitor gefitinib (Okamura, Morimoto et al. 1992; Hirata, Ogawa et al. 2002). In addition human umbilical vein EC (HUVECs) which do not express EGFR, do not migrate in the presence of EGF or TGF-α; however, these cells do migrate when co-cultered with cells expressing high levels of EGFR and they then produce VEGF and IL-8 following stimulation of EGF, thus inducing endothelial growth through paracrine mechanisms (Okamura, Morimoto et al. 1992). Other workers have investigated the effects of targeted combination therapy. Combined anti-TNF and anti-IL-1 therapy showed initial promise in animal models of arthritis (Bendele, Chlipala et al. 2000; Feige, Hu et al. 2000). However, this success was not replicated in RA patients treated with combination therapy who had failed to show clinical improvement following methotrexate therapy. In addition there was an increased incidence of infection in the combination treatment group (Genovese, Cohen et al. 2004). The data presented here suggest that combining drugs which target both a central component in the cytokine cascade (TNFα) and abrogate neoangiogenesis (via modulation of EGFR and VEGF) may therefore hold significant promise in RA.

Taken together the above work has validated E-selectin targeted optical *in vivo* imaging as a novel modality for investigating animal models of inflammation and arthritis. It has also demonstrated the practical use for measuring and interrogating the effect of novel therapeutic strategies that may ultimately be of benefit to patients with RA. The following sections detail how this technology could be deployed further.

6.1 Future Work

6.1.1 Short Term Objectives

6.1.1.1 Methods of intensifying E-selectin targeted signal

The technique of fluorescent imaging by a NIR labelled MoAb directed at E-selectin has demonstrated specificity as an *in vivo* imaging technique. However despite the affinity and specificity of anti-E-selectin for its intended target, there were still significant levels of background signal due to non-specific uptake of antibody into tissue and prolonged clearance from the blood. This reduced the target to background ratio. A potential advantage of optically labelled probes is that they can be activated or switched on by a variety of mechanisms at their intended target. This compares to

other imaging modalities such as radioisotopes where a constant (but gradually decaying) signal will be emitted. A number of different activatable optical probes have been described and the principles behind these are discussed in introductory Section 1.3.2.2.2. These are largely based on a quenching mechanism whereby enzymatic cleavage of fluorophore and quencher held in close steric alignment results in fluorescent activation as the fluorophore and quencher move away from each other.

6.1.1.1.1 Investigation of altering fluorophore ratios to target moiety: increasing specificity of E-selectin targeted signal

Another potential approach that may be possible to explore is the autoquenching that can occur between identical fluorescent molecules if they are held in close proximity. This has been investigated by Ogawa and colleagues. They have developed a molecular imaging probe consisting of multiple self quenching fluorophores (Cy5.5 or Alexa Fluor 680) conjugated to a MoAb (the HER-2 blocker trastuzumab). This agent only becomes fluorescently active after cellular internalisation where the fluorescent molecules dissociate from the antibody and then fluoresce without auto-quenching of adjacent fluorescent molecules. They demonstrated higher tumour to background ratios of fluorescent signal intensity for this conjugate with up to a nine fold increase in quenching with the addition of multiple fluorophores (Ogawa, Regino et al. 2009).

→Further work would be required however, to delineate how this may translate into increased signal intensity at the intended target *in vivo*. Differing fluorophore combinations could be validated in the TNFα induced paw inflammation model and compared to the labelling experiments already performed.

Following expression on the activated endothelium it appears that E-selectin is rapidly internalised into endosomes (von Asmuth, Smeets et al. 1992). The internalisation of this glycoprotein was investigated on TNFα-activated HUVEC. Internalisation studies were performed with radioiodinated antibodies in an acid elution endocytosis assay and by immunohistology. Kinetics of intercellular adhesion molecule-1 (ICAM-1) were compared in parallel experiments. A monoclonal antibody specific for E-selectin, was internalized at a rate of approximately 1.7% of the membrane-bound monoclonal antibody per minute. In contrast, less than 0.1% of membrane antibody specific for ICAM-1 was internalized per minute. TNF-activated HUVEC were immunostained and examined by light microscopy and electron microscopy (EM). A

study by Subramaniam and colleagues demonstrated that P- and E-selectins are internalised differently following their expression (Subramaniam, Koedam et al. 1993). The endocytosis pattern visualised by immunofluorescent staining in this paper are very similar to those seen following stimulation of PY4.1 cells with TNFα at 4 hours as described in Section 3.3.4.2.

→The physiological significance of E-selectin internalization compared to the internalisation of a novel conjugated probe in the regulation of E-selectin membrane expression and clearance of E-selectin from the circulation would require further investigation. Similarly if multiple fluorophores were placed on the antibody the pharmokinetics and clearance of the novel conjugate would also require verification.

6.1.1.1.2 Labeling to minimal E-selectin antibody fragment

Labelling to a fragment of antibody can have advantages since the clearance from the blood pool may be quicker than a full sized monoclonal antibody. This may help to increase background to target levels. In addition antibody imaging methods can be problematic due to nonspecific adhesion, the human anti-mouse antibody (HAMA) response and uncertainty in the labelling site, which may interfere with the biospecificity. To investigate these properties, an anti E-selectin Fab fragment has been utilised to demonstrate that ^{99m}Tc-anti-E-selectin Fab scintigraphy can be used successfully to image synovitis with improved specificity than ^{99m}Tc-HDP bone scanning (Jamar, Houssiau et al. 2002). Other approaches include using humanised or chimeric monoclonal antibodies or smaller fragments such as single-chain variable fragment antibodies (sFV) which can be produced by bacterial systems (Huston, George et al. 1996). These are minimal antibody binding sites engineered as single polypeptide chains. The sFv can be as small as 26 kDa monomers or can be engineered as larger fusion proteins designed to self associate into dimeric or multimeric species. They typically exhibit rapid clearance that results in high targeting specificity within a matter of hours. In this study Huston and colleagues compared different modes of administration (i.v. and i.p) of radiolabelled sFVs to investigate their biodistribution and targeting properties. Administration by either the i.p. or i.v. route showed comparable long-term retention in the circulation, but the i.v. route showed an initially high peak blood level while i.p. injection did not. As with a single sFv dose, repeated bolus injections of sFv attained high target-to-background

ratios, whereas continuous sFv infusion reached a steady state level of free sFv in blood and kidney that exceeded that in tumor xenografts.

→Investigation of the biokinetics of sFVs for fluorescent imaging in arthritis would also warrant investigation to determine whether this conferred additional accelerated clearance and targeting properties.

6.1.1.1.3 Labelling to other smaller targeted molecules – aptamer based technology

As oligonucleotide ligands, aptamers are comparable to antibodies in specificity and affinity for their target molecule, typically a protein (Gold, Polisky et al. 1995; Famulok and Mayer 1999). At 8-15 kDa, aptamers are intermediate in size between antibodies (150 kDa) and small peptides (15 kDa) and are slightly smaller than sFv (25 kDa). As polyanions, aptamers are quite different in composition from sFv. As synthetic molecules, aptamers readily support site-specific modifications that maintain structure and activity. Aptamers can be coupled to diagnostic or therapeutic agents and to bioconjugates, such as polyethyleneglycol (PEG) polymers, that can alter aptamer pharmacokinetics. The parameters for the *in vivo* activity of aptamers have been investigated in rats with an aptamer directed against L-selectin (Watson, Chang et al. 2000). Previous therapeutic work with aptamers has focused on blocking protein function; by far the most advanced work is represented by the use of a vascular endothelial growth factor aptamer, pegaptanib sodium (Macugen; Pfizer and Eyetech) (Ruckman, Green et al. 1998), now approved for treatment of macular degeneration (Csaky 2003). The small size and polyanionic nature of aptamers may lead to rapid blood clearance and tissue uptake and may minimize the residence in liver and kidney, providing some potentially useful features for imaging and radiotherapy. Initial experiments to address aptamer suitability for *in vivo* imaging have been reported (Charlton, Sennello et al. 1997; Hicke, Stephens et al. 2006).

→Comparing the kinetics of optical *in vivo* targeted single chain dye labelled molecules to alternative targets such as aptamer based technology may therefore be a useful way of optimising inflamed/arthritic signal to background ratio thereby maximising signal specificity.

6.1.1.1.4 Indocyanine green (ICG) as an optical imaging agent

Another method of achieving a greater ratio of specific targeting has also been deployed by Ogawa and colleagues. This utilises some of the unique spectral properties of indocyanine green (ICG). This is already routinely used in the clinic for retinal angiography (Slakter, Yannuzzi et al. 1995) and liver function testing (Cherrick, Stein et al. 1960; Weissleder and Ntziachristos 2003). Most recently, ICG has been tested for use during liver cancer surgery by two groups to identify small and macroscopically unidentifiable liver cancers in real time which were confirmed microscopically (Gotoh, Yamada et al. 2009; Ishizawa, Fukushima et al. 2009). ICG has also been tested in the real time identification of sentinel lymph nodes in small numbers of breast cancer patients (Sevick-Muraca, Sharma et al. 2008; Tagaya, Yamazaki et al. 2008; Troyan, Kianzad et al. 2009). As ICG is non-targeted, however, a small number of false positives were detected (Ishizawa, Fukushima et al. 2009). Conjugation of ICG to a molecule that would enable tumour-specific targeting would reduce this. However, ICG's use as a conjugated NIR probe is limited as upon protein binding, fluorescence is lost. In an animal model, this property was exploited by conjugation with antibodies to CD25 which upon CD25 positive tumour cell binding become internalised leading to catabolism in lysosomes, with release of fluorescence from unbound ICG (Ogawa, Kosaka et al. 2009). ICG unbound to a target has been used to detect arthritis in a rat model of arthritis. This demonstrated that native dye was able to provide a significant increase in the fluorescent signal of arthritic joints compared to baseline values (Meier, Krug et al. 2010). Several translational optical imaging devices have recently been introduced to the clinic. This includes a custom built ICG enhanced optical imaging device that has recently been shown by Fischer *et al* to correlate well to MRI changes in the detection of pathological change in RA (Fischer, Ebert et al.). Five patients and a corresponding number of normal controls were studied using 0.1mg/kg by body weight of ICG as an unconjugated non-specific contrast agent. Fluorescence images were acquired continuously over a 15 minute period. Findings were also compared directly to contrast enhanced MR images taken concurrently. This demonstrated that ICG levels were increased in inflammatory joints although specific sensitivity and specificity was not clearly defined. They did conclude however, that NIR imaging was limited to the finger and foot joints because the strong scattering and absorption of light would preclude imaging beyond a few

centimetres of tissue depth. The specificity could be amplified beyond this by conjugating fluorescent dye to a particular target such as E-selectin.

→A possible longer term goal of this work would be to consider targeting activated endothelium in humans by linking ICG to E-selectin and constructing the conjugate so that it could dissociate following internalisation into endosomes where the emission wavelength would increase into the NIR range. Because both the human E-selectin antibody and fluorophore are approved for human administration, the likelihood of clinical translation may be improved. The resulting conjugate may well have different toxicities to the individual molecules, however the presence of two approved agents in the conjugate bodes well for its eventual clearance for human use.

6.1.1.1.5 Use of alternative imaging hardware

The challenge of overcoming light scattering and propagation for the imaging of deep joints and tissues remains to be resolved (Ntziachristos, Ripoll et al. 2002). This issue may not pose such a great problem for imaging distal joint disease. One of the major limitations of optical imaging is the loss of signal specificity due to light scattering. Although this may be decreased by imaging peripheral arthritis such as the mouse paw, this factor can potentially limit analysis of more proximal joints such as the knee or deeper tissues. This can be overcome by use of more intense dyes or by maximising the sensitivity of the optical imaging device. Advances in imaging methods that offer novel ways of visualizing and quantifying fluorescent signal will also have significant impact on fluorescent *in vivo* imaging techniques (Ntziachristos 2006) and many of these may be very useful for the future imaging of arthritis.

→Novel imaging techniques and systems could readily be analysed using the TNFα induced paw model for rapid turnover of experiments and validation of initial results from novel imaging platforms. For example exploring the specific signal returned from novel tomographic techniques for optical imaging would help to further determine the potential of this system to generate additional in vivo molecular information.

6.1.1.2 Alternative animal models

While CIA has served as an important model for investigating the aetiopathogenesis of RA, and for developing new treatments, it is not identical to RA. An ideal *in vivo* model of human synovitis would include human synovium but be readily available in

an animal host for study of the cellular mechanisms of disease and for assessment of novel molecular targets.

Investigating the *in vivo* action of novel conjugates on RA synovium in the animal model is possible by examining the action of agents on rheumatoid synovial tissue transplanted into severe combined immunodeficient (SCID) mice. The SCID model, with defects in both humoral and cell-mediated immunity, can serve as a recipient for grafts derived from numerous human tissues (McCune, Namikawa et al. 1988). In this particular RA model synovial grafts are implanted subcutaneously. The transplants remain viable and become vascularised by mouse subdermal vessels. There are connections between the mouse and transplant vasculature, with the transplant vasculature maintaining the ability to express human cell adhesion molecules (Wahid, Blades et al. 2000). This model has provided direct evidence that intragraft injection of TNFα upregulates the expression of human microvascular EC adhesion molecules. The model has also been used for investigating the use of NanoSPECT/CT imaging in the animal model. This has demonstrated that this imaging platform can be both sensitive and specific for the detection of ^{111}In-labelled anti-E-selectin or isotype control antibody.

→Hence novel human E-selectin targeted imaging agents with differing fluorophore combinations could be tested following direct stimulation of the grafts with TNFα over an acute time period, (similar to the way that TNFα injections into the paw have been used as an acute model of inflammation for initial optical imaging experiments).

→This model has also been used for the identification of novel synovium-specific peptides by *in vivo* phage display selection (Lee, Buckley et al. 2002). It may be possible to compare the honing of these peptides to either the E-selectin or a minimal E-selectin fragment (sFV). With the latter being of comparable size to novel synovium specific peptides. It would then also be possible to generate a control for both novel fluorescently conjugated molecules for *in vivo* validation.

6.1.2 Long Term Future Work and Clinical Perspectives

The work suggested above has indicated that optical imaging in humans may hold potential. As optical imaging becomes more targeted through the use of specific antibodies, activateable probes, as well as brighter, more photostable dyes, human targeted fluorescence optical imaging is a realistic possibility. Indeed, non-specific

optical imaging of patients with RA has already taken place with some initial optical imaging studies undertaken following the injection of ICG into patients with RA as described above. The addition of TNFα blockade to the therapeutic armamentarium for patients with RA has had a revolutionary impact on the treatment of both RA and other inflammatory diseases with differing molecular approaches used to target TNFα (Isaacs 2009). This has paved the way for many other agents other than TNFα blockade to be validated as therapeutic agents, but there still remains considerable uncertainty about which individual patients will respond to any particular treatment (Feldmann, Williams et al.). Increasingly as further agents become clinically available the complexity of individual treatment plans for patients with RA is likely to increase. Biomarkers are therefore required that enable both the early diagnosis of RA and help to identify particular patients that may respond positively to tailored biological therapy. Furthermore early synovitis destined to develop into RA is characterised by a distinct and transient cytokine profile that may be different to that in established disease (Raza, Falciani et al. 2005). There is much need therefore, to determine how levels of cytokines and other inflammatory mediators change during the evolution of disease both systemically and in local sites of inflammation. It is the latter that will be most amenable to examination by novel bioimaging techniques such as optical imaging. With the added molecular perspective to diagnosis, this may translate into improved targeting of treatments to particular patients depending on the phenotype of the disease thereby helping to determine appropriate treatment.

E-selectin represents an excellent molecular imaging target in humans. E-selectin can be expressed at low levels in uninflamed tissue including synovial tissue (Fairburn, Kunaver et al. 1993) but is upregulated in inflammatory synovitis (Kriegsmann, Keyszer et al. 1995) and reduced following anti-TNFα therapy (Paleolog, Hunt et al. 1996; Tak, Taylor et al. 1996). It is also expressed on activated endothelium of patients with a variety of other inflammatory conditions (Bevilacqua and Nelson 1993). Understanding the kinetics of trafficking of specific *versus* non-specific molecules to sites of inflammation *in vivo* can provide useful therapeutic information. For example, given there is a substantial proportion of antibody that tracks to sites of inflammation that is non targeted, it might be better to administer antibody targeted therapy prior to other immunomodulating drugs that decrease joint swelling in order to enhance local drug delivery to inflamed areas.

6.2 Conclusion

In summary, I have shown that E-selectin targeted imaging of joints of mice with inflammatory arthritis using fluorescently labelled anti-E-selectin is feasible *in vivo*. Furthermore, I have applied fluorescence imaging to investigate the *in vivo* mode of action of vascular-targeted therapies in murine inflammatory arthritis.

In summary E-selectin targeted *in vivo* optical imaging is an effective quantifiable imaging technique that is likely to be of significant use in the animal model and has potential to be translated into the clinic for targeted optical imaging of patients with arthritis and other inflammatory conditions. Utilising a targeted optical imaging technique to visualise endothelial activation during the evolution of inflammation in conditions such as RA will further assist in understanding disease pathogenesis and developing novel therapies.

REFERENCES

Adams, B. K., H. M. Al Attia, et al. (2001). "99Tc(m) nanocolloid scintigraphy: a reliable way to detect active joint disease in patients with peripheral joint pain." Nucl Med Commun **22**(3): 315-8.

Adams, K. E., S. Ke, et al. (2007). "Comparison of visible and near-infrared wavelength-excitable fluorescent dyes for molecular imaging of cancer." J Biomed Opt **12**(2): 024017.

Albelda, S. M., P. D. Oliver, et al. (1990). "EndoCAM: a novel endothelial cell-cell adhesion molecule." J Cell Biol **110**(4): 1227-37.

Amin, M. A., P. J. Mansfield, et al. (2007). "Interleukin-18 induces angiogenic factors in rheumatoid arthritis synovial tissue fibroblasts via distinct signaling pathways." Arthritis Rheum **56**(6): 1787-97.

Andersson, S. E., A. Johansson, et al. (1998). "Physiological characterization of mBSA antigen induced arthritis in the rat. II. Joint blood flow, glucose metabolism, and cell proliferation." J Rheumatol **25**(9): 1778-84.

Arzu Gencoglu, E., G. Aras, et al. (2003). "Comparison of Tc-99m HIG and three-phase Tc-99m MDP bone scintigraphy for evaluating the efficacy of Yttrium-90 silicate radionuclide synovectomy." Clin Nucl Med **28**(4): 277-85.

Ballara, S., P. C. Taylor, et al. (2001). "Raised serum vascular endothelial growth factor levels are associated with destructive change in inflammatory arthritis." Arthritis Rheum **44**(9): 2055-64.

Ballou, B., G. W. Fisher, et al. (1995). "Tumor labeling in vivo using cyanine-conjugated monoclonal antibodies." Cancer Immunol Immunother **41**(4): 257-63.

Barrera, P., W. J. Oyen, et al. (2003). "Scintigraphic detection of tumour necrosis factor in patients with rheumatoid arthritis." Ann Rheum Dis **62**(9): 825-8.

Barrera, P., C. J. van der Laken, et al. (2000). "Radiolabelled interleukin-1 receptor antagonist for detection of synovitis in patients with rheumatoid arthritis." Rheumatology (Oxford) **39**(8): 870-4.

Baselga, J. and C. L. Arteaga (2005). "Critical update and emerging trends in epidermal growth factor receptor targeting in cancer." J Clin Oncol **23**(11): 2445-59.

Baselga, J., D. Tripathy, et al. (1996). "Phase II study of weekly intravenous recombinant humanized anti-p185HER2 monoclonal antibody in patients with HER2/neu-overexpressing metastatic breast cancer." J Clin Oncol **14**(3): 737-44.

Bates, D. O., R. I. Heald, et al. (2001). "Vascular endothelial growth factor increases Rana vascular permeability and compliance by different signalling pathways." J Physiol **533**(Pt 1): 263-72.

Beckers, C., X. Jeukens, et al. (2006). "(18)F-FDG PET imaging of rheumatoid knee synovitis correlates with dynamic magnetic resonance and sonographic assessments as well as with the serum level of metalloproteinase-3." Eur J Nucl Med Mol Imaging **33**(3): 275-80.

Beckers, C., C. Ribbens, et al. (2004). "Assessment of disease activity in rheumatoid arthritis with (18)F-FDG PET." J Nucl Med **45**(6): 956-64.

Bendele, A. M., E. S. Chlipala, et al. (2000). "Combination benefit of treatment with the cytokine inhibitors interleukin-1 receptor antagonist and PEGylated soluble tumor necrosis factor receptor type I in animal models of rheumatoid arthritis." Arthritis Rheum **43**(12): 2648-59.

Bevilacqua, M., E. Butcher, et al. (1991). "Selectins: a family of adhesion receptors." Cell **67**(2): 233.

Bevilacqua, M. P. and R. M. Nelson (1993). "Selectins." J Clin Invest **91**(2): 379-87.

Bevilacqua, M. P., J. S. Pober, et al. (1987). "Identification of an inducible endothelial-leukocyte adhesion molecule." Proc Natl Acad Sci U S A **84**(24): 9238-42.

Bevilacqua, M. P., J. S. Pober, et al. (1985). "Interleukin 1 acts on cultured human vascular endothelium to increase the adhesion of polymorphonuclear leukocytes, monocytes, and related leukocyte cell lines." J Clin Invest **76**(5): 2003-11.

Bevilacqua, M. P., S. Stengelin, et al. (1989). "Endothelial leukocyte adhesion molecule 1: an inducible receptor for neutrophils related to complement regulatory proteins and lectins." Science **243**(4895): 1160-5.

Bhaumik, S. and S. S. Gambhir (2002). "Optical imaging of Renilla luciferase reporter gene expression in living mice." Proc Natl Acad Sci U S A **99**(1): 377-82.

Bhushan, M., T. O. Bleiker, et al. (2002). "Anti-E-selectin is ineffective in the treatment of psoriasis: a randomized trial." Br J Dermatol **146**(5): 824-31.

Binns, R. M., S. T. Licence, et al. (1996). "In vivo E-selectin upregulation correlates early with infiltration of PMN, later with PBL entry: MAbs block both." Am J Physiol **270**(1 Pt 2): H183-93.

Binns, R. M., S. T. Licence, et al. (1992). "Active lymphocyte traffic induced in the periphery by cytokines and phytohemagglutinin: three different mechanisms?" Eur J Immunol **22**(9): 2195-203.

Binns, R. M., A. Whyte, et al. (1996). "The role of E-selectin in lymphocyte and polymorphonuclear cell recruitment into cutaneous delayed hypersensitivity reactions in sensitized pigs." J Immunol **157**(9): 4094-9.

Binstadt, B. A., P. R. Patel, et al. (2006). "Particularities of the vasculature can promote the organ specificity of autoimmune attack." Nat Immunol **7**(3): 284-92.

Biswal, S., D. L. Resnick, et al. (2007). "Molecular imaging: integration of molecular imaging into the musculoskeletal imaging practice." Radiology **244**(3): 651-71.

Blann, A. D., A. Herrick, et al. (1995). "Altered levels of soluble adhesion molecules in rheumatoid arthritis, vasculitis and systemic sclerosis." Br J Rheumatol **34**(9): 814-9.

Blum, G., G. von Degenfeld, et al. (2007). "Noninvasive optical imaging of cysteine protease activity using fluorescently quenched activity-based probes." Nat Chem Biol **3**(10): 668-77.

Blum, G., R. M. Weimer, et al. (2009). "Comparative assessment of substrates and activity based probes as tools for non-invasive optical imaging of cysteine protease activity." PLoS One **4**(7): e6374.

Brahn, E., D. J. Peacock, et al. (1992). "Effects of tumor necrosis factor alpha (TNF-alpha) on collagen arthritis." Lymphokine Cytokine Res **11**(5): 253-6.

Breedveld, F. C., C. Han, et al. (2005). "Association between baseline radiographic damage and improvement in physical function after treatment of patients with rheumatoid arthritis." Ann Rheum Dis **64**(1): 52-5.

Brennan, F. M., D. Chantry, et al. (1989). "Inhibitory effect of TNF alpha antibodies on synovial cell interleukin-1 production in rheumatoid arthritis." Lancet **2**(8657): 244-7.

Bresnihan, B., J. M. Alvaro-Gracia, et al. (1998). "Treatment of rheumatoid arthritis with recombinant human interleukin-1 receptor antagonist." Arthritis Rheum **41**(12): 2196-204.

Bublil, E. M. and Y. Yarden (2007). "The EGF receptor family: spearheading a merger of signaling and therapeutics." Curr Opin Cell Biol **19**(2): 124-34.

Buch, M. and P. Emery (2002). "The aetiology and pathogenesis of rheumatoid arthritis." Hospital Pharmacist **9**: 5-10.

Buch, M. H., E. M. Vital, et al. (2008). "Abatacept in the treatment of rheumatoid arthritis." Arthritis Res Ther **10 Suppl 1**: S5.

Butcher, E. C. (1991). "Leukocyte-endothelial cell recognition: three (or more) steps to specificity and diversity." Cell **67**(6): 1033-6.

Butler, D. M., R. N. Maini, et al. (1995). "Modulation of proinflammatory cytokine release in rheumatoid synovial membrane cell cultures. Comparison of monoclonal anti TNF-alpha antibody with the interleukin-1 receptor antagonist." Eur Cytokine Netw **6**(4): 225-30.

Campos, M. M., G. E. Souza, et al. (1998). "Modulation of kinin B1 but not B2 receptors-mediated rat paw edema by IL-1beta and TNFalpha." Peptides **19**(7): 1269-76.

Cao, T., N. P. Gerard, et al. (1999). "Use of NK(1) knockout mice to analyze substance P-induced edema formation." Am J Physiol **277**(2 Pt 2): R476-81.

Cao, T., E. Pinter, et al. (2000). "Neurokinin-1 receptor agonists are involved in mediating neutrophil accumulation in the inflamed, but not normal, cutaneous microvasculature: an in vivo study using neurokinin-1 receptor knockout mice." J Immunol **164**(10): 5424-9.

Carmeliet, P. (2000). "Mechanisms of angiogenesis and arteriogenesis." Nat Med **6**(4): 389-95.

Carmeliet, P. (2003). "Angiogenesis in health and disease." Nat Med **9**(6): 653-60.

Carson, C. W., L. D. Beall, et al. (1994). "Soluble E-selectin is increased in inflammatory synovial fluid." J Rheumatol **21**(4): 605-11.

Chapman, P. T., F. Jamar, et al. (1994). "Noninvasive imaging of E-selectin expression by activated endothelium in urate crystal-induced arthritis." Arthritis Rheum **37**(12): 1752-6.

Chapman, P. T., F. Jamar, et al. (1996). "Use of a radiolabeled monoclonal antibody against E-selectin for imaging of endothelial activation in rheumatoid arthritis." Arthritis Rheum **39**(8): 1371-5.

Charlton, J., J. Sennello, et al. (1997). "In vivo imaging of inflammation using an aptamer inhibitor of human neutrophil elastase." Chem Biol **4**(11): 809-16.

Chen, J., C. H. Tung, et al. (2005). "Near-infrared fluorescent imaging of matrix metalloproteinase activity after myocardial infarction." Circulation **111**(14): 1800-5.

Chen, J., C. H. Tung, et al. (2002). "In vivo imaging of proteolytic activity in atherosclerosis." Circulation **105**(23): 2766-71.

Chen, W. T., U. Mahmood, et al. (2005). "Arthritis imaging using a near-infrared fluorescence folate-targeted probe." Arthritis Res Ther **7**(2): R310-7.

Cherrick, G. R., S. W. Stein, et al. (1960). "Indocyanine green: observations on its physical properties, plasma decay, and hepatic extraction." J Clin Invest **39**: 592-600.

Choy, E. H. and G. S. Panayi (2001). "Cytokine pathways and joint inflammation in rheumatoid arthritis." N Engl J Med **344**(12): 907-16.

Citri, A. and Y. Yarden (2006). "EGF-ERBB signalling: towards the systems level." Nat Rev Mol Cell Biol **7**(7): 505-16.

Cohen, S., E. Hurd, et al. (2002). "Treatment of rheumatoid arthritis with anakinra, a recombinant human interleukin-1 receptor antagonist, in combination with

methotrexate: results of a twenty-four-week, multicenter, randomized, double-blind, placebo-controlled trial." Arthritis Rheum **46**(3): 614-24.

Cohnheim (1889). "Lectures on General Pathology: A Handbook for Practitioners and Students."

Colville-Nash, P. R. and D. L. Scott (1992). "Angiogenesis and rheumatoid arthritis: pathogenic and therapeutic implications." Ann Rheum Dis **51**(7): 919-25.

Contag, C. H., P. R. Contag, et al. (1995). "Photonic detection of bacterial pathogens in living hosts." Mol Microbiol **18**(4): 593-603.

Corkill, M. M., B. W. Kirkham, et al. (1991). "Gold treatment of rheumatoid arthritis decreases synovial expression of the endothelial leukocyte adhesion receptor ELAM-1." J Rheumatol **18**(10): 1453-60.

Courtenay, J. S., M. J. Dallman, et al. (1980). "Immunisation against heterologous type II collagen induces arthritis in mice." Nature **283**(5748): 666-8.

Crockett-Torabi, E. (1998). "Selectins and mechanisms of signal transduction." J Leukoc Biol **63**(1): 1-14.

Csaky, K. (2003). "Anti-vascular endothelial growth factor therapy for neovascular age-related macular degeneration: promises and pitfalls." Ophthalmology **110**(5): 879-81.

Cunha, F. Q., S. Poole, et al. (1992). "The pivotal role of tumour necrosis factor alpha in the development of inflammatory hyperalgesia." Br J Pharmacol **107**(3): 660-4.

Cunha, T. M., W. A. Verri, Jr., et al. (2008). "Crucial role of neutrophils in the development of mechanical inflammatory hypernociception." J Leukoc Biol **83**(4): 824-32.

Dams, E. T., W. J. Oyen, et al. (2000). "99mTc-PEG liposomes for the scintigraphic detection of infection and inflammation: clinical evaluation." J Nucl Med **41**(4): 622-30.

Dean, J. A. (1992). lange's handbook of chemistry, McCraw Hill.

Deguchi, J. O., M. Aikawa, et al. (2006). "Inflammation in atherosclerosis: visualizing matrix metalloproteinase action in macrophages in vivo." Circulation **114**(1): 55-62.

Denk, W., J. H. Strickler, et al. (1990). "Two-photon laser scanning fluorescence microscopy." Science **248**(4951): 73-6.

Desaulniers, M., A. Fuks, et al. (1974). "Radiotechnetium polyphosphate joint imaging." J Nucl Med **15**(6): 417-23.

Di Rosa, M., Giroud, J.P, Willoughby, D.A (1971). "Studies of mediators of acute inflammatory responses induced in rats in different sites by carrageenin and turpentine." J pathol **104**: 15-21.

Di Rosa, M., J. M. Papadimitriou, et al. (1971). "A histopathological and pharmacological analysis of the mode of action of nonsteroidal anti-inflammatory drugs." J Pathol **105**(4): 239-56.

Di Rosa, M., Willoughby, D.A. (1971). "Screens for anti inflammatory drugs." J Pharm. Pharmacol. **23**: 297-300.

Diaz, R., P. A. Nguewa, et al. "Antitumor and antiangiogenic effect of the dual EGFR and HER-2 tyrosine kinase inhibitor lapatinib in a lung cancer model." BMC Cancer **10**(1): 188.

Doherty, J. K., C. Bond, et al. (1999). "The HER-2/neu receptor tyrosine kinase gene encodes a secreted autoinhibitor." Proc Natl Acad Sci U S A **96**(19): 10869-74.

Drickamer, K. (1988). "Two distinct classes of carbohydrate-recognition domains in animal lectins." J Biol Chem **263**(20): 9557-60.

Dubois, N. A., L. C. Kolpack, et al. (1991). "Isolation and characterization of an established endothelial cell line from transgenic mouse hemangiomas." Exp Cell Res **196**(2): 302-13.

Edwards, J. C. and G. Cambridge (2001). "Sustained improvement in rheumatoid arthritis following a protocol designed to deplete B lymphocytes." Rheumatology (Oxford) **40**(2): 205-11.

Edwards, J. C., L. Szczepanski, et al. (2004). "Efficacy of B-cell-targeted therapy with rituximab in patients with rheumatoid arthritis." N Engl J Med **350**(25): 2572-81.

Elliott, M. J., R. N. Maini, et al. (1994). "Randomised double-blind comparison of chimeric monoclonal antibody to tumour necrosis factor alpha (cA2) versus placebo in rheumatoid arthritis." Lancet **344**(8930): 1105-10.

Elliott, M. J., R. N. Maini, et al. (1993). "Treatment of rheumatoid arthritis with chimeric monoclonal antibodies to tumor necrosis factor alpha." Arthritis Rheum **36**(12): 1681-90.

Esdaile, J. M., M. Abrahamowicz, et al. (2001). "Traditional Framingham risk factors fail to fully account for accelerated atherosclerosis in systemic lupus erythematosus." Arthritis Rheum **44**(10): 2331-7.

Everts, M., S. A. Asgeirsdottir, et al. (2003). "Comparison of E-selectin expression at mRNA and protein levels in murine models of inflammation." Inflamm Res **52**(12): 512-8.

Fairburn, K., M. Kunaver, et al. (1993). "Intercellular adhesion molecules in normal synovium." Br J Rheumatol **32**(4): 302-6.

Famulok, M. and G. Mayer (1999). "Aptamers as tools in molecular biology and immunology." Curr Top Microbiol Immunol **243**: 123-36.

Fassbender, H. G. and M. Simmling-Annefeld (1983). "The potential aggressiveness of synovial tissue in rheumatoid arthritis." J Pathol **139**(3): 399-406.

Fassbender, K., T. Bertsch, et al. (1999). "Adhesion molecules in cerebrovascular diseases. Evidence for an inflammatory endothelial activation in cerebral large- and small-vessel disease." Stroke **30**(8): 1647-50.

Fava, R. A., N. J. Olsen, et al. (1994). "Vascular permeability factor/endothelial growth factor (VPF/VEGF): accumulation and expression in human synovial fluids and rheumatoid synovial tissue." J Exp Med **180**(1): 341-6.

Feige, U., Y. L. Hu, et al. (2000). "Anti-interleukin-1 and anti-tumor necrosis factor-alpha synergistically inhibit adjuvant arthritis in Lewis rats." Cell Mol Life Sci **57**(10): 1457-70.

Feldmann, M., F. M. Brennan, et al. (1996). "Rheumatoid arthritis." Cell **85**(3): 307-10.

Feldmann, M., F. M. Brennan, et al. (1996). "Role of cytokines in rheumatoid arthritis." Annu Rev Immunol **14**: 397-440.

Feldmann, M. and R. N. Maini (2003). "Lasker Clinical Medical Research Award. TNF defined as a therapeutic target for rheumatoid arthritis and other autoimmune diseases." Nat Med **9**(10): 1245-50.

Feldmann, M., R. O. Williams, et al. "What have we learnt from targeted anti-TNF therapy?" Ann Rheum Dis **69 Suppl 1**: i97-99.

Fidarova, E. F., E. El-Emir, et al. (2008). "Microdistribution of targeted, fluorescently labeled anti-carcinoembryonic antigen antibody in metastatic colorectal cancer: implications for radioimmunotherapy." Clin Cancer Res **14**(9): 2639-46.

Figueiredo, J. L., H. Alencar, et al. (2006). "Near infrared thoracoscopy of tumoral protease activity for improved detection of peripheral lung cancer." Int J Cancer **118**(11): 2672-7.

Fischer, T., B. Ebert, et al. "Detection of rheumatoid arthritis using non-specific contrast enhanced fluorescence imaging." Acad Radiol **17**(3): 375-81.

Fischer, T., I. Gemeinhardt, et al. (2006). "Assessment of unspecific near-infrared dyes in laser-induced fluorescence imaging of experimental arthritis." Acad Radiol **13**(1): 4-13.

FitzGerald, O. and B. Bresnihan (1995). "Synovial membrane cellularity and vascularity." Annals of the Rheumatic Diseases **54** 511-515.

FitzGerald, O., M. Soden, et al. (1991). "Morphometric analysis of blood vessels in synovial membranes obtained from clinically affected and unaffected knee joints of patients with rheumatoid arthritis." Ann Rheum Dis **50**(11): 792-6.

Fogelman, I. (1980). "Skeletal uptake of diphosphonate: a review." Eur J Nucl Med **5**(6): 473-6.

Ford, W. L. and J. L. Gowans (1969). "The traffic of lymphocytes." Semin Hematol **6**(1): 67-83.

Frijns, C. J., L. J. Kappelle, et al. (1997). "Soluble adhesion molecules reflect endothelial cell activation in ischemic stroke and in carotid atherosclerosis." Stroke **28**(11): 2214-8.

Furchgott, R. F. and J. V. Zawadzki (1980). "The obligatory role of endothelial cells in the relaxation of arterial smooth muscle by acetylcholine." Nature **288**(5789): 373-6.

Gabay, C., L. Marinova-Mutafchieva, et al. (2001). "Increased production of intracellular interleukin-1 receptor antagonist type I in the synovium of mice with collagen-induced arthritis: a possible role in the resolution of arthritis." Arthritis Rheum **44**(2): 451-62.

Gado, K. and G. Gigler (1991). "Zymosan inflammation: a new method suitable for evaluating new antiinflammatory drugs." Agents Actions **32**(1-2): 119-21.

Gallatin, W. M., I. L. Weissman, et al. (1983). "A cell-surface molecule involved in organ-specific homing of lymphocytes." Nature **304**(5921): 30-4.

Garrood, T., M. Blades, et al. (2009). "A novel model for the pre-clinical imaging of inflamed human synovial vasculature." Rheumatology (Oxford) **48**(8): 926-31.

Genovese, M. C., S. Cohen, et al. (2004). "Combination therapy with etanercept and anakinra in the treatment of patients with rheumatoid arthritis who have been treated unsuccessfully with methotrexate." Arthritis Rheum **50**(5): 1412-9.

Genovese, M. C., J. D. McKay, et al. (2008). "Interleukin-6 receptor inhibition with tocilizumab reduces disease activity in rheumatoid arthritis with inadequate response to disease-modifying antirheumatic drugs: the tocilizumab in combination with traditional disease-modifying antirheumatic drug therapy study." Arthritis Rheum **58**(10): 2968-80.

Giatromanolaki, A., E. Sivridis, et al. (2001). "The angiogenic pathway "vascular endothelial growth factor/flk-1(KDR)-receptor" in rheumatoid arthritis and osteoarthritis." The Journal of Pathology **194**: 101-108.

Gill, S. C. and P. H. von Hippel (1989). "Calculation of protein extinction coefficients from amino acid sequence data." Anal Biochem **182**(2): 319-26.

Gleysteen, J. P., J. R. Newman, et al. (2008). "Fluorescent labeled anti-EGFR antibody for identification of regional and distant metastasis in a preclinical xenograft model." Head Neck **30**(6): 782-9.

Gold, L., B. Polisky, et al. (1995). "Diversity of oligonucleotide functions." Annu Rev Biochem **64**: 763-97.

Goldman, C. K., J. Kim, et al. (1993). "Epidermal growth factor stimulates vascular endothelial growth factor production by human malignant glioma cells: a model of glioblastoma multiforme pathophysiology." Mol Biol Cell **4**(1): 121-33.

Gotoh, K., T. Yamada, et al. (2009). "A novel image-guided surgery of hepatocellular carcinoma by indocyanine green fluorescence imaging navigation." J Surg Oncol **100**(1): 75-9.

Gounaris, E., C. H. Tung, et al. (2008). "Live imaging of cysteine-cathepsin activity reveals dynamics of focal inflammation, angiogenesis, and polyp growth." PLoS One **3**(8): e2916.

Graves, B. J., R. L. Crowther, et al. (1994). "Insight into E-selectin/ligand interaction from the crystal structure and mutagenesis of the lec/EGF domains." Nature **367**(6463): 532-8.

Guillemin, F., L. Billot, et al. (2005). "Reproducibility and sensitivity to change of 5 methods for scoring hand radiographic damage in patients with rheumatoid arthritis." J Rheumatol **32**(5): 778-86.

Hahne, M., U. Jager, et al. (1993). "Five tumor necrosis factor-inducible cell adhesion mechanisms on the surface of mouse endothelioma cells mediate the binding of leukocytes." J Cell Biol **121**(3): 655-64.

Hallbeck, A. L., T. M. Walz, et al. (2005). "TGF-alpha and ErbB2 production in synovial joint tissue: increased expression in arthritic joints." Scand J Rheumatol **34**(3): 204-11.

Hanahan, D. and J. Folkman (1996). "Patterns and emerging mechanisms of the angiogenic switch during tumorigenesis." Cell **86**(3): 353-64.

Hansch, A., O. Frey, et al. (2004). "Diagnosis of arthritis using near-infrared fluorochrome Cy5.5." Invest Radiol **39**(10): 626-32.

Hansch, A., O. Frey, et al. (2004). "In vivo imaging of experimental arthritis with near-infrared fluorescence." Arthritis Rheum **50**(3): 961-7.

Hansch, A., D. Sauner, et al. (2003). "Noninvasive diagnosis of arthritis by autofluorescence." Invest Radiol **38**(9): 578-83.

Hansen, A., A. Kumar, et al. (2004). "Evaluation of cardioprotective effects of recombinant soluble P-selectin glycoprotein ligand-immunoglobulin in myocardial ischemia-reperfusion injury by real-time myocardial contrast echocardiography." J Am Coll Cardiol **44**(4): 887-91.

Harari, O. A., D. Marshall, et al. (2001). "Limited endothelial E- and P-selectin expression in MRL/lpr lupus-prone mice." Rheumatology (Oxford) **40**(8): 889-95.

Harari, O. A., J. F. McHale, et al. (1999). "Endothelial cell E- and P-selectin up-regulation in murine contact sensitivity is prolonged by distinct mechanisms occurring in sequence." J Immunol **163**(12): 6860-6.

Harris, J. M. and R. B. Chess (2003). "Effect of pegylation on pharmaceuticals." Nat Rev Drug Discov **2**(3): 214-21.

Haworth, C., F. M. Brennan, et al. (1991). "Expression of granulocyte-macrophage colony-stimulating factor in rheumatoid arthritis: regulation by tumor necrosis factor-alpha." Eur J Immunol **21**(10): 2575-9.

Helfgott, S., L. Rosenthall, et al. (1982). "Generalized skeletal response to 99mtechnetium methylene diphosphonate in rheumatoid arthritis." J Rheumatol **9**(6): 939-41.

Herschman, H. R. (2003). "Molecular imaging: looking at problems, seeing solutions." Science **302**(5645): 605-8.

Heyward, S. A., N. Dubois-Stringfellow, et al. (1995). "Expression and inducibility of vascular adhesion receptors in development." FASEB J **9**(10): 956-62.

Hicke, B. J., A. W. Stephens, et al. (2006). "Tumor targeting by an aptamer." J Nucl Med **47**(4): 668-78.

Hirata, A., S. Ogawa, et al. (2002). "ZD1839 (Iressa) induces antiangiogenic effects through inhibition of epidermal growth factor receptor tyrosine kinase." Cancer Res **62**(9): 2554-60.

Hodgson, R. J., P. O'Connor, et al. (2008). "MRI of rheumatoid arthritis image quantitation for the assessment of disease activity, progression and response to therapy." Rheumatology (Oxford) **47**(1): 13-21.

Holmdahl, R., M. E. Andersson, et al. (1989). "Collagen induced arthritis as an experimental model for rheumatoid arthritis. Immunogenetics, pathogenesis and autoimmunity." Apmis **97**(7): 575-84.

Holmdahl, R., R. Bockermann, et al. (2002). "The molecular pathogenesis of collagen-induced arthritis in mice--a model for rheumatoid arthritis." Ageing Res Rev **1**(1): 135-47.

Holmdahl, R., L. Jansson, et al. (1990). "Arthritis in DBA/1 mice induced with passively transferred type II collagen immune serum. Immunohistopathology and serum levels of anti-type II collagen auto-antibodies." Scand J Immunol **31**(2): 147-57.

Holmdahl, R., L. Jansson, et al. (1986). "Homologous type II collagen induces chronic and progressive arthritis in mice." Arthritis Rheum **29**(1): 106-13.

Hsu-Lin, S., C. L. Berman, et al. (1984). "A platelet membrane protein expressed during platelet activation and secretion. Studies using a monoclonal antibody specific for thrombin-activated platelets." J Biol Chem **259**(14): 9121-6.

Huang, Z., C. Brdlik, et al. (2009). "A pan-HER approach for cancer therapy: background, current status and future development." Expert Opin Biol Ther **9**(1): 97-110.

Huber, L. C., P. Kunzler, et al. (2008). "Effects of a novel tyrosine kinase inhibitor in rheumatoid arthritis synovial fibroblasts." Ann Rheum Dis **67**(3): 389-94.

Huston, J. S., A. J. George, et al. (1996). "Single-chain Fv radioimmunotargeting." Q J Nucl Med **40**(3): 320-33.

Hynes, N. E. and H. A. Lane (2005). "ERBB receptors and cancer: the complexity of targeted inhibitors." Nat Rev Cancer **5**(5): 341-54.

Inglis, J. J., G. Criado, et al. (2007). "Collagen-induced arthritis in C57BL/6 mice is associated with a robust and sustained T-cell response to type II collagen." Arthritis Res Ther **9**(5): R113.

Inglis, J. J., E. Simelyte, et al. (2008). "Protocol for the induction of arthritis in C57BL/6 mice." Nat Protoc **3**(4): 612-8.

Isaacs, J. D. (2009). "Antibody engineering to develop new antirheumatic therapies." Arthritis Res Ther **11**(3): 225.

Ishizawa, T., N. Fukushima, et al. (2009). "Real-time identification of liver cancers by using indocyanine green fluorescent imaging." Cancer **115**(11): 2491-504.

Izmailova, E. S., N. Paz, et al. (2007). "Use of molecular imaging to quantify response to IKK-2 inhibitor treatment in murine arthritis." Arthritis Rheum **56**(1): 117-28.

Izquierdo, E., J. D. Canete, et al. (2009). "Immature blood vessels in rheumatoid synovium are selectively depleted in response to anti-TNF therapy." PLoS One **4**(12): e8131.

Jaffe, E. A., R. L. Nachman, et al. (1973). "Culture of human endothelial cells derived from umbilical veins. Identification by morphologic and immunologic criteria." J Clin Invest **52**(11): 2745-56.

Jamar, F., P. T. Chapman, et al. (1997). "A comparison between 111In-anti-E-selectin mAb and 99Tcm-labelled human non-specific immunoglobulin in radionuclide imaging of rheumatoid arthritis." Br J Radiol **70**(833): 473-81.

Jamar, F., F. A. Houssiau, et al. (2002). "Scintigraphy using a technetium 99m-labelled anti-E-selectin Fab fragment in rheumatoid arthritis." Rheumatology (Oxford) **41**(1): 53-61.

Jayson, M. I. and J. S. Barks (1971). "Oedema in rheumatoid arthritis: changes in the coefficient of capillary filtration." Br Med J **2**(5761): 555-7.

Jiang, T., E. S. Olson, et al. (2004). "Tumor imaging by means of proteolytic activation of cell-penetrating peptides." Proc Natl Acad Sci U S A **101**(51): 17867-72.

Jin, P., J. Zhang, et al. (2009). "Rational optimization of a bispecific ligand trap targeting EGF receptor family ligands." Mol Med **15**(1-2): 11-20.

Johnston, G. I., R. G. Cook, et al. (1989). "Cloning of GMP-140, a granule membrane protein of platelets and endothelium: sequence similarity to proteins involved in cell adhesion and inflammation." Cell **56**(6): 1033-44.

Johnston, J. B., S. Navaratnam, et al. (2006). "Targeting the EGFR pathway for cancer therapy." Curr Med Chem **13**(29): 3483-92.

Jorissen, R. N., F. Walker, et al. (2003). "Epidermal growth factor receptor: mechanisms of activation and signalling." Exp Cell Res **284**(1): 31-53.

Joyce, J. A., A. Baruch, et al. (2004). "Cathepsin cysteine proteases are effectors of invasive growth and angiogenesis during multistage tumorigenesis." Cancer Cell **5**(5): 443-53.

Kameda, H., H. Ishigami, et al. (2006). "Imatinib mesylate inhibits proliferation of rheumatoid synovial fibroblast-like cells and phosphorylation of Gab adapter proteins activated by platelet-derived growth factor." Clin Exp Immunol **144**(2): 335-41.

Kaushal, S., M. K. McElroy, et al. (2008). "Fluorophore-conjugated anti-CEA antibody for the intraoperative imaging of pancreatic and colorectal cancer." J Gastrointest Surg **12**(11): 1938-50.

Kavanaugh, A., J. S. Smolen, et al. (2009). "Effect of certolizumab pegol with methotrexate on home and work place productivity and social activities in patients with active rheumatoid arthritis." Arthritis Rheum **61**(11): 1592-600.

Kaya, M., H. Tuna, et al. (2004). "(99m)Tc-dextran scintigraphy to detect disease activity in patients with rheumatoid arthritis." Nucl Med Commun **25**(6): 597-601.

Keeble, J., M. Blades, et al. (2005). "The role of substance P in microvascular responses in murine joint inflammation." Br J Pharmacol **144**(8): 1059-66.

Keelan, E. T., A. A. Harrison, et al. (1994). "Imaging vascular endothelial activation: an approach using radiolabeled monoclonal antibodies against the endothelial cell adhesion molecule E-selectin." J Nucl Med **35**(2): 276-81.

Keelan, E. T., S. T. Licence, et al. (1994). "Characterization of E-selectin expression in vivo with use of a radiolabeled monoclonal antibody." Am J Physiol **266**(1 Pt 2): H278-90.

Kelloff, G. J., K. A. Krohn, et al. (2005). "The progress and promise of molecular imaging probes in oncologic drug development." Clin Cancer Res **11**(22): 7967-85.

Keystone, E., D. Heijde, et al. (2008). "Certolizumab pegol plus methotrexate is significantly more effective than placebo plus methotrexate in active rheumatoid arthritis: findings of a fifty-two-week, phase III, multicenter, randomized, double-blind, placebo-controlled, parallel-group study." Arthritis Rheum **58**(11): 3319-29.

Keystone, E. C., M. C. Genovese, et al. (2009). "Golimumab, a human antibody to tumour necrosis factor {alpha} given by monthly subcutaneous injections, in active rheumatoid arthritis despite methotrexate therapy: the GO-FORWARD Study." Ann Rheum Dis **68**(6): 789-96.

Keystone, E. C., H. U. Schorlemmer, et al. (1977). "Zymosan-induced arthritis: a model of chronic proliferative arthritis following activation of the alternative pathway of complement." Arthritis Rheum **20**(7): 1396-1401.

Kidd, B. L., J. J. Inglis, et al. (2003). "Inhibition of inflammation and hyperalgesia in NK-1 receptor knock-out mice." Neuroreport **14**(17): 2189-92.

Kim, J. S., H. An, et al. (2009). "Multimodal optical and Gd-based nanoparticles for imaging in inflammatory arthritis." Clin Exp Rheumatol **27**(4): 580-6.

Kimball, E. S. and J. L. Gross (1991). "Angiogenesis in pannus formation." Agents Actions **34**(3-4): 329-31.

Klareskog, L., J. Ronnelid, et al. (2008). "Immunity to citrullinated proteins in rheumatoid arthritis." Annu Rev Immunol **26**: 651-75.

Klareskog, L., P. Stolt, et al. (2006). "A new model for an etiology of rheumatoid arthritis: smoking may trigger HLA-DR (shared epitope)-restricted immune reactions to autoantigens modified by citrullination." Arthritis Rheum **54**(1): 38-46.

Koch, A. E., J. C. Burrows, et al. (1991). "Immunolocalization of endothelial and leukocyte adhesion molecules in human rheumatoid and osteoarthritic synovial tissues." Lab Invest **64**(3): 313-20.

Koch, A. E., M. M. Halloran, et al. (1995). "Angiogenesis mediated by soluble forms of E-selectin and vascular cell adhesion molecule-1." Nature **376**(6540): 517-9.

Koch, A. E., L. A. Harlow, et al. (1994). "Vascular endothelial growth factor. A cytokine modulating endothelial function in rheumatoid arthritis." J Immunol **152**(8): 4149-56.

Konecny, G. E., Y. G. Meng, et al. (2004). "Association between HER-2/neu and vascular endothelial growth factor expression predicts clinical outcome in primary breast cancer patients." Clin Cancer Res **10**(5): 1706-16.

Kovar, J. L., M. A. Johnson, et al. (2006). "Hyaluronidase expression induces prostate tumor metastasis in an orthotopic mouse model." Am J Pathol **169**(4): 1415-26.

Kovar, J. L., M. A. Simpson, et al. (2007). "A systematic approach to the development of fluorescent contrast agents for optical imaging of mouse cancer models." Anal Biochem **367**(1): 1-12.

Koyama, Y., Y. Hama, et al. (2007). "Spectral fluorescence molecular imaging of lung metastases targeting HER2/neu." Clin Cancer Res **13**(10): 2936-45.

Kriegsmann, J., G. M. Keyszer, et al. (1995). "Expression of E-selectin messenger RNA and protein in rheumatoid arthritis." Arthritis Rheum **38**(6): 750-4.

Kulka, J. P., D. Bocking, et al. (1955). "Early joint lesions of rheumatoid arthritis; report of eight cases, with knee biopsies of lesions of less than one year's duration." AMA Arch Pathol **59**(2): 129-50.

Kumar, P., S. Hosaka, et al. (2001). "Soluble E-selectin induces monocyte chemotaxis through Src family tyrosine kinases." J Biol Chem **276**(24): 21039-45.

Kumar, R. and R. Yarmand-Bagheri (2001). "The role of HER2 in angiogenesis." Semin Oncol **28**(5 Suppl 16): 27-32.

Kusada, J., T. Otsuka, et al. (1993). "Immuno-reactive human epidermal growth factor (h-EGF) in rheumatoid synovial fluids." Nippon Seikeigeka Gakkai Zasshi **67**(9): 859-65.

Kuuliala, A., K. Eberhardt, et al. (2002). "Circulating soluble E-selectin in early rheumatoid arthritis: a prospective five year study." Ann Rheum Dis **61**(3): 242-6.

Lai, W. F., C. H. Chang, et al. (2004). "Early diagnosis of osteoarthritis using cathepsin B sensitive near-infrared fluorescent probes." Osteoarthritis Cartilage **12**(3): 239-44.

Lang, A., D. Horler, et al. (2000). "The relative importance of cysteine peptidases in osteoarthritis." J Rheumatol **27**(8): 1970-9.

Lasky, L. A., M. S. Singer, et al. (1989). "Cloning of a lymphocyte homing receptor reveals a lectin domain." Cell **56**(6): 1045-55.

Lee, D. M. and M. E. Weinblatt (2001). "Rheumatoid arthritis." THE LANCET **358**: 903-911.

Lee, L., C. Buckley, et al. (2002). "Identification of synovium-specific homing peptides by in vivo phage display selection." Arthritis Rheum **46**(8): 2109-20.

Lefer, D. J. (2000). "Pharmacology of selectin inhibitors in ischemia/reperfusion states." Annu Rev Pharmacol Toxicol **40**: 283-94.

Levick, J. R. (1981). "Permeability of rheumatoid and normal human synovium to specific plasma proteins." Arthritis Rheum **24**(12): 1550-60.

Levine, J. D., S. J. Dardick, et al. (1986). "Contribution of sensory afferents and sympathetic efferents to joint injury in experimental arthritis." J Neurosci **6**(12): 3423-9.

Ley, K. and G. S. Kansas (2004). "Selectins in T-cell recruitment to non-lymphoid tissues and sites of inflammation." Nat Rev Immunol **4**(5): 325-35.

Lipsky, P. E. (2007). "Why does rheumatoid arthritis involve the joints?" N Engl J Med **356**(23): 2419-20.

Lipsky, P. E., D. M. van der Heijde, et al. (2000). "Infliximab and methotrexate in the treatment of rheumatoid arthritis. Anti-Tumor Necrosis Factor Trial in Rheumatoid Arthritis with Concomitant Therapy Study Group." N Engl J Med **343**(22): 1594-602.

Lisy, M. R., A. Goermar, et al. (2008). "In vivo near-infrared fluorescence imaging of carcinoembryonic antigen-expressing tumor cells in mice." Radiology **247**(3): 779-87.

Lo, S. K., S. Lee, et al. (1991). "Endothelial-leukocyte adhesion molecule 1 stimulates the adhesive activity of leukocyte integrin CR3 (CD11b/CD18, Mac-1, alpha m beta 2) on human neutrophils." J Exp Med **173**(6): 1493-500.

Lobb, R., G. Chi-Rosso, et al. (1991). "Expression and functional characterization of a soluble form of vascular cell adhesion molecule 1." Biochem Biophys Res Commun **178**(3): 1498-504.

Lobb, R. R., G. Chi-Rosso, et al. (1991). "Expression and functional characterization of a soluble form of endothelial-leukocyte adhesion molecule 1." J Immunol **147**(1): 124-9.

Lopes, F. P., M. N. de Azevedo, et al. "Use of 99mTc-anti-CD3 scintigraphy in the differential diagnosis of rheumatic diseases." Rheumatology (Oxford) **49**(5): 933-9.

Los, M., J. M. Roodhart, et al. (2007). "Target practice: lessons from phase III trials with bevacizumab and vatalanib in the treatment of advanced colorectal cancer." Oncologist **12**(4): 443-50.

Lubberts, E., M. I. Koenders, et al. (2004). "Treatment with a neutralizing anti-murine interleukin-17 antibody after the onset of collagen-induced arthritis reduces joint inflammation, cartilage destruction, and bone erosion." Arthritis Rheum **50**(2): 650-9.

Lundberg, C. and K. E. Arfors (1983). "Polymorphonuclear leukocyte accumulation in inflammatory dermal sites as measured by 51Cr-labeled cells and myeloperoxidase." Inflammation **7**(3): 247-55.

Mahdi, H., B. A. Fisher, et al. (2009). "Specific interaction between genotype, smoking and autoimmunity to citrullinated alpha-enolase in the etiology of rheumatoid arthritis." Nat Genet **41**(12): 1319-24.

Mahmood, U. and R. Weissleder (2003). "Near-infrared optical imaging of proteases in cancer." Mol Cancer Ther **2**(5): 489-96.

Maini, R. N., F. C. Breedveld, et al. (1998). "Therapeutic efficacy of multiple intravenous infusions of anti-tumor necrosis factor alpha monoclonal antibody combined with low-dose weekly methotrexate in rheumatoid arthritis." Arthritis Rheum **41**(9): 1552-63.

Maini, R. N., P. C. Taylor, et al. (2006). "Double-blind randomized controlled clinical trial of the interleukin-6 receptor antagonist, tocilizumab, in European patients with rheumatoid arthritis who had an incomplete response to methotrexate." Arthritis Rheum **54**(9): 2817-29.

Marinova-Mutafchieva, L., R. O. Williams, et al. (1997). "Dynamics of proinflammatory cytokine expression in the joints of mice with collagen-induced arthritis (CIA)." Clin Exp Immunol **107**(3): 507-12.

Marinova-Mutafchieva, L., R. O. Williams, et al. (2000). "A comparative study into the mechanisms of action of anti-tumor necrosis factor alpha, anti-CD4, and combined anti-tumor necrosis factor alpha/anti-CD4 treatment in early collagen-induced arthritis." Arthritis Rheum **43**(3): 638-44.

Marshall, D. and D. O. Haskard (2002). "Clinical overview of leukocyte adhesion and migration: where are we now?" Semin Immunol **14**(2): 133-40.

Massoud, T. F. and S. S. Gambhir (2003). "Molecular imaging in living subjects: seeing fundamental biological processes in a new light." Genes Dev **17**(5): 545-80.

McCune, J. M., R. Namikawa, et al. (1988). "The SCID-hu mouse: murine model for the analysis of human hematolymphoid differentiation and function." Science **241**(4873): 1632-9.

McDonald, D. M. and P. Baluk (2002). "Significance of blood vessel leakiness in cancer." Cancer Res **62**(18): 5381-5.

McElroy, M., K. Hayashi, et al. (2009). "Fluorescent LYVE-1 antibody to image dynamically lymphatic trafficking of cancer cells in vivo." J Surg Res **151**(1): 68-73.

Meier, R., C. Krug, et al. (2010). "ICG-enhanced imaging of arthritis with an integrated optical imaging/X-ray system." Arthritis Rheum **62**(8): 2322-7.

Melancon, M. P., W. Wang, et al. (2007). "A novel method for imaging in vivo degradation of poly(L-glutamic acid), a biodegradable drug carrier." Pharm Res **24**(6): 1217-24.

Mendelsohn, J. and J. Baselga (2003). "Status of epidermal growth factor receptor antagonists in the biology and treatment of cancer." J Clin Oncol **21**(14): 2787-99.

Mendelsohn, J. and J. Baselga (2006). "Epidermal growth factor receptor targeting in cancer." Semin Oncol **33**(4): 369-85.

Menger, M. D. and H. A. Lehr (1993). "Scope and perspectives of intravital microscopy--bridge over from in vitro to in vivo." Immunol Today **14**(11): 519-22.

Michel, C. C. and F. E. Curry (1999). "Microvascular permeability." Physiol Rev **79**(3): 703-61.

Midwood, K., S. Sacre, et al. (2009). "Tenascin-C is an endogenous activator of Toll-like receptor 4 that is essential for maintaining inflammation in arthritic joint disease." Nat Med **15**(7): 774-80.

Miller, E. J. (1972). "Structural studies on cartilage collagen employing limited cleavage and solubilization with pepsin." Biochemistry **11**(26): 4903-9.

Mima, T., Y. Saeki, et al. (1995). "Transfer of rheumatoid arthritis into severe combined immunodeficient mice. The pathogenetic implications of T cell populations oligoclonally expanding in the rheumatoid joints." J Clin Invest **96**(4): 1746-58.

Miotla, J., R. Maciewicz, et al. (2000). "Treatment with soluble VEGF receptor reduces disease severity in murine collagen-induced arthritis." Lab Invest **80**(8): 1195-205.

Moore, K. L. (1998). "Structure and function of P-selectin glycoprotein ligand-1." Leuk Lymphoma **29**(1-2): 1-15.

Mor, A., S. B. Abramson, et al. (2005). "The fibroblast-like synovial cell in rheumatoid arthritis: a key player in inflammation and joint destruction." Clin Immunol **115**(2): 118-28.

Moreland, L. W., S. W. Baumgartner, et al. (1997). "Treatment of rheumatoid arthritis with a recombinant human tumor necrosis factor receptor (p75)-Fc fusion protein." N Engl J Med **337**(3): 141-7.

Moreland, L. W., D. P. McCabe, et al. (2000). "Phase I/II trial of recombinant methionyl human tumor necrosis factor binding protein PEGylated dimer in patients with active refractory rheumatoid arthritis." J Rheumatol **27**(3): 601-9.

Moreland, L. W., M. H. Schiff, et al. (1999). "Etanercept therapy in rheumatoid arthritis. A randomized, controlled trial." Ann Intern Med **130**(6): 478-86.

Muller, W. A., C. M. Ratti, et al. (1989). "A human endothelial cell-restricted, externally disposed plasmalemmal protein enriched in intercellular junctions." J Exp Med **170**(2): 399-414.

Myers, L. K., E. F. Rosloniec, et al. (1997). "Collagen-induced arthritis, an animal model of autoimmunity." Life Sci **61**(19): 1861-78.

Nah, S. S., H. J. Won, et al. (2009). "Epidermal growth factor increases prostaglandin E(2) production via ERK1/2 MAPK and NF-kappaB pathway in fibroblast like synoviocytes from patients with rheumatoid arthritis." Rheumatol Int.

Nahta, R., L. X. Yuan, et al. (2007). "Lapatinib induces apoptosis in trastuzumab-resistant breast cancer cells: effects on insulin-like growth factor I signaling." Mol Cancer Ther **6**(2): 667-74.

Nakatsu, T., S. Ichiyama, et al. (2006). "Structural basis for the spectral difference in luciferase bioluminescence." Nature **440**(7082): 372-6.

Newman, J. R., J. P. Gleysteen, et al. (2008). "Stereomicroscopic fluorescence imaging of head and neck cancer xenografts targeting CD147." Cancer Biol Ther **7**(7): 1063-70.

Newman, W., L. D. Beall, et al. (1993). "Soluble E-selectin is found in supernatants of activated endothelial cells and is elevated in the serum of patients with septic shock." J Immunol **150**(2): 644-54.

Niedre, M. J., R. H. de Kleine, et al. (2008). "Early photon tomography allows fluorescence detection of lung carcinomas and disease progression in mice in vivo." Proc Natl Acad Sci U S A **105**(49): 19126-31.

Noss, E. H. and M. B. Brenner (2008). "The role and therapeutic implications of fibroblast-like synoviocytes in inflammation and cartilage erosion in rheumatoid arthritis." Immunol Rev **223**: 252-70.

Notley, C. A., F. E. McCann, et al. "ANTI-CD3 therapy expands the numbers of CD4+ and CD8+ Treg cells and induces sustained amelioration of collagen-induced arthritis." Arthritis Rheum **62**(1): 171-8.

Ntziachristos, V. (2006). "Fluorescence molecular imaging." Annu Rev Biomed Eng **8**: 1-33.

Ntziachristos, V., J. Ripoll, et al. (2005). "Looking and listening to light: the evolution of whole-body photonic imaging." Nat Biotechnol **23**(3): 313-20.

Ntziachristos, V., J. Ripoll, et al. (2002). "Would near-infrared fluorescence signals propagate through large human organs for clinical studies?" Opt Lett **27**(5): 333-5.

O'Dell, J. R., C. E. Haire, et al. (1996). "Treatment of rheumatoid arthritis with methotrexate alone, sulfasalazine and hydroxychloroquine, or a combination of all three medications." N Engl J Med **334**(20): 1287-91.

O'Shaughnessy, M. C., E. K. Vetsika, et al. (2006). "The effect of substance P on nitric oxide release in a rheumatoid arthritis model." Inflamm Res **55**(6): 236-40.

Ogawa, M., N. Kosaka, et al. (2009). "In vivo molecular imaging of cancer with a quenching near-infrared fluorescent probe using conjugates of monoclonal antibodies and indocyanine green." Cancer Res **69**(4): 1268-72.

Ogawa, M., C. A. Regino, et al. (2009). "In vivo target-specific activatable near-infrared optical labeling of humanized monoclonal antibodies." Mol Cancer Ther **8**(1): 232-9.

Okamura, K., A. Morimoto, et al. (1992). "A model system for tumor angiogenesis: involvement of transforming growth factor-alpha in tube formation of human microvascular endothelial cells induced by esophageal cancer cells." Biochem Biophys Res Commun **186**(3): 1471-9.

Olayioye, M. A., R. M. Neve, et al. (2000). "The ErbB signaling network: receptor heterodimerization in development and cancer." EMBO J **19**(13): 3159-67.

Oliver, S. J., M. L. Banquerigo, et al. (1994). "Suppression of collagen-induced arthritis using an angiogenesis inhibitor, AGM-1470, and a microtubule stabilizer, taxol." Cell Immunol **157**(1): 291-9.

Oliver, S. J. and E. Brahn (1996). "Combination therapy in rheumatoid arthritis: the animal model perspective." J Rheumatol Suppl **44**: 56-60.

Oyen, W. J., O. C. Boerman, et al. (1996). "The uptake mechanisms of inflammation- and infection-localizing agents." Eur J Nucl Med **23**(4): 459-65.

Pace, C. N., F. Vajdos, et al. (1995). "How to measure and predict the molar absorption coefficient of a protein." Protein Sci **4**(11): 2411-23.

Paleolog, E. M. (2002). "Angiogenesis in rheumatoid arthritis." Arthritis Research **4**(suppl 3): S81-S90.

Paleolog, E. M. (2009). "The vasculature in rheumatoid arthritis: cause or consequence?" Int J Exp Pathol **90**(3): 249-61.

Paleolog, E. M., M. Hunt, et al. (1996). "Deactivation of vascular endothelium by monoclonal anti-tumor necrosis factor alpha antibody in rheumatoid arthritis." Arthritis Rheum **39**(7): 1082-91.

Paleolog, E. M., S. Young, et al. (1998). "Modulation of angiogenic vascular endothelial growth factor by tumor necrosis factor alpha and interleukin-1 in rheumatoid arthritis." Arthritis Rheum **41**(7): 1258-65.

Palframan, R., M. Airey, et al. (2009). "Use of biofluorescence imaging to compare the distribution of certolizumab pegol, adalimumab, and infliximab in the inflamed paws of mice with collagen-induced arthritis." J Immunol Methods **348**(1-2): 36-41.

Palosaari, K., J. Vuotila, et al. (2006). "Bone oedema predicts erosive progression on wrist MRI in early RA--a 2-yr observational MRI and NC scintigraphy study." Rheumatology (Oxford) **45**(12): 1542-8.

Pasceri, V. and E. T. Yeh (1999). "A tale of two diseases: atherosclerosis and rheumatoid arthritis." Circulation **100**(21): 2124-6.

Peacock, D. J., M. L. Banquerigo, et al. (1992). "Angiogenesis inhibition suppresses collagen arthritis." J Exp Med **175**(4): 1135-8.

Peterson, J. D., T. P. Labranche, et al. "Optical tomographic imaging discriminates between disease-modifying anti-rheumatic drug (DMARD) and non-DMARD efficacy in collagen antibody-induced arthritis." Arthritis Res Ther **12**(3): R105.

Petit, A. M., J. Rak, et al. (1997). "Neutralizing antibodies against epidermal growth factor and ErbB-2/neu receptor tyrosine kinases down-regulate vascular endothelial growth factor production by tumor cells in vitro and in vivo: angiogenic implications for signal transduction therapy of solid tumors." Am J Pathol **151**(6): 1523-30.

Piguet, P. F., G. E. Grau, et al. (1992). "Evolution of collagen arthritis in mice is arrested by treatment with anti-tumour necrosis factor (TNF) antibody or a recombinant soluble TNF receptor." Immunology **77**(4): 510-4.

Pitzalis, C. and T. Garrood (2006). "From ubiquitous antigens to joint-specific inflammation: could local vascular permeability be the missing link?" Trends Immunol **27**(7): 299-302.

Pober, J. S., M. P. Bevilacqua, et al. (1986). "Two distinct monokines, interleukin 1 and tumor necrosis factor, each independently induce biosynthesis and transient expression of the same antigen on the surface of cultured human vascular endothelial cells." J Immunol **136**(5): 1680-7.

Pober, J. S., M. A. Gimbrone, Jr., et al. (1986). "Overlapping patterns of activation of human endothelial cells by interleukin 1, tumor necrosis factor, and immune interferon." J Immunol **137**(6): 1893-6.

Pober, J. S., L. A. Lapierre, et al. (1987). "Activation of cultured human endothelial cells by recombinant lymphotoxin: comparison with tumor necrosis factor and interleukin 1 species." J Immunol **138**(10): 3319-24.

Ravindranath, N., D. Wion, et al. (2001). "Epidermal growth factor modulates the expression of vascular endothelial growth factor in the human prostate." J Androl **22**(3): 432-43.

RayChaudhury, A., W. A. Frazier, et al. (1994). "Comparison of normal and tumorigenic endothelial cells: differences in thrombospondin production and responses to transforming growth factor-beta." J Cell Sci **107 (Pt 1)**: 39-46.

Raza, K., F. Falciani, et al. (2005). "Early rheumatoid arthritis is characterized by a distinct and transient synovial fluid cytokine profile of T cell and stromal cell origin." Arthritis Res Ther **7**(4): R784-95.

Remmers, E. F., H. Sano, et al. (1991). "Production of platelet derived growth factor B chain (PDGF-B/c-sis) mRNA and immunoreactive PDGF B-like

polypeptide by rheumatoid synovium: coexpression with heparin binding acidic fibroblast growth factor-1." J Rheumatol **18**(1): 7-13.

Remmers, E. F., H. Sano, et al. (1991). "Platelet-derived growth factors and heparin-binding (fibroblast) growth factors in the synovial tissue pathology of rheumatoid arthritis." Semin Arthritis Rheum **21**(3): 191-9.

Reynolds, P. R., D. J. Larkman, et al. (2006). "Detection of vascular expression of E-selectin in vivo with MR imaging." Radiology **241**(2): 469-76.

Riese, D. J., 2nd and D. F. Stern (1998). "Specificity within the EGF family/ErbB receptor family signaling network." Bioessays **20**(1): 41-8.

Roivainen, A., R. Parkkola, et al. (2003). "Use of positron emission tomography with methyl-11C-choline and 2-18F-fluoro-2-deoxy-D-glucose in comparison with magnetic resonance imaging for the assessment of inflammatory proliferation of synovium." Arthritis Rheum **48**(11): 3077-84.

Romas, E., N. A. Sims, et al. (2002). "Osteoprotegerin reduces osteoclast numbers and prevents bone erosion in collagen-induced arthritis." Am J Pathol **161**(4): 1419-27.

Rooney, M., D. Condell, et al. (1988). "Analysis of the histologic variation of synovitis in rheumatoid arthritis." Arthritis Rheum **31**(8): 956-63.

Rosenthal, E. L., B. D. Kulbersh, et al. (2007). "Use of fluorescent labeled anti-epidermal growth factor receptor antibody to image head and neck squamous cell carcinoma xenografts." Mol Cancer Ther **6**(4): 1230-8.

Ruchaud-Sparagano, M. H., E. M. Drost, et al. (1998). "Potential pro-inflammatory effects of soluble E-selectin upon neutrophil function." Eur J Immunol **28**(1): 80-9.

Ruchaud-Sparagano, M. H., T. R. Walker, et al. (2000). "Soluble E-selectin acts in synergy with platelet-activating factor to activate neutrophil beta 2-integrins. Role of tyrosine kinases and Ca2+ mobilization." J Biol Chem **275**(21): 15758-64.

Ruckman, J., L. S. Green, et al. (1998). "2'-Fluoropyrimidine RNA-based aptamers to the 165-amino acid form of vascular endothelial growth factor (VEGF165). Inhibition of receptor binding and VEGF-induced vascular permeability through interactions requiring the exon 7-encoded domain." J Biol Chem **273**(32): 20556-67.

Salvemini, D., Z. Q. Wang, et al. (1996). "Nitric oxide: a key mediator in the early and late phase of carrageenan-induced rat paw inflammation." Br J Pharmacol **118**(4): 829-38.

Sampath, L., S. Kwon, et al. (2007). "Dual-labeled trastuzumab-based imaging agent for the detection of human epidermal growth factor receptor 2 overexpression in breast cancer." J Nucl Med **48**(9): 1501-10.

Sano, H., K. Engleka, et al. (1993). "Coexpression of phosphotyrosine-containing proteins, platelet-derived growth factor-B, and fibroblast growth factor-1 in situ in synovial tissues of patients with rheumatoid arthritis and Lewis rats with adjuvant or streptococcal cell wall arthritis." J Clin Invest **91**(2): 553-65.

Sano, H., R. Forough, et al. (1990). "Detection of high levels of heparin binding growth factor-1 (acidic fibroblast growth factor) in inflammatory arthritic joints." J Cell Biol **110**(4): 1417-26.

Sarup, J., P. Jin, et al. (2008). "Human epidermal growth factor receptor (HER-1:HER-3) Fc-mediated heterodimer has broad antiproliferative activity in vitro and in human tumor xenografts." Mol Cancer Ther **7**(10): 3223-36.

Satoh, K., S. Kikuchi, et al. (2001). "Involvement of ErbB-2 in rheumatoid synovial cell growth." Arthritis Rheum **44**(2): 260-5.

Sattar, N., D. W. McCarey, et al. (2003). "Explaining how "high-grade" systemic inflammation accelerates vascular risk in rheumatoid arthritis." Circulation **108**(24): 2957-63.

Schellekens, G. A., H. Visser, et al. (2000). "The diagnostic properties of rheumatoid arthritis antibodies recognizing a cyclic citrullinated peptide." Arthritis Rheum **43**(1): 155-63.

Scherer, R. L., M. N. VanSaun, et al. (2008). "Optical imaging of matrix metalloproteinase-7 activity in vivo using a proteolytic nanobeacon." Mol Imaging **7**(3): 118-31.

Schmitt-Sody, M., J. Landes, et al. (2003). "Quantitative assessment of angiogenesis in murine antigen-induced arthritis by intravital fluorescence microscopy." J Vasc Res **40**(5): 460-6.

Schreiber, A. B., M. E. Winkler, et al. (1986). "Transforming growth factor-alpha: a more potent angiogenic mediator than epidermal growth factor." Science **232**(4755): 1250-3.

Schumacher, H. R. and R. C. Kitridou (1972). "Synovitis of recent onset. A clinicopathologic study during the first month of disease." Arthritis Rheum **15**(5): 465-85.

Sehnert, B., P. Gierer, et al. (2006). "Modulation of granulocyte-endothelium interactions by antileukoproteinase: inhibition of anti-type II collagen antibody-induced leukocyte attachment to the synovial endothelium." Arthritis Res Ther **8**(4): R95.

Sevick-Muraca, E. M., R. Sharma, et al. (2008). "Imaging of lymph flow in breast cancer patients after microdose administration of a near-infrared fluorophore: feasibility study." Radiology **246**(3): 734-41.

Shepard, H. M., C. M. Brdlik, et al. (2008). "Signal integration: a framework for understanding the efficacy of therapeutics targeting the human EGFR family." J Clin Invest **118**(11): 3574-81.

Sheth, R. A., R. Upadhyay, et al. (2009). "Improved detection of ovarian cancer metastases by intraoperative quantitative fluorescence protease imaging in a pre-clinical model." Gynecol Oncol **112**(3): 616-22.

Shiozawa, S., K. Shiozawa, et al. (1989). "Human epidermal growth factor for the stratification of synovial lining layer and neovascularisation in rheumatoid arthritis." Ann Rheum Dis **48**(10): 820-8.

Siegelman, M. H., M. van de Rijn, et al. (1989). "Mouse lymph node homing receptor cDNA clone encodes a glycoprotein revealing tandem interaction domains." Science **243**(4895): 1165-72.

Silman, A. J., J. Newman, et al. (1996). "Cigarette smoking increases the risk of rheumatoid arthritis. Results from a nationwide study of disease-discordant twins." Arthritis Rheum **39**(5): 732-5.

Simon, G. H., H. E. Daldrup-Link, et al. (2006). "Optical imaging of experimental arthritis using allogeneic leukocytes labeled with a near-infrared fluorescent probe." Eur J Nucl Med Mol Imaging **33**(9): 998-1006.

Slakter, J. S., L. A. Yannuzzi, et al. (1995). "Indocyanine-green angiography." Curr Opin Ophthalmol **6**(3): 25-32.

Slamon, D. J., B. Leyland-Jones, et al. (2001). "Use of chemotherapy plus a monoclonal antibody against HER2 for metastatic breast cancer that overexpresses HER2." N Engl J Med **344**(11): 783-92.

Smolen, J., R. B. Landewe, et al. (2009). "Efficacy and safety of certolizumab pegol plus methotrexate in active rheumatoid arthritis: the RAPID 2 study. A randomised controlled trial." Ann Rheum Dis **68**(6): 797-804.

Smolen, J. S., A. Beaulieu, et al. (2008). "Effect of interleukin-6 receptor inhibition with tocilizumab in patients with rheumatoid arthritis (OPTION study): a double-blind, placebo-controlled, randomised trial." Lancet **371**(9617): 987-97.

Somers, W. S., J. Tang, et al. (2000). "Insights into the molecular basis of leukocyte tethering and rolling revealed by structures of P- and E-selectin bound to SLe(X) and PSGL-1." Cell **103**(3): 467-79.

Spibey, C. A., P. Jackson, et al. (2001). "A unique charge-coupled device/xenon arc lamp based imaging system for the accurate detection and quantitation of multicolour fluorescence." Electrophoresis **22**(5): 829-36.

Springer, T. A. (1990). "Adhesion receptors of the immune system." Nature **346**(6283): 425-34.

Springer, T. A. (1994). "Traffic signals for lymphocyte recirculation and leukocyte emigration: the multistep paradigm." Cell **76**(2): 301-14.

Stamper, H. B., Jr. and J. J. Woodruff (1976). "Lymphocyte homing into lymph nodes: in vitro demonstration of the selective affinity of recirculating lymphocytes for high-endothelial venules." J Exp Med **144**(3): 828-33.

Stehle, G., A. Wunder, et al. (1997). "Pharmacokinetics of methotrexate-albumin conjugates in tumor-bearing rats." Anticancer Drugs **8**(9): 835-44.

Stevens, C. R., D. R. Blake, et al. (1991). "A comparative study by morphometry of the microvasculature in normal and rheumatoid synovium." Arthritis Rheum **34**(12): 1508-13.

Subramaniam, M., J. A. Koedam, et al. (1993). "Divergent fates of P- and E-selectins after their expression on the plasma membrane." Mol Biol Cell **4**(8): 791-801.

Sumariwalla, P. F., Y. Cao, et al. (2003). "The angiogenesis inhibitor protease-activated kringles 1-5 reduces the severity of murine collagen-induced arthritis." Arthritis Res Ther **5**(1): R32-9.

Sumariwalla, P. F., P. Jin, et al. (2008). "Antagonism of the human epidermal growth factor receptor family controls disease severity in murine collagen-induced arthritis." Arthritis Rheum **58**(10): 3071-80.

Sumariwalla, P. F., A. M. Malfait, et al. (2004). "P-selectin glycoprotein ligand 1 therapy ameliorates established collagen-induced arthritis in DBA/1 mice partly through the suppression of tumour necrosis factor." Clin Exp Immunol **136**(1): 67-75.

Svensson, L., J. Jirholt, et al. (1998). "B cell-deficient mice do not develop type II collagen-induced arthritis (CIA)." Clin Exp Immunol **111**(3): 521-6.

Szekanecz, Z. and A. E. Koch (2008). "Vascular involvement in rheumatic diseases: 'vascular rheumatology'." Arthritis Res Ther **10**(5): 224.

Tagaya, N., R. Yamazaki, et al. (2008). "Intraoperative identification of sentinel lymph nodes by near-infrared fluorescence imaging in patients with breast cancer." Am J Surg **195**(6): 850-3.

Tak, P. P., P. C. Taylor, et al. (1996). "Decrease in cellularity and expression of adhesion molecules by anti-tumor necrosis factor alpha monoclonal antibody treatment in patients with rheumatoid arthritis." Arthritis Rheum **39**(7): 1077-81.

Taurog, J. D., S. S. Kerwar, et al. (1985). "Synergy between adjuvant arthritis and collagen-induced arthritis in rats." J Exp Med **162**(3): 962-78.

Taylor, P. C., A. Steuer, et al. (2004). "Comparison of ultrasonographic assessment of synovitis and joint vascularity with radiographic evaluation in a randomized, placebo-controlled study of infliximab therapy in early rheumatoid arthritis." Arthritis Rheum **50**(4): 1107-16.

Thorbecke, G. J., R. Shah, et al. (1992). "Involvement of endogenous tumor necrosis factor alpha and transforming growth factor beta during induction of collagen type II arthritis in mice." Proc Natl Acad Sci U S A **89**(16): 7375-9.

Tracey, D., L. Klareskog, et al. (2008). "Tumor necrosis factor antagonist mechanisms of action: a comprehensive review." Pharmacol Ther **117**(2): 244-79.

Trentham, D. E., A. S. Townes, et al. (1977). "Autoimmunity to type II collagen an experimental model of arthritis." J Exp Med **146**(3): 857-68.

Troyan, S. L., V. Kianzad, et al. (2009). "The FLARE() Intraoperative Near-Infrared Fluorescence Imaging System: A First-in-Human Clinical Trial in Breast Cancer Sentinel Lymph Node Mapping." Ann Surg Oncol.

Tsien, R. Y. (2009). "Constructing and Exploiting the Fluorescent Protein Paintbox (Nobel Lecture)." Angew Chem Int Ed Engl.

Urano, Y., D. Asanuma, et al. (2009). "Selective molecular imaging of viable cancer cells with pH-activatable fluorescence probes." Nat Med **15**(1): 104-9.

van der Heijde, D. M., M. A. van Leeuwen, et al. (1995). "Radiographic progression on radiographs of hands and feet during the first 3 years of rheumatoid arthritis measured according to Sharp's method (van der Heijde modification)." J Rheumatol **22**(9): 1792-6.

van Gaalen, F. A., S. P. Linn-Rasker, et al. (2004). "Autoantibodies to cyclic citrullinated peptides predict progression to rheumatoid arthritis in patients with undifferentiated arthritis: a prospective cohort study." Arthritis Rheum **50**(3): 709-15.

van Mourik, J. A., O. C. Leeksma, et al. (1985). "Vascular endothelial cells synthesize a plasma membrane protein indistinguishable from the platelet membrane glycoprotein IIa." J Biol Chem **260**(20): 11300-6.

Veale, D. J., C. Maple, et al. (1998). "Soluble cell adhesion molecules--P-selectin and ICAM-1, and disease activity in patients receiving sulphasalazine for active rheumatoid arthritis." Scand J Rheumatol **27**(4): 296-9.

Veihelmann, A., A. G. Harris, et al. (1999). "In vivo assessment of synovial microcirculation and leukocyte-endothelial cell interaction in mouse antigen-induced arthritis." Microcirculation **6**(4): 281-90.

Veihelmann, A., G. Szczesny, et al. (1998). "A novel model for the study of synovial microcirculation in the mouse knee joint in vivo." Res Exp Med (Berl) **198**(1): 43-54.

Vincent, C., L. Nogueira, et al. (2002). "Detection of antibodies to deiminated recombinant rat filaggrin by enzyme-linked immunosorbent assay: a highly effective test for the diagnosis of rheumatoid arthritis." Arthritis Rheum **46**(8): 2051-8.

von Asmuth, E. J., E. F. Smeets, et al. (1992). "Evidence for endocytosis of E-selectin in human endothelial cells." Eur J Immunol **22**(10): 2519-26.

Voskuyl, A. E., S. Martin, et al. (1995). "Levels of circulating intercellular adhesion molecule-1 and -3 but not circulating endothelial leucocyte adhesion molecule are increased in patients with rheumatoid vasculitis." Br J Rheumatol **34**(4): 311-5.

Wahid, S., M. C. Blades, et al. (2000). "Tumour necrosis factor-alpha (TNF-alpha) enhances lymphocyte migration into rheumatoid synovial tissue transplanted into severe combined immunodeficient (SCID) mice." Clin Exp Immunol **122**(1): 133-42.

Walsh, D. (1999). "Angiogenesis and arthritis." Rheumatology **38**: 103–12.

Walsh, D. A., P. I. Mapp, et al. (1992). "Localisation and characterisation of substance P binding to human synovial tissue in rheumatoid arthritis." Ann Rheum Dis **51**(3): 313-7.

Watson, S. R., Y. F. Chang, et al. (2000). "Anti-L-selectin aptamers: binding characteristics, pharmacokinetic parameters, and activity against an intravascular target in vivo." Antisense Nucleic Acid Drug Dev **10**(2): 63-75.

Weber, A. J. and M. De Bandt (2000). "Angiogenesis: general mechanisms and implications for rheumatoid arthritis." Joint Bone Spine **67**(5): 366-83.

Weinblatt, M. E., E. C. Keystone, et al. (2003). "Adalimumab, a fully human anti-tumor necrosis factor alpha monoclonal antibody, for the treatment of rheumatoid arthritis in patients taking concomitant methotrexate: the ARMADA trial." Arthritis Rheum **48**(1): 35-45.

Weinblatt, M. E., J. M. Kremer, et al. (1999). "A trial of etanercept, a recombinant tumor necrosis factor receptor:Fc fusion protein, in patients with rheumatoid arthritis receiving methotrexate." N Engl J Med **340**(4): 253-9.

Weiss, T. E., W. S. Maxfield, et al. (1965). "Iodinated human serum albumin (I-131) localization studies of rheumatoid arthritis joints by scintillation scanning. (Preliminary report)." Arthritis Rheum **8**(5): 976-87.

Weissleder, R. and U. Mahmood (2001). "Molecular imaging." Radiology **219**(2): 316-33.

Weissleder, R. and V. Ntziachristos (2003). "Shedding light onto live molecular targets." Nat Med **9**(1): 123-8.

Weissleder, R. and M. J. Pittet (2008). "Imaging in the era of molecular oncology." Nature **452**(7187): 580-9.

Weissleder, R., C. H. Tung, et al. (1999). "In vivo imaging of tumors with protease-activated near-infrared fluorescent probes." Nat Biotechnol **17**(4): 375-8.

Weller, A., S. Isenmann, et al. (1992). "Cloning of the mouse endothelial selectins. Expression of both E- and P-selectin is inducible by tumor necrosis factor alpha." J Biol Chem **267**(21): 15176-83.

Wellicome, S. M., P. Kapahi, et al. (1993). "Detection of a circulating form of vascular cell adhesion molecule-1: raised levels in rheumatoid arthritis and systemic lupus erythematosus." Clin Exp Immunol **92**(3): 412-8.

Wellicome, S. M., M. H. Thornhill, et al. (1990). "A monoclonal antibody that detects a novel antigen on endothelial cells that is induced by tumor necrosis factor, IL-1, or lipopolysaccharide." J Immunol **144**(7): 2558-65.

Whyte, A., D. O. Haskard, et al. (1994). "Infiltrating gamma delta T-cells and selectin endothelial ligands in the cutaneous phytohaemagglutinin-induced inflammatory reaction." Vet Immunol Immunopathol **41**(1-2): 31-40.

Williams, P. J., R. H. Jones, et al. (1998). "Correlation between IgG anti-type II collagen levels and arthritic severity in murine arthritis." Autoimmunity **27**(4): 201-7.

Williams, R. O., M. Feldmann, et al. (1992). "Anti-tumor necrosis factor ameliorates joint disease in murine collagen-induced arthritis." Proc Natl Acad Sci U S A **89**(20): 9784-8.

Williams, R. O., J. J. Inglis, et al. (2005). "Analysing the effect of novel therapies on cytokine expression in experimental arthritis." Int J Exp Pathol **86**(5): 267-78.

Wilson, T. and J. W. Hastings (1998). "Bioluminescence." Annu Rev Cell Dev Biol **14**: 197-230.

Winnard, P. T., Jr., J. B. Kluth, et al. (2006). "Noninvasive optical tracking of red fluorescent protein-expressing cancer cells in a model of metastatic breast cancer." Neoplasia **8**(10): 796-806.

Winter, C. A., E. A. Risley, et al. (1962). "Carrageenin-induced edema in hind paw of the rat as an assay for antiiflammatory drugs." Proc Soc Exp Biol Med **111**: 544-7.

Withrow, K. P., J. R. Newman, et al. (2008). "Assessment of bevacizumab conjugated to Cy5.5 for detection of head and neck cancer xenografts." Technol Cancer Res Treat **7**(1): 61-6.

Woodfin, A., M. B. Voisin, et al. (2007). "PECAM-1: a multi-functional molecule in inflammation and vascular biology." Arterioscler Thromb Vasc Biol **27**(12): 2514-23.

Wooley, P., H. Luthera, et al. (1981). "Type II collagen-induced arthritis in mice I. Major Histocompatibility Complex (I Region) Linkage and Antibody Correlates." Jr. Exp. Med **154**: 688-700.

Wooley, P. H., J. Dutcher, et al. (1993). "Influence of a recombinant human soluble tumor necrosis factor receptor FC fusion protein on type II collagen-induced arthritis in mice." J Immunol **151**(11): 6602-7.

Woolf, C. J., A. Allchorne, et al. (1997). "Cytokines, nerve growth factor and inflammatory hyperalgesia: the contribution of tumour necrosis factor alpha." Br J Pharmacol **121**(3): 417-24.

Workman, P., E. O. Aboagye, et al. (2010). "Guidelines for the welfare and use of animals in cancer research." Br J Cancer **102**(11): 1555-77.

Wunder, A., U. Muller-Ladner, et al. (2003). "Albumin-based drug delivery as novel therapeutic approach for rheumatoid arthritis." J Immunol **170**(9): 4793-801.

Wunder, A., R. H. Straub, et al. (2005). "Molecular imaging: novel tools in visualizing rheumatoid arthritis." Rheumatology (Oxford) **44**(11): 1341-9.

Wunder, A., C. H. Tung, et al. (2004). "In vivo imaging of protease activity in arthritis: a novel approach for monitoring treatment response." Arthritis Rheum **50**(8): 2459-65.

Xu, H., K. Baidoo, et al. (2007). "Design, synthesis, and characterization of a dual modality positron emission tomography and fluorescence imaging agent for monoclonal antibody tumor-targeted imaging." J Med Chem **50**(19): 4759-65.

Yamane, S., S. Ishida, et al. (2008). "Proinflammatory role of amphiregulin, an epidermal growth factor family member whose expression is augmented in rheumatoid arthritis patients." J Inflamm (Lond) **5**: 5.

Yarden, Y. and M. X. Sliwkowski (2001). "Untangling the ErbB signalling network." Nat Rev Mol Cell Biol **2**(2): 127-37.

Zhao, H., T. C. Doyle, et al. (2005). "Emission spectra of bioluminescent reporters and interaction with mammalian tissue determine the sensitivity of detection in vivo." J Biomed Opt **10**(4): 41210.

Zou, P., S. Xu, et al. (2009). "Near-Infrared Fluorescence Labeled Anti-TAG-72 Monoclonal Antibodies for Tumor Imaging in Colorectal Cancer Xenograft Mice." Mol Pharm.

PUBLICATIONS AND PRIZES

Abstracts

Gompels, Luke L, Inglis, Julia, Vincent, Tonia, Madden, Leigh, McNamee, Kay, McConnell, Ellen, Haskard Dorian; Paleolog, Ewa. In Vivo Fluorescence Imaging of TNF-Induced Endothelial Inflammation by Targeting E-Selectin [abstract]. Arthritis Rheum 2009;60 Suppl 10 :1997. (Oral presentation of abstract, American College of Rheumatology, Conference, November 2009)

Gompels LL; Vincent T; Madden L; Lim NH; McConnell E; Mcnamee K; Haskard DO; Paleolog EM. QUANTIFYING IN VIVO FLUORESCENCE IMAGING IN MURINE ARTHRITIS BY TARGETING E-SELECTIN. Annual Meeting of the British-Society-Rheumatology/Spring Meeting of British-Health-Professional-in-Rheumatology, 21 Apr 2010 - 23 Apr 2010. 49:I27-I27. OXFORD UNIV PRESS (Apr 2010) (Oral presentation of abstract: Young Investigator Prize Winner, BSR, April, 2010)

Gompels LL; Vincent T; Madden L; Lim NH; McConnell E; Mcnamee K; Haskard DO; Paleolog EM. In Vivo Fluorescence imaging of E-Selectin: Quantitative Detection of Endothelial Inflammation in Arthritis Models. Medical Research Society 25th February 2010.

Publications

Gompels LL; Lim NH; Vincent T; Paleolog EM. (Aug 2010). In vivo optical imaging in arthritis--an enlightening future?. Rheumatology (Oxford). 49:1436-1446.

Gompels LL, Paleolog EM. Molecular Imaging Techniques for Rheumatology Practice: Offering a Window on Disease Pathogenesis and Paving the Way for Novel Molecular Therapies. International Journal of Clinical Rheumatology (In press).

Prizes

British Society of Rheumatology Young Investigator 2010.